



Characterization of low-volatile oxygenated organic molecules and their impacts on particle formation

Dandan Li

► To cite this version:

Dandan Li. Characterization of low-volatile oxygenated organic molecules and their impacts on particle formation. *Catalysis*. Université Claude Bernard - Lyon I, 2022. English. NNT : 2022LYO10146 . tel-04860599

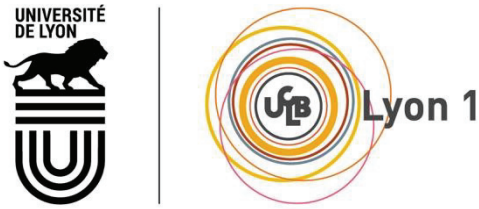
HAL Id: tel-04860599

<https://theses.hal.science/tel-04860599v1>

Submitted on 1 Jan 2025

HAL is a multi-disciplinary open access archive for the deposit and dissemination of scientific research documents, whether they are published or not. The documents may come from teaching and research institutions in France or abroad, or from public or private research centers.

L'archive ouverte pluridisciplinaire **HAL**, est destinée au dépôt et à la diffusion de documents scientifiques de niveau recherche, publiés ou non, émanant des établissements d'enseignement et de recherche français ou étrangers, des laboratoires publics ou privés.



**THESE de DOCTORAT DE
L'UNIVERSITE CLAUDE BERNARD LYON 1**

**Ecole Doctorale ED n°206
Ecole Doctorale de chimie de Lyon**

Discipline : Chimie

Soutenue publiquement le 05/12/22 par :

Dandan LI

**Characterization of low-volatile
oxygenated organic molecules and their
impacts on particle formation**

Devant le jury composé de :

Dr. Agnès BORBON	LAMP, CNRS, Clermont-Ferrand	Rapporteur
Pr. Bénédicte PICQUET-VARRAULT	Université Paris Est Créteil	Rapporteure
Dr. Sonia GIL	IRCELYON, UCBL1, Lyon	Examinateuse
Dr. Julien KAMMER	Aix-Marseille Université	Examinateur
Dr. Abdelwahid MELLOUKI	ICARE, CNRS, Orléans	Président
Pr. Eric VILLENAVE	Université de Bordeaux	Examinateur
Dr. Christian GEORGE	IRCELYON, CNRS, Lyon	Directeur de thèse
Dr. Matthieu RIVA	IRCELYON, CNRS, Lyon	Co-directeur de thèse

Université Claude Bernard – LYON 1

Administrateur provisoire de l'Université	M. Frédéric FLEURY
Président du Conseil Académique	M. Hamda BEN HADID
Vice-Président du Conseil d'Administration	M. Didier REVEL
Vice-Président du Conseil des Etudes et de la Vie Universitaire	M. Philippe CHEVALLIER
Vice-Président de la Commission de Recherche	M. Jean-François MORNEX
Directeur Général des Services	M. Pierre ROLLAND

COMPOSANTES SANTE

Département de Formation et Centre de Recherche en Biologie Humaine	Directrice : Mme Anne-Marie SCHOTT
Faculté d'Odontologie	Doyenne : Mme Dominique SEUX
Faculté de Médecine et Maïeutique Lyon Sud - Charles Mérieux	Doyenne : Mme Carole BURILLON
Faculté de Médecine Lyon-Est	Doyen : M. Gilles RODE
Institut des Sciences et Techniques de la Réadaptation (ISTR)	Directeur : M. Xavier PERROT
Institut des Sciences Pharmaceutiques et Biologiques (ISBP)	Directrice: Mme Christine VINCIGUERRA

COMPOSANTES & DEPARTEMENTS DE SCIENCES & TECHNOLOGIE

Département Génie Electrique et des Procédés (GEP)	Directrice : Mme Rosaria FERRIGNO
Département Informatique	Directeur : M. Behzad SHARIAT
Département Mécanique	Directeur M. Marc BUFFAT
Ecole Supérieure de Chimie, Physique, Electronique (CPE Lyon)	Directeur : Gérard PIGNAULT
Institut de Science Financière et d'Assurances (ISFA)	Directeur : M. Nicolas LEBOISNE
Institut National du Professorat et de l'Education	Administrateur Provisoire : M. Pierre CHAREYRON
Institut Universitaire de Technologie de Lyon 1	Directeur : M. Christophe VITON
Observatoire de Lyon	Directrice : Mme Isabelle DANIEL
Polytechnique Lyon	Directeur : Emmanuel PERRIN
UFR Biosciences	Administratrice provisoire : Mme Kathrin GIESELER
UFR des Sciences et Techniques des Activités Physiques et Sportives (STAPS)	Directeur : M. Yannick VANPOULLE
UFR Faculté des Sciences	Directeur : M. Bruno ANDRIOLETTI

Résumé de thèse

Caractérisation des molécules organiques oxygénées peu volatiles et leurs impacts sur la formation de particules

Les travaux présentés dans cette thèse portent sur le développement d'un nouveau spectromètre de masse à ionisation chimique pour l'observation d'espèces organiques réactives, et l'étude de ces derniers dans la formation de nouvelles particules dans l'atmosphère. Cette thèse est composée de six parties, qui seront brièvement présentées dans ce résumé.

Le premier chapitre est une introduction du contexte scientifique, présentant la composition de l'atmosphère, les sources et la caractérisation physico-chimique des aérosols atmosphériques et le mécanisme de formation des aérosols organiques secondaires (AOS). Plus précisément, les processus d'oxydation des composés organiques volatils (COV) sont détaillés, avec une mention particulière à la détection des molécules hautement oxygénées (HOM), ainsi que leur rôle dans la formation de nouvelles particules. Les polluants atmosphériques, en particulier les aérosols atmosphériques, jouent un rôle important dans la qualité de l'air, la visibilité, le climat et la santé humaine. Cependant, la composition complexe de l'atmosphère ainsi que les limites des outils analytiques existants rendent difficile une compréhension complète des processus d'oxydation des COV et leur rôle dans la formation de nouvelles particules.

Le deuxième chapitre décrit les différents dispositifs expérimentaux et les méthodes analytiques utilisées pour mener à bien ce travail. Les systèmes expérimentaux comprennent un réacteur à aérosol pour étudier l'oxydation des COV, la chambre de simulation atmosphérique Cosmics Leaving Outdoor Droplets (CLOUD) pour la formation de nouvelles particules. Une grande diversité de spectromètres de masse à ionisation chimique (CIMS) est présentée, notamment l'ionisation chimique à base de $\text{NO}_3^-/\text{NH}_4^+$ couplée à un spectromètre de masse à haute résolution Orbitrap (CI-Orbitrap). Les performances des différents instruments pour mesurer les produits

Résumé de thèse

d'oxydation formés lors de l'oxydation de l'alpha-pinène sont détaillées. Enfin, des analyseurs standards pour mesurer la concentration des oxydes d'azote ainsi que de l'ozone sont détaillés dans ce chapitre.

Il a été démontré que les HOM contribuent aux processus de nucléation et à la croissance de particules nouvellement formées. Dans le troisième chapitre, un spectromètre de masse à haute résolution (Orbitrap) avec une source d'ionisation chimique ont été utilisées avec succès pour caractériser ces espèces organiques réactives. Ce nouveau couplage présente un pouvoir de résolution de masse 10 à 20 fois plus élevé (c'est-à-dire $R = 140\,000$ à m/z 200) par rapport aux spectromètres de masse traditionnellement utilisés. Ainsi, les incertitudes liées à l'identification et la quantification des espèces isobares sont considérablement réduites en utilisant le CI-Orbitrap. Sa capacité à séparer avec précision les espèces formées lors de l'ozonolyse de monoterpènes a été démontrée. La quantification des énergies de liaison entre l'agent ionisant et les analytes a également été explorée via l'utilisation de la spectrométrie de masse en tandem (MS/MS). Cette dernière option permet également de fournir des informations structurelles sur des molécules hautement oxygénées. Par conséquent, la chimie et les propriétés physicochimiques de ces molécules gazeuses complexes peuvent être mieux appréhendées. Dans l'ensemble, le développement de ce nouvel outil analytique pourrait marquer une avancée cruciale dans notre capacité à comprendre la formation et le devenir des espèces organiques dans l'atmosphère.

Compte tenu du succès de l'utilisation du CI-Orbitrap avec les ions nitrate comme agent ionisant, les ions ammonium (NH_4^+) ont été explorés pour caractériser une plus large gamme de produits d'oxydation et d'espèces radicalaires formées à partir de l'oxydation de COV. Une intercomparaison des performances de divers spectromètres de masse déployés lors de la campagne Cloud 14 est proposée dans le chapitre IV. La quantification des produits d'oxydation formés lors de l'ozonolyse de l' α -pinène, a révélée que le CI- (NH_4^+) -Orbitrap est un système analytique très prometteur pour obtenir une évaluation détaillée de l'ensemble des produits formés lors de processus d'oxydation. Parmi les quatre spectromètres de masse, le CI- (NH_4^+) -Orbitrap a identifié la plus large gamme de produits, y compris les molécules organiques hautement oxygénées (HOM) et des espèces radicalaires.

Résumé de thèse

Grâce aux récents développements analytiques, le rôle des espèces oxydées dans la formation et la croissance des aérosols a été mieux compris. Les molécules organiques oxygénées (MOO), qui sont produites à partir de l'oxydation des COV, contribuent à la formation et à la croissance des aérosols organiques. En ce qui concerne l'oxydation diurne des COV, elle est principalement due aux radicaux hydroxyles et à l'ozone (O_3). La nuit, outre l' O_3 , les radicaux nitrates (NO_3) sont impliqués dans la dégradation des COV et la formation d'une grande variété d'espèces oxygénées, dont les HOM. Fait intéressant, la formation nocturne de nouvelles particules (NPF) est que très peu rapportée dans la littérature, bien que des concentrations importantes d'espèces dimériques ont également été observées. Ici, nous montrons que la chimie du NO_3 inhibe la formation de nouvelles particules lors de l'oxydation des monoterpènes et explique probablement l'absence d'événement nocturne de NPF dans des environnements dominés par les émissions de monoterpènes. Les expériences en laboratoire et les observations dans l'atmosphère ont montré que les radicaux peroxyles formés par la chimie du radical NO_3 produisent non seulement des espèces dimériques de plus grande volatilité, mais modifient entièrement les réactions de terminaison des autres radicaux RO_2 , produits à partir de la chimie O_3/OH . La volatilité des produits d'oxydation contenant de l'azote, produits par la chimie du NO_3 , est trop importante pour initier la nucléation et la croissance des particules. Par conséquent, les rendements en espèces organiques à ultra-faible volatilité (ULVOC) ont diminué d'un facteur 5 et les taux de formation de particules ont chuté d'un facteur 4 lorsque seulement 20 à 30 % de la réactivité du monoterpène est liée aux radicaux NO_3 . Les expériences en laboratoire sont étayées par des observations ambiantes montrant que le nombre de particules a été réduit jusqu'à un ordre de grandeur lorsque la chimie du NO_3 est présente. Nos résultats expliquent pourquoi la formation de nouvelles particules ne se produit pas tout le temps et partout dans une certaine mesure.

Enfin, le sixième chapitre résume ce travail de thèse et présente les perspectives des études futures.

Résumé de thèse

List of used abbreviations

APi-TOF: Atmospheric Pressure Interface Time of Flight Mass Spectrometer

AVOC: Anthropogenic Volatile Organic Compound

BVOC: Biogenic Volatile Organic Compound

CCN: Cloud Condensation Nuclei

CERN: European Organization for Nuclear Research

CI: Chemical Ionization

CIMS: Chemical Ionization Mass Spectrometry

CLOUD: Cosmics Leaving OUtdoor Droplets

EI: Electron Impact

ELVOC: Extremely Low Volatility Organic Compound

ESI: Electrospray Ionization

F0AM: Framework for 0-D Atmospheric Modeling

FFT: Fast Fourier Transformation

FIGAERO-ToF-CIMS: Time of Flight Chemical Ionization Mass Spectrometer equipped with a Filter Inlet for Gases and AEROsols

GUI: Graphical User Interface

HCD: Higher Energy Collisional Dissociation

HOM: Highly Organic Oxygenated Molecule

IMR: Ion Molecule Reaction

IVOC: Intermediate volatility organic compound

KMD: Kendrick Mass Defect

LVOC: Low Volatility Organic Compound

List of abbreviations

MCM: Master Chemical Mechanism

MCP: Micro-channel Plates

MS²: tandem mass spectral

m/z: mass-to-charge ratio

NPF: New Particle Formation

OFR: Oxidation Flow Reactor

OOM: Oxygenated organic molecules

OVOC: Oxygenated Volatile Organic Compound

PA: Proton Affinities

POA: Primary Organic Aerosol

ppmv: parts per trillion (10^6) by volume

ppbv: parts per trillion (10^9) by volume

pptv: parts per trillion (10^{12}) by volume

PTR-QMS: Proton Transfer Reaction Quadrupole Mass Spectrometer

PTR-ToF-MS: Proton Transfer Reaction Time of Flight Mass Spectrometer

RF: Radio Frequency

RH: Relative Humidity

RO₂: Peroxy Radicals

sCI: Stabilised Criegee Intermediate

slpm: standard liter per minute

SOA: Secondary Organic Aerosol

SRI: Switchable Reagent Ionization

SVOC: Semi-volatile Organic Compound

T: Temperature

List of abbreviations

TDC: Time-to-Digital Converter

ToF: Time-of-Flight

ULVOC: Ultra-low Volatility Organic Compound

UV: Ultraviolet

VBS: Volatility Basis Set

List of abbreviations

Publications included in this thesis

I Riva, M., Ehn, M., **Li, D.**, Tomaz, S., Bourgain, F., Perrier, S., and George, C. (2019), CI-Orbitrap: An Analytical Instrument To Study Atmospheric Reactive Organic Species, *Analytical chemistry*, 91(15), 9419-9423, doi:10.1021/acs.analchem.9b02093. (Chapter III)

II Riva, M., Bruggemann, M., **Li, D.**, Perrier, S., George, C., Herrmann, H., and Berndt, T. (2020), Capability of CI-Orbitrap for Gas-Phase Analysis in Atmospheric Chemistry: A Comparison with the CI-APi-TOF Technique, *Analytical chemistry*, doi:10.1021/acs.analchem.0c00111. (Chapter III)

III **Li, D.**, Wang D., Caudillo L., Scholz W., Wang M., Marie G., CLOUD COLLABORATION, Perrier S., Kirkby J., Donahue M. N., George C., Haddad El- I., Riva M., Ammonium CI-Orbitrap: a tool for characterizing the reactivity of oxygenated organic molecules (2023). (Chapter IV)

IV **Li, D.***, Huang W.*., Wang D., Wang M., Thornton J. A., Caudillo L., Rörup B., Marten R., Scholz W., Finkenzeller H., Marie G., CLOUD COLLABORATION, Kirkby J., Donahue M. N., George C., Haddad El- I., Bianchi F., Riva M., Nitrate radicals suppress biogenic new particle formation from monoterpene oxidation (2023). *: contributed equally. (Chapter V)

Contribution report

I Dandan Li (DDL) participated in the development of CI-Orbitrap technology. DDL learned how the Orbitrap mass spectrometer and CI inlet work, participated in coupling the CI inlet to Orbitrap and tuning the instrument. DDL performed the experiments together with Matthieu Riva (MR). DDL wrote the experimental section of the paper.

II DDL performed experiments to help characterize the performance of the CI-Orbitrap and help analyze data collected in Lyon but also in Tropos.

III DDL worked on packaging, deploying and maintaining CI-Orbitrap to the CLOUD chamber in CLOUD14 campaign at CERN, Switzerland. DDL worked shifts for the experiments, took charge of Orbitrap data analysis, and coordinated with 4-5 members or students for comparing NH₄⁺-Orbitrap with the other mass spectrometers deployed during Cloud14. DDL did not run other instruments, but participated in the review and discussion of the data used in Chapter IV. DDL wrote the paper under the supervision of MR and Christian George (CG).

IV DDL extended the preliminary results obtained from the CLOUD14 campaign, by performing flow tube experiments and coordinating the analysis of field data with the University of Helsinki. DDL performed data analysis and modeling with MR. DDL compiled with different data sets and interpreted them with the help of co-author. DDL wrote the paper under the supervision of MR and CG.

Table of contents

Table of contents

<i>Résumé de thèse</i>	<i>i</i>
<i>List of used abbreviations.....</i>	<i>v</i>
<i>Publications included in this thesis</i>	<i>ix</i>
<i>Contribution report</i>	<i>x</i>
<i>Table of contents.....</i>	<i>1</i>
<i>Chapter I: Introduction</i>	<i>7</i>
I.1. The atmosphere.....	7
I.2. Atmospheric aerosols	8
I.2.1. Sources and composition of aerosols	8
I.2.2 Impact of aerosols	10
I.3. Formation of secondary organic aerosol from volatile precursors	12
I.3.1. Oxidation of VOCs	12
I.3.2. Formation of highly oxygenated molecules.....	14
I.3.3. Volatility classes of oxidation products	15
I.3.4. Role of OVOCs in SOA	17
I.3.5 Oxygenated molecules detection in gas phase.....	17
I.4. Motivation for this study	18
I.5. References	20
<i>Chapter II: Experimental methods</i>	<i>33</i>
II.0. Motivation	33
II.1. Experimental systems	33
II.1.1. Oxidation flow reactor (OFR) for radical chemistry	33

Table of contents

II.1.2. CLOUD (Cosmics Leaving Outdoor Droplets) chamber for new particle formation	34
II.2. Chemical characterization	36
II.2.1. NO _x and O ₃ analyzers.....	36
II.2.2. Chemical ionization mass spectrometry	37
II.2.2.1 Chemical ionization schemes	37
II.2.2.2 Proton transfer reaction mass spectrometer (PTR-MS)	39
II.2.2.3 CI-Orbitrap.....	41
II.2.2.4 CI-APi-LTOF.....	46
II.2.2.5. PTR3-TOF	48
II.2.2.6 FIGAERO-CIMS.....	49
II.2.3. Orbitool software for analyzing Orbitrap data.....	50
II.3. References	52
<i>Chapter III: CI-Orbitrap: An Analytical Instrument To Study Atmospheric Reactive Organic Species</i>	<i>61</i>
III.1. Introduction.....	62
III.2. Experimental section	64
III.2.1. Oxidation Flow Reactor	64
III.2.2. Free-Jet Flow System	66
III.3. Results and discussion	67
III.4. Conclusion	75
III.5. References	76
<i>Chapter IV: Ammonium CI-Orbitrap: a tool for characterizing the reactivity of oxygenated organic molecules</i>	<i>83</i>
IV.1. Introduction	84
IV.2. Experimental approach and product analysis.....	85

Table of contents

IV.2.1. CLOUD chamber experiments.....	85
IV.2.2. Product analysis by Cl-(NH ₄ ⁺)-Orbitrap.....	86
IV.2.3 Product analysis by Cl-(NO ₃ ⁻)-APi-LTOF.....	88
IV.2.4 Product analysis by PTR3-TOF	89
IV.2.5 Product analysis by I ⁻ -FIGAERO-CIMS.....	90
IV.2.6 Volatility of OOMs	90
IV.3. Results and discussion	92
IV.3.1 Characterization of NH ₄ ⁺ -Orbitrap	92
IV.3.2 Characterization of OVOC by four instruments	96
IV.3.3 Instrumental comparisons: correlations	97
IV.3.4 Instrumental comparisons: concentration estimates	100
IV.3.5 RH dependance of NH ₄ ⁺ -Orbitrap.....	103
IV.3.6 Volatility distribution by four instruments	106
IV.4. Conclusion	108
IV.5. References.....	108
Chapter V: Nitrate radicals suppress biogenic new particle formation from monoterpene oxidation.....	119
V.1. Introduction	121
V.2. Materials and methods.....	122
V.2.1. Kinetic and product characterization in the oxidation flow reactor	122
V.2.2. Particle formation in CLOUD chamber	122
V.2.3. Field campaign in Siikaneva, Finland	124
V.2.4. Orbitrap technology	124
V.2.5. Volatility of HOMs.	125
V.2.6. Kinetic model simulations.....	126

Table of contents

V.3. Results.....	126
V.3.1. NPF with different oxidants	127
V.3.2. HOM distribution at different NO ₃ levels	130
V.3.3. Change of HOM volatility distribution by NO ₃	133
V.3.4. Nocturnal NPF in a wetland	136
V.4. Discussion.....	138
V.5. References.....	138
V.6. Supplementary information.....	148
<i>Chapter VI: Conclusions and perspectives</i>	173

Chapter I: Introduction

Chapter I: Introduction

I.1. The atmosphere

The atmosphere, a thin layer of gas containing a variety of diverse species, surrounds the Earth and allows life by absorbing ultraviolet solar radiation, warming the surface, and maintaining a relatively constant diurnal variation in temperature near the ground. As illustrated in Table I-1, the main constituents of dry atmospheric air are nitrogen (N_2 , 78%), oxygen (O_2 , 21%), and Argon (Ar, 1%) (Seinfeld and Pandis, 2016). Water vapor, the most significant trace gases, has a highly varied composition through the atmosphere, fluctuating with weather, latitude, and altitude. Less than 1% of the atmosphere is made up of the remaining trace gases. But despite this, they are extremely important for the chemical composition and radiative balance of the atmosphere. For example, carbon dioxide (CO_2), nitrous oxide (N_2O), and methane (CH_4) are the most abundant greenhouse gases after water vapor.

Table I-1: The major atmospheric components and their residence time at ground level (Seinfeld and Pandis, 2016; Wang, 2021).

Atmospheric species	Volume fraction (%)	Mean atmospheric residence time
Nitrogen (N_2)	78.1	15×10^{16} years
oxygen (O_2)	20.9	8×10^3 years
H_2O (g)	0-4	6-15 days
Argon (Ar)	0.9	infinite
H_2O (l)	< 0.3	1-20 days
Carbon dioxide (CO_2)	> 0.04	15 years
Neon (Ne)	1.8×10^{-3}	infinite
Helium (He)	1.8×10^{-3}	infinite
Methane (CH_4)	$\sim 1.7 \times 10^{-4}$	9 years
Hydrogen (H_2)	$\sim 5 \times 10^{-5}$	10 years
Nitrous oxide (N_2O)	$\sim 3.1 \times 10^{-5}$	150 years

Carbon monoxide (CO)	$\sim 1.2 \times 10^{-4}$	2 months
ozone (O_3)	$2-200 \times 10^{-6}$	1-2 months
Ammonia (NH_3)	$\sim 0.1 - 1 \times 10^{-6}$	20 days
Nitrogen dioxide (NO_2)	$\sim 1 \times 10^{-7}$	1 day
VOCs	$\sim 0.1-1 \times 10^{-4}$	hours-days
Sulfur dioxide (SO_2)	$\sim 2 \times 10^{-8}$	1 day
Particles	$< 10^{-5}$	minutes-weeks

Nitrogen oxides (NO_x), tropospheric ozone (O_3), and aerosol particles are the major atmospheric pollutants that are harmful to human health. NO_x are emitted by combustion engines or produced naturally by lightning. Tropospheric ozone, commonly referred to as ground-level ozone, is created when volatile organic compounds (VOCs) are photochemically oxidized in the presence of NO_x (Finlayson-Pitts and Pitts, 2000). The atmosphere is regarded to be oxidizing due to the abundance of oxidants, including O_3 , free radicals such as hydroxyl (OH), hydroperoxyl (HO_2), and nitrate (NO_3) radicals. The presence of oxidants transforms sulfur dioxide (SO_2) and VOCs into highly oxygenated species that can further affect air quality, notably by forming new particles (Bianchi et al., 2019). Although free radicals are typically less than one part in billion parts of air (ppbv), they have the capability of altering the chemical composition of the atmosphere.

I.2. Atmospheric aerosols

The terminology “atmospheric aerosols” refer to fine solid or liquid particles suspended in a gaseous medium, which are ubiquitous components of the atmosphere. Contrary to long-lived greenhouse gases, aerosol particles in the troposphere typically only last from a few hours to up to a few weeks in the atmosphere (Table I-1). Aerosols have significant effects in climate and atmospheric chemistry although making up less than 10^{-5} of atmospheric volume fraction. For example, they can scatter sunlight, serve as cloud condensation nuclei (CCN), and take part in heterogeneous chemical reactions (Andreae and Crutzen, 1997).

I.2.1. Sources and composition of aerosols

Aerosol particles originate from natural and anthropogenic sources (Seinfeld and Pankow, 2003). They can be directly released as primary aerosols, either as liquids or solids, such as desert dust,

fossil fuel combustion, and sea spray. Others, referred to as secondary particles, are produced by chemical reaction and gas-to-particle conversion of gaseous inorganic and organic precursors in the atmosphere, namely new particle formation (NPF) (Borduas and Lin, 2016; Calvo et al., 2013; George et al., 2015; Pöschl, 2005). NPF represents a significant load of atmospheric particles, contributing to 45% of global low-level cloud CCN and 35% of CCN in the free troposphere (Merikanto et al., 2009). As a rule, NPF happens in two stages: the nucleation of a critical cluster (2 nm) from vapor transform to liquid or solid, and following growth of the critical cluster to a bigger size (Kulmala et al., 2013; Zhang, 2010). During the growth, the newly formed particles may be removed by pre-existing particles, as illustrated in Figure I-1.

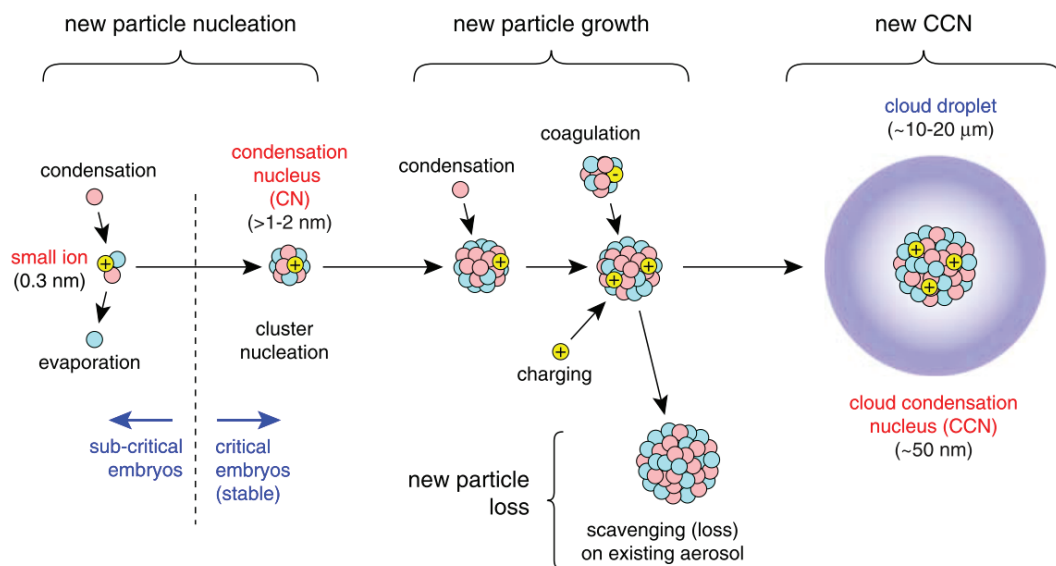


Figure I-1: Schematic description of ion-induced nucleation and growth of atmospheric aerosol particles (Kirkby, 2007).

The chemical composition of secondary particles is extremely complex, and the physiochemical nature of these particles remains poorly understood (Jimenez et al., 2009; Kwon et al., 2020; Wilczyńska-Michalik et al., 2021). As shown in Figure I-2, sulfate, nitrate, ammonium, and chloride ions are the most prevalent inorganic species of secondary particles, while organics comprise up to 90% to the submicron aerosol mass. SOA formation and aging involve a wide range of VOCs which is estimated to be up to 10^5 distinct organic molecules in the atmosphere (Goldstein and Galbally, 2007). Each of these compounds can go through a variety of atmospheric oxidation

processes to yield various oxidized products, which may contribute to the formation and growth of SOA.

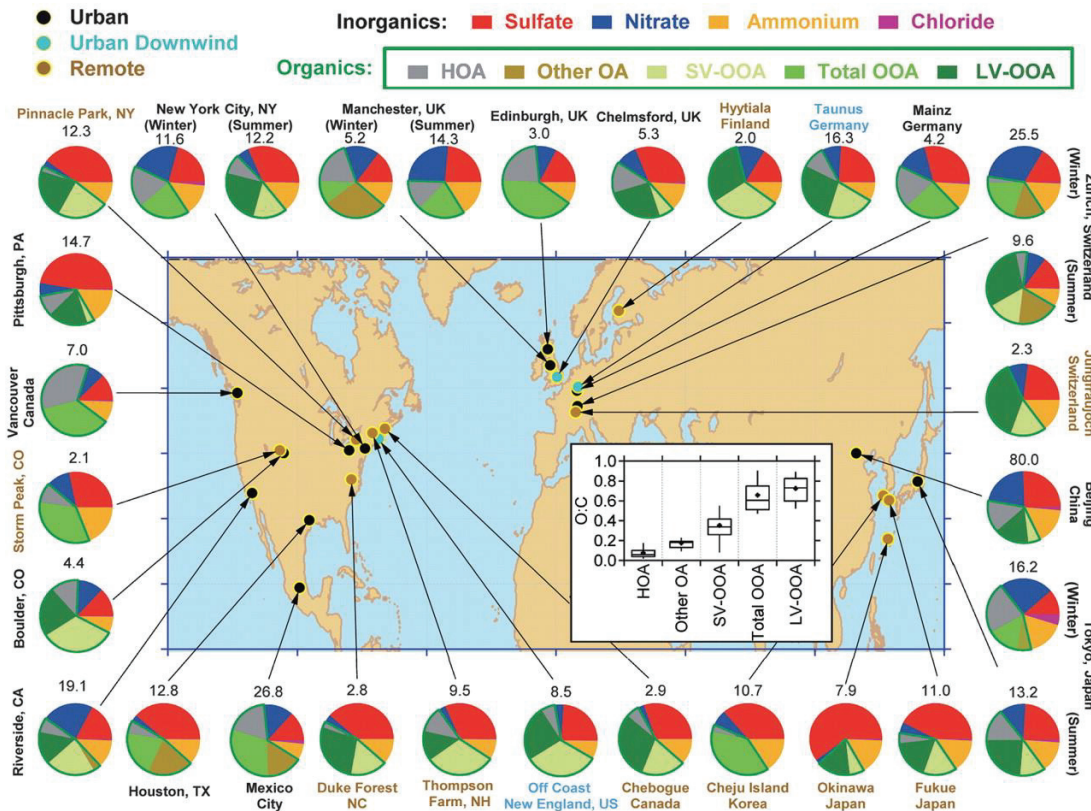


Figure I-2: Total mass concentration (in micrograms per cubic meter) and mass fractions of inorganic species and organic components in sub-micrometer aerosols measured with the Aerosol Mass Spectrometer at multiple surface locations in the northern Hemisphere (Jimenez et al., 2009).

I.2.2 Impact of aerosols

Aerosols are typically between 1 nm (lower limit: clusters of few molecules) and 100 μm (upper limit: rapid sedimentation) (Pöschl, 2005; Seinfeld and Pandis, 2016), resulting in a volume difference over a trillion. Typically, soot and other dark-colored aerosol particles absorb sunlight and warm the atmosphere. Light-colored ones, such as sea spray, on the other hand, reflect sunlight, cooling the atmosphere. Aerosol particles not only have these direct effects, but they are also essential for cloud formation as every cloud droplet and ice crystal involve an aerosol particle, as shown in Figure I-2. The surface provided by atmospheric particles allows the condensation of

water vapor, which leads to the production of clouds and rain. In general, an increase in aerosol particle concentration causes brighter clouds consisting of more, but smaller cloud droplet with longer lifetime. The resulting clouds reflect more sunlight back into space, which further cool down the atmosphere (Boucher et al., 2013; Twomey, 1977).

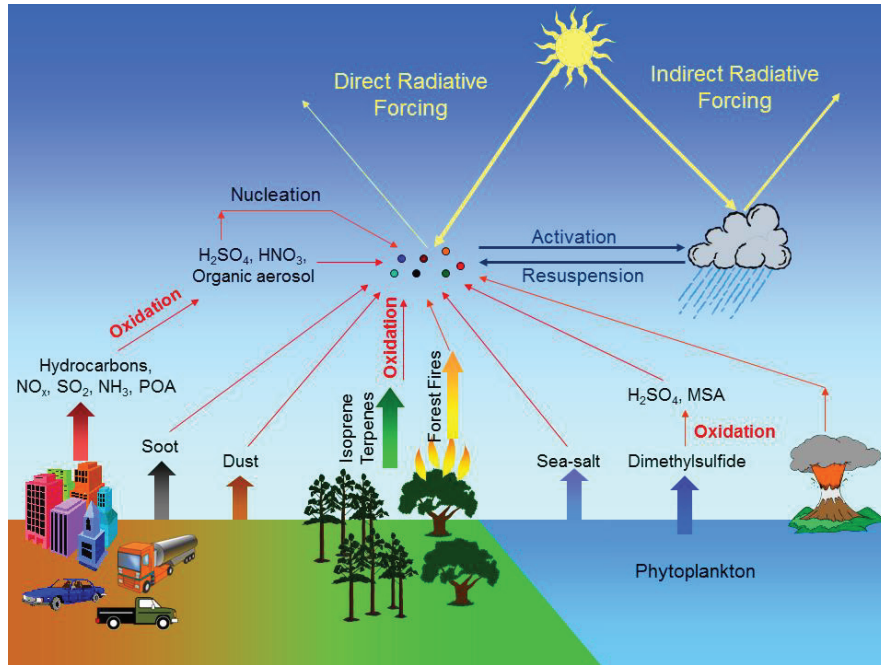


Figure I-3: A schematic showing the different sources of aerosols in the atmosphere and their effect on climate (Fadnavis et al., 2020).

Besides those on the climate, aerosol particles have various effects on our lives. Being the fifth most significant risk factor for early mortality and disability, they have negative health implications (Fowler et al., 2020; Lelieveld et al., 2015). The fate of aerosol particles in the respiratory system might vary greatly depending on their size (Rostami, 2009). For instance, larger aerosol particles are primarily deposited in the upper respiratory system whereas smaller ones can enter the lungs deeply. They also worsen visibility, as is seen in polluted areas. Large aerosol particles can absorb and scatter light, preventing it from reaching an object in the distance and getting reflected back to a viewer's eye, leading to visibility degradation (Eidels-Dubovoi, 2002).

Overall, aerosols are by far the most uncertain of all the factors influencing the climate (IPCC, 2013; IPCC, 2022). As a result, predicting accurately how climate will evolve remain challenging. For example, as we do not know how aerosol particles looked in the preindustrial atmosphere, it is

impossible to gauge accurately aerosol climate effects and how humankind has modified it (Carslaw et al., 2013). Hence, it would be particularly crucial to understand the atmosphere's natural state to reduce uncertainties. Before the advent of industry, the primary sources of aerosols were natural, with a significant contribution from biogenic activity (Andreae, 2007). Thus, studies on biogenic vapors-formed aerosols shed light on aerosols in both the present-day and pre-industrial atmosphere.

I.3. Formation of secondary organic aerosol from volatile precursors

I.3.1. Oxidation of VOCs

SOA formation begins with the release of precursor VOCs into the atmosphere. Both anthropogenic and natural VOCs come with a huge variety, with biogenic VOCs, being the most significant source in the atmosphere (Guenther et al., 2012; Lamarque et al., 2010). For example, isoprene emissions dominate tropical forests (Müller et al., 2008) and monoterpenes including α -pinene predominate in boreal forests (Hakola et al., 2012). Biogenic VOCs (BVOCs) chemistry significantly contributes to global SOA mass due to their abundance, although recent studies have shown that isoprene chemistry can reduce monoterpene derived SOA formation when co-emitted. (Heinritzi et al., 2020; McFiggans et al., 2019).

Although BVOCs dominate on a global scale, anthropogenic VOC (AVOC) emissions can be significant regionally. AVOCs are mainly dominated by aromatics, alkanes, and alkenes in urban areas (Li et al., 2019), and are emitted by a variety of human activities, including traffic and cleaning agents. Numerous studies on the oxidation of aromatic compounds have demonstrated their substantial SOA yields (Gentner et al., 2017; Ng et al., 2007).

Gas-phase oxidation is the main process for converting and degrading VOCs either by reacting with atmospheric oxidants, such as the hydroxyl radical (OH), ozone (O_3), or nitrate radical (NO_3) or via photolysis (Kroll and Seinfeld, 2008). The oxidants initiating the degradation of a VOC play a major role in determining the product distribution and thus is assumed to be a controlling factor in the product volatility (Kroll and Seinfeld, 2008).

Table I-2 summarizes the average concentrations of these three oxidants in a polluted urban environment. The OH radical is the main oxidant in the troposphere. The concentration of OH can

be low as 1×10^5 molecules cm⁻³, with the tropics and summer having the greatest levels (Finlayson-Pitts and Pitts, 2000; Lelieveld et al., 2016). Daytime OH concentrations are much higher than nighttime levels. OH radicals react with practically everything quickly and have a lifetime of a few seconds (Isaksen and Dalsøren, 2011).

Table I-2: Average oxidant mixing ratios and concentrations in a polluted urban atmosphere (Calvert et al., 2002).

Oxidant	Daytime		Nighttime	
	Volume mixing ratio	molecules cm ⁻³	Volume mixing ratio	molecules cm ⁻³
OH	0.16 pptv	3.9×10^6	0.0007 pptv	1.4×10^4
O ₃	110 ppbv	2.7×10^{12}	80 ppbv	2.0×10^{12}
NO ₃	3 pptv	7.0×10^7	100 pptv	2.5×10^9

O₃ is a significant oxidant due to its large concentrations, especially for unsaturated compounds, although generally having lower reaction rate constants than OH radicals. Alkenes are more reactive with O₃ since a double bond is required to start the oxidation process. Furthermore, elevated concentrations of O₃ during nighttime compared to OH, making it an important oxidant throughout the day. The global average lifetime of O₃ is estimated to be 19 days (Seinfeld and Pandis, 2016).

The NO₃-initiated oxidation is not significant during daytime because NO₃ radicals are quickly photolyzed. However, NO₃ chemistry has been observed during daytime beneath thick clouds or forest canopies (Liebmann et al., 2019; Wennberg et al., 2018). NO₃ is generally highly reactive with unsaturated VOCs, some of which having similar reaction rate constant compared to OH radicals. The nighttime NO₃ mixing ratio in the boundary layer is typically hundreds of ppt, thus it can be readily shown that reaction with NO₃ radical is the major degradation pathway for VOCs at night due to the high reactivity and much higher mixing ratio of NO₃ radical than OH radical (Kurtenbach et al., 2002).

I.3.2. Formation of highly oxygenated molecules

The oxidation of VOCs will produce a large pool of oxygenated VOC (OVOC), some of which possess (extremely) low vapor pressure, namely highly oxygenated organic molecules (HOMs) (Ehn et al., 2014). During the oxidation processes, HOMs are formed via autoxidation involving peroxy radicals (RO_2), starting with an intramolecular hydrogen-atom shift forming a hydroperoxyalkyl radical and subsequent rapid addition of O_2 forming a new and more oxidized peroxy radical (Crounse et al., 2013). The presence of functional groups in larger RO_2 can lower the energy barriers of the initial steps, allowing H-shift reactions under tropospheric conditions. The repetitive chain reaction leads to a wide variety of multifunctional products containing six or more oxygen atoms typically (Bianchi et al., 2019). Figure I-4 provides a schematic representation of the mechanism.

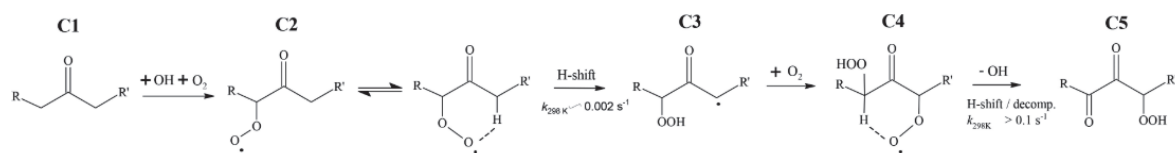


Figure I-4: Autoxidation mechanism in OH-initiated oxidation of ketones (Bianchi et al., 2019).

Within a few seconds of the ozone attack, highly oxidized and low volatility products are produced either through unimolecular termination of RO_2 radicals with NO_x , HO_2 , etc., or bimolecular reaction involving two RO_2 radicals (Berndt et al., 2018b; Tuija Jokinen et al., 2014). In particular, the reaction between two RO_2 radicals can produce a stable covalently bond dimer (I-1), whose volatility is instantly decreased by accreted functionality.



The definitions by Bianchi et al. (2019) on what compounds are thought to be HOMs are applied in this thesis. These are:

1. *HOMs are formed via autoxidation involving peroxy radicals.* This criterion distinguishes HOMs from other organic molecules with a high oxygen content, for example sugars.
2. *HOMs are formed in the gas phase under atmospherically relevant conditions.* This condition distinguishes HOMs from compounds formed in many system, such as combustion where autoxidation is known to be important (Cox and Cole, 1985).

3. *HOMs typically contain six or more oxygen atoms.* Compared to the previous two, this last criterion is less strict. Its primary purpose is to highlight the absolute number of oxygen atoms as a distinguishing feature of HOMs.

HOMs have been observed in the boreal forest (Ehn et al., 2012), suburban (Jokinen et al., 2014), rural (Kürten et al., 2016), and urban areas (Wang et al., 2022b), as well as in the free troposphere (Bianchi et al., 2016). All major oxidants have been found to produce HOMs (Bianchi et al., 2019). Most of the studies focused on the oxidation process initiated by O₃ and OH radical, notably involving BVOCs and fewer about the formation mechanism of HOMs from NO₃ radical reaction (Berndt et al., 2018a; Jokinen et al., 2015; Liebmann et al., 2019). Comparatively fewer investigations have been performed on the formation of HOMs from AVOCs (Molteni et al., 2018; Rissanen, 2021).

HOMs exhibit low or extremely low volatilities with a significant mass yield due to their large number of functional groups. As a result, they can nucleate together with other precursors and actively participate in condensational growth at all sizes, from new particle formation (NPF) to cloud condensation nuclei (CCN) (Ehn et al., 2014; Kirkby et al., 2016; Riccobono et al., 2014).

I.3.3. Volatility classes of oxidation products

Atmospheric VOC oxidation products either partition between gas and particle phase or get eliminated from the atmosphere by wet or dry deposition. The vapor pressure of the products determines whether they stay in the gas phase or transition to the condensed phase. The saturation vapor pressure refers to the pressure when the number of evaporated molecules is equal to the condensed phase at a certain temperature (Vehkamaki and Riipinen, 2012). The physical procedure that determines how a chemical is distributed between the gas and particle phases is known as the gas-particle partitioning. The equilibrium partitioning coefficient of molecules or the saturation vapor pressure serve as indicators of partitioning (Pankow, 1994). The following formula provides the partitioning coefficient, K_i :

$$K_i = \frac{[i]_{particle}}{[i]_{gas} \times M_{org}} = \frac{RT}{MW\gamma_i p_i^0} \quad (I-2)$$

where $[i]_{particle}$ and $[i]_{gas}$ are the concentrations of a compound i in the particle and gas phase, respectively, and M_{org} is the total aerosol organic mass. R is the gas constant and T the temperature;

MW is the mean molecular mass of the particle components; γ_i is the activity coefficient, and p_i^0 is the saturation vapor pressure of the given compound.

Volatility is a property of a compound that refers to its propensity to exist as a vapor, which decreases with decreasing saturation vapor pressure. Since the volatility is proportional to saturation vapor pressure, it is represented in terms of saturation mass concentration C^0 ($\mu\text{g m}^{-3}$). C^0 is the saturation concentration of a vapor over a single component, whereas the saturation concentration over a mixture is determined by the effective saturation concentration C^* , the inverse of partitioning coefficient, K_i :

$$C^* = \gamma \times C^0 = \frac{[i]_{gas}}{[i]_{particle}} \times M_{org} \quad (\text{I-3})$$

Volatility basis set (VBS), a categorization framework based on quantifiable organic property-volatility, has been established and is frequently used to characterize oxidation chemistry in a straightforward but coherent manner (Donahue et al., 2011; Li et al., 2016). The volatility of VOC oxidation products can vary by several orders of magnitude. The VBS parameterization is useful for classifying the wide range of OVOCs into the multiple groups. Products are grouped into broad categories based on C^* :

1. Ultra-low volatility organic compounds (ULVOC), $C^* < 10^{-8.5} \mu\text{g m}^{-3}$;
2. Extremely low volatility organic compounds (ELVOC), $10^{-8.5} < C^* < 10^{-4.5} \mu\text{g m}^{-3}$;
3. Low volatility organic compounds (LVOC), $10^{-4.5} < C^* < 10^{-0.5} \mu\text{g m}^{-3}$;
4. Semi-volatile organic compounds (SVOC), $10^{-0.5} < C^* < 10^{2.5} \mu\text{g m}^{-3}$;
5. Intermediate volatility organic compounds (IVOC), $10^{2.5} < C^* < 10^{6.5} \mu\text{g m}^{-3}$;
6. Volatile organic compounds (VOC), $10^{6.5} < C^* \mu\text{g m}^{-3}$.

ULVOCs can usually drive nucleation alone, at rates and under conditions observed in the atmosphere. ELVOCs condensation drive initial growth of nucleated particles up to 2 nm. As the particles increase in size and the Kelvin barrier progressively falls, subsequent growth is dominated by more abundant LVOCs (Trostl et al., 2016). HOMs are mostly classified as ULVOC, ELVOC, and LVOC, with a little subset in SVOC. Therefore, HOMs may play a role in NPF and SOA growth (Ehn et al., 2014; Kirkby et al., 2016; Trostl et al., 2016).

I.3.4. Role of OVOCs in SOA

Depending on the environment, different vapors participate in the initial stages of NPF. The specifics of their identities remain unknown. Likely candidates include sulfuric acid, ammonia, nitric acid (Kirkby et al., 2011; Lovejoy et al., 2004; Sipilä et al., 2010; Wang et al., 2020), iodine oxoacids (He et al., 2021; Sipilä et al., 2016) and organic molecules (Bianchi et al., 2016; Kirkby et al., 2016).

Organic compounds have a significant role in NPF events in addition of making up a sizable portion of the total aerosol mass (Kerminen et al., 2018). Low volatility vapors cluster together to generate particles during NPF occurrences. As more vapors condense on these particles, they grow to bigger sizes. It is generally acknowledged that HOMs play a significant role in both nucleation and particle growth, either independently or via stabilizing sulfuric acid clusters (Ehn et al., 2014; Gordon et al., 2017; Kirkby et al., 2016). They are capable of participating in the very first steps of NPF, in the early growth of the newly formed particles, or by condensing on pre-existing aerosol particles. It has long been hypothesized that the vapors that cause the particles to enlarge, reaching CCN sizes, are often organic (Kerminen et al., 2012; Kulmala et al., 1998; Riipinen et al., 2011; Smith et al., 2008; Tunved et al., 2006). Instead of their formation rate, the major factor that determines whether NPF events form climate-active aerosol particles is the growth rate of particles, since these smallest particles are most vulnerable to scavenging by coagulation into larger particles (Kerminen et al., 2004; Kerminen et al., 2012). As a result, organic molecules play a pivotal role in NPF-derived climate-relevant particles.

I.3.5 Oxygenated molecules detection in gas phase

HOM researches have progressed dramatically thanks to the instrumental advancements that enable their direct detection (Breitenlechner et al., 2017; Ehn et al., 2010; Ehn et al., 2014; Riva et al., 2019a). Chemical ionization mass spectrometry (CIMS) has become a particularly effective method for detecting and characterizing a wide variety of oxygenated gas-phase species, including free radicals (Bianchi et al., 2019; Huey, 2007; Laskin et al., 2018). The MS is an online method that can separately detect individual gaseous ionized molecules in a mixture based on their mass-to-charge (m/z) ratio (Bianchi et al., 2019; Ehn et al., 2014; Riva et al., 2020). A mass spectrometer mainly consists of an ionization source, a mass analyzer, and an ion detection system. The

commonly used methods in atmospheric science to ionize the molecules of interest are electron impact (EI), chemical ionization (CI) and electrospray ionization (ESI). And the commonly used mass analyzers include quadrupole, time-of-flight (TOF), and ion trap mass analyzer, which differ in their mass resolving power and therefore their capabilities for distinguishing isobaric ions. As for the detector, ions are detected in proportion to their abundance by micro-channel plates (MCP), electron multipliers, or image currents.

HOMs were originally found in the form of N-containing ambient ions using atmospheric pressure interface time-of-flight mass spectrometer (APi-TOF) in the boreal forest, and the element compositions were attempted to be identified at the time (Ehn et al., 2010). The definitive elemental identification of HOMs was later confirmed by a combination of new long-term measurements in the boreal forest and a targeted chamber investigation looking at naturally charged ions produced from monoterpene oxidation by ozone (Ehn et al., 2012). As a result, the research interest in atmospheric HOMs greatly increased, and many follow-up studies have been inspired, including theoretical and experimental exploration of the formation mechanism, the contribution to the newly formed particles and even to cloud condensation nucleus (CCN) on a global scale of HOMs (Bianchi et al., 2016; Ehn et al., 2014; Kirkby et al., 2016; Trostl et al., 2016).

But the APi-TOF detects only naturally charged positive and negative ions with m/z up to thousand Th due to the lack of an ion source and thus the measurement of neutral HOM molecules. Given that HOMs were primarily observed as clusters with NO_3^- (Ehn et al., 2010; Ehn et al., 2012), an APi-TOF attached to a chemical ionization source employing nitrate as the reagent ion should effectively detect HOMs. Since that time, CIMS has been commonly used in the identification, structure elucidation and quantification of organic compounds (Bianchi et al., 2019; Cappellin et al., 2012; Lee et al., 2016; Riva et al., 2019b).

I.4. Motivation for this study

SOA make up between 20-90% of the fine tropospheric particles (Hallquist et al., 2009; Jimenez et al., 2009; Kroll and Seinfeld, 2008). For example, new particle formation, condensation, and heterogeneous chemistry cause SOA to form in the atmosphere (Hallquist et al., 2009; Kroll and Seinfeld, 2008). The chemical decomposition of VOCs is an important contributor to SOA (Hallquist et al., 2009). A variety of products with various functionalities and volatilities are

produced because of VOC oxidation. Additionally, the products with low enough volatility can contribute to NPF or the growth of pre-existing particles. A new subgroup of organic vapors, highly oxygenated organic molecules (HOMs), was demonstrated to play a significant role in nucleation and growth of aerosol particles (Bianchi et al., 2019; Ehn et al., 2014). Despite their significance, the current understanding of SOA formation mechanism and evolution remain uncertainty, due to the complexity of aerosol particles and the limitations of existing instrumentation. As a result, the origins of SOA are typically considered in a relatively simple manner in climate models, resulting in large uncertainties (Shrivastava et al., 2017; Tsagiris et al., 2014). In this work, we are attempting to investigate several unknown questions about new particle formation.

First of all, major breakthroughs have been made in the study of atmospheric oxidation processes and aerosol particle formation, which attribute to a key point being the identification of trace amounts of highly oxygenated multifunctional organic molecules (Bianchi et al., 2019; Ehn et al., 2014). Therefore, we developed a new coupling to take advantage of the high resolving-power of the Orbitrap mass spectrometer for the first time to measure oxygenated species. The CI-Orbitrap could easily separate multiple overlapping ions of different elemental composition in situations where the widely used TOF mass analyzers would not have been able to identify all ions. We developed nitrate chemistry that analyzed gas-phase HOMs formed during monoterpenes' oxidation as they have been shown to be highly selective HOMs. Moreover, the possibility of ammonium chemistry to characterize OVOCs, including HOMs and less oxidized species, was explored. In contrast to other mass spectrometry, NH_4^+ -Orbitrap is a good potential CIMS technique for comprehensive measurement of the entire product distribution without switching reagent ions or running 2-3 mass spectrometers with only one reagent ion in parallel.

Given that Orbitrap has been successfully applied to characterize in real time gaseous and particle phases, a new software tool for analyzing long-term MS data is needed as the commercial software XcaliburTM provides only basic data analysis (Lee et al., 2020; Riva et al., 2020; Riva et al., 2019a). Therefore, a new software tool was developed with a graphical user interface (GUI), named Orbitool, for analyzing online Orbitrap mass spectrometry data. Orbitool includes data reading and average, background noise determination and reduction, peak shape determination, mass calibration, chemical composition and signal abundance determination via peak fitting, and data output. Long-term data could be averaged while maintaining mass accuracy. Orbitool is

designed for in-depth laboratory research and long-term atmospheric measurements. The interaction between Orbitool and other software is made easier via flexible input and output interfaces.

Daytime VOC oxidation occurs mainly through the reaction with OH radicals and ozone (Jokinen et al., 2015; Lim and Ziemann, 2005). For nocturnal oxidation processes, NO₃ radical represents an important or even dominant atmospheric oxidant and exhibits a very high reactivity with VOCs (Asaf et al., 2009; Kurtenbach et al., 2002). Although the extremely low-volatility organic compounds that most effectively drive NPF can form at night, particularly from ozone chemistry, nocturnal NPF involving organic species is not frequently detected. The exact mechanism preventing NPF at night is yet unknown, but NO₃ is thought to be a potential contributor. As a result, we combined NPF experiments in the Cosmics Leaving OUtdoor Droplets (CLOUD) chamber at European Organization for Nuclear Research (CERN), radical chemistry experiments using an Oxidation Flow Reactor (OFR), and field observations of pure biogenic NPF to study the impact of NO₃ radicals on product distribution and NPF.

I.5. References

- Andreae, M. O. (2007), Aerosols Before Pollution, *Science*, 315(5808), 50-51, doi:doi:10.1126/science.1136529.
- Andreae, M. O., and Crutzen, P. J. (1997), Atmospheric Aerosols: Biogeochemical Sources and Role in Atmospheric Chemistry, *Science*, 276(5315), 1052-1058, doi:doi:10.1126/science.276.5315.1052.
- Asaf, D., Pedersen, D., Matveev, V., Peleg, M., Kern, C., Zingler, J., Platt, U., and Luria, M. (2009), Long-Term Measurements of NO₃ Radical at a Semiarid Urban Site: 1. Extreme Concentration Events and Their Oxidation Capacity, *Environmental science & technology*, 43(24), 9117-9123, doi:10.1021/es900798b.
- Berndt, T., Mentler, B., Scholz, W., Fischer, L., Herrmann, H., Kulmala, M., and Hansel, A. (2018a), Accretion Product Formation from Ozonolysis and OH Radical Reaction of alpha-Pinene: Mechanistic Insight and the Influence of Isoprene and Ethylene, *Environmental science & technology*, 52(19), 11069-11077, doi:10.1021/acs.est.8b02210.
- Berndt, T., Scholz, W., Mentler, B., Fischer, L., Herrmann, H., Kulmala, M., and Hansel, A. (2018b), Accretion Product Formation from Self- and Cross-Reactions of RO₂ Radicals in the Atmosphere, *Angewandte Chemie*, 57(14), 3820-3824, doi:10.1002/anie.201710989.
- Bianchi, F., Kurten, T., Riva, M., Mohr, C., Rissanen, M. P., Roldin, P., Berndt, T., Crounse, J. D., Wennberg, P. O., Mentel, T. F., Wildt, J., Junninen, H., Jokinen, T., Kulmala, M., Worsnop, D. R., Thornton, J. A., Donahue, N., Kjaergaard, H. G., and Ehn, M. (2019), Highly Oxygenated Organic Molecules (HOM) from Gas-Phase Autoxidation Involving Peroxy

Chapter I: Introduction

- Radicals: A Key Contributor to Atmospheric Aerosol, *Chemical reviews*, 119(6), 3472-3509, doi:10.1021/acs.chemrev.8b00395.
- Bianchi, F., Tröstl, J., Junninen, H., Frege, C., Henne, S., Hoyle, C. R., Molteni, U., Herrmann, E., Adamov, A., Bukowiecki, N., Chen, X., Duplissy, J., Gysel, M., Hutterli, M., Kangasluoma, J., Kontkanen, J., Kürten, A., Manninen, H. E., Münch, S., Peräkylä, O., Petäjä, T., Rondo, L., Williamson, C., Weingartner, E., Curtius, J., Worsnop, D. R., Kulmala, M., Dommen, J., and Baltensperger, U. (2016), New particle formation in the free troposphere: A question of chemistry and timing, *Science*, 352(6289), 1109-1112, doi:10.1126/science.aad5456.
- Borduas, N., and Lin, V. S. (2016), Research highlights: laboratory studies of the formation and transformation of atmospheric organic aerosols, *Environmental science. Processes & impacts*, 18(4), 425-428, doi:10.1039/c6em90012g.
- Boucher, O., Randall, D., Artaxo, P., Bretherton, C., and Feingold, G. (2013), Clouds and Aerosols, in *Clouds and Aerosols. In: Climate Change 2013: The Physical Science Basis.* , edited.
- Breitenlechner, M., Fischer, L., Hainer, M., Heinritzi, M., Curtius, J., and Hansel, A. (2017), PTR3: An Instrument for Studying the Lifecycle of Reactive Organic Carbon in the Atmosphere, *Analytical chemistry*, 89(11), 5824-5831, doi:10.1021/acs.analchem.6b05110.
- Calvert, J. G., Atkinson, R., Becker, K. H., Kamens, R. M., Seinfeld, J. H., Wallington, T. H., and Yarwood, G. (2002), The mechanisms of atmospheric oxidation of the aromatic hydrocarbons.
- Calvo, A. I., Alves, C., Castro, A., Pont, V., Vicente, A. M., and Fraile, R. (2013), Research on aerosol sources and chemical composition: Past, current and emerging issues, *Atmospheric Research*, 120-121, 1-28, doi:<https://doi.org/10.1016/j.atmosres.2012.09.021>.
- Cappellin, L., Karl, T., Probst, M., Ismailova, O., Winkler, P. M., Soukoulis, C., Aprea, E., Mark, T. D., Gasperi, F., and Biasioli, F. (2012), On quantitative determination of volatile organic compound concentrations using proton transfer reaction time-of-flight mass spectrometry, *Environmental science & technology*, 46(4), 2283-2290, doi:10.1021/es203985t.
- Carslaw, K. S., Lee, L. A., Reddington, C. L., Pringle, K. J., Rap, A., Forster, P. M., Mann, G. W., Spracklen, D. V., Woodhouse, M. T., Regayre, L. A., and Pierce, J. R. (2013), Large contribution of natural aerosols to uncertainty in indirect forcing, *Nature*, 503(7474), 67-71, doi:10.1038/nature12674.
- Cox, R. A., and Cole, J. A. (1985), Chemical aspects of the autoignition of hydrocarbon air mixtures, *Combustion and Flame*, 60(2), 109-123, doi:[https://doi.org/10.1016/0010-2180\(85\)90001-X](https://doi.org/10.1016/0010-2180(85)90001-X).
- Crounse, J. D., Nielsen, L. B., Jørgensen, S., Kjaergaard, H. G., and Wennberg, P. O. (2013), Autoxidation of Organic Compounds in the Atmosphere, *The Journal of Physical Chemistry Letters*, 4(20), 3513-3520, doi:10.1021/jz4019207.
- Donahue, N. M., Epstein, S. A., Pandis, S. N., and Robinson, A. L. (2011), A two-dimensional volatility basis set: 1. organic-aerosol mixing thermodynamics, *Atmospheric Chemistry and Physics*, 11(7), 3303-3318, doi:10.5194/acp-11-3303-2011.
- Ehn, M., Junninen, H., Petäjä, T., Kurtén, T., Kerminen, V. M., Schobesberger, S., Manninen, H. E., Ortega, I. K., Vehkamäki, H., Kulmala, M., and Worsnop, D. R. (2010), Composition and temporal behavior of ambient ions in the boreal forest, *Atmospheric Chemistry and Physics*, 10(17), 8513-8530, doi:10.5194/acp-10-8513-2010.
- Ehn, M., Kleist, E., Junninen, H., Petäjä, T., Lönn, G., Schobesberger, S., Dal Maso, M., Trimborn, A., Kulmala, M., Worsnop, D. R., Wahner, A., Wildt, J., and Mentel, T. F. (2012), Gas

phase formation of extremely oxidized pinene reaction products in chamber and ambient air, *Atmospheric Chemistry and Physics*, 12(11), 5113-5127, doi:10.5194/acp-12-5113-2012.

Ehn, M., Thornton, J. A., Kleist, E., Sipila, M., Junninen, H., Pullinen, I., Springer, M., Rubach, F., Tillmann, R., Lee, B., Lopez-Hilfiker, F., Andres, S., Acir, I. H., Rissanen, M., Jokinen, T., Schobesberger, S., Kangasluoma, J., Kontkanen, J., Nieminen, T., Kurten, T., Nielsen, L. B., Jorgensen, S., Kjaergaard, H. G., Canagaratna, M., Maso, M. D., Berndt, T., Petaja, T., Wahner, A., Kerminen, V. M., Kulmala, M., Worsnop, D. R., Wildt, J., and Mentel, T. F. (2014), A large source of low-volatility secondary organic aerosol, *Nature*, 506(7489), 476-479, doi:10.1038/nature13032.

Eidels-Dubovoi, S. (2002), Aerosol impacts on visible light extinction in the atmosphere of Mexico City, *Science of The Total Environment*, 287(3), 213-220, doi:[https://doi.org/10.1016/S0048-9697\(01\)00983-4](https://doi.org/10.1016/S0048-9697(01)00983-4).

Fadnavis, S., Mahajan, A. S., Choudhury, A. D., Roy, C., Singh, M., Biswas, M. S., Pandithurai, G., Prabhakaran, T., Lal, S., Venkatraman, C., Ganguly, D., Sinha, V., and Sarin, M. M. (2020), Atmospheric Aerosols and Trace Gases, in *Assessment of Climate Change over the Indian Region: A Report of the Ministry of Earth Sciences (MoES), Government of India*, edited by R. Krishnan, J. Sanjay, C. Gnanaseelan, M. Mujumdar, A. Kulkarni and S. Chakraborty, pp. 93-116, Springer Singapore, Singapore, doi:10.1007/978-981-15-4327-2_5.

Finlayson-Pitts, B. J., and Pitts, J. N. (2000), Preface, in *Chemistry of the Upper and Lower Atmosphere*, edited by B. J. Finlayson-Pitts and J. N. Pitts, pp. xvii-xviii, Academic Press, San Diego, doi:<https://doi.org/10.1016/B978-012257060-5/50000-9>.

Fowler, D., Brimblecombe, P., Burrows, J., Heal, M. R., Grennfelt, P., Stevenson, D. S., Jowett, A., Nemitz, E., Coyle, M., Liu, X., Chang, Y., Fuller, G. W., Sutton, M. A., Klimont, Z., Unsworth, M. H., and Vieno, M. (2020), A chronology of global air quality, *Philosophical Transactions of the Royal Society A: Mathematical, Physical and Engineering Sciences*, 378(2183), 20190314, doi:doi:10.1098/rsta.2019.0314.

Gentner, D. R., Jathar, S. H., Gordon, T. D., Bahreini, R., Day, D. A., El Haddad, I., Hayes, P. L., Pieber, S. M., Platt, S. M., de Gouw, J., Goldstein, A. H., Harley, R. A., Jimenez, J. L., Prévôt, A. S. H., and Robinson, A. L. (2017), Review of Urban Secondary Organic Aerosol Formation from Gasoline and Diesel Motor Vehicle Emissions, *Environmental science & technology*, 51(3), 1074-1093, doi:10.1021/acs.est.6b04509.

George, C., Ammann, M., D'Anna, B., Donaldson, D. J., and Nizkorodov, S. A. (2015), Heterogeneous photochemistry in the atmosphere, *Chemical reviews*, 115(10), 4218-4258, doi:10.1021/cr500648z.

Goldstein, A. H., and Galbally, I. E. (2007), Known and unknown organic constituents in the Earth's atmosphere, *Environmental science & technology*, 41(5), 1514-1521, doi:10.1021/es072476p.

Gordon, H., Kirkby, J., Baltensperger, U., Bianchi, F., Breitenlechner, M., Curtius, J., Dias, A., Dommen, J., Donahue, N. M., Dunne, E. M., Duplissy, J., Ehrhart, S., Flagan, R. C., Frege, C., Fuchs, C., Hansel, A., Hoyle, C. R., Kulmala, M., Kürten, A., Lehtipalo, K., Makhmutov, V., Molteni, U., Rissanen, M. P., Stozkhov, Y., Tröstl, J., Tsagkogeorgas, G., Wagner, R., Williamson, C., Wimmer, D., Winkler, P. M., Yan, C., and Carslaw, K. S. (2017), Causes and importance of new particle formation in the present-day and preindustrial atmospheres,

Chapter I: Introduction

- Journal of Geophysical Research: Atmospheres*, 122(16), 8739-8760, doi:10.1002/2017jd026844.
- Guenther, A. B., Jiang, X., Heald, C. L., Sakulyanontvittaya, T., Duhl, T., Emmons, L. K., and Wang, X. (2012), The Model of Emissions of Gases and Aerosols from Nature version 2.1 (MEGAN2.1): an extended and updated framework for modeling biogenic emissions, *Geosci. Model Dev.*, 5(6), 1471-1492, doi:10.5194/gmd-5-1471-2012.
- Hakola, H., Hellén, H., Hemmilä, M., Rinne, J., and Kulmala, M. (2012), In situ measurements of volatile organic compounds in a boreal forest, *Atmospheric Chemistry and Physics*, 12(23), 11665-11678, doi:10.5194/acp-12-11665-2012.
- Hallquist, M., Wenger, J. C., Baltensperger, U., Rudich, Y., Simpson, D., Claeys, M., Dommen, J., Donahue, N. M., George, C., Goldstein, A. H., Hamilton, J. F., Herrmann, H., Hoffmann, T., Inuma, Y., Jang, M., Jenkin, M. E., Jimenez, J. L., Kiendler-Scharr, A., Maenhaut, W., McFiggans, G., Mentel, T. F., Monod, A., Prévôt, A. S. H., Seinfeld, J. H., Surratt, J. D., Szmigielski, R., and Wildt, J. (2009), The formation, properties and impact of secondary organic aerosol: current and emerging issues, *Atmospheric Chemistry and Physics*, 9(14), 5155-5236, doi:10.5194/acp-9-5155-2009.
- He, X. C., Tham, Y. J., Dada, L., Wang, M., Finkenzeller, H., Stolzenburg, D., Iyer, S., Simon, M., Kurten, A., Shen, J., Rorup, B., Rissanen, M., Schobesberger, S., Baalbaki, R., Wang, D. S., Koenig, T. K., Jokinen, T., Sarnela, N., Beck, L. J., Almeida, J., Amanatidis, S., Amorim, A., Ataei, F., Baccarini, A., Bertozi, B., Bianchi, F., Brilke, S., Caudillo, L., Chen, D., Chiu, R., Chu, B., Dias, A., Ding, A., Dommen, J., Duplissy, J., El Haddad, I., Gonzalez Carracedo, L., Granzin, M., Hansel, A., Heinritzi, M., Hofbauer, V., Junninen, H., Kangasluoma, J., Kemppainen, D., Kim, C., Kong, W., Krechmer, J. E., Kvashin, A., Laitinen, T., Lamkaddam, H., Lee, C. P., Lehtipalo, K., Leiminger, M., Li, Z., Makhmutov, V., Manninen, H. E., Marie, G., Marten, R., Mathot, S., Mauldin, R. L., Mentler, B., Mohler, O., Muller, T., Nie, W., Onnela, A., Petaja, T., Pfeifer, J., Philippov, M., Ranjithkumar, A., Saiz-Lopez, A., Salma, I., Scholz, W., Schuchmann, S., Schulze, B., Steiner, G., Stozhkov, Y., Tauber, C., Tome, A., Thakur, R. C., Vaisanen, O., Vazquez-Pufleau, M., Wagner, A. C., Wang, Y., Weber, S. K., Winkler, P. M., Wu, Y., Xiao, M., Yan, C., Ye, Q., Ylisirnio, A., Zauner-Wieczorek, M., Zha, Q., Zhou, P., Flagan, R. C., Curtius, J., Baltensperger, U., Kulmala, M., Kerminen, V. M., Kurten, T., Donahue, N. M., Volkamer, R., Kirkby, J., Worsnop, D. R., and Sipila, M. (2021), Role of iodine oxoacids in atmospheric aerosol nucleation, *Science*, 371(6529), 589-595, doi:10.1126/science.abe0298.
- Heinritzi, M., Dada, L., Simon, M., Stolzenburg, D., Wagner, A. C., Fischer, L., Ahonen, L. R., Amanatidis, S., Baalbaki, R., Baccarini, A., Bauer, P. S., Baumgartner, B., Bianchi, F., Brilke, S., Chen, D., Chiu, R., Dias, A., Dommen, J., Duplissy, J., Finkenzeller, H., Frege, C., Fuchs, C., Garmash, O., Gordon, H., Granzin, M., El Haddad, I., He, X., Helm, J., Hofbauer, V., Hoyle, C. R., Kangasluoma, J., Keber, T., Kim, C., Kürten, A., Lamkaddam, H., Laurila, T. M., Lampilahti, J., Lee, C. P., Lehtipalo, K., Leiminger, M., Mai, H., Makhmutov, V., Manninen, H. E., Marten, R., Mathot, S., Mauldin, R. L., Mentler, B., Molteni, U., Müller, T., Nie, W., Nieminen, T., Onnela, A., Partoll, E., Passananti, M., Petäjä, T., Pfeifer, J., Pospisilova, V., Quéléver, L. L. J., Rissanen, M. P., Rose, C., Schobesberger, S., Scholz, W., Scholze, K., Sipilä, M., Steiner, G., Stozhkov, Y., Tauber, C., Tham, Y. J., Vazquez-Pufleau, M., Virtanen, A., Vogel, A. L., Volkamer, R., Wagner, R., Wang, M., Weitz, L., Wimmer, D., Xiao, M., Yan, C., Ye, P., Zha, Q., Zhou, X.,

Chapter I: Introduction

- Amorim, A., Baltensperger, U., Hansel, A., Kulmala, M., Tomé, A., Winkler, P. M., Worsnop, D. R., Donahue, N. M., Kirkby, J., and Curtius, J. (2020), Molecular understanding of the suppression of new-particle formation by isoprene, *Atmospheric Chemistry and Physics*, 20(20), 11809-11821, doi:10.5194/acp-20-11809-2020.
- Huey, L. G. (2007), Measurement of trace atmospheric species by chemical ionization mass spectrometry: Speciation of reactive nitrogen and future directions, *Mass spectrometry reviews*, 26(2), 166-184, doi:<https://doi.org/10.1002/mas.20118>.
- IPCC (2013), Climate Change 2013: The Physical Science Basis. *Rep.*
- IPCC (2022), Climate Change 2022: Impacts, Adaptation and Vulnerability Working Group II Contribution to the Sixth Assessment Report of the Intergovernmental Panel on Climate Change *Rep.*
- Isaksen, I. S. A., and Dalsøren, S. B. (2011), Getting a Better Estimate of an Atmospheric Radical, *Science*, 331(6013), 38-39, doi:[doi:10.1126/science.1199773](https://doi.org/10.1126/science.1199773).
- Jimenez, J. L., Canagaratna, M. R., Donahue, N. M., Prevot, A. S. H., Zhang, Q., Kroll, J. H., DeCarlo, P. F., Allan, J. D., Coe, H., Ng, N. L., Aiken, A. C., Docherty, K. S., Ulbrich, I. M., Grieshop, A. P., Robinson, A. L., Duplissy, J., Smith, J. D., Wilson, K. R., Lanz, V. A., Hueglin, C., Sun, Y. L., Tian, J., Laaksonen, A., Raatikainen, T., Rautiainen, J., Vaattovaara, P., Ehn, M., Kulmala, M., Tomlinson, J. M., Collins, D. R., Cubison, M. J., Dunlea, J., Huffman, J. A., Onasch, T. B., Alfarra, M. R., Williams, P. I., Bower, K., Kondo, Y., Schneider, J., Drewnick, F., Borrmann, S., Weimer, S., Demerjian, K., Salcedo, D., Cottrell, L., Griffin, R., Takami, A., Miyoshi, T., Hatakeyama, S., Shimono, A., Sun, J. Y., Zhang, Y. M., Dzepina, K., Kimmel, J. R., Sueper, D., Jayne, J. T., Herndon, S. C., Trimborn, A. M., Williams, L. R., Wood, E. C., Middlebrook, A. M., Kolb, C. E., Baltensperger, U., and Worsnop, D. R. (2009), Evolution of Organic Aerosols in the Atmosphere, *Science*, 326(5959), 1525-1529, doi:[doi:10.1126/science.1180353](https://doi.org/10.1126/science.1180353).
- Jokinen, T., Berndt, T., Makkonen, R., Kerminen, V. M., Junninen, H., Paasonen, P., Stratmann, F., Herrmann, H., Guenther, A. B., Worsnop, D. R., Kulmala, M., Ehn, M., and Sipila, M. (2015), Production of extremely low volatile organic compounds from biogenic emissions: Measured yields and atmospheric implications, *Proceedings of the National Academy of Sciences of the United States of America*, 112(23), 7123-7128, doi:[10.1073/pnas.1423977112](https://doi.org/10.1073/pnas.1423977112).
- Jokinen, T., Sipilä, M., Richters, S., Kerminen, V.-M., Paasonen, P., Stratmann, F., Worsnop, D., Kulmala, M., Ehn, M., Herrmann, H., and Berndt, T. (2014), Rapid Autoxidation Forms Highly Oxidized RO₂ Radicals in the Atmosphere, *Angewandte Chemie International Edition*, 53(52), 14596-14600, doi:<https://doi.org/10.1002/anie.201408566>.
- Kürten, A., Bergen, A., Heinritzi, M., Leiminger, M., Lorenz, V., Piel, F., Simon, M., Sitals, R., Wagner, A. C., and Curtius, J. (2016), Observation of new particle formation and measurement of sulfuric acid, ammonia, amines and highly oxidized organic molecules at a rural site in central Germany, *Atmospheric Chemistry and Physics*, 16(19), 12793-12813, doi:10.5194/acp-16-12793-2016.
- Kerminen, V.-M., Chen, X., Vakkari, V., Petäjä, T., Kulmala, M., and Bianchi, F. (2018), Atmospheric new particle formation and growth: review of field observations, *Environmental Research Letters*, 13(10), 103003, doi:10.1088/1748-9326/aadf3c.

Chapter I: Introduction

- Kerminen, V.-M., Lehtinen, K. E. J., Anttila, T., and Kulmala, M. (2004), Dynamics of atmospheric nucleation mode particles: a timescale analysis, *Tellus B: Chemical and Physical Meteorology*, 56(2), 135-146, doi:10.3402/tellusb.v56i2.16411.
- Kerminen, V. M., Paramonov, M., Anttila, T., Riipinen, I., Fountoukis, C., Korhonen, H., Asmi, E., Laakso, L., Lihavainen, H., Swietlicki, E., Svenningsson, B., Asmi, A., Pandis, S. N., Kulmala, M., and Petäjä, T. (2012), Cloud condensation nuclei production associated with atmospheric nucleation: a synthesis based on existing literature and new results, *Atmospheric Chemistry and Physics*, 12(24), 12037-12059, doi:10.5194/acp-12-12037-2012.
- Kirkby, J. (2007), Cosmic Rays and Climate, *Surveys in Geophysics*, 28(5), 333-375, doi:10.1007/s10712-008-9030-6.
- Kirkby, J., Curtius, J., Almeida, J., Dunne, E., Duplissy, J., Ehrhart, S., Franchin, A., Gagné, S., Ickes, L., Kürten, A., Kupc, A., Metzger, A., Riccobono, F., Rondo, L., Schobesberger, S., Tsagkogeorgas, G., Wimmer, D., Amorim, A., Bianchi, F., Breitenlechner, M., David, A., Dommen, J., Downard, A., Ehn, M., Flagan, R. C., Haider, S., Hansel, A., Hauser, D., Jud, W., Junninen, H., Kreissl, F., Kvashin, A., Laaksonen, A., Lehtipalo, K., Lima, J., Lovejoy, E. R., Makhmutov, V., Mathot, S., Mikkilä, J., Minginette, P., Mogo, S., Nieminen, T., Onnela, A., Pereira, P., Petäjä, T., Schnitzhofer, R., Seinfeld, J. H., Sipilä, M., Stozhkov, Y., Stratmann, F., Tomé, A., Vanhanen, J., Viisanen, Y., Vrtala, A., Wagner, P. E., Walther, H., Weingartner, E., Wex, H., Winkler, P. M., Carslaw, K. S., Worsnop, D. R., Baltensperger, U., and Kulmala, M. (2011), Role of sulphuric acid, ammonia and galactic cosmic rays in atmospheric aerosol nucleation, *Nature*, 476(7361), 429-433, doi:10.1038/nature10343.
- Kirkby, J., Duplissy, J., Sengupta, K., Frege, C., Gordon, H., Williamson, C., Heinritzi, M., Simon, M., Yan, C., Almeida, J., Tröstl, J., Nieminen, T., Ortega, I. K., Wagner, R., Adamov, A., Amorim, A., Bernhammer, A.-K., Bianchi, F., Breitenlechner, M., Brilke, S., Chen, X., Craven, J., Dias, A., Ehrhart, S., Flagan, R. C., Franchin, A., Fuchs, C., Guida, R., Hakala, J., Hoyle, C. R., Jokinen, T., Junninen, H., Kangasluoma, J., Kim, J., Krapf, M., Kürten, A., Laaksonen, A., Lehtipalo, K., Makhmutov, V., Mathot, S., Molteni, U., Onnela, A., Peräkylä, O., Piel, F., Petäjä, T., Praplan, A. P., Pringle, K., Rap, A., Richards, N. A. D., Riipinen, I., Rissanen, M. P., Rondo, L., Sarnela, N., Schobesberger, S., Scott, C. E., Seinfeld, J. H., Sipilä, M., Steiner, G., Stozhkov, Y., Stratmann, F., Tomé, A., Virtanen, A., Vogel, A. L., Wagner, A. C., Wagner, P. E., Weingartner, E., Wimmer, D., Winkler, P. M., Ye, P., Zhang, X., Hansel, A., Dommen, J., Donahue, N. M., Worsnop, D. R., Baltensperger, U., Kulmala, M., Carslaw, K. S., and Curtius, J. (2016), Ion-induced nucleation of pure biogenic particles, *Nature*, 533, 521, doi:10.1038/nature17953.
- Kroll, J. H., and Seinfeld, J. H. (2008), Chemistry of secondary organic aerosol: Formation and evolution of low-volatility organics in the atmosphere, *Atmospheric Environment*, 42(16), 3593-3624, doi:10.1016/j.atmosenv.2008.01.003.
- Kulmala, M., Kontkanen, J., Junninen, H., Lehtipalo, K., Manninen, H. E., Nieminen, T., Petäjä, T., Sipilä, M., Schobesberger, S., Rantala, P., Franchin, A., Jokinen, T., Järvinen, E., Äijälä, M., Kangasluoma, J., Hakala, J., Aalto, P. P., Paasonen, P., Mikkilä, J., Vanhanen, J., Aalto, J., Hakola, H., Makkonen, U., Ruuskanen, T., Mauldin, R. L., Duplissy, J., Vehkamäki, H., Bäck, J., Kortelainen, A., Riipinen, I., Kurtén, T., Johnston, M. V., Smith, J. N., Ehn, M., Mentel, T. F., Lehtinen, K. E. J., Laaksonen, A., Kerminen, V.-M., and Worsnop, D. R.

- (2013), Direct Observations of Atmospheric Aerosol Nucleation, *Science*, 339(6122), 943-946, doi:doi:10.1126/science.1227385.
- Kulmala, M., Toivonen, A., Mäkelä, J. M., and Laaksonen, A. (1998), Analysis of the growth of nucleation mode particles observed in Boreal forest, *Tellus B: Chemical and Physical Meteorology*, 50(5), 449-462, doi:10.3402/tellusb.v50i5.16229.
- Kurtenbach, R., Ackermann, R., Becker, K. H., Geyer, A., Gomes, J. A. G., Lörzer, J. C., Platt, U., and Wiesen, P. (2002), Verification of the Contribution of Vehicular Traffic to the Total NMVOC Emissions in Germany and the Importance of the NO₃ Chemistry in the City Air, *Journal of Atmospheric Chemistry*, 42(1), 395-411, doi:10.1023/A:1015778616796.
- Kwon, H.-S., Ryu, M. H., and Carlsten, C. (2020), Ultrafine particles: unique physicochemical properties relevant to health and disease, *Experimental & Molecular Medicine*, 52(3), 318-328, doi:10.1038/s12276-020-0405-1.
- Lamarque, J. F., Bond, T. C., Eyring, V., Granier, C., Heil, A., Klimont, Z., Lee, D., Liousse, C., Mieville, A., Owen, B., Schultz, M. G., Shindell, D., Smith, S. J., Stehfest, E., Van Aardenne, J., Cooper, O. R., Kainuma, M., Mahowald, N., McConnell, J. R., Naik, V., Riahi, K., and van Vuuren, D. P. (2010), Historical (1850–2000) gridded anthropogenic and biomass burning emissions of reactive gases and aerosols: methodology and application, *Atmospheric Chemistry and Physics*, 10(15), 7017-7039, doi:10.5194/acp-10-7017-2010.
- Laskin, J., Laskin, A., and Nizkorodov, S. A. (2018), Mass Spectrometry Analysis in Atmospheric Chemistry, *Analytical chemistry*, 90(1), 166-189, doi:10.1021/acs.analchem.7b04249.
- Lee, B. H., Mohr, C., Lopez-Hilfiker, F. D., Lutz, A., Hallquist, M., Lee, L., Romer, P., Cohen, R. C., Iyer, S., Kurtén, T., Hu, W., Day, D. A., Campuzano-Jost, P., Jimenez, J. L., Xu, L., Ng, N. L., Guo, H., Weber, R. J., Wild, R. J., Brown, S. S., Koss, A., de Gouw, J., Olson, K., Goldstein, A. H., Seco, R., Kim, S., McAvey, K., Shepson, P. B., Starn, T., Baumann, K., Edgerton, E. S., Liu, J., Shilling, J. E., Miller, D. O., Brune, W., Schobesberger, S., D'Ambro, E. L., and Thornton, J. A. (2016), Highly functionalized organic nitrates in the southeast United States: Contribution to secondary organic aerosol and reactive nitrogen budgets, *Proceedings of the National Academy of Sciences*, 113(6), 1516-1521, doi:10.1073/pnas.1508108113.
- Lee, C. P., Riva, M., Wang, D., Tomaz, S., Li, D., Perrier, S., Slowik, J. G., Bourgain, F., Schmale, J., Prevot, A. S. H., Baltensperger, U., George, C., and El Haddad, I. (2020), Online Aerosol Chemical Characterization by Extractive Electrospray Ionization-Ultrahigh-Resolution Mass Spectrometry (EESI-Orbitrap), *Environmental science & technology*, 54(7), 3871-3880, doi:10.1021/acs.est.9b07090.
- Lelieveld, J., Evans, J. S., Fnais, M., Giannadaki, D., and Pozzer, A. (2015), The contribution of outdoor air pollution sources to premature mortality on a global scale, *Nature*, 525(7569), 367-371, doi:10.1038/nature15371.
- Lelieveld, J., Gromov, S., Pozzer, A., and Taraborrelli, D. (2016), Global tropospheric hydroxyl distribution, budget and reactivity, *Atmospheric Chemistry and Physics*, 16(19), 12477-12493, doi:10.5194/acp-16-12477-2016.
- Li, J., Hao, Y., Simayi, M., Shi, Y., Xi, Z., and Xie, S. (2019), Verification of anthropogenic VOC emission inventory through ambient measurements and satellite retrievals, *Atmospheric Chemistry and Physics*, 19(9), 5905-5921, doi:10.5194/acp-19-5905-2019.

Chapter I: Introduction

- Li, Y., Pöschl, U., and Shiraiwa, M. (2016), Molecular corridors and parameterizations of volatility in the chemical evolution of organic aerosols, *Atmospheric Chemistry and Physics*, 16(5), 3327-3344, doi:10.5194/acp-16-3327-2016.
- Liebmann, J., Sobanski, N., Schuladen, J., Karu, E., Hellén, H., Hakola, H., Zha, Q., Ehn, M., Riva, M., Heikkinen, L., Williams, J., Fischer, H., Lelieveld, J., and Crowley, J. N. (2019), Alkyl nitrates in the boreal forest: formation via the NO_3^- , OH^- and O_3 -induced oxidation of biogenic volatile organic compounds and ambient lifetimes, *Atmospheric Chemistry and Physics*, 19(15), 10391-10403, doi:10.5194/acp-19-10391-2019.
- Lim, Y. B., and Ziemann, P. J. (2005), Products and Mechanism of Secondary Organic Aerosol Formation from Reactions of n-Alkanes with OH Radicals in the Presence of NO_x , *Environmental science & technology*, 39(23), 9229-9236, doi:10.1021/es051447g.
- Lovejoy, E. R., Curtius, J., and Froyd, K. D. (2004), Atmospheric ion-induced nucleation of sulfuric acid and water, *Journal of Geophysical Research: Atmospheres*, 109(D8), doi:<https://doi.org/10.1029/2003JD004460>.
- Müller, J. F., Stavrakou, T., Wallens, S., De Smedt, I., Van Roozendael, M., Potosnak, M. J., Rinne, J., Munger, B., Goldstein, A., and Guenther, A. B. (2008), Global isoprene emissions estimated using MEGAN, ECMWF analyses and a detailed canopy environment model, *Atmospheric Chemistry and Physics*, 8(5), 1329-1341, doi:10.5194/acp-8-1329-2008.
- McFiggans, G., Mentel, T. F., Wildt, J., Pullinen, I., Kang, S., Kleist, E., Schmitt, S., Springer, M., Tillmann, R., Wu, C., Zhao, D., Hallquist, M., Faxon, C., Le Breton, M., Hallquist, A. M., Simpson, D., Bergstrom, R., Jenkin, M. E., Ehn, M., Thornton, J. A., Alfarra, M. R., Bannan, T. J., Percival, C. J., Priestley, M., Topping, D., and Kiendler-Scharr, A. (2019), Secondary organic aerosol reduced by mixture of atmospheric vapours, *Nature*, 565(7741), 587-593, doi:10.1038/s41586-018-0871-y.
- Merikanto, J., Spracklen, D. V., Mann, G. W., Pickering, S. J., and Carslaw, K. S. (2009), Impact of nucleation on global CCN, *Atmospheric Chemistry and Physics*, 9(21), 8601-8616, doi:10.5194/acp-9-8601-2009.
- Molteni, U., Bianchi, F., Klein, F., El Haddad, I., Frege, C., Rossi, M. J., Dommen, J., and Baltensperger, U. (2018), Formation of highly oxygenated organic molecules from aromatic compounds, *Atmospheric Chemistry and Physics*, 18(3), 1909-1921, doi:10.5194/acp-18-1909-2018.
- Ng, N. L., Kroll, J. H., Chan, A. W. H., Chhabra, P. S., Flagan, R. C., and Seinfeld, J. H. (2007), Secondary organic aerosol formation from m-xylene, toluene, and benzene, *Atmospheric Chemistry and Physics*, 7(14), 3909-3922, doi:10.5194/acp-7-3909-2007.
- Pöschl, U. (2005), Atmospheric Aerosols: Composition, Transformation, Climate and Health Effects, *Angewandte Chemie International Edition*, 44(46), 7520-7540, doi:<https://doi.org/10.1002/anie.200501122>.
- Pankow, J. F. (1994), An absorption model of the gas/aerosol partitioning involved in the formation of secondary organic aerosol, *Atmospheric Environment*, 28(2), 189-193, doi:[https://doi.org/10.1016/1352-2310\(94\)90094-9](https://doi.org/10.1016/1352-2310(94)90094-9).
- Riccobono, F., Schobesberger, S., Scott, C. E., Dommen, J., Ortega, I. K., Rondo, L., Almeida, J., Amorim, A., Bianchi, F., Breitenlechner, M., David, A., Downard, A., Dunne, E. M., Duplissy, J., Ehrhart, S., Flagan, R. C., Franchin, A., Hansel, A., Junninen, H., Kajos, M., Keskinen, H., Kupc, A., Kürten, A., Kvashin, A. N., Laaksonen, A., Lehtipalo, K., Makhmutov, V., Mathot, S., Nieminen, T., Onnela, A., Petäjä, T., Praplan, A. P., Santos, F.

Chapter I: Introduction

- D., Schallhart, S., Seinfeld, J. H., Sipilä, M., Spracklen, D. V., Stozhkov, Y., Stratmann, F., Tomé, A., Tsagkogeorgas, G., Vaattovaara, P., Viisanen, Y., Vrtala, A., Wagner, P. E., Weingartner, E., Wex, H., Wimmer, D., Carslaw, K. S., Curtius, J., Donahue, N. M., Kirkby, J., Kulmala, M., Worsnop, D. R., and Baltensperger, U. (2014), Oxidation Products of Biogenic Emissions Contribute to Nucleation of Atmospheric Particles, *Science*, 344(6185), 717-721, doi:10.1126/science.1243527.
- Riipinen, I., Pierce, J. R., Yli-Juuti, T., Nieminen, T., Häkkinen, S., Ehn, M., Junninen, H., Lehtipalo, K., Petäjä, T., Slowik, J., Chang, R., Shantz, N. C., Abbatt, J., Leaitch, W. R., Kerminen, V. M., Worsnop, D. R., Pandis, S. N., Donahue, N. M., and Kulmala, M. (2011), Organic condensation: a vital link connecting aerosol formation to cloud condensation nuclei (CCN) concentrations, *Atmospheric Chemistry and Physics*, 11(8), 3865-3878, doi:10.5194/acp-11-3865-2011.
- Rissanen, M. (2021), Anthropogenic Volatile Organic Compound (AVOC) Autoxidation as a Source of Highly Oxygenated Organic Molecules (HOM), *The Journal of Physical Chemistry A*, 125(41), 9027-9039, doi:10.1021/acs.jpca.1c06465.
- Riva, M., Brüggemann, M., Li, D., Perrier, S., George, C., Herrmann, H., and Berndt, T. (2020), Capability of CI-Orbitrap for Gas-Phase Analysis in Atmospheric Chemistry: A Comparison with the CI-APi-TOF Technique, *Analytical chemistry*, 92(12), 8142-8150, doi:10.1021/acs.analchem.0c00111.
- Riva, M., Ehn, M., Li, D., Tomaz, S., Bourgain, F., Perrier, S., and George, C. (2019a), CI-Orbitrap: An Analytical Instrument To Study Atmospheric Reactive Organic Species, *Analytical chemistry*, 91(15), 9419-9423, doi:10.1021/acs.analchem.9b02093.
- Riva, M., Rantala, P., Krechmer, J. E., Peräkylä, O., Zhang, Y., Heikkilä, L., Garmash, O., Yan, C., Kulmala, M., Worsnop, D., and Ehn, M. (2019b), Evaluating the performance of five different chemical ionization techniques for detecting gaseous oxygenated organic species, *Atmospheric Measurement Techniques*, 12(4), 2403-2421, doi:10.5194/amt-12-2403-2019.
- Rostami, A. A. (2009), Computational Modeling of Aerosol Deposition in Respiratory Tract: A Review, *Inhalation Toxicology*, 21(4), 262-290, doi:10.1080/08958370802448987.
- Seinfeld, J. H., and Pandis, S. N. (2016), *Atmospheric Chemistry and Physics: From Air Pollution to Climate Change, 3rd Edition*.
- Seinfeld, J. H., and Pankow, J. F. (2003), Organic Atmospheric Particulate Material, *Annual Review of Physical Chemistry*, 54(1), 121-140, doi:10.1146/annurev.physchem.54.011002.103756.
- Shrivastava, M., Cappa, C. D., Fan, J., Goldstein, A. H., Guenther, A. B., Jimenez, J. L., Kuang, C., Laskin, A., Martin, S. T., Ng, N. L., Petaja, T., Pierce, J. R., Rasch, P. J., Roldin, P., Seinfeld, J. H., Shilling, J., Smith, J. N., Thornton, J. A., Volkamer, R., Wang, J., Worsnop, D. R., Zaveri, R. A., Zelenyuk, A., and Zhang, Q. (2017), Recent advances in understanding secondary organic aerosol: Implications for global climate forcing, *Reviews of Geophysics*, 55(2), 509-559, doi:<https://doi.org/10.1002/2016RG000540>.
- Sipilä, M., Berndt, T., Petäjä, T., Brus, D., Vanhanen, J., Stratmann, F., Patokoski, J., Mauldin, R. L., Hyvärinen, A.-P., Lihavainen, H., and Kulmala, M. (2010), The Role of Sulfuric Acid in Atmospheric Nucleation, *Science*, 327(5970), 1243-1246, doi:doi:10.1126/science.1180315.
- Sipilä, M., Sarnela, N., Jokinen, T., Henschel, H., Junninen, H., Kontkanen, J., Richters, S., Kangasluoma, J., Franchin, A., Peräkylä, O., Rissanen, M. P., Ehn, M., Vehkamäki, H.,

Chapter I: Introduction

- Kurten, T., Berndt, T., Petäjä, T., Worsnop, D., Ceburnis, D., Kerminen, V.-M., Kulmala, M., and O'Dowd, C. (2016), Molecular-scale evidence of aerosol particle formation via sequential addition of HIO_3 , *Nature*, 537(7621), 532-534, doi:10.1038/nature19314.
- Smith, J. N., Dunn, M. J., VanReken, T. M., Iida, K., Stolzenburg, M. R., McMurry, P. H., and Huey, L. G. (2008), Chemical composition of atmospheric nanoparticles formed from nucleation in Tecamac, Mexico: Evidence for an important role for organic species in nanoparticle growth, *Geophysical Research Letters*, 35(4), doi:<https://doi.org/10.1029/2007GL032523>.
- Trostl, J., Chuang, W. K., Gordon, H., Heinritzi, M., Yan, C., Molteni, U., Ahlm, L., Frege, C., Bianchi, F., Wagner, R., Simon, M., Lehtipalo, K., Williamson, C., Craven, J. S., Duplissy, J., Adamov, A., Almeida, J., Bernhammer, A. K., Breitenlechner, M., Brilke, S., Dias, A., Ehrhart, S., Flagan, R. C., Franchin, A., Fuchs, C., Guida, R., Gysel, M., Hansel, A., Hoyle, C. R., Jokinen, T., Junninen, H., Kangasluoma, J., Keskinen, H., Kim, J., Krapf, M., Kurten, A., Laaksonen, A., Lawler, M., Leiminger, M., Mathot, S., Mohler, O., Nieminen, T., Onnela, A., Petaja, T., Piel, F. M., Miettinen, P., Rissanen, M. P., Rondo, L., Sarnela, N., Schobesberger, S., Sengupta, K., Sipila, M., Smith, J. N., Steiner, G., Tome, A., Virtanen, A., Wagner, A. C., Weingartner, E., Wimmer, D., Winkler, P. M., Ye, P., Carslaw, K. S., Curtius, J., Dommen, J., Kirkby, J., Kulmala, M., Riipinen, I., Worsnop, D. R., Donahue, N. M., and Baltensperger, U. (2016), The role of low-volatility organic compounds in initial particle growth in the atmosphere, *Nature*, 533(7604), 527-531, doi:10.1038/nature18271.
- Tsigaridis, K., Daskalakis, N., Kanakidou, M., Adams, P. J., Artaxo, P., Bahadur, R., Balkanski, Y., Bauer, S. E., Bellouin, N., Benedetti, A., Bergman, T., Berntsen, T. K., Beukes, J. P., Bian, H., Carslaw, K. S., Chin, M., Curci, G., Diehl, T., Easter, R. C., Ghan, S. J., Gong, S. L., Hodzic, A., Hoyle, C. R., Iversen, T., Jathar, S., Jimenez, J. L., Kaiser, J. W., Kirkevåg, A., Koch, D., Kokkola, H., Lee, Y. H., Lin, G., Liu, X., Luo, G., Ma, X., Mann, G. W., Mihalopoulos, N., Morcrette, J. J., Müller, J. F., Myhre, G., Myriokefalitakis, S., Ng, N. L., O'Donnell, D., Penner, J. E., Pozzoli, L., Pringle, K. J., Russell, L. M., Schulz, M., Sciare, J., Seland, Ø., Shindell, D. T., Sillman, S., Skeie, R. B., Spracklen, D., Stavrakou, T., Steenrod, S. D., Takemura, T., Tiitta, P., Tilmes, S., Tost, H., van Noije, T., van Zyl, P. G., von Salzen, K., Yu, F., Wang, Z., Wang, Z., Zaveri, R. A., Zhang, H., Zhang, K., Zhang, Q., and Zhang, X. (2014), The AeroCom evaluation and intercomparison of organic aerosol in global models, *Atmospheric Chemistry and Physics*, 14(19), 10845-10895, doi:10.5194/acp-14-10845-2014.
- Tunved, P., Hansson, H.-C., Kerminen, V.-M., Ström, J., Maso, M. D., Lihavainen, H., Viisanen, Y., Aalto, P. P., Komppula, M., and Kulmala, M. (2006), High Natural Aerosol Loading over Boreal Forests, *Science*, 312(5771), 261-263, doi:doi:10.1126/science.1123052.
- Twomey, S. (1977), The Influence of Pollution on the Shortwave Albedo of Clouds, *Journal of Atmospheric Sciences*, 34(7), 1149-1152, doi:10.1175/1520-0469(1977)034<1149:tiopot>2.0.co;2.
- Vehkamaki, H., and Riipinen, I. (2012), Thermodynamics and kinetics of atmospheric aerosol particle formation and growth, *Chemical Society reviews*, 41(15), 5160-5173, doi:10.1039/c2cs00002d.
- Wang, M., Kong, W., Marten, R., He, X.-C., Chen, D., Pfeifer, J., Heitto, A., Kontkanen, J., Dada, L., Kürten, A., Yli-Juuti, T., Manninen, H. E., Amanatidis, S., Amorim, A., Baalbaki, R., Baccarini, A., Bell, D. M., Bertozzi, B., Bräkling, S., Brilke, S., Murillo, L. C., Chiu, R.,

Chapter I: Introduction

- Chu, B., De Menezes, L.-P., Duplissy, J., Finkenzeller, H., Carracedo, L. G., Granzin, M., Guida, R., Hansel, A., Hofbauer, V., Krechmer, J., Lehtipalo, K., Lamkaddam, H., Lampimäki, M., Lee, C. P., Makhmutov, V., Marie, G., Mathot, S., Mauldin, R. L., Mentler, B., Müller, T., Onnela, A., Partoll, E., Petäjä, T., Philippov, M., Pospisilova, V., Ranjithkumar, A., Rissanen, M., Rörup, B., Scholz, W., Shen, J., Simon, M., Sipilä, M., Steiner, G., Stolzenburg, D., Tham, Y. J., Tomé, A., Wagner, A. C., Wang, D. S., Wang, Y., Weber, S. K., Winkler, P. M., Wlasits, P. J., Wu, Y., Xiao, M., Ye, Q., Zauner-Wieczorek, M., Zhou, X., Volkamer, R., Riipinen, I., Dommen, J., Curtius, J., Baltensperger, U., Kulmala, M., Worsnop, D. R., Kirkby, J., Seinfeld, J. H., El-Haddad, I., Flagan, R. C., and Donahue, N. M. (2020), Rapid growth of new atmospheric particles by nitric acid and ammonia condensation, *Nature*, 581(7807), 184-189, doi:10.1038/s41586-020-2270-4.
- Wang, X. (2021), Impact of atmospheric photochemical reactions on air quality.
- Wang, Y., Clusius, P., Yan, C., Dallenbach, K., Yin, R., Wang, M., He, X. C., Chu, B., Lu, Y., Dada, L., Kangasluoma, J., Rantala, P., Deng, C., Lin, Z., Wang, W., Yao, L., Fan, X., Du, W., Cai, J., Heikkinen, L., Tham, Y. J., Zha, Q., Ling, Z., Junninen, H., Petaja, T., Ge, M., Wang, Y., He, H., Worsnop, D. R., Kerminen, V. M., Bianchi, F., Wang, L., Jiang, J., Liu, Y., Boy, M., Ehn, M., Donahue, N. M., and Kulmala, M. (2022b), Molecular Composition of Oxygenated Organic Molecules and Their Contributions to Organic Aerosol in Beijing, *Environmental science & technology*, 56(2), 770-778, doi:10.1021/acs.est.1c05191.
- Wennberg, P. O., Bates, K. H., Crounse, J. D., Dodson, L. G., McVay, R. C., Mertens, L. A., Nguyen, T. B., Praske, E., Schwantes, R. H., Smarte, M. D., St Clair, J. M., Teng, A. P., Zhang, X., and Seinfeld, J. H. (2018), Gas-Phase Reactions of Isoprene and Its Major Oxidation Products, *Chemical reviews*, 118(7), 3337-3390, doi:10.1021/acs.chemrev.7b00439.
- Wilczyńska-Michalik, W., Różańska, A., Bulanda, M., Chmielarczyk, A., Pietras, B., and Michalik, M. (2021), Physicochemical and microbiological characteristics of urban aerosols in Krakow (Poland) and their potential health impact, *Environmental Geochemistry and Health*, 43(11), 4601-4626, doi:10.1007/s10653-021-00950-x.
- Zhang, R. (2010), Getting to the Critical Nucleus of Aerosol Formation, *Science*, 328(5984), 1366-1367, doi:doi:10.1126/science.1189732.

Chapter II: Experimental methods

Chapter II: Experimental methods

II.0. Motivation

This chapter describes all the experimental setups, techniques, and data analysis methods used for the work performed within this thesis. The general setup and working principles behind the used methods and instruments will be presented here. Specific analytical methods and experimental details are discussed in the following chapters presenting the results. For Orbitrap mass spectrometry techniques applied in this work, some specific methods were developed and will be of particular interest here.

II.1. Experimental systems

II.1.1. Oxidation flow reactor (OFR) for radical chemistry

The oxidation flow reactor (OFR) is designed to study radical chemistry. As shown in Figure II-1, an 18-liter Pyrex glass tube (12 cm i.d. × 158 cm length) mounted with a fan and 7-UV lamps (Philips CLEO) was used to perform the experiments. Total flow in the OFR was maintained in the range of 15-16 standard liter per minute (slpm), giving an average residence time of 67-72 s. Ozone was generated by an ozone generator (Fisher Scientific, SOG-1) and continuously injected into the system. For the experiments conducted in the presence of nitrogen oxides (NO_x), nitric oxide (NO) was added into the system, ranging from 0 to 1.8 ppbv. Concentrations of limonene ranged from 0.4 to 2 ppmv and α -pinene from 1 to 4 ppmv. The initial O_3 concentration was set at 40 ppbv. For the nitrate radicals-derived experiments, an external 1-liter pre-reactor was designed to generate steady state concentrations of NO_3 radicals from the reaction of NO_2 with O_3 , which was dimmed to prevent the NO_3 photolysis by ambient lights. During the experiments, the total flow in pre-reactor was fixed at 1 slpm, giving a reaction time of 60 s. Concentration of NO_2 varied from 0 to 75 ppbv, while initial O_3 and α -pinene concentrations were fixed at 50 and 8 ppbv, respectively.

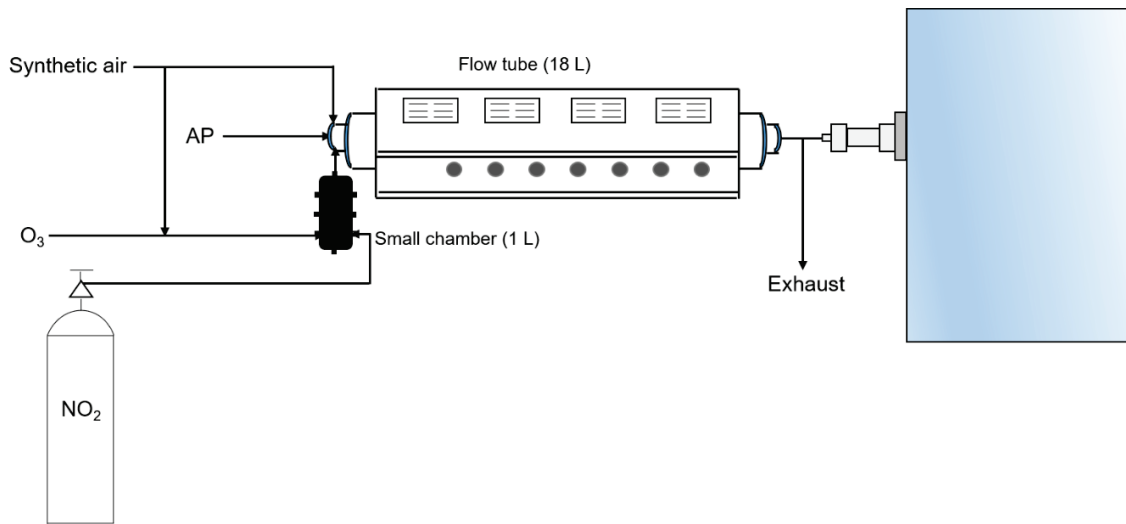


Figure II-1: Schematic of the oxidation flow reactor experiments.

II.1.2. CLOUD (Cosmics Leaving Outdoor Droplets) chamber for new particle formation

The Cosmics Leaving OUtdoor Droplets (CLOUD) chamber is a 26.1 m³ and 3-m-stainless steel vessel at CERN (European Organization for Nuclear Research), which is designed to study the formation and growth of aerosol particles from a wide variety of precursor vapors (Kirkby et al., 2011; Kirkby et al., 2016). CLOUD is the largest and most advanced laboratory experiment to study how ions produced by cosmic rays affect aerosol formation (Duplissy et al., 2010; Kirkby et al., 2011). It provides temperature-controlled over the entire range of atmosphere-relevant temperatures (208 to 373 K) with an accuracy of 0.01 K by circulating air in the space between the chamber and its insulation. A schematic drawing of the CLOUD chamber is shown in Figure II-2.

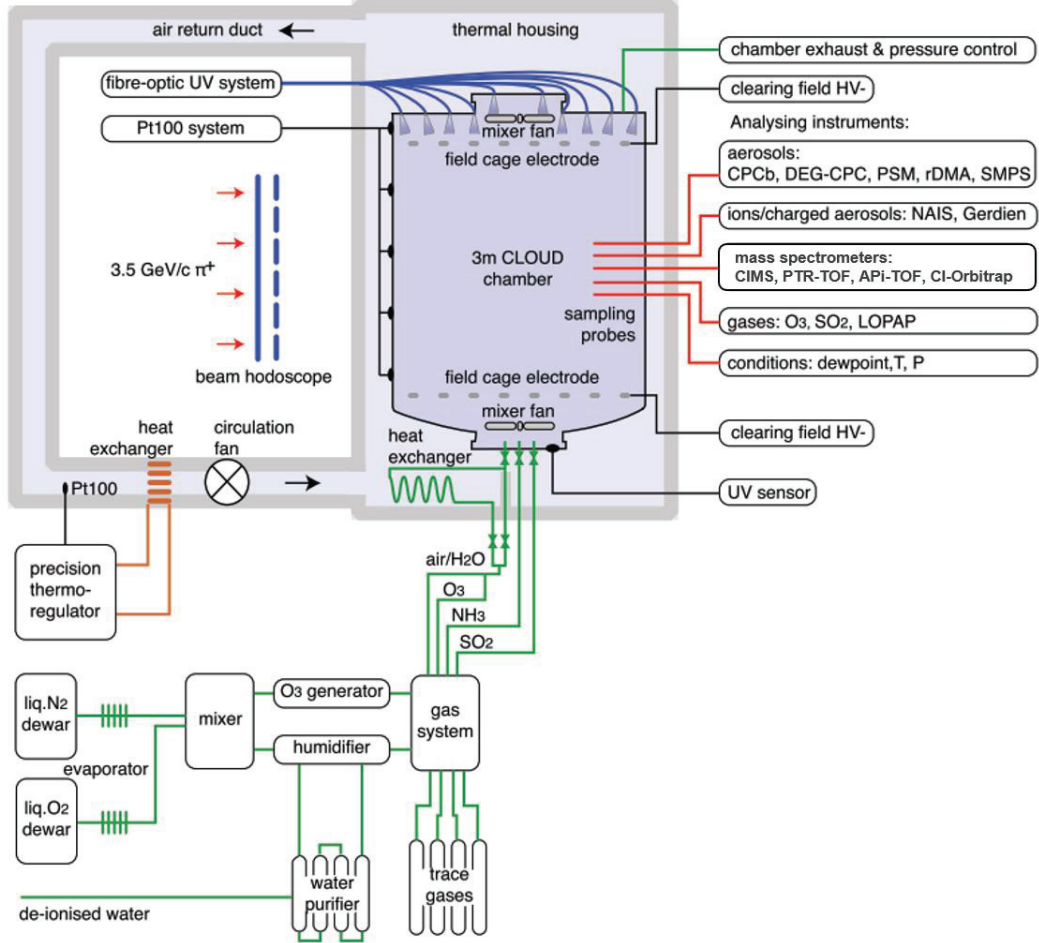


Figure II-2: Schematic of the CLOUD chamber experiments (Kirkby et al., 2011).

The evaporation of cryogenic liquid nitrogen (N_2) and liquid oxygen (O_2) was blended at a ratio of 79:21 to produce pure synthetic air, which flushed the chamber constantly. 250 optical fiber-optic systems installed on top of the chamber to avoid disturbing chamber temperature are utilized to initiate photolytic reactions, including Hg-Xe UV lamps, and UV excimer laser (Kupc et al., 2011). Variable amounts of trace gases, for example, O_3 , VOCs, NO_x , SO_2 , NH_3 , and CO were precisely injected into the system as needed and monitored (Voigtländer et al., 2012). The contents of the chamber were ceaselessly detected and analyzed by a wide range of external instruments connected to the sampling probes ~1 m protruding into the chamber. The CLOUD chamber reaches extremely standards of cleanliness, which is cleaned by irrigating the walls with ultra-pure water, heating to 373 K, and flushed with humidified pure air and the high ozone,

declining the contaminant levels such as VOCs to less than 1 ppbv (Duplissy et al., 2010). The particles were wiped out using a high voltage electric field.

II.2. Chemical characterization

II.2.1. NO_x and O₃ analyzers

- NO_x analyzer

The CLD 88 CY p (ECO PHYSICS) is capable to measure NO_x in the range of parts per trillion (ppt). In this work, an ECO PHYSICS analyzer equipped with a photolytic converter PLC 860 was used to monitor NO_x for the experiments performed using the OFR, having a detection limit of 0.05‰ of the max range and an efficiency of >90% for NO₂ measurement. NO₂ is converted into NO through the reaction with carbon (C) in the heated converter (>300 °C) as the following reaction:



NO is measured by chemiluminescence method:



The radiation emission is in the wavelength between 600 and 3000 nm with a maximum intensity of around 1200 nm. The chemiluminescence signal is detected photo-electrically. The pressure in the reaction chamber is reduced in order to enhance the light yield and use a less collision effective molecule M, for instance, N₂ or O₂, to reduce quenching (II-5). The NO_x analyzer was calibrated with theoretically known amounts of NO and NO₂ concentrations (0-100 ppbv) prior to the experiments.

- O₃ analyzer

The concentration of ozone (O₃) is measured by a Thermo 49C based on the principle that ozone molecules absorb ultraviolet (UV) light at a wavelength of 254 nm. According to the Lambert-Beer law, the degree to which the UV light is absorbed is directly related to the O₃ concentration. The

sample is drawn into the instrument chamber and is divided into two gas streams. One gas stream flows through an O₃ scrubber as the “reference gas” and then flows to the reference solenoid valve. The other gas flow directly flows to the sample solenoid valve as the “sample gas”. The two solenoid valves are automatically switched every 10 seconds so that the two gas flows alternately pass through each absorption cell, and the corresponding two detectors are used to detect the light intensity. The instrument calculates the O₃ concentration for each cell and outputs the average concentration. The range of the instrument is 0-200 ppmv and the detection limit is 1.0 ppbv.

II.2.2. Chemical ionization mass spectrometry

In this PhD work, there are results presented by proton transfer reaction mass spectrometer (PTR-MS), chemical ionization coupled to an Orbitrap mass spectrometer (CI-Orbitrap), a chemical ionization atmospheric pressure interface long time of flight mass spectrometer (CI-APi-LTOF), a newly-developed prototype of the proton transfer reaction time-of-flight mass spectrometer (PTR3-TOF), and a time-of-flight mass spectrometer equipped with a Filter Inlet for Gases and AEROSols (FIGAERO-CIMS). Among them, I was in charge of PTR-QMS for monitoring VOC precursor, and CI-Orbitrap for retrieving the evolution of oxidation products. The remaining other mass spectrometers were operated and maintained by colleagues in CLOUD consortium. I was involved in data analysis and discussions. Therefore, the working principles of these instruments are only briefly described in the corresponding subsections below.

II.2.2.1 Chemical ionization schemes

Chemical ionization is a soft ionization technique used in mass spectrometry. Analyte ions are created by the collisions of neutral molecules with the reagent ions through ion-molecule reactions in the gas phase. Reagent ions, including nitrate, acetate, iodide, amine, and ammonia, are formed by soft ionization (radioactive, corona discharge, and x-ray) of gaseous molecules (Berndt et al., 2018a; Berndt et al., 2016; Berndt et al., 2018b; Breitenlechner et al., 2017; Hansel et al., 2018; Jokinen et al., 2012; Lopez-Hilfiker et al., 2014; Rissanen et al., 2019; Riva et al., 2020; Riva et al., 2019a; Riva et al., 2019b). Compared to electron ionization (EI) ionization, chemical ionization generally provide much less energy to neutral molecules, resulting in fragmentation free ionization process and leading to an accurate molecular weight determination of labile analytes (Field, 1968).

Chapter II: Experimental methods

Various reagent ions have different sensitivity to organic molecules, which determine the ability to detect specific compounds or classes of compounds with the same or comparable functional groups (Aljawhary et al., 2013; Berndt et al., 2018b; Riva et al., 2019b). Table II-1 provides a few examples. Negative ion-based techniques, notably using nitrate (NO_3^-) or iodide (I^-), can nicely detect HOMs, whereas negative mode is selective and only a small subset of the OOMs can be characterized (Berndt et al., 2015; Berndt et al., 2018b; Lee et al., 2014; Riva et al., 2019b). Recently, positive ion-based techniques have been developed and shown to have good response to HOMs and the less oxidized products, providing the possibility of achieving carbon-closure (Berndt et al., 2018a; Berndt et al., 2018b; Hansel et al., 2018; Praplan et al., 2015; Riva et al., 2020; Riva et al., 2019b). Hence the full detection of organic compounds can be achieved using both negative and positive ionization techniques coupled with several mass spectrometers (Hansel et al., 2018; Isaacman-VanWertz et al., 2018; Isaacman-VanWertz et al., 2017).

Table II-1: Selectivity of several chemical ionization schemes coupled to MS used in atmospheric measurements.

Reagent ion	Favorable detected compounds	Reference
NO_3^-	H_2SO_4 , HOMs, RO_2	(Berndt et al., 2015; Ehn et al., 2014; Jokinen et al., 2012; Riva et al., 2019a; Riva et al., 2019b)
$\text{C}_2\text{H}_3\text{O}_2^-$ $\text{C}_3\text{H}_3\text{O}_3^-$ $\text{C}_3\text{H}_5\text{O}_3^-$	O VOCs, acids	(Berndt et al., 2016; Berndt et al., 2015; Bertram et al., 2011; Brophy and Farmer, 2016; Hansel et al., 2018; Veres et al., 2008)
CF_3O^-	Inorganic acids, carboxylic acids, peroxides, hydroxynitrates	(Amelynck et al., 2000; Beaver et al., 2012; Crounse et al., 2006; Crounse et al., 2011)
I^-	O VOCs, HOMs, ONs, HO_2 , HO_2NO_2 , Halogens	(Lee et al., 2014; Lee et al., 2016; Riedel et al., 2012; Riva et al., 2019b; Wang et al., 2020a)
Br^-	HO_2 , ONs, inorganic acids	(Rissanen et al., 2019; Sanchez et al., 2016; Wang et al., 2020b; Wu et al., 2021)
$(\text{H}_2\text{O})_n\text{H}^+$	VOCs, SVOCs	(Breitenlechner et al., 2017; Yuan et al., 2016)

Amines	O VOCs, HOMs, RO ₂	(Berndt et al., 2018b; Riva et al., 2020; Riva et al., 2019b)
NH ₄ ⁺	O VOCs, HOMs, RO ₂	(Berndt et al., 2018b; Hansel et al., 2018; Zaytsev et al., 2019)

II.2.2.2 Proton transfer reaction mass spectrometer (PTR-MS)

- Proton transfer reaction quadrupole mass spectrometer (QMS)

In the nitrate radicals-derived OFR experiments, a proton transfer reaction quadrupole mass spectrometer (PTR-QMS 300, Ionicon Analytik) coupled to a switchable reagent ionization (SRI) source was used to monitor VOC continuously. The instrument consists of three main parts as shown in Figure II-3: an ion source, drift tube, and a quadrupole mass filter. PTR-QMS could be used with H₃O⁺, NO⁺, or O₂⁺ ionization mode. Only H₃O⁺ ionization mode was employed in this study. Production of H₃O⁺ ions with a high purity level (up to 98%) occurs in the ion source from ultra-pure water vapor. Then H₃O⁺ ions are extracted towards the drift tube, where the continuously introduced sample gas containing VOCs undergoes proton transfer from H₃O⁺ ions. VOCs could be ionized when their proton affinities (PA) are higher than water, show as follows:



Water has a PA of 166.5 kcal mol⁻¹, which is lower than most VOC trace gases in the ambient air but greater than the common constituents in the air, such as N₂, O₂, CO₂ etc. Hence, air does not react with H₃O⁺ and acts as a buffer gas.

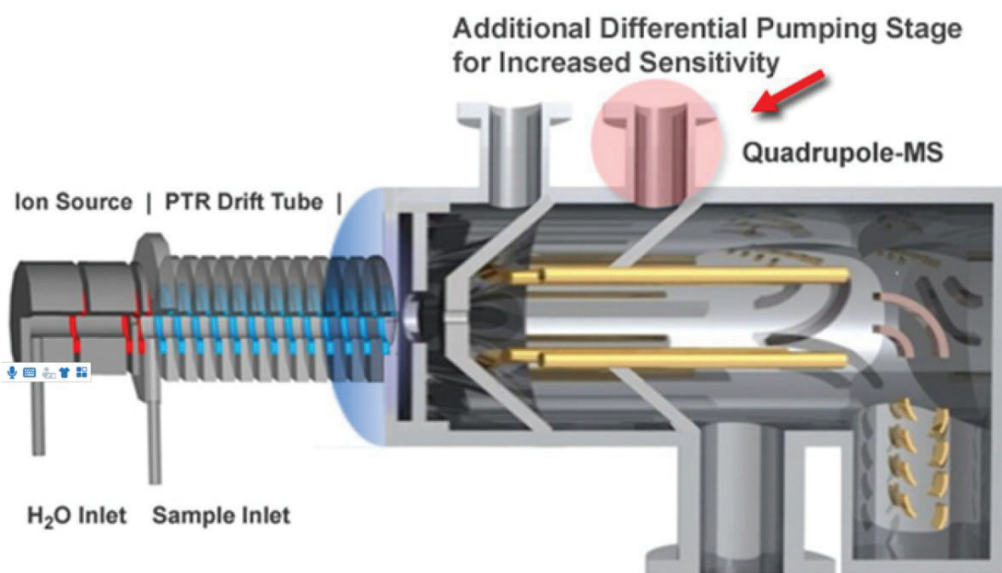


Figure II-3: Schematic view of the PTR-QMS (adapted from ionicon.com)

Then an electric drift field pulls primary and product ions towards the detection part. The drift tube voltage (E , $V\text{ cm}^{-1}$) can supply necessary kinetic energy to help reduce cluster formation, but fragmentation could occur. Hence, the ratio of E/N is an important parameter for PTR-MS analysis, where N denotes the number density of the gas (cm^{-3}) in the drift tube. E/N ratio is expressed in Td ($1\text{ Td} = 10^{-17}\text{ V cm}^2$). In general, a high E/N ratio often results in greater fragmentation, whereas a low E/N ratio leads to more water cluster formation.

A quadrupole mass filter combined with a secondary electron multiplier enables mass separation and detection of ions. A DC voltage and a high frequency AC voltage are applied to four rods. The ions, which are injected parallel to the rods, oscillate perpendicular to their direction of travel. Only ions with a specific m/Q ratio are transmitted. As a result, the quadrupole must repeatedly cycle through a set of m/Q in order to measure several compounds.

- Proton transfer reaction-time of flight-mass spectrometer (PTR-ToF-MS)

The online monitoring of changes in limonene and α -pinene was done with a high-resolution proton transfer reaction-time of flight-mass spectrometer (PTR-ToF-MS 8000, Ionicon Analytik) coupled to a SRI source. This instrument was developed to provide gentle ionization, a high mass resolution ($4500\text{ m}/\Delta m$), and a detection limit of pptv level.

As shown in Figure II-4, PTR-ToF-MS has a similar ion source, drift tube as PTR-QMS but different mass analyzer. It works based on the principle that the mass to charge ratios (m/z) of an accelerated ion determine the time of flight in a field-free region. By measuring the time between the accelerating pulse provided at the extraction of the ions and the arrival of an ion on the detector, the m/z can be determined. The flight trajectory is typically a V-shape or W-shape which doubles the resolution but with less sensitivity.

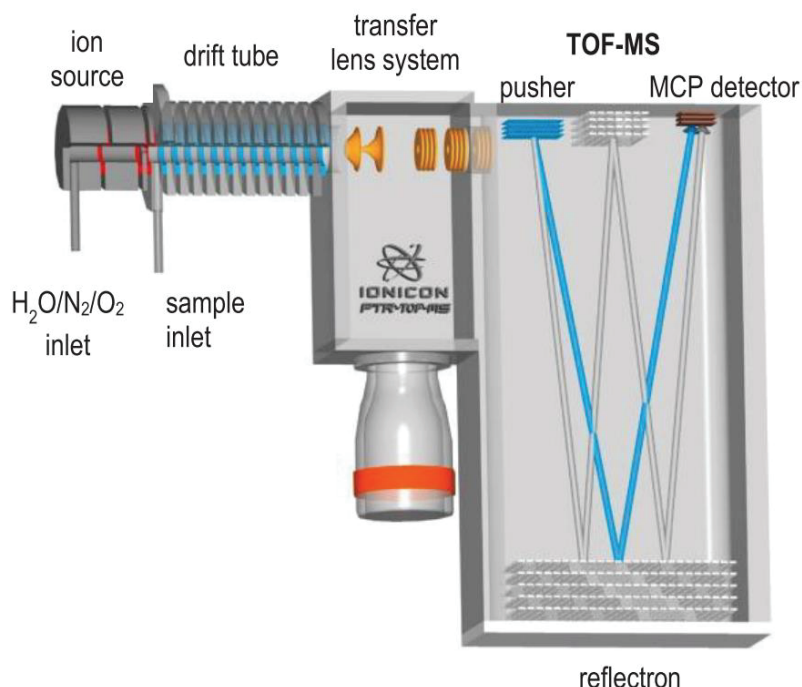


Figure II-4: Schematic view of the PTR-ToF-MS (adapted from ionicon.com)

II.2.2.3 CI-Orbitrap

The chemical composition of RO₂ radicals and closed-shell molecules were retrieved in real-time by means of a high-resolution mass spectrometer (Orbitrap) coupled with a CI inlet. The method and the inlet used in this work was adopted from earlier studies where they successfully detected sulfuric acid by chemical ionization in very low quantities (Eisele and Tanner, 1993). The CI inlet is a home-built version with minor modifications regarding the commercial inlet, as shown in

Chapter II: Experimental methods

Figure II-5 (Riva et al., 2019a). A special connector flange was constructed for interfacing to the Orbitrap. The Eisele-type inlet minimizes the wall losses by the use of a coaxial sample flow of 10 lpm and a sheath flow of 30 lpm, facilitating the characterization of low-volatile and radical species.

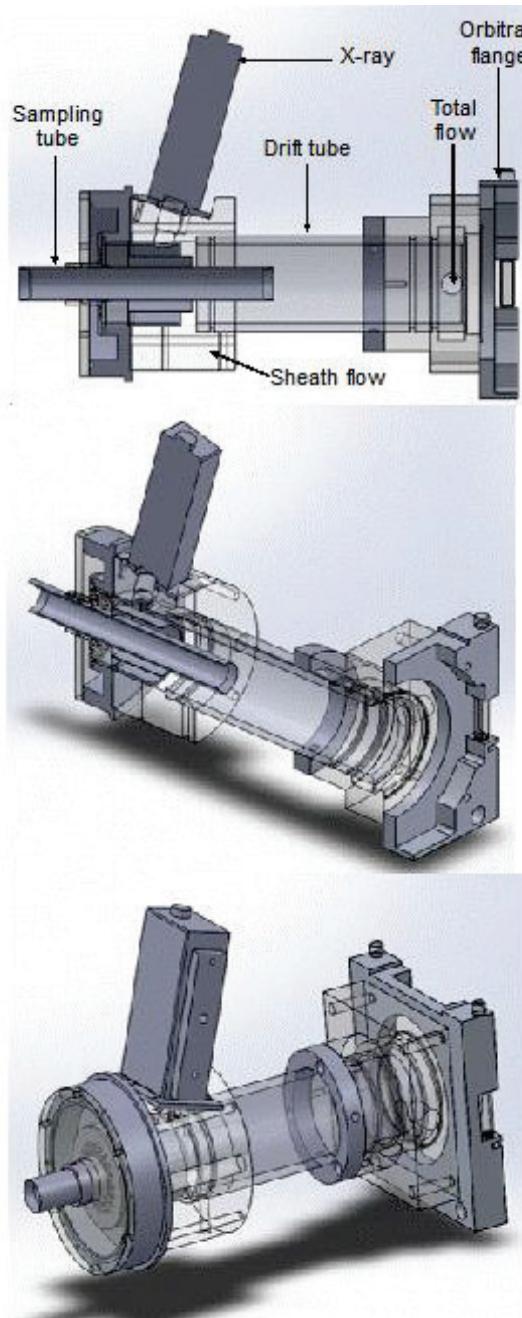


Figure II-5: Schematic of the homemade atmospheric pressure chemical ionization interface (Riva et al., 2019a).

Chapter II: Experimental methods

The sample enters the CI with a flow rate of 10 lpm and is kept in the center, surrounded by the concentric sheath flow of 30 lpm, which is optimized for minimal contact and loss to the wall of the sample. The clean air containing the reagent molecules is ionized to form the reagent ions using a soft X-ray photo-ionizer (Hamamatsu, L9491). Then the reagent ions in the sheath flow are guided into the sample flow by means of an electric field. Once in the ion-molecule-reaction (IMR) zone, the sample molecules are charged by the reaction with the reagent ions forming a stable cluster or transferring a proton. The interaction time between the reagent ions and the neutral molecules within the IMR zone is approximately 200-300 ms.

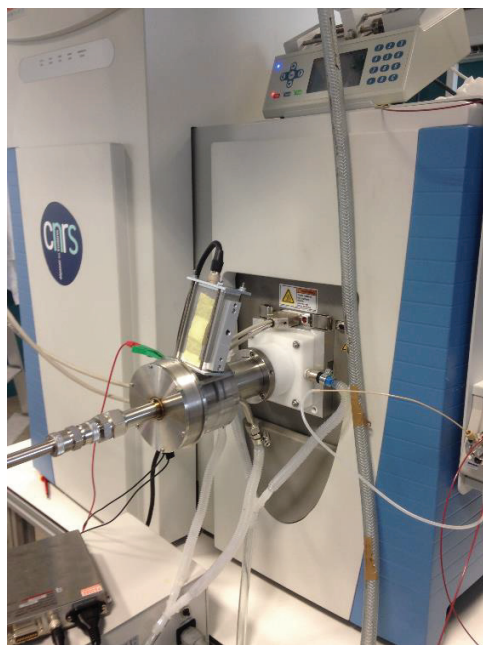


Figure II-6: Home-made chemical ionization inlet coupled to Orbitrap mass spectrometer.

The ions are then introduced within the Orbitrap mass spectrometer at a flow rate of 2 lpm. A special connector flange was constructed for interfacing to the Orbitrap (Figure II-6). The chemical compositions of the organic compounds are analyzed in real time by Q Exactive Orbitrap mass spectrometer (Thermo Scientific, US) (Riva et al., 2019a; Zuth et al., 2018). As schematized in Figure II-7, the Orbitrap consists of five main components: an ion source, ion optics for focusing and transmitting the ions produced in the source, an intermediate storage device (C-Trap) for short pulse injection, an optional collision cell for performing higher energy collisional dissociation (HCD) experiments, and the Orbitrap analyzer for Fourier transform mass analysis.

Chapter II: Experimental methods

Ions from the ion transfer capillary enter an ion transmission device consisting of progressively spaced, stainless-steel electrodes (S-lens). As the amplitude of radio frequency (RF) applied to the electrodes of S-lens increases, ions of progressively higher m/Q pass through to the exit lens. Then ions move toward the injection flatapole, a square array of flat metal electrodes. Incoming ions are bent to a 90° arc by flatapole to remove the neutral molecules and then guided into the quadrupole. Quadrupole includes a symmetrical, parallel array of four hyperbolic rods and provides the first mass filter and efficiently transmit a certain m/Q ion. On their way from the ion source to the Orbitrap analyzer, the transmitted ions are stored and cooled in the gas-filled curved linear trap (C-Trap). Their kinetic energy is dissipated by collision with nitrogen bath gas. Ions are cooled down to the axis of the C-Trap and get collected near the middle part. An electric field is applied to the electrodes of C-Trap and pushes ions into the Orbitrap analyzer.

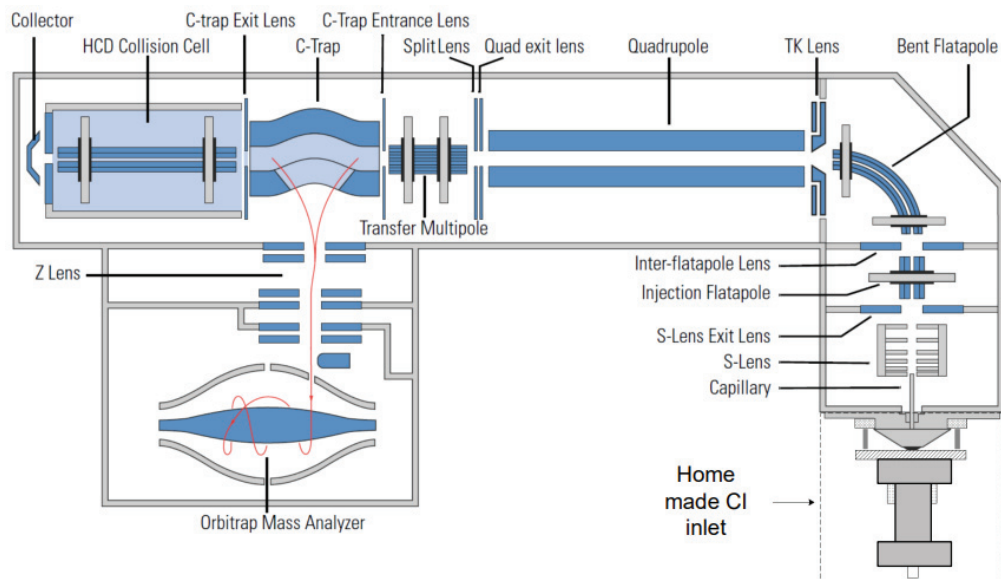


Figure II-7: Schematic of the Q Exactive mass spectrometer (adapted from the manual of the manufacturer, Thermo).

The Orbitrap analyzer consists of a spindle-shaped central electrode surrounded by a pair of bell-shaped outer electrode (Figure II-8). In the mass analyzer, stable ion trajectories combine rotation around an axial central electrode with harmonic oscillations along it. For any given m/Q, rotational and radial frequencies exhibit strong dependence on initial radius and energy, whereas the frequency ω_z of these harmonic oscillations along the z-axis depends only on the ion m/Q ratio

and the instrumental constant k , the curvature of the field determined by the shape of the electrodes and the applied potential:

$$\omega_z = \sqrt{\frac{k}{m/Q}} \quad (\text{II-1})$$

These oscillating ions produce the image current which is detected by the two split halves of the outer electrode of the Orbital trap. By Fast Fourier Transformation (FFT) of the amplified image current, the time signals are converted to frequency and the instrument obtains the frequencies and then m/z .

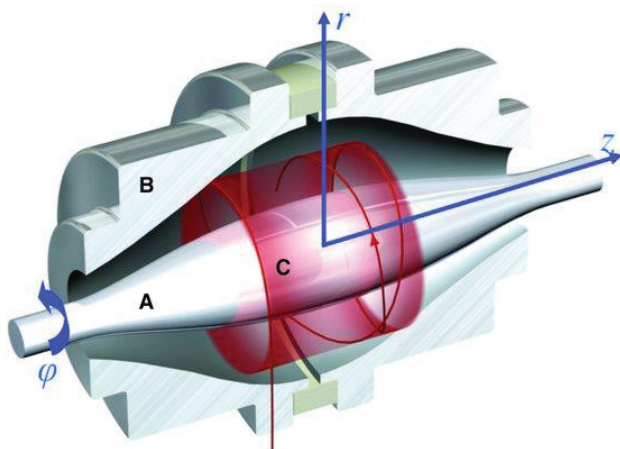


Figure II-8: Cutaway view of the Orbitrap mass analyzer. A) Central electrode, B) An outer electrode, split in half by an insulating ceramic ring, C) Complex orbital path of an ion (Snow, 2014).

The Q-Exactive Orbitrap also allows conducting tandem mass spectral (MS^2) analyses to obtain chemical structure information on the compounds by using HCD cell, see Figure II-6. It consists of a straight multipole mounted inside a metal tube, which is connected in direct line-of-sight to the C-Trap. Nitrogen gases are filled to increase gas pressure inside the multipole and collide with selected sample molecules. The generated fragments go back to C-Trap and are detected in the Orbitrap analyzer.

Overall, the mass spectrometer used in this study has a mass resolution of 140 000 at m/Q 200, allowing the mass determination of a wider variety of species. Isobaric ions and isotopes were more clearly separated thanks to the high resolving power of Orbitrap mass analyzer. In addition, the scanning range is configured to m/Q 50-750 with a scan rate of 0.2 scans/s. The calibration of the Q-Exactive mass spectrometer was externally performed daily by a 2 Mm sodium acetate solution which provided a suite of positive and negative adduct ions in the desired m/Q range. The mass accuracy is <5 ppm with external calibration and <1 ppm using internal standard. Orbitrap data were analyzed by the XCalibur 2.2 (Thermo Scientific) software package and newly developed Orbitool software which will describe in the following section.

II.2.2.4 CI-APi-LTOF

Detection of RO₂ radicals and accretion products were also measured by a chemical ionization atmospheric pressure interface long time of flight mass spectrometer (CI-APi-LTOF) at the Cloud chamber, as shown in Figure II-9. The design of CI-inlet coupled to an APi-TOF was first introduced by (Jokinen et al., 2012) and described elsewhere (Kürten et al., 2016; Kurten et al., 2014). The CI-APi-LTOF offers a mass resolving power up to 12 000 and can detected HOMs (mass 300-650 Da) as clusters with the reagent ions using a corona discharge (Kürten et al., 2011). The sample flow enters the ion drift tube where it is surrounded concentrically by the sheath gas. The primary ions are directed towards the center of the sample flow by means of an electrostatic field so that they can interact with sampled compounds. These compounds can be ionized through proton-transfer reaction or via clustering with the primary ions. A core-sampling technique was applied to prevent losses in the sampling inlet (Knopf et al., 2015). Most of the flow is used to protect the core flow that is analyzed. This setup reduces the sampling loss rate of HOMs to less than 30% (Simon et al., 2020).

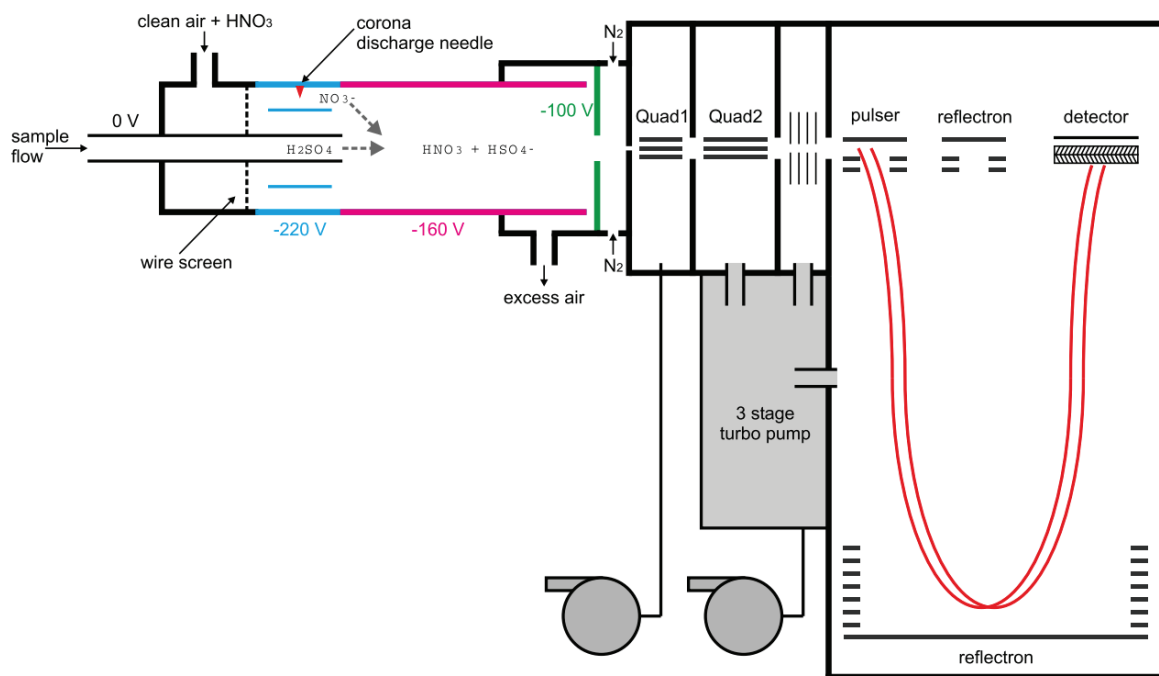


Figure II-9: Schematic of the CI-APi-TOF mass spectrometer (Kürten et al., 2014).

The APi-TOF has three differentially pumped chambers, the first two containing short segmented quadrupoles used in ion guide mode, and the third containing an ion lens assembly (Junninen et al., 2010). The primary and sample ions are drawn into the first stage of a vacuum chamber through a pinhole with a pressure of ~ 2 mbar. Quadrupoles in the first and second stages of the chamber are operated in RF-only mode for guiding the ions. The second chamber is pumped down to $\sim 10^{-3}$ mbar. A lens stack in a third stage focuses and prepares the ions energetically before they enter the time-of-flight mass spectrometer (Aerodyne Research Inc., USA, and Tofwerk AG, Switzerland). The final pressure in the TOF is nearly 10^{-6} mbar. The APi-TOF can be operated in either *V* or *W* mode, with the letters symbolizing the flight path of the ions inside the instrument. The greater the ion mass, the longer it takes to reach the detector. Data are recorded using time-to-digital converter (TDC) by co-adding spectra for 5 s and processed in IGOR Pro 7 (WaveMetrics, Inc., USA), using the software package Tofware (Version 3.2, Aerodyne Inc., USA) and MATLAB R2019b (MathWorks, Inc., USA).

II.2.2.5. PTR3-TOF

A newly-developed prototype of the proton transfer reaction time-of-flight mass spectrometer (PTR3-TOF) was used to measure the concentration of VOCs and other oxygenated compounds also during the Cloud experiments. Compared to the conventional PTR-TOF, PTR3 significantly improves the detection of low volatility compounds by reducing the wall loss and increasing the sensitivity. As shown in Figure II-10, PTR3 consists of a corona discharge ion source, a tripole reaction chamber, a drift region, a quadrupole transfer unit, and TOF-MS. Reagent ions are produced in the corona discharge from humidified nitrogen or NH₃/H₂O introduced as CI gas. The majority of organic compounds are ionized by using proton transfer or ligand switch reactions from (H₃O⁺)(H₂O)_n clusters (Breitenlechner et al., 2017) or NH₄⁺X_n (X being NH₃/H₂O, n=1, 2) (Hansel et al., 2018). In order to reduce transmission losses, a core flow was drawn from the center of a laminar sample flow through a critical orifice into the tripole reaction chamber where the ion-molecule reactions take place. In addition, the sheath gas surrounding the core flow is pumped out symmetrically, ensuring to minimize wall contact of the sample gas and hence reduce wall losses of OVOC for instance RO₂.

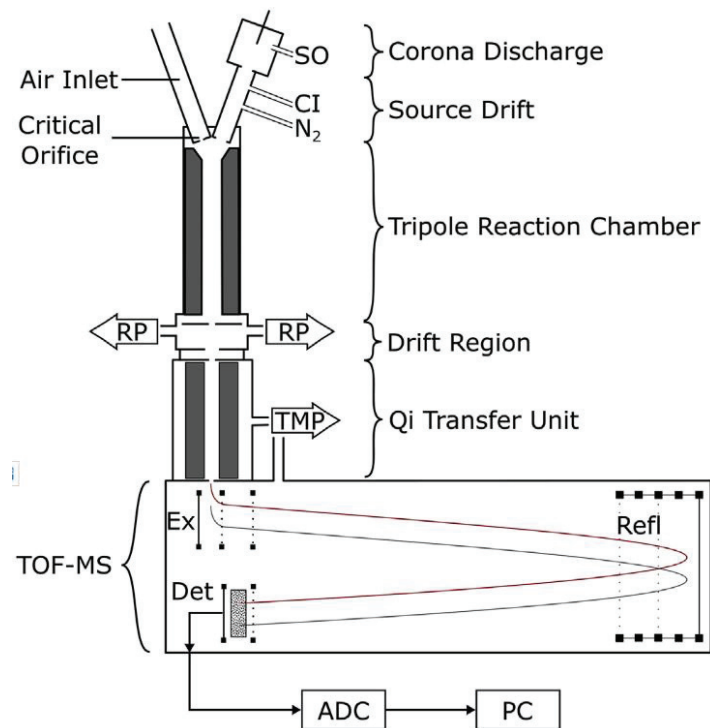


Figure II-10: Schematics of PTR3-TOF (Hansel et al., 2018).

The pressure in this reaction region was maintained at ~80 mbar. The distribution of primary ions and sample molecules can be adjusted by a tunable radio frequency signal applied to the tripole rods. The pressure drops to 2-4 mbar in the drift region due to the coupling of PTR3 to the mass spectrometer, which leads to a different distribution of primary and product ion clusters than in the tripole reaction chamber. Overall, increased pressure in the tripole and longer reaction time result in a 500-fold increase in sensitivity to various organics compared to conventional PTR instruments. PTR3-TOF are calibrated using a gas standard containing 1 ppm of 3-hexanone, heptanone and α -pinene in nitrogen. The concentrations of oxygenated products are estimated by using the sensitivity of 3-hexanone as lower-limit values due to possible fragmentation. All data were acquired using TofDaq recorder by Tofwerk and analyzed with TOF-Tracer software running on Julia 0.6.

II.2.2.6 FIGAERO-CIMS

A time of flight mass spectrometer equipped with a Filter Inlet for Gases and AEROsols (FIGAERO-CIMS) is capable of measuring both gas and particle composition of secondary organic aerosols (SOA) with a multi-port inlet manifold (Lopez-Hilfiker et al., 2014) and was deployed during the Cloud campaign. As schematized in Figure II-11, one exit port is used for sampling and analyzing gases, and the other for sampling and analyzing desorption vapors from the collected aerosols. A removable tray with a filter is used to change between these two states. In gas mode, trace gases are directly sampled into a turbulent ion-molecule reactor simultaneous particles are collected on a polytetrafluoroethylene (PTFE) filter via a separate dedicated port. In the particle mode, the filter is automatically moved into a pure N₂ gas stream flowing into the ion-molecule reactor, while the N₂ is progressively heated to evaporate the particles via temperature-programmed thermal desorption. Hence, the ion thermogram for individual ions can be obtained from the resulting signal versus desorption temperature curves. Each desorption cycle includes two parts: the particle collection and the linear increase in desorption temperature (i.e., ~25 °C → ~150 °C in 15 mins). The filter-related background signals are determined by a particle blanking manifold which periodically prevent particles from reaching the primary collection filter in the FIGAERO.

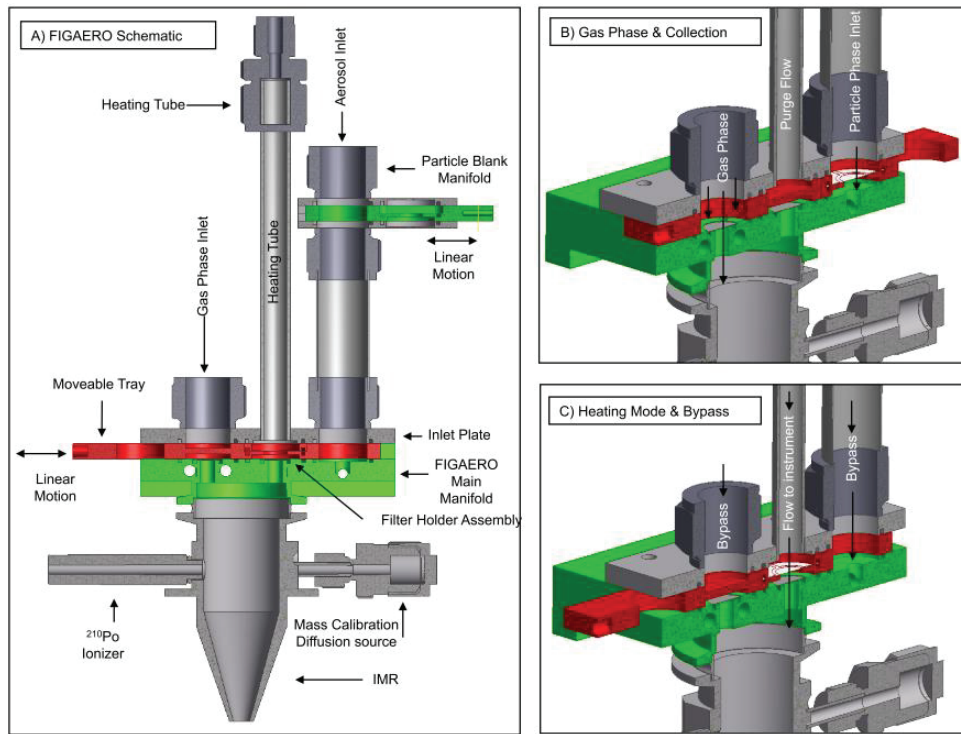


Figure II-11: Schematic of FIGAERO assembly (Lopez-Hilfiker et al., 2014).

Both modes are fully automated and programmable for continuous online sampling. Analytes are then chemically ionized and extracted into a TOF-MS (Wang et al., 2020b). Measurement cycle of two modes was set to 30 minutes, 15 mins in gas and 15 mins in particle mode. As a result, FIGAERO enables the alternate measurements of gas and particle samples. Iodide (I^-) or acetate can be used as reagent ions, achieving highly selective determined analytes with very low detection limits. Data were analyzed using Tofware (version 2.5.11_FIGAERO) giving 10 s average mass spectra.

II.2.3. Orbitool software for analyzing Orbitrap data

The high resolution Orbitrap spectra were analyzed using a new-developed software “Orbitool” with a graphical user interface (GUI) (Cai et al., 2020). The gas-phase oxidation of one single VOC can yield thousands of oxidized products. And the application of CI-Orbitrap achieve much greater mass resolving power to distinguish isobaric species. As a result, the chemical diversity of OVOCs presents a significant challenge in detecting, quantifying, and characterizing such a large number and wide variety of organic compounds. The commercial software, XcaliburTM, which was used in

our initial studies (Riva et al., 2019a), provides an interface for basic data processing, e.g., reading single or averaged scans and exporting the time evolution of selected signal peaks. However, more comprehensive data analysis is usually needed in order to investigate complexities and chemical processes that occur in the atmosphere. Furthermore, the use of Orbitrap in long-term continuous online measurements necessitates the development of a new software tool for interpreting Orbitrap data. Therefore, Orbitool came into being.

The basic working principle of Orbitool is shown in Figure II-12. Orbitool enables data averaging, noise determination and reduction, the single peak fitting, mass calibration, peak assignment and export of time series and mass defect plots. The user has the option of averaging all imported files or only a portion of them. Either the scan count or the scan time are used to determine the average spectra. Orbitool takes the peaks which is lower than a certain percentile of the peak heights in the mass defect range of [0.5, 0.8] Da as noise peaks. The users can choose remove noise peaks, remove noise peaks and subtract noise level, or no denoising. A normal distribution is used by Orbitool to characterize the single peak shape. The users can remove deviated peaks manually on the GUI. Orbitool can automatically locate the peaks of user-provided calibration species within a preset uncertainty range. A polynomial function is then used to fit a calibration curve. By utilizing various calibration species, the users can set the degree of polynomial and adjust the calibration curve.

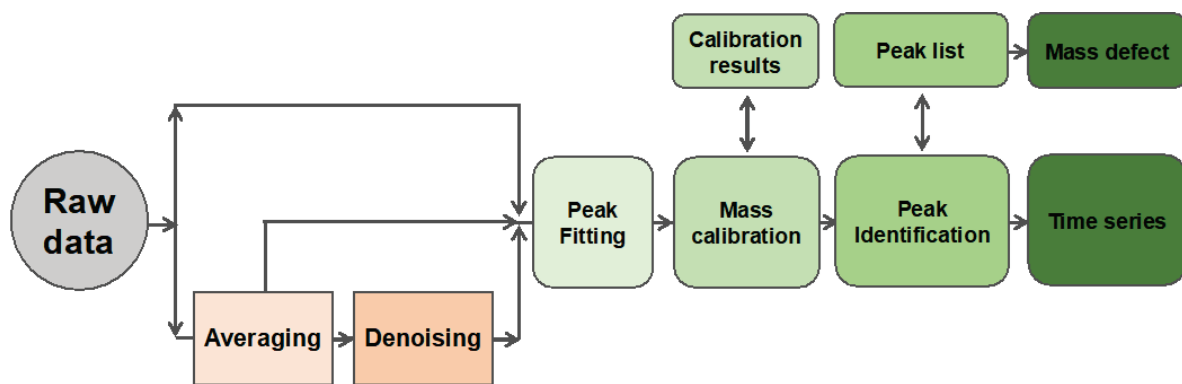


Figure II-12: Simplified schematics of the working principle of Orbitool (Cai et al., 2020).

Orbitool fit single peak to the calibrated average spectrum and usually conducts a default peak fitting to the whole spectra. And the users can merge the peaks in a given mass range using a customized mass tolerance. When assigning chemical formulae for a given mass, Orbitool searches

for all possible chemical formulae satisfying configured boundary conditions. Isotope identification is also supported at the same time. A mass list is created using the fitted peak location and their corresponding chemical formulas once all the single peaks have been identified. The users can get the temporal evolution of abundance for given chemical species and export them. In addition, the mass defect plot is provided on the GUI for an intuitive and rapid characterization of an averaged spectrum.

Orbitool is mostly coded in Python, with the supports from several third-party libraries. To enhance computational speed, the mass spectra are processed using the Numba package (Lam et al., 2015) and chemical composition and signal abundance are determined using the Cython package 5 (Behnel et al., 2011). Orbitool was tested in Python 3.6 on the Microsoft Windows operating system. An executable version of Orbitool and its open-source codes are publicly available (<https://orbitrap.catalyse.cnrs.fr>)

II.3. References

- Aljawhary, D., Lee, A. K. Y., and Abbatt, J. P. D. (2013), High-resolution chemical ionization mass spectrometry (ToF-CIMS): application to study SOA composition and processing, *Atmospheric Measurement Techniques*, 6(11), 3211-3224, doi:10.5194/amt-6-3211-2013.
- Amelynck, C., Schoon, N., and Arijs, E. (2000), Gas phase reactions of CF_3O^- and $\text{CF}_3\text{O}-\text{H}_2\text{O}$ with nitric, formic, and acetic acid, *International Journal of Mass Spectrometry*, 203(1), 165-175, doi:[https://doi.org/10.1016/S1387-3806\(00\)00321-3](https://doi.org/10.1016/S1387-3806(00)00321-3).
- Beaver, M. R., Clair, J. M. S., Paulot, F., Spencer, K. M., Crounse, J. D., LaFranchi, B. W., Min, K. E., Pusede, S. E., Wooldridge, P. J., Schade, G. W., Park, C., Cohen, R. C., and Wennberg, P. O. (2012), Importance of biogenic precursors to the budget of organic nitrates: observations of multifunctional organic nitrates by CIMS and TD-LIF during BEARPEX 2009, *Atmospheric Chemistry and Physics*, 12(13), 5773-5785, doi:10.5194/acp-12-5773-2012.
- Berndt, T., Mentler, B., Scholz, W., Fischer, L., Herrmann, H., Kulmala, M., and Hansel, A. (2018a), Accretion Product Formation from Ozonolysis and OH Radical Reaction of alpha-Pinene: Mechanistic Insight and the Influence of Isoprene and Ethylene, *Environmental science & technology*, 52(19), 11069-11077, doi:10.1021/acs.est.8b02210.
- Berndt, T., Richters, S., Jokinen, T., Hyttinen, N., Kurten, T., Otkjaer, R. V., Kjaergaard, H. G., Stratmann, F., Herrmann, H., Sipila, M., Kulmala, M., and Ehn, M. (2016), Hydroxyl radical-induced formation of highly oxidized organic compounds, *Nature communications*, 7, 13677, doi:10.1038/ncomms13677.
- Berndt, T., Richters, S., Kaethner, R., Voigtlander, J., Stratmann, F., Sipila, M., Kulmala, M., and Herrmann, H. (2015), Gas-Phase Ozonolysis of Cycloalkenes: Formation of Highly Oxidized RO_2 Radicals and Their Reactions with NO , NO_2 , SO_2 , and Other RO_2 Radicals, *The journal of physical chemistry. A*, 119(41), 10336-10348, doi:10.1021/acs.jpca.5b07295.

Chapter II: Experimental methods

- Berndt, T., Scholz, W., Mentler, B., Fischer, L., Herrmann, H., Kulmala, M., and Hansel, A. (2018b), Accretion Product Formation from Self- and Cross-Reactions of RO₂ Radicals in the Atmosphere, *Angewandte Chemie*, 57(14), 3820-3824, doi:10.1002/anie.201710989.
- Bertram, T. H., Kimmel, J. R., Crisp, T. A., Ryder, O. S., Yatavelli, R. L. N., Thornton, J. A., Cubison, M. J., Gonin, M., and Worsnop, D. R. (2011), A field-deployable, chemical ionization time-of-flight mass spectrometer, *Atmospheric Measurement Techniques*, 4(7), 1471-1479, doi:10.5194/amt-4-1471-2011.
- Breitenlechner, M., Fischer, L., Hainer, M., Heinritzi, M., Curtius, J., and Hansel, A. (2017), PTR3: An Instrument for Studying the Lifecycle of Reactive Organic Carbon in the Atmosphere, *Analytical chemistry*, 89(11), 5824-5831, doi:10.1021/acs.analchem.6b05110.
- Brophy, P., and Farmer, D. K. (2016), Clustering, methodology, and mechanistic insights into acetate chemical ionization using high-resolution time-of-flight mass spectrometry, *Atmospheric Measurement Techniques*, 9(8), 3969-3986, doi:10.5194/amt-9-3969-2016.
- Cai, R., Li, Y., Clément, Y., Li, D., Dubois, C., Fabre, M., Besson, L., Perrier, S., George, C., Ehn, M., Huang, C., Yi, P., Ma, Y., and Riva, M. (2021), Orbitool: A software tool for analyzing online Orbitrap mass spectrometry data, *Atmospheric Measurement Techniques*, 14(3), 2377-2387, doi:10.5194/amt-14-2377-2021.
- Crounse, J. D., McKinney, K. A., Kwan, A. J., and Wennberg, P. O. (2006), Measurement of Gas-Phase Hydroperoxides by Chemical Ionization Mass Spectrometry, *Analytical chemistry*, 78(19), 6726-6732, doi:10.1021/ac0604235.
- Crounse, J. D., Paulot, F., Kjaergaard, H. G., and Wennberg, P. O. (2011), Peroxy radical isomerization in the oxidation of isoprene, *Physical chemistry chemical physics : PCCP*, 13(30), 13607-13613, doi:10.1039/c1cp21330j.
- Duplissy, J., Enghoff, M. B., Aplin, K. L., Arnold, F., Aufmhoff, H., Avnggaard, M., Baltensperger, U., Bondo, T., Bingham, R., Carslaw, K., Curtius, J., David, A., Fastrup, B., Gagné, S., Hahn, F., Harrison, R. G., Kellett, B., Kirkby, J., Kulmala, M., Laakso, L., Laaksonen, A., Lillestol, E., Lockwood, M., Mäkelä, J., Makhmutov, V., Marsh, N. D., Nieminen, T., Onnela, A., Pedersen, E., Pedersen, J. O. P., Polny, J., Reichl, U., Seinfeld, J. H., Sipilä, M., Stozhkov, Y., Stratmann, F., Svensmark, H., Svensmark, J., Veenhof, R., Verheggen, B., Viisanen, Y., Wagner, P. E., Wehrle, G., Weingartner, E., Wex, H., Wilhelmsson, M., and Winkler, P. M. (2010), Results from the CERN pilot CLOUD experiment, *Atmospheric Chemistry and Physics*, 10(4), 1635-1647, doi:10.5194/acp-10-1635-2010.
- Ehn, M., Thornton, J. A., Kleist, E., Sipila, M., Junninen, H., Pullinen, I., Springer, M., Rubach, F., Tillmann, R., Lee, B., Lopez-Hilfiker, F., Andres, S., Acir, I. H., Rissanen, M., Jokinen, T., Schobesberger, S., Kangasluoma, J., Kontkanen, J., Nieminen, T., Kurten, T., Nielsen, L. B., Jorgensen, S., Kjaergaard, H. G., Canagaratna, M., Maso, M. D., Berndt, T., Petaja, T., Wahner, A., Kerminen, V. M., Kulmala, M., Worsnop, D. R., Wildt, J., and Mentel, T. F. (2014), A large source of low-volatility secondary organic aerosol, *Nature*, 506(7489), 476-479, doi:10.1038/nature13032.
- Eisele, F. L., and Tanner, D. J. (1993), Measurement of the gas phase concentration of H₂SO₄ and methane sulfonic acid and estimates of H₂SO₄ production and loss in the atmosphere, *Journal of Geophysical Research: Atmospheres*, 98(D5), 9001-9010, doi:10.1029/93jd00031.
- Field, F. H. (1968), Chemical ionization mass spectrometry, *Accounts of Chemical Research*, 1(2), 42-49, doi:10.1021/ar50002a002.

Chapter II: Experimental methods

- Hansel, A., Scholz, W., Mentler, B., Fischer, L., and Berndt, T. (2018), Detection of RO₂ radicals and other products from cyclohexene ozonolysis with NH₄⁺ and acetate chemical ionization mass spectrometry, *Atmospheric Environment*, 186, 248-255, doi:10.1016/j.atmosenv.2018.04.023.
- Isaacman-VanWertz, G., Massoli, P., O'Brien, R., Lim, C., Franklin, J. P., Moss, J. A., Hunter, J. F., Nowak, J. B., Canagaratna, M. R., Misztal, P. K., Arata, C., Roscioli, J. R., Herndon, S. T., Onasch, T. B., Lambe, A. T., Jayne, J. T., Su, L., Knopf, D. A., Goldstein, A. H., Worsnop, D. R., and Kroll, J. H. (2018), Chemical evolution of atmospheric organic carbon over multiple generations of oxidation, *Nature chemistry*, 10(4), 462-468, doi:10.1038/s41557-018-0002-2.
- Isaacman-VanWertz, G., Massoli, P., O'Brien, R., Nowak, J., Canagaratna, M., Jayne, J., Worsnop, D., Su, L., Knopf, D., and Misztal, P. (2017), Using advanced mass spectrometry techniques to fully characterize atmospheric organic carbon: current capabilities and remaining gaps, *Faraday discussions*, 200, 579-598.
- Jokinen, T., Sipilä, M., Junninen, H., Ehn, M., Lönn, G., Hakala, J., Petäjä, T., Mauldin, R. L., Kulmala, M., and Worsnop, D. R. (2012), Atmospheric sulphuric acid and neutral cluster measurements using CI-APi-TOF, *Atmospheric Chemistry and Physics*, 12(9), 4117-4125, doi:10.5194/acp-12-4117-2012.
- Junninen, H., Ehn, M., Petäjä, T., Luosujärvi, L., Kotiaho, T., Kostiainen, R., Rohner, U., Gonin, M., Fuhrer, K., Kulmala, M., and Worsnop, D. R. (2010), A high-resolution mass spectrometer to measure atmospheric ion composition, *Atmospheric Measurement Techniques*, 3(4), 1039-1053, doi:10.5194/amt-3-1039-2010.
- Kürten, A., Bergen, A., Heinritzi, M., Leiminger, M., Lorenz, V., Piel, F., Simon, M., Sitals, R., Wagner, A. C., and Curtius, J. (2016), Observation of new particle formation and measurement of sulfuric acid, ammonia, amines and highly oxidized organic molecules at a rural site in central Germany, *Atmospheric Chemistry and Physics*, 16(19), 12793-12813, doi:10.5194/acp-16-12793-2016.
- Kürten, A., Jokinen, T., Simon, M., Sipila, M., Sarnela, N., Junninen, H., Adamov, A., Almeida, J., Amorim, A., Bianchi, F., Breitenlechner, M., Dommen, J., Donahue, N. M., Duplissy, J., Ehrhart, S., Flagan, R. C., Franchin, A., Hakala, J., Hansel, A., Heinritzi, M., Hutterli, M., Kangasluoma, J., Kirkby, J., Laaksonen, A., Lehtipalo, K., Leiminger, M., Makhmutov, V., Mathot, S., Onnela, A., Petaja, T., Praplan, A. P., Riccobono, F., Rissanen, M. P., Rondo, L., Schobesberger, S., Seinfeld, J. H., Steiner, G., Tome, A., Trostl, J., Winkler, P. M., Williamson, C., Wimmer, D., Ye, P., Baltensperger, U., Carslaw, K. S., Kulmala, M., Worsnop, D. R., and Curtius, J. (2014), Neutral molecular cluster formation of sulfuric acid-dimethylamine observed in real time under atmospheric conditions, *Proceedings of the National Academy of Sciences of the United States of America*, 111(42), 15019-15024, doi:10.1073/pnas.1404853111.
- Kürten, A., Rondo, L., Ehrhart, S., and Curtius, J. (2011), Performance of a corona ion source for measurement of sulfuric acid by chemical ionization mass spectrometry, *Atmospheric Measurement Techniques*, 4(3), 437-443, doi:10.5194/amt-4-437-2011.
- Kirkby, J., Curtius, J., Almeida, J., Dunne, E., Duplissy, J., Ehrhart, S., Franchin, A., Gagné, S., Ickes, L., Kürten, A., Kupc, A., Metzger, A., Riccobono, F., Rondo, L., Schobesberger, S., Tsagkogeorgas, G., Wimmer, D., Amorim, A., Bianchi, F., Breitenlechner, M., David, A., Dommen, J., Downard, A., Ehn, M., Flagan, R. C., Haider, S., Hansel, A., Hauser, D., Jud,

Chapter II: Experimental methods

- W., Junninen, H., Kreissl, F., Kvashin, A., Laaksonen, A., Lehtipalo, K., Lima, J., Lovejoy, E. R., Makhmutov, V., Mathot, S., Mikkilä, J., Minginette, P., Mogo, S., Nieminen, T., Onnela, A., Pereira, P., Petäjä, T., Schnitzhofer, R., Seinfeld, J. H., Sipilä, M., Stozhkov, Y., Stratmann, F., Tomé, A., Vanhanen, J., Viisanen, Y., Vrtala, A., Wagner, P. E., Walther, H., Weingartner, E., Wex, H., Winkler, P. M., Carslaw, K. S., Worsnop, D. R., Baltensperger, U., and Kulmala, M. (2011), Role of sulphuric acid, ammonia and galactic cosmic rays in atmospheric aerosol nucleation, *Nature*, 476(7361), 429-433, doi:10.1038/nature10343.
- Kirkby, J., Duplissy, J., Sengupta, K., Frege, C., Gordon, H., Williamson, C., Heinritzi, M., Simon, M., Yan, C., Almeida, J., Tröstl, J., Nieminen, T., Ortega, I. K., Wagner, R., Adamov, A., Amorim, A., Bernhammer, A.-K., Bianchi, F., Breitenlechner, M., Brilke, S., Chen, X., Craven, J., Dias, A., Ehrhart, S., Flagan, R. C., Franchin, A., Fuchs, C., Guida, R., Hakala, J., Hoyle, C. R., Jokinen, T., Junninen, H., Kangasluoma, J., Kim, J., Krapf, M., Kürten, A., Laaksonen, A., Lehtipalo, K., Makhmutov, V., Mathot, S., Molteni, U., Onnela, A., Peräkylä, O., Piel, F., Petäjä, T., Praplan, A. P., Pringle, K., Rap, A., Richards, N. A. D., Riipinen, I., Rissanen, M. P., Rondo, L., Sarnela, N., Schobesberger, S., Scott, C. E., Seinfeld, J. H., Sipilä, M., Steiner, G., Stozhkov, Y., Stratmann, F., Tomé, A., Virtanen, A., Vogel, A. L., Wagner, A. C., Wagner, P. E., Weingartner, E., Wimmer, D., Winkler, P. M., Ye, P., Zhang, X., Hansel, A., Dommen, J., Donahue, N. M., Worsnop, D. R., Baltensperger, U., Kulmala, M., Carslaw, K. S., and Curtius, J. (2016), Ion-induced nucleation of pure biogenic particles, *Nature*, 533, 521, doi:10.1038/nature17953.
- Knopf, D. A., Poschl, U., and Shiraiwa, M. (2015), Radial diffusion and penetration of gas molecules and aerosol particles through laminar flow reactors, denuders, and sampling tubes, *Analytical chemistry*, 87(7), 3746-3754, doi:10.1021/ac5042395.
- Kupc, A., Amorim, A., Curtius, J., Danielczok, A., Duplissy, J., Ehrhart, S., Walther, H., Ickes, L., Kirkby, J., Kürten, A., Lima, J. M., Mathot, S., Minginette, P., Onnela, A., Rondo, L., and Wagner, P. E. (2011), A fibre-optic UV system for H₂SO₄ production in aerosol chambers causing minimal thermal effects, *Journal of Aerosol Science*, 42(8), 532-543, doi:10.1016/j.jaerosci.2011.05.001.
- Lee, B. H., Lopez-Hilfiker, F. D., Mohr, C., Kurten, T., Worsnop, D. R., and Thornton, J. A. (2014), An iodide-adduct high-resolution time-of-flight chemical-ionization mass spectrometer: application to atmospheric inorganic and organic compounds, *Environmental science & technology*, 48(11), 6309-6317, doi:10.1021/es500362a.
- Lee, B. H., Mohr, C., Lopez-Hilfiker, F. D., Lutz, A., Hallquist, M., Lee, L., Romer, P., Cohen, R. C., Iyer, S., Kurtén, T., Hu, W., Day, D. A., Campuzano-Jost, P., Jimenez, J. L., Xu, L., Ng, N. L., Guo, H., Weber, R. J., Wild, R. J., Brown, S. S., Koss, A., de Gouw, J., Olson, K., Goldstein, A. H., Seco, R., Kim, S., McAvey, K., Shepson, P. B., Starn, T., Baumann, K., Edgerton, E. S., Liu, J., Shilling, J. E., Miller, D. O., Brune, W., Schobesberger, S., D'Ambro, E. L., and Thornton, J. A. (2016), Highly functionalized organic nitrates in the southeast United States: Contribution to secondary organic aerosol and reactive nitrogen budgets, *Proceedings of the National Academy of Sciences*, 113(6), 1516-1521, doi:10.1073/pnas.1508108113.
- Lopez-Hilfiker, F. D., Mohr, C., Ehn, M., Rubach, F., Kleist, E., Wildt, J., Mentel, T. F., Lutz, A., Hallquist, M., Worsnop, D., and Thornton, J. A. (2014), A novel method for online analysis of gas and particle composition: description and evaluation of a Filter Inlet for Gases and

Chapter II: Experimental methods

- AEROSols (FIGAERO), *Atmospheric Measurement Techniques*, 7(4), 983-1001, doi:10.5194/amt-7-983-2014.
- Praplan, A. P., Schobesberger, S., Bianchi, F., Rissanen, M. P., Ehn, M., Jokinen, T., Junninen, H., Adamov, A., Amorim, A., Dommen, J., Duplissy, J., Hakala, J., Hansel, A., Heinritzi, M., Kangasluoma, J., Kirkby, J., Krapf, M., Kürten, A., Lehtipalo, K., Riccobono, F., Rondo, L., Sarnela, N., Simon, M., Tomé, A., Tröstl, J., Winkler, P. M., Williamson, C., Ye, P., Curtius, J., Baltensperger, U., Donahue, N. M., Kulmala, M., and Worsnop, D. R. (2015), Elemental composition and clustering behaviour of α -pinene oxidation products for different oxidation conditions, *Atmospheric Chemistry and Physics*, 15(8), 4145-4159, doi:10.5194/acp-15-4145-2015.
- Riedel, T. P., Bertram, T. H., Crisp, T. A., Williams, E. J., Lerner, B. M., Vlasenko, A., Li, S.-M., Gilman, J., de Gouw, J., Bon, D. M., Wagner, N. L., Brown, S. S., and Thornton, J. A. (2012), Nitryl Chloride and Molecular Chlorine in the Coastal Marine Boundary Layer, *Environmental science & technology*, 46(19), 10463-10470, doi:10.1021/es204632r.
- Rissanen, M. P., Mikkilä, J., Iyer, S., and Hakala, J. (2019), Multi-scheme chemical ionization inlet (MION) for fast switching of reagent ion chemistry in atmospheric pressure chemical ionization mass spectrometry (CIMS) applications, *Atmospheric Measurement Techniques*, 12(12), 6635-6646, doi:10.5194/amt-12-6635-2019.
- Riva, M., Brüggemann, M., Li, D., Perrier, S., George, C., Herrmann, H., and Berndt, T. (2020), Capability of CI-Orbitrap for Gas-Phase Analysis in Atmospheric Chemistry: A Comparison with the CI-APi-TOF Technique, *Analytical chemistry*, 92(12), 8142-8150, doi:10.1021/acs.analchem.0c00111.
- Riva, M., Ehn, M., Li, D., Tomaz, S., Bourgain, F., Perrier, S., and George, C. (2019a), CI-Orbitrap: An Analytical Instrument To Study Atmospheric Reactive Organic Species, *Analytical chemistry*, 91(15), 9419-9423, doi:10.1021/acs.analchem.9b02093.
- Riva, M., Rantala, P., Krechmer, J. E., Peräkylä, O., Zhang, Y., Heikkinen, L., Garmash, O., Yan, C., Kulmala, M., Worsnop, D., and Ehn, M. (2019b), Evaluating the performance of five different chemical ionization techniques for detecting gaseous oxygenated organic species, *Atmospheric Measurement Techniques*, 12(4), 2403-2421, doi:10.5194/amt-12-2403-2019.
- Sanchez, J., Tanner, D. J., Chen, D., Huey, L. G., and Ng, N. L. (2016), A new technique for the direct detection of HO₂ radicals using bromide chemical ionization mass spectrometry (Br-CIMS): initial characterization, *Atmospheric Measurement Techniques*, 9(8), 3851-3861, doi:10.5194/amt-9-3851-2016.
- Simon, M., Dada, L., Heinritzi, M., Scholz, W., Stolzenburg, D., Fischer, L., Wagner, A. C., Kürten, A., Rörup, B., He, X.-C., Almeida, J., Baalbaki, R., Baccarini, A., Bauer, P. S., Beck, L., Bergen, A., Bianchi, F., Bräkling, S., Brilke, S., Caudillo, L., Chen, D., Chu, B., Dias, A., Draper, D. C., Duplissy, J., El-Haddad, I., Finkenzeller, H., Frege, C., Gonzalez-Carracedo, L., Gordon, H., Granzin, M., Hakala, J., Hofbauer, V., Hoyle, C. R., Kim, C., Kong, W., Lamkaddam, H., Lee, C. P., Lehtipalo, K., Leiminger, M., Mai, H., Manninen, H. E., Marie, G., Marten, R., Mentler, B., Molteni, U., Nichman, L., Nie, W., Ojdanic, A., Onnela, A., Partoll, E., Petäjä, T., Pfeifer, J., Philippov, M., Quéléver, L. L. J., Ranjithkumar, A., Rissanen, M. P., Schallhart, S., Schobesberger, S., Schuchmann, S., Shen, J., Sipilä, M., Steiner, G., Stozhkov, Y., Tauber, C., Tham, Y. J., Tomé, A. R., Vazquez-Pufleau, M., Vogel, A. L., Wagner, R., Wang, M., Wang, D. S., Wang, Y., Weber, S. K., Wu, Y., Xiao, M., Yan, C., Ye, P., Ye, Q., Zauner-Wieczorek, M., Zhou, X., Baltensperger, U., Dommen,

Chapter II: Experimental methods

- J., Flagan, R. C., Hansel, A., Kulmala, M., Volkamer, R., Winkler, P. M., Worsnop, D. R., Donahue, N. M., Kirkby, J., and Curtius, J. (2020), Molecular understanding of new-particle formation from α -pinene between -50 and $+25$ °C, *Atmospheric Chemistry and Physics*, 20(15), 9183-9207, doi:10.5194/acp-20-9183-2020.
- Snow, J. (2014), The environmental, elemental and proteomic plasticity of Trichodesmium in the (sub) tropical atlantic.
- Veres, P., Roberts, J. M., Warneke, C., Welsh-Bon, D., Zahniser, M., Herndon, S., Fall, R., and de Gouw, J. (2008), Development of negative-ion proton-transfer chemical-ionization mass spectrometry (NI-PT-CIMS) for the measurement of gas-phase organic acids in the atmosphere, *International Journal of Mass Spectrometry*, 274(1-3), 48-55, doi:10.1016/j.ijms.2008.04.032.
- Voigtlander, J., Duplissy, J., Rondo, L., Kürten, A., and Stratmann, F. (2012), Numerical simulations of mixing conditions and aerosol dynamics in the CERN CLOUD chamber, *Atmospheric Chemistry and Physics*, 12(4), 2205-2214, doi:10.5194/acp-12-2205-2012.
- Wang, M., Chen, D., Xiao, M., Ye, Q., Stolzenburg, D., Hofbauer, V., Ye, P., Vogel, A. L., Mauldin, R. L., 3rd, Amorim, A., Baccarini, A., Baumgartner, B., Brilke, S., Dada, L., Dias, A., Duplissy, J., Finkenzeller, H., Garmash, O., He, X. C., Hoyle, C. R., Kim, C., Kvashnin, A., Lehtipalo, K., Fischer, L., Molteni, U., Petaja, T., Pospisilova, V., Quelever, L. L. J., Rissanen, M., Simon, M., Tauber, C., Tome, A., Wagner, A. C., Weitz, L., Volkamer, R., Winkler, P. M., Kirkby, J., Worsnop, D. R., Kulmala, M., Baltensperger, U., Dommen, J., El-Haddad, I., and Donahue, N. M. (2020a), Photo-oxidation of Aromatic Hydrocarbons Produces Low-Volatility Organic Compounds, *Environmental science & technology*, 54(13), 7911-7921, doi:10.1021/acs.est.0c02100.
- Wang, M., Kong, W., Marten, R., He, X.-C., Chen, D., Pfeifer, J., Heitto, A., Kontkanen, J., Dada, L., Kürten, A., Yli-Juuti, T., Manninen, H. E., Amanatidis, S., Amorim, A., Baalbaki, R., Baccarini, A., Bell, D. M., Bertozi, B., Bräkling, S., Brilke, S., Murillo, L. C., Chiu, R., Chu, B., De Menezes, L.-P., Duplissy, J., Finkenzeller, H., Carracedo, L. G., Granzin, M., Guida, R., Hansel, A., Hofbauer, V., Krechmer, J., Lehtipalo, K., Lamkaddam, H., Lampimäki, M., Lee, C. P., Makhmutov, V., Marie, G., Mathot, S., Mauldin, R. L., Mentler, B., Müller, T., Onnela, A., Partoll, E., Petäjä, T., Philippov, M., Pospisilova, V., Ranjithkumar, A., Rissanen, M., Rörup, B., Scholz, W., Shen, J., Simon, M., Sipilä, M., Steiner, G., Stolzenburg, D., Tham, Y. J., Tomé, A., Wagner, A. C., Wang, D. S., Wang, Y., Weber, S. K., Winkler, P. M., Wlasits, P. J., Wu, Y., Xiao, M., Ye, Q., Zauner-Wieczorek, M., Zhou, X., Volkamer, R., Riipinen, I., Dommen, J., Curtius, J., Baltensperger, U., Kulmala, M., Worsnop, D. R., Kirkby, J., Seinfeld, J. H., El-Haddad, I., Flagan, R. C., and Donahue, N. M. (2020b), Rapid growth of new atmospheric particles by nitric acid and ammonia condensation, *Nature*, 581(7807), 184-189, doi:10.1038/s41586-020-2270-4.
- Wu, R., Vereecken, L., Tsiligiannis, E., Kang, S., Albrecht, S. R., Hantschke, L., Zhao, D., Novelli, A., Fuchs, H., Tillmann, R., Hohaus, T., Carlsson, P. T. M., Shenolikar, J., Bernard, F., Crowley, J. N., Fry, J. L., Brownwood, B., Thornton, J. A., Brown, S. S., Kiendler-Scharr, A., Wahner, A., Hallquist, M., and Mentel, T. F. (2021), Molecular composition and volatility of multi-generation products formed from isoprene oxidation by nitrate radical, *Atmospheric Chemistry and Physics*, 21(13), 10799-10824, doi:10.5194/acp-21-10799-2021.

Chapter II: Experimental methods

- Yuan, B., Koss, A., Warneke, C., Gilman, J. B., Lerner, B. M., Stark, H., and de Gouw, J. A. (2016), A high-resolution time-of-flight chemical ionization mass spectrometer utilizing hydronium ions (H_3O^+ ToF-CIMS) for measurements of volatile organic compounds in the atmosphere, *Atmospheric Measurement Techniques*, 9(6), 2735-2752, doi:10.5194/amt-9-2735-2016.
- Zaytsev, A., Breitenlechner, M., Koss, A. R., Lim, C. Y., Rowe, J. C., Kroll, J. H., and Keutsch, F. N. (2019), Using collision-induced dissociation to constrain sensitivity of ammonia chemical ionization mass spectrometry (NH_4^+ CIMS) to oxygenated volatile organic compounds, *Atmospheric Measurement Techniques*, 12(3), 1861-1870, doi:10.5194/amt-12-1861-2019.
- Zuth, C., Vogel, A. L., Ockenfeld, S., Huesmann, R., and Hoffmann, T. (2018), Ultrahigh-Resolution Mass Spectrometry in Real Time: Atmospheric Pressure Chemical Ionization Orbitrap Mass Spectrometry of Atmospheric Organic Aerosol, *Analytical chemistry*, 90(15), 8816-8823, doi:10.1021/acs.analchem.8b00671.

Chapter III: CI-Orbitrap: An Analytical
Instrument To Study Atmospheric
Reactive Organic Species

Chapter III: CI-Orbitrap: An Analytical Instrument To Study Atmospheric Reactive Organic Species

This chapter summarized the analytical developments performed with the CI-Orbitrap. The results presented here were published in *Anal. Chem.*, 2019, DOI: 10.1021/acs.analchem.9b02093 and *Anal. Chem.*, 2020, DOI: 10.1021/acs.analchem.0c00111

III.1. Introduction

Atmospheric aerosols, a mixture of solid and liquid particles of organic and inorganic substances suspended in the air, make up less than a millionth of a percent of the atmosphere, yet they still produce a significant cooling effect on our planet. They do this in two ways: by directly reflecting solar radiation back into space, and by acting as nuclei for cloud droplet formation, whereby they regulate cloud reflectivity and lifetimes (Albrecht, 1989; Rosenfeld et al., 2008). Typically, only particles larger than 100 nm in diameter result in cloud condensation nuclei, and therefore the chemical components and the processes contributing to the growth of such particles are extremely important. Atmospheric aerosols are also recognized to adversely impact air quality and human health, representing nowadays the fifth-ranking human health risk factor, globally (Gakidou et al., 2017).

Depending on the geographic region, organic aerosol on average contributes 20-90% to the submicron aerosol mass (Jimenez et al., 2009), with secondary organic aerosol (SOA) as the largest source of atmospheric organic aerosol (Hallquist et al., 2009; Jimenez et al., 2009). The organic vapors able to grow aerosols by gas-to-particle conversion, thus forming SOA, are primarily formed through the oxidation of volatile organic compounds (VOC), yielding a wide variety of oxygenated VOC (OVOC) (Hallquist et al., 2009). Characterization of all these OVOC represents a unique analytical challenge (Glasius & Goldstein, 2016; Goldstein & Galbally, 2007). Over the last five years, major breakthroughs have been achieved within the field of atmospheric oxidation processes and aerosol particle formation (Berndt et al., 2015; Bianchi et al., 2019; Ehn et al., 2014; Jokinen et al., 2014). A pivotal starting point was the identification of highly oxygenated organic molecules (HOM) (Ehn et al., 2014), formed through a process called autoxidation (Crounse et al., 2013). In this process, peroxy radicals formed from the oxidation of a VOC undergo intramolecular hydrogen abstraction, followed by the addition of molecular oxygen. This results in the formation of a new peroxy radical, with an additional hydroperoxy group. This chain reaction can be repeated and lead to a wide variety of products depending on the termination mechanisms (Bianchi et al., 2019). HOM have been shown to contribute to the nucleation and growth of new particles both in atmospheric simulation chambers and in the atmosphere (Bianchi et al., 2019; Tröstl et al., 2016). However, a complete understanding of how VOC oxidation processes contribute to new particle

and SOA formation is still lacking, and the quantitative evaluation of the impact of aerosol on air quality and climate remains poorly understood (Glasisius & Goldstein, 2016).

Over the last ten years, mass spectrometric techniques have made dramatic improvements in detecting and characterizing gas-phase oxygenated species, including radicals, of varying volatilities (Donahue et al., 2011; Kurtén et al., 2016). In particular, chemical ionization mass spectrometry (CIMS) has emerged as a powerful tool to characterize a wide range of different gaseous compounds (Berndt et al., 2018; Bianchi et al., 2019; Lee et al., 2014; Riva et al., 2019). CI is a soft ionization technique where the analyte is ionized through clustering process with the reagent ions and undergoes only minimal fragmentation or via proton transfer processes (Crounse et al., 2006; Jokinen et al., 2012; Lee et al., 2014). As part of the rapid development, multiple reagent ion schemes have been tested over the last few years. Due to the improvements in sensitivity and/or selectivity, a wide variety of oxygenated species, including RO₂ radicals and stabilized Criegee intermediates, can now be directly analyzed (Berndt et al., 2015; Berndt et al., 2018b; Breitenlechner et al., 2017; Krechmer et al., 2018). While CIMS provides very good sensitivities (detection limit as low as 10⁴ molecules cm⁻³) (Jokinen et al., 2012), they are commonly coupled to TOF mass analyzers having limited mass resolving power. This typically ranges from 4000 for a medium-resolution (e.g., the Tofwerk AG HTOF) to 14 000 for a high-performance TOF (e.g., Tofwerk AG LTOF) (Riva et al., 2019). These resolving powers make identification and quantification of individual organic molecules extremely challenging in cases with multiple overlapping ions, yielding significant uncertainties (Cubison & Jimenez, 2015; Riva et al., 2019; Stark et al., 2015). Indeed, “atmospheric” mass spectra acquired using the CIMS technique typically contain a large amount of information, and therefore remain complex in nature, representing a significant challenge for data analysis. Computational approaches, including ion deconvolution procedures, are required to solve this limitation in order to extract the maximum possible information content (Cubison & Jimenez, 2015; Meija & Caruso, 2004).

In this work, we successfully coupled a high-resolution mass spectrometer (Orbitrap) with a CI source to overcome many current instrumental limitations. The CI-Orbitrap combines the benefits of soft atmospheric pressure ionization, high mass resolving power ($R = 140\ 000$ at m/z 200), and high time resolution (~10 s). As a proof of concept, we analyzed gas-phase OVOC formed during the oxidation of two monoterpenes using nitrate-ion-based (NO₃⁻) chemical

ionization in an oxidation flow reactor. We used this chemistry as it has been shown to be highly selective towards atmospheric reactive species, including HOM (Bianchi et al., 2019; Riva et al., 2019). We characterized the time evolution of the HOM under varying VOC precursor, O₃, and NO_x concentrations.

In addition, the sensitivity, as well as the linearity of the CI-Orbitrap with different reagent ions operated in the positive or negative mode, were determined and compared to those of the CI-APi-TOF. To do so, we performed the first side-by-side comparison between a CI-Orbitrap and a CI-APi-TOF applying two different chemical ionization schemes, i.e., the acetate-ion-based (CH₃COO⁻) (Berndt et al., 2015; Berndt et al., 2018) and the aminium-ion-based (n-C₃H₇NH₃⁺) (Berndt et al., 2015) product ionization in a free-jet system designed to probe the early stage of a given reaction. Very low concentrations of RO₂ radicals and OVOCs are produced from the ozone and OH radical initiated oxidation of α -pinene in order to ascertain the benefit and the limitation of the CI-Orbitrap.

III.2. Experimental section

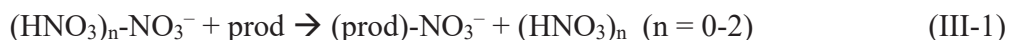
For this study, the chemical composition of the oxygenated products was retrieved in real time by a Q-Exactive Orbitrap Plus mass spectrometer (Thermo Scientific) coupled with a chemical ionization (CI) inlet (Figure II-5, 6). While the design of the CI inlet is based on that of Eisele and Tanner (1993), we constructed a special connector flange as well as optimized the dimensions of the CI inlet for coupling to the Orbitrap (Figure II-5), details in Chapter II.2. The Eisele-type inlet minimizes the wall losses through the use of coaxial sample and sheath flows, facilitating the characterization of (extremely) low-volatile and radical species. The results presented here are coming from two systems-oxidation Flow Reactor for the first characterization of CI-Orbitrap and Free-Jet Flow System for a side-by-side comparison between CI-Orbitrap and a CI-APi-TOF. And the parameters used for the mass spectrometers are mentioned in the corresponding sections below.

III.2.1. Oxidation Flow Reactor

The ozonolysis experiments were conducted at room temperature and atmospheric pressure in an oxidation flow reactor and in the absence of an OH scavenger. The reactor was a ~18-litres Pyrex glass tube (12 cm i.d. \times 158 cm length), which has been described in more detail previously (Aregahegn et al., 2013). The total flow rate of synthetic air (N₂/O₂ 80:20) was set at 15 liter per

minute (L/min) giving an average residence time of 72 seconds. Ozone, generated by an ozone generator (Fisher Scientific, SOG-1) was continuously injected into the flow tube. For the experiments performed in the presence of nitrogen oxides (NO_x), nitric oxide (NO) was added into the flow tube reactor. The concentrations of ozone (initial concentration 40 ppb) and NO (ranging from 0 to 1.8 ppb) were measured using a Thermo 49C and an Ecophysics CLD 88p equipped with a photolytic converter PLC 860, respectively. Concentrations of limonene varied from 0.4 to 2 ppm and α -pinene from 1 to 4 ppm, both measured using a proton transfer reaction time-of-flight mass spectrometer (PTR-TOF 8000, Ionicon Analytik GmbH).

NO_3^- reagent ions were used to characterize HOMs due to its high sensitivity and selectivity in this system. NO_3^- ions were generated by passing clean air (10 mL/min) containing nitric acid through a soft X-ray photoionizer (Hamamatsu, L9491) and guided into the sample flow by an electric field. RO_2 radicals as well as closed-shell products, called “prod” for all together, were charged by binding to the nitrate ion clusters $(\text{HNO}_3)_n(\text{NO}_3^-)$, $n = 0-2$ according to the following reaction (III-1). The interaction time between NO_3^- ions and the sample was approximately 200 ms.



It is important to mention that the absolute calibration of the detected oxygenated products is impossible due to a lack of authentic reference substances for RO_2 radicals and the majority of closed-shell products. Thus, the product signals were normalized to the sum of the reagent ions, i.e., $\Sigma[(\text{HNO}_3)_n-\text{NO}_3^- (n = 0-2)]$.

The Q Exactive Orbitrap mass spectrometers have been described elsewhere (Michalski et al., 2011) and recently used for online measurements of atmospheric gases and particles (Brüggemann et al., 2017; Zuth et al., 2018). The Q Exactive has a high mass resolving power of 140 000 (at m/z 200), allowing an accurate identification of a wide variety of species at a time resolution of 10 s. The instrument was operated in negative mode, scanning from m/z 50 to 750 with a scan rate of 0.2 scans/s. External mass calibration of the Q Exactive mass spectrometer was performed using the traditional electrospray ionization source by using a 2 mM sodium acetate solution. This approach provided a suite of negative adduct ions in the desired mass range. The high-resolution

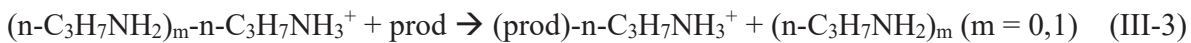
data were analyzed by XCalibur 2.2 (Thermo Scientific) software package to determine accurate formula and the abundance of the compounds of interest.

III.2.2. Free-Jet Flow System

Ozonolysis and OH radical initiated oxidation of α -pinene ($C_{10}H_{16}$) were performed under dry conditions ($RH < 0.1\%$) in a free-jet flow system at a temperature of 297 ± 1 K and atmospheric pressure (Berndt et al., 2015; Berndt et al., 2018). This flow system allows the investigation of VOC oxidation under atmospheric conditions with negligible wall effects and a reaction time of 7.9 s. Ozone produced from a low-pressure mercury lamp or isopropyl nitrite (IPN) was premixed with air (5 L/min (STP)) and injected through the inner tube into the main gas stream (95 L/min (STP)) containing α -pinene diluted in air. Ozonolysis experiments (dark reaction) were performed in the absence of an OH scavenger, i.e., the in-situ OH radical formation from ozonolysis led to a combined $O_3/OH + \alpha$ -pinene reaction. In the pure OH experiments based on IPN photolysis, 8 NARVA 36W Blacklight Blue lamps were used for illuminating the flow system. All gas flows were set by means of calibrated gas flow controllers (MKS 1259/1179). The concentration of α -pinene was maintained at 5.0×10^{11} molecules cm^{-3} , while ozone and IPN were ramping up from 2.5×10^{10} to 5.6×10^{11} and from 1.7×10^{10} to 6.7×10^{11} molecules cm^{-3} , respectively.

The chemical composition of the oxygenated products was retrieved in real time by a Q-Exactive Orbitrap Plus mass spectrometer and a chemical ionization - atmospheric pressure interface - time-of-flight mass spectrometer (CI-APi-TOF, Tofwerk AG). Both instruments have been described elsewhere and were equipped with a similar Eisele-type inlet (Eisele and Tanner, 1993; Jokinen et al., 2012; Michalski et al., 2011; Zuth et al., 2018). While the CI inlet mounted on the APi-TOF is manufactured by Airmodus (Finland), the CI inlet installed on the Orbitrap is a home-built version with minor modifications regarding to the commercially available inlet (Figure II-5). The sample flow rate for both instruments was set at ~ 10 L/min (STP). Protonated n-propylamine ($n-C_3H_7NH_3^+$) or acetate (CH_3COO^-) ions were produced using an X-ray source or an Am-241 source for the Orbitrap and the APi-TOF, respectively.

The reagent ions were $(CH_3COOH)_n-CH_3COO^-$ ($n = 0,1$) and $(n-C_3H_7NH_2)_m-n-C_3H_7NH_3^+$ ($m = 0,1$) in the negative and positive mode, respectively. The sample molecules were detected as clusters with the respective reagent ions according to the following reactions (III-2) and (III-3):



Similarly, the product signals of both mass spectrometers were normalized to the sum of the reagent ions, i.e., $\Sigma[(\text{CH}_3\text{COOH})_n\text{-CH}_3\text{COO}^- \quad (n = 0,1)]$ or $\Sigma[(\text{n-C}_3\text{H}_7\text{NH}_2)_m\text{-n-C}_3\text{H}_7\text{NH}_3^+ \quad (m = 0,1)]$. The resulting normalized signals were used for the comparison in order to evaluate the performance of both techniques.

The Q Exactive Plus Orbitrap (Orbitrap-Tropos) was used in positive (i.e., $\text{n-C}_3\text{H}_7\text{NH}_3^+$) and negative mode (i.e., CH_3COO^-) and connected to a free-jet flow system. The Q Exactive Orbitrap in Oxidation Flow Reactor system (Orbitrap-IRCELYON) was solely used in negative mode (NO_3^-) to determine the ion transmission and to develop the linearity correction. Both CI-Orbitrap and CI-APi-TOF instruments were operated using the same settings and were run in full scan mode, allowing the identification of a wide variety of species. The instruments were operated in negative or positive mode with an automatic gain control (AGC) target of 1×10^5 charges, a maximum injection time of 1 s. Spectra were averaged of 5 microscans (1 microscan corresponding to 1 ion injection). The stacked-ring ion guide (or S-Lens) is a radio frequency (RF) device efficiently capturing and focusing the ions into a tight beam. As previously described it contains a series of electrodes where voltages are applied in order to focus the ions. The S-lens level was maintained at 60%, to maximize ion transmission and the limit of detection. The C-Trap consist of a RF-based ion collecting trap (Figure II-7), which is automatically controlled by the AGC (automatic gain control) in order to prevent space-charge effect. In order to evaluate the impact of the number of charges collected in the C-trap, the AGC target of the Orbitrap-Tropos instrument was scanned from 5×10^4 to 1×10^6 charges. External mass calibrations were performed prior to the experiments by injecting a 2 mM sodium acetate solution using an electrospray ionization source, providing a suite of negative and positive adduct ions in the desired mass range of m/z 59 – 700 Th.

III.3. Results and discussion

To highlight the features of this CI-Orbitrap, we focused our attention on the analysis of products from the ozonolysis of α -pinene and limonene, as they constitute a major fraction of the global monoterpene emissions (Messina et al., 2016). In addition, both systems have been previously studied (Ehn et al., 2014; Jokinen et al., 2015), which is a pivotal point to evaluate the performance

of the CI-Orbitrap and validate our results. Using the CI-Orbitrap, we characterized the formation of HOM spanning from m/z 250 to 650. HOM were detected as clusters with the reagent ions. Figure III-1 presents typical mass spectra obtained from the gas phase oxidation of both VOC with and without NO using NO_3^- reagent ion. As previously reported, NO_3^- -based chemistry is highly sensitive and selective towards HOM, including monomers ($\text{C}_{8-10}\text{H}_{14-18}\text{O}_{6-11}$), organonitrates ($\text{C}_{8-10}\text{H}_{11-17}\text{NO}_{6-11}$) and dimers ($\text{C}_{18-20}\text{H}_{26-34}\text{O}_{9-18}$), formed from the ozonolysis of monoterpenes.

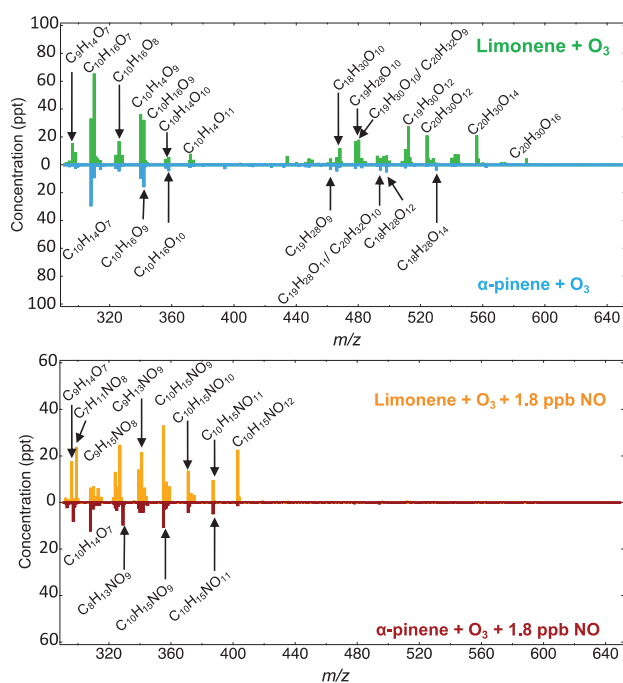


Figure III-1: Mass spectra of HOM formed from limonene and α -pinene ozonolysis without (upper) and with (lower) NO addition. HOM are detected as clusters with the nitrate (NO_3^-) ion and measured by the CI-Orbitrap. Concentration is reported in parts per trillion (i.e., 2.46×10^7 molecule cm^{-3}).

One main benefit of the CI-Orbitrap is the high mass resolving power, allowing unambiguous identification of the diverse products formed from a given reaction. As shown in Figure III-2, we are now able to accurately distinguish organonitrates and peroxy radicals (e.g., C₉H₁₃O₈N / C₁₀H₁₅O₈ at *m/z* 325.05344 / 325.06499 and C₉H₁₃O₁₀N / C₁₀H₁₅O₁₀ at *m/z* 357.04118 / 357.05382, respectively), which has often been impossible with typical CI-API-TOF instruments with HTOF

(mass resolving power ~ 5000) mass analyzers, and challenging even with LTOF (mass resolving power $\sim 10\,000$) mass analyzers.

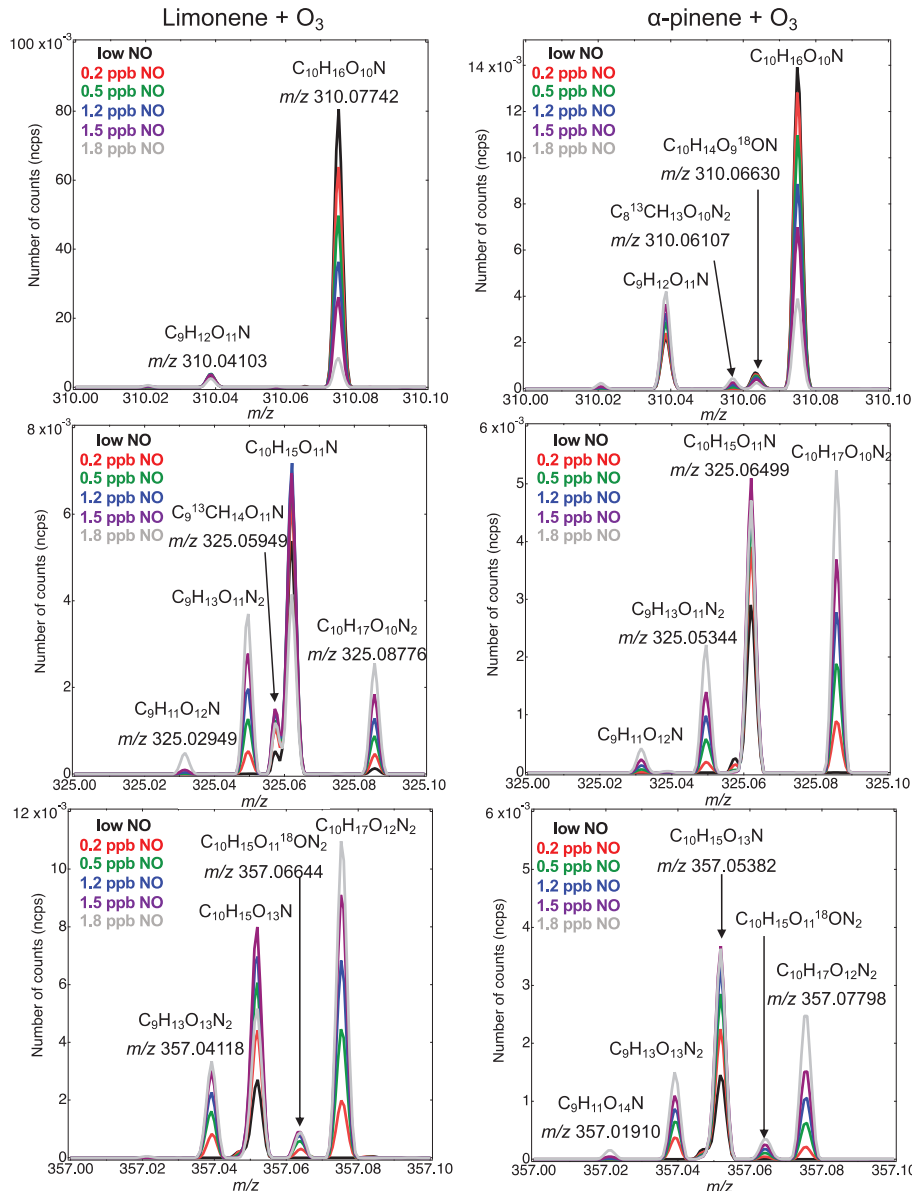


Figure III-2: Mass spectra of ions at m/z 310, 325 and 357 measured during the ozonolysis of limonene (left column) and α-pinene (right column) using different concentrations of NO. HOM are detected as clusters with the nitrate (NO₃⁻) ion and measured by the CI-Orbitrap.

To further illustrate the performance of the CI-Orbitrap compared to state-of-the-art CI-APi-TOF, we simulated the spectra of the latter at four ions, representing monomers (m/z 342),

organonitrate/peroxy radicals (m/z 325 and 357) and dimers (m/z 484). The CI-Orbitrap data for these ions are presented in Figure III-3, while the corresponding TOF data were generated using a mass resolving power of 10 000 (Figure III-3). It is evident that in most of these examples, the TOF instruments would struggle, while the CI-Orbitrap easily separated the ions of different elemental compositions. Further, a larger mass resolving power (i.e., narrower peak) helps to decrease the detection limit. In other words, less signal is required to reach above the background noise level of the instrument, providing additional confidence in the quantification of the products observed in very low abundance.

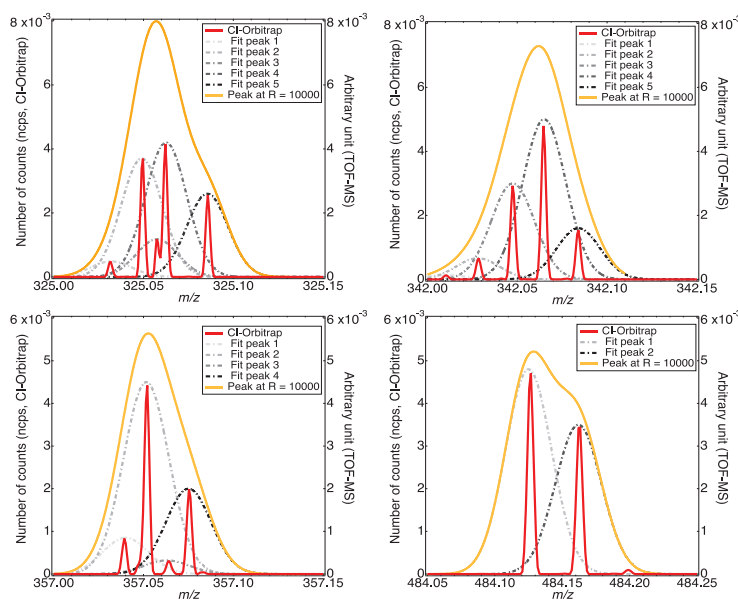


Figure III-3: Mass spectra (red) of different HOM, at m/z 325, 342, 357, and 484, measured by a nitrate CI-Orbitrap during limonene ozonolysis. The orange trace represents the spectrum that would be observed using an instrument with a mass resolving power of 10 000. Dashed lines stand for the fits of individual ions. The TOF-MS signals represent synthetic data using arbitrary units and do not aim at matching the surface area measured using the CI-Orbitrap.

Despite the wealth of studies using the Orbitrap technique, little is known about the capability of the Orbitrap in measuring compounds at extremely low concentrations. For example, it has been suggested that the Orbitrap can provide a non-linear response, potentially impacting isotope ratios, determination, and the quantification of compounds present at extremely low concentrations (Eiler et al., 2017). In view of these findings available from the literature, we evaluated the performance

of the CI-Orbitrap by comparing the measured vs. the theoretical isotopic intensities using product ions analyzed by the Orbitrap-Tropos using protonated n-propylamine ($n\text{-C}_3\text{H}_7\text{NH}_3^+$) and acetate (CH_3COO^-). To further estimate the impact of different reagent ions, results using the Orbitrap-IRCELYON (nitrate-ion based chemistry) are also compared here. In both cases, OVOCs were continuously generated either in the Oxidation Flow Reactor or in Free-Jet Flow System.

Hence, the abundance of the main OVOCs (e.g., $\text{C}_{10}\text{H}_{14,16}\text{O}_x$; $\text{C}_{20}\text{H}_{30,32}\text{O}_x$) and RO_2 radicals (e.g., $\text{C}_{10}\text{H}_{15,17}\text{O}_x$) at nominal masses M , $(M + 1)$ and $(M + 2)$, corresponding to their ^{13}C atom and ^{18}O atom fraction, were measured to cover a wide range of normalized product signals in the range of 5×10^{-7} to 5×10^{-2} . Signal intensities reported in Figure III-4A were obtained with an AGC target of 1×10^5 charges. As depicted in Figure III-4A, when the ratio is equal to 1.0 for normalized signal $> \sim 4 \times 10^{-4}$ to ($\sim 1 \times 10^6$ molecules cm^{-3}), the Orbitrap is providing a linear measure of the ion intensity. However, this ratio dropped significantly for normalized signals below $\sim 4 \times 10^{-4}$. Such a situation occurs when the ion intensity is close to the instrumental threshold, i.e., by using standard settings the Orbitrap mass analyzer records only signal if $\text{S/N} > 1.3$. The ion signals below this threshold are treated as undetected by the acquisition software. Due to the statistics, peaks with an average $\text{S/N} = 1.5$ for example will appear above this threshold only in a limited amount of cases reducing the resulting peak intensity (Makarov and Denisov, 2009). As a result, for a normalized signal smaller than 1×10^{-5} , the CI-Orbitrap only detects 5 – 10 % of the “true ion number distribution”. That means, using the instrumental parameters and the calibration factor employed here (1.85×10^9 molecules cm^{-3}) the limit of quantification (LoQ, corresponding to lowest normalized signal observed within the linear range) of the Orbitrap was evaluated to be $\sim 1 \times 10^6$ molecules cm^{-3} at a 10-minute integration time. It is worth pointing out that the limit of detection (LoD, corresponding to the lowest normalized signal observed) is likely one or two orders of magnitude lower than the LoQ but due to the lack of linearity, accurate numbers cannot be directly provided. By adjusting the AGC target the linear range can be shifted towards lower ion concentrations as shown in Figure III-4B. This can be explained by a larger number of ions trapped within the C-trap prior to the Orbitrap scan resulting in more ions entering the Orbitrap mass analyzer. This leads to an enhanced S/N ratio and better statistics. Hence, we have evaluated the impact of the AGC target (scanned from 5×10^4 to 1×10^6 charges) on the linearity and found that by optimizing the AGC target, the LoQ of the CI-Orbitrap is anticipated to be greatly extended.

However, as most of our previous experiments were performed using an AGC target of 1×10^5 charges, we kept this setting to perform the side-by-side comparison.

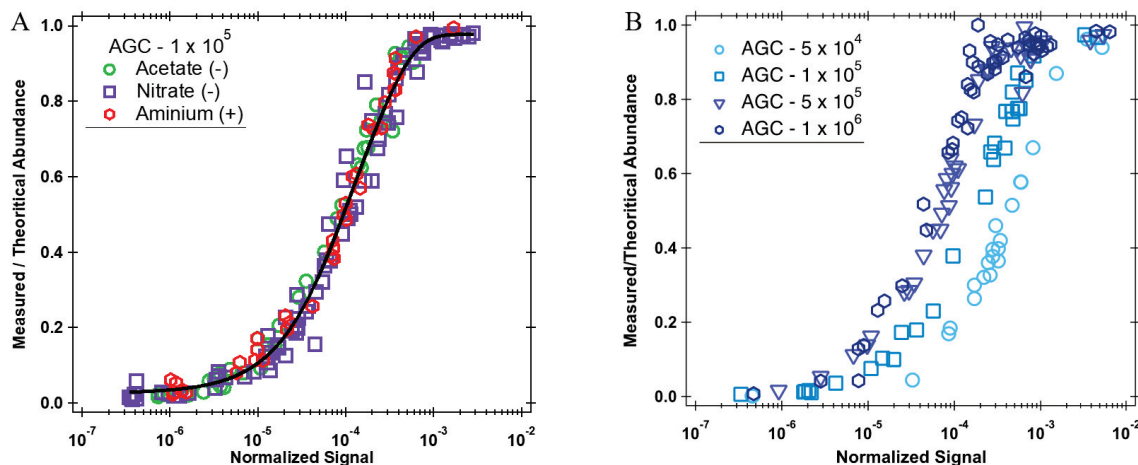


Figure III-4: (A) Linearity of the Orbitrap as a function of normalized signal measured with protonated n-propylamine ($n\text{-C}_3\text{H}_7\text{NH}_3^+$) and acetate (CH_3COO^-) reagent ions with the Orbitrap-Tropos and nitrate-ion based chemistry with the Orbitrap-IRCELYON, using identical parameter settings. All signal intensities were corrected with respect to the sum of $(\text{CH}_3\text{COOH})_n\text{-CH}_3\text{COO}^-$ ($n = 0,1$) at nominal 59 Th and 119 Th; to the sum of $(n\text{-C}_3\text{H}_7\text{NH}_2)_m\text{-n-C}_3\text{H}_7\text{NH}_3^+$ ($m = 0,1$) at nominal 60 Th and 119 Th; and to the sum of $(\text{HNO}_3)_p\text{-NO}_3^-$ ($p = 0,1,2$) at nominal 62, 125, 188 Th, for the respective reagent ions. The black fit is the “sigmoidal correction function” based on a sigmoidal fitting algorithm. (B) Impact of the AGC target on the linearity of the CI-Orbitrap-Tropos using aminium ($n\text{-C}_3\text{H}_7\text{NH}_3^+$) as the reagent ion.

To evaluate the performance of the CI-Orbitrap compared to the widely used CI-APi-TOF technique we directly performed side-by-side experiments. Both instruments sampled concurrently RO_2 radicals as well as OVOCs produced under well-controlled reaction conditions. We focused on the detection of RO_2 radicals produced from the oxidation of α -pinene. Figure III-5 shows the results of the OH radical-initiated oxidation of α -pinene. The OH radicals were generated by isopropyl nitrite (IPN) photolysis. The formation of the additional RO_2 radical $\text{HO-C}_{10}\text{H}_{15}(\text{OH})(\text{O}_2)\text{O}_2$ can be explained by the reaction of $\text{HO-C}_{10}\text{H}_{16}(\text{O}_2)_2\text{O}_2$ with NO and subsequent radical isomerization as discussed in a former study (Berndt et al., 2018). NO is formed from the IPN photolysis. In addition to the RO_2 radicals, also closed-shell products were detected including carbonyls and organic nitrates produced from the $\text{RO}_2 + \text{NO}$ reactions (Ziemann and Atkinson,

2012). Lastly, products arising from other bimolecular RO₂ reactions were not detected or were below the detection limit under the selected experimental conditions due to the relatively low RO₂ radical concentrations < 10⁸ molecules cm⁻³ and the very short reaction time of 7.9 s.

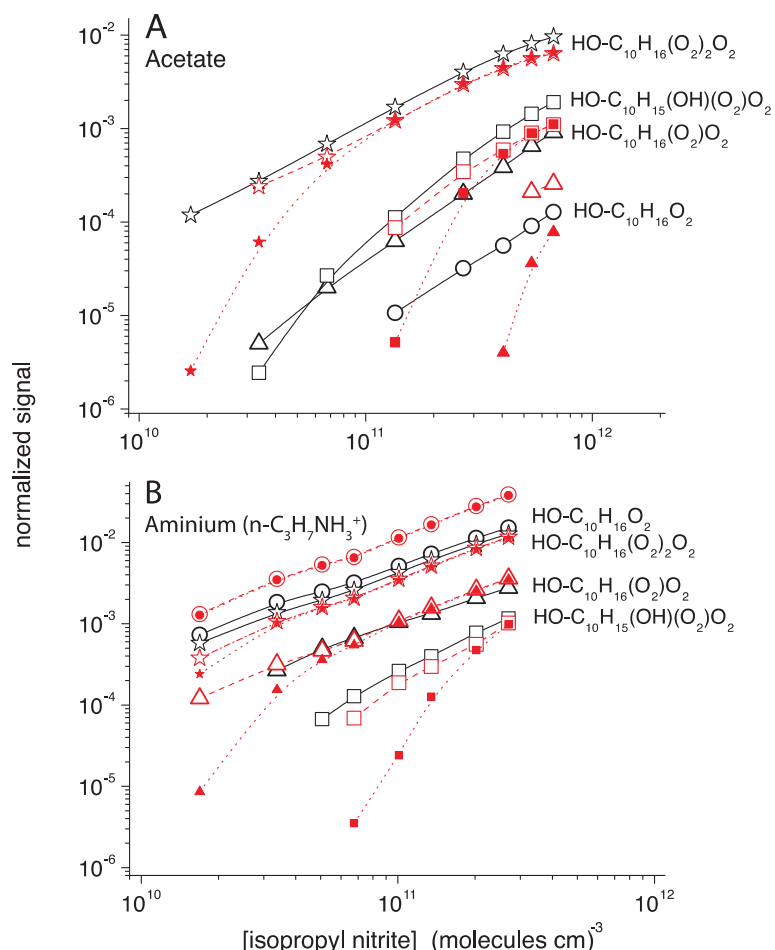


Figure III-5: Normalized signals of RO₂ radicals produced from the OH radical-initiated oxidation of α -pinene as a function of initial IPN concentration measured by the CI-APi-TOF (black) and the CI-Orbitrap (red). OH radicals have been formed via IPN photolysis. Full and open markers in red correspond to raw and corrected (using the sigmoidal correction function) signals measured with the Orbitrap, respectively. **(A)** Acetate and **(B)** aminium ($n\text{-C}_3\text{H}_7\text{NH}_3^+$) served as the reagent ion for otherwise identical reaction conditions in both cases.

As shown in Figure III-5, for uncorrected normalized intensities above $2\text{--}3 \times 10^{-4}$ (corresponding to $\sim 5\text{--}7 \times 10^5$ molecules cm⁻³) both techniques are in very good agreement. The

lack of linearity hampers the Orbitrap, unlike the APi-TOF, to accurately measure lower concentrations. However, this lack of linearity appears to be independent of the instrument and the type of reagent ions (Figure III-4A). This behavior indicates that this instrumental limitation can be overcome in order to retrieve the “correct” signal strength for peaks with the lowest signal intensity. Indeed, using all measurements from multiple experiments and reagent ions, a function named “sigmoidal correction function” based on a fitting algorithm using a characteristic sigmoidal shape can be determined. Therefore, raw normalized signals (corrected for sampling losses) measured with the CI-Orbitrap were further corrected using the “sigmoidal correction function”, see also Figure III-4. By applying this method, all the data were corrected (open markers), which greatly helps maintaining the good agreement between both techniques (Figure III-5). However, for uncorrected signal intensities below a threshold of $5 \times 10^{-6} - 1 \times 10^{-5}$ this approach results in an overestimation of the ion concentrations as the signal is likely very close to the noise level of the instrument. As a result, such data points were not included in Figure III-5. While the APi-TOF can further help correcting this lack of linearity we preferred to propose a method based only on the signal acquired by the Orbitrap. Hence, the LoD is likely an upper limit and might be even pushed further with appropriate and collocated instrumentations.

Overall, product signals measured by CI-Orbitrap and the CI-APi-TOF are mostly within a factor of 2 (Figure III-6), providing a good agreement between these two analytical techniques for corrected normalized signal intensity ranging from $\sim 5 \times 10^{-5}$ to 1×10^{-2} (corresponding to $\sim 1 \times 10^5$ to 2.5×10^8 molecules cm $^{-3}$). Exception are the measurements of highly oxidized products using acetate ionization. The reason for that is not clear at the moment. It is worth pointing out that the positive mode measurements were less impacted by the lack of linearity compared to negative mode measurements. This is explained by the fact that at a given product concentration, the resulting ion intensity measured by aminium ($n\text{-C}_3\text{H}_7\text{NH}_3^+$) ionization is much greater than for acetate ionization. In the case of the highest oxidized RO₂ radicals, i.e., HO-C₁₀H₁₆(O₂)₂O₂ and HO-C₁₀H₁₅(OH)(O₂)O₂ bearing -OH and -OOH moieties, the obtained corrected signal intensities are almost identical within a factor of two applying either acetate or aminium ($n\text{-C}_3\text{H}_7\text{NH}_3^+$) for product ionization. This fact is obviously due to strong binding of these RO₂ radicals to both reagent ions. Thus, a near-maximum detection sensitivity can be expected for these reagent ions (Berndt et al., 2019; Hyttinen et al., 2018). On the other hand, for the less oxidized RO₂ radicals HO-C₁₀H₁₆O₂

and HO-C₁₀H₁₆(O₂)O₂ the detection sensitivity based on aminium (n-C₃H₇NH₃⁺) ionization is definitely higher compared to acetate ionization, i.e., by a factor of 500 – 1000 in the case of HO-C₁₀H₁₆O₂ (Torsten Berndt et al., 2019).

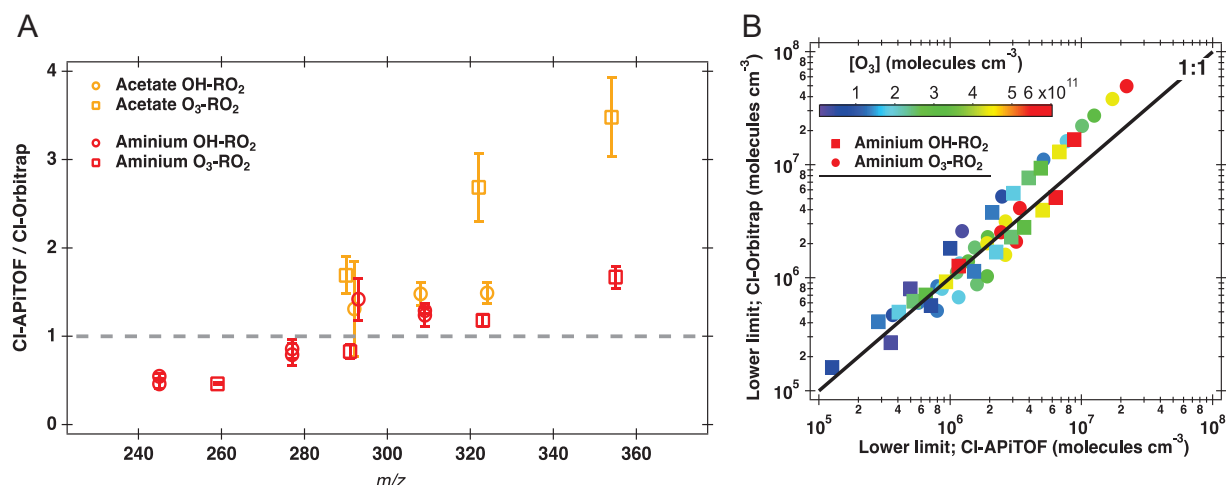


Figure III-6: (A) Comparison between lower limit RO₂ radical concentrations measured with the CI-APiTof and the CI-Orbitrap in the different experiments. (B) Correlation of the concentrations of OVOC and RO₂ radicals formed from the O₃/OH + α -pinene reaction measured by the CI-APiTof and the CI-Orbitrap using aminium (n-C₃H₇NH₃⁺) ionization.

III.4. Conclusion

In this work we demonstrated, the possibility of interfacing a CI inlet with an ultrahigh-resolution mass spectrometer. We showed its ability to unambiguously resolve all ions from the complex gas phase mixture generated from the oxidation of monoterpenes. We demonstrated the capability of the CI-Orbitrap in measuring RO₂ radicals as well as OVOCs at atmospherically relevant concentrations and compared them to simultaneous CI-APi-TOF measurements. We explored the current limitations of this new analytical technique and demonstrated that these can be partially overcome through a careful determination of a sigmoidal correction function. In addition, to unambiguously identify OVOCs formed in the gas phase, the analysis by means of the CI-Orbitrap can accurately quantify organic species at concentrations down to 1×10^5 molecules cm⁻³. This LoQ is \sim one order of magnitude higher in comparison to the APi-TOF used in this study. Overall, the combination of the high-mass resolving power of the Orbitrap and the high sensitivity of the

aminium/ammonium CI represents a powerful analytical tool that can improve our current knowledge regarding the complexity of the atmospheric gaseous composition. Thus, this new technique can help to answer some of the questions that so far were unable to be answered due to the pre-existing instrument limitations. In summary, the development of this new analytical instrument can be a pivotal step forward for an accurate understanding of the formation and fate of atmospheric reactive organic species.

III.5. References

- Albrecht, B. A. (1989). Aerosols, Cloud Microphysics, and Fractional Cloudiness. *Science*, 245(4923), 1227–1230. <https://doi.org/10.1126/science.245.4923.1227>.
- Aregahegn, K. Z., Nozière, B., & George, C. (2013). Organic aerosol formation photo-enhanced by the formation of secondary photosensitizers in aerosols. *Faraday Discussions*, 165, 123. <https://doi.org/10.1039/c3fd00044c>.
- Berndt, T., Hyttinen, N., Herrmann, H., and Hansel, A. (2019), First oxidation products from the reaction of hydroxyl radicals with isoprene for pristine environmental conditions, *Communications Chemistry*, 2(1), 21, doi:10.1038/s42004-019-0120-9.
- Berndt, T., Mentler, B., Scholz, W., Fischer, L., Herrmann, H., Kulmala, M., and Hansel, A. (2018), Accretion Product Formation from Ozonolysis and OH Radical Reaction of alpha-Pinene: Mechanistic Insight and the Influence of Isoprene and Ethylene, *Environmental science & technology*, 52(19), 11069-11077, doi:10.1021/acs.est.8b02210.
- Berndt, T., Richters, S., Kaethner, R., Voigtländer, J., Stratmann, F., Sipilä, M., Kulmala, M., & Herrmann, H. (2015). Gas-Phase Ozonolysis of Cycloalkenes: Formation of Highly Oxidized RO₂ Radicals and Their Reactions with NO, NO₂, SO₂, and Other RO₂ Radicals. *The Journal of Physical Chemistry A*, 119(41), 10336–10348. <https://doi.org/10.1021/acs.jpca.5b07295>.
- Berndt, T., Scholz, W., Mentler, B., Fischer, L., Herrmann, H., Kulmala, M., & Hansel, A. (2018). Accretion Product Formation from Self- and Cross-Reactions of RO₂ Radicals in the Atmosphere. *Angewandte Chemie International Edition*, 57(14), 3820–3824. <https://doi.org/10.1002/anie.201710989>.
- Bianchi, F., Kurtén, T., Riva, M., Mohr, C., Rissanen, M. P., Roldin, P., Berndt, T., Crounse, J. D., Wennberg, P. O., Mentel, T. F., Wildt, J., Junninen, H., Jokinen, T., Kulmala, M., Worsnop, D. R., Thornton, J. A., Donahue, N., Kjaergaard, H. G., & Ehn, M. (2019). Highly Oxygenated Organic Molecules (HOM) from Gas-Phase Autoxidation Involving Peroxy Radicals: A Key Contributor to Atmospheric Aerosol. *Chemical Reviews*. <https://doi.org/10.1021/acs.chemrev.8b00395>.
- Breitenlechner, M., Fischer, L., Hainer, M., Heinritzi, M., Curtius, J., and Hansel, A. (2017), PTR3: An Instrument for Studying the Lifecycle of Reactive Organic Carbon in the Atmosphere, *Analytical chemistry*, 89(11), 5824-5831, doi:10.1021/acs.analchem.6b05110.
- Brüggemann, M., Hayeck, N., Bonnneau, C., Pesce, S., Alpert, P. A., Perrier, S., Zuth, C., Hoffmann, T., Chen, J., & George, C. (2017). Interfacial photochemistry of biogenic

- surfactants: A major source of abiotic volatile organic compounds. *Faraday Discussions*, 200, 59–74. <https://doi.org/10.1039/C7FD00022G>.
- Crounse, J. D., McKinney, K. A., Kwan, A. J., & Wennberg, P. O. (2006). Measurement of Gas-Phase Hydroperoxides by Chemical Ionization Mass Spectrometry. *Analytical Chemistry*, 78(19), 6726–6732. <https://doi.org/10.1021/ac0604235>.
- Crounse, J. D., Nielsen, L. B., Jørgensen, S., Kjaergaard, H. G., & Wennberg, P. O. (2013). Autoxidation of Organic Compounds in the Atmosphere. *The Journal of Physical Chemistry Letters*, 4(20), 3513–3520. <https://doi.org/10.1021/jz4019207>.
- Cubison, M. J., & Jimenez, J. L. (2015). Statistical precision of the intensities retrieved from constrained fitting of overlapping peaks in high-resolution mass spectra. *Atmospheric Measurement Techniques*, 8(6), 2333–2345. <https://doi.org/10.5194/amt-8-2333-2015>.
- Donahue, N. M., Epstein, S. A., Pandis, S. N., & Robinson, A. L. (2011). A two-dimensional volatility basis set: 1. organic-aerosol mixing thermodynamics. *Atmospheric Chemistry and Physics*, 11(7), 3303–3318. <https://doi.org/10.5194/acp-11-3303-2011>.
- Ehn, M., Thornton, J. A., Kleist, E., Sipilä, M., Junninen, H., Pullinen, I., Springer, M., Rubach, F., Tillmann, R., Lee, B., Lopez-Hilfiker, F., Andres, S., Acir, I.-H., Rissanen, M., Jokinen, T., Schobesberger, S., Kangasluoma, J., Kontkanen, J., Nieminen, T., ... Mentel, T. F. (2014). A large source of low-volatility secondary organic aerosol. *Nature*, 506(7489), 476–479. <https://doi.org/10.1038/nature13032>.
- Eiler, J., Cesar, J., Chimiak, L., Dallas, B., Grice, K., Griep-Raming, J., Juchelka, D., Kitchen, N., Lloyd, M., Makarov, A., Robins, R., and Schwieters, J. (2017), Analysis of molecular isotopic structures at high precision and accuracy by Orbitrap mass spectrometry, *International Journal of Mass Spectrometry*, 422, 126–142, doi:10.1016/j.ijms.2017.10.002.
- Eisele, F. L., & Tanner, D. J. (1993). Measurement of the gas phase concentration of H₂SO₄ and methane sulfonic acid and estimates of H₂SO₄ production and loss in the atmosphere. *Journal of Geophysical Research: Atmospheres*, 98(D5), 9001–9010. <https://doi.org/10.1029/93JD00031>.
- Gakidou, E., Afshin, A., Abajobir, A. A., Abate, K. H., Abbafati, C., Abbas, K. M., Abd-Allah, F., Abdulle, A. M., Abera, S. F., Aboyans, V., Abu-Raddad, L. J., Abu-Rmeileh, N. M. E., Abyu, G. Y., Adedeji, I. A., Adetokunboh, O., Afarideh, M., Agrawal, A., Agrawal, S., Ahmadieh, H., ... Murray, C. J. L. (2017). Global, regional, and national comparative risk assessment of 84 behavioural, environmental and occupational, and metabolic risks or clusters of risks, 1990–2016: A systematic analysis for the Global Burden of Disease Study 2016. *The Lancet*, 390(10100), 1345–1422. [https://doi.org/10.1016/S0140-6736\(17\)32366-8](https://doi.org/10.1016/S0140-6736(17)32366-8).
- Glasius, M., & Goldstein, A. H. (2016). Recent Discoveries and Future Challenges in Atmospheric Organic Chemistry. *Environmental Science & Technology*, 50(6), 2754–2764. <https://doi.org/10.1021/acs.est.5b05105>.
- Goldstein, A. H., & Galbally, I. E. (2007). Known and Unexplored Organic Constituents in the Earth's Atmosphere. *Environmental Science & Technology*, 41(5), 1514–1521. <https://doi.org/10.1021/es072476p>.
- Hallquist, M., Wenger, J. C., Baltensperger, U., Rudich, Y., Simpson, D., Claeys, M., Dommen, J., Donahue, N. M., George, C., Goldstein, A. H., Hamilton, J. F., Herrmann, H., Hoffmann, T., Inuma, Y., Jang, M., Jenkin, M. E., Jimenez, J. L., Kiendler-Scharr, A., Maenhaut, W., McFiggans, G., Mentel, T. F., Monod, A., Prévôt, A. S. H., Seinfeld, J. H., Surratt, J. D.,

- Szmigielski, R., and Wildt, J. (2009). The formation, properties and impact of secondary organic aerosol: Current and emerging issues. *Atmospheric Chemistry and Physics*, 9(14), 5155–5236. <https://doi.org/10.5194/acp-9-5155-2009>.
- Heinritzi, M., Simon, M., Steiner, G., Wagner, A. C., Kürten, A., Hansel, A., & Curtius, J. (2016). Characterization of the mass-dependent transmission efficiency of a CIMS. *Atmospheric Measurement Techniques*, 9(4), 1449–1460. <https://doi.org/10.5194/amt-9-1449-2016>.
- Hyttinen, N., Otkjaer, R. V., Iyer, S., Kjaergaard, H. G., Rissanen, M. P., Wennberg, P. O., and Kurten, T. (2018), Computational Comparison of Different Reagent Ions in the Chemical Ionization of Oxidized Multifunctional Compounds, *The journal of physical chemistry. A*, 122(1), 269-279, doi:10.1021/acs.jpca.7b10015.
- Isaacman-VanWertz, G., Massoli, P., O'Brien, R., Lim, C., Franklin, J. P., Moss, J. A., Hunter, J. F., Nowak, J. B., Canagaratna, M. R., Misztal, P. K., Arata, C., Roscioli, J. R., Herndon, S. T., Onasch, T. B., Lambe, A. T., Jayne, J. T., Su, L., Knopf, D. A., Goldstein, A. H., ... Kroll, J. H. (2018). Chemical evolution of atmospheric organic carbon over multiple generations of oxidation. *Nature Chemistry*, 10(4), 462–468. <https://doi.org/10.1038/s41557-018-0002-2>.
- Jimenez, J. L., Canagaratna, M. R., Donahue, N. M., Prevot, A. S. H., Zhang, Q., Kroll, J. H., DeCarlo, P. F., Allan, J. D., Coe, H., Ng, N. L., Aiken, A. C., Docherty, K. S., Ulbrich, I. M., Grieshop, A. P., Robinson, A. L., Duplissy, J., Smith, J. D., Wilson, K. R., Lanz, V. A., Hueglin, C., Sun, Y. L., Tian, J., Laaksonen, A., Raatikainen, T., Rautiainen, J., Vaattovaara, P., Ehn, M., Kulmala, M., Tomlinson, J. M., Collins, D. R., Cubison, M. J., Dunlea, J., Huffman, J. A., Onasch, T. B., Alfarra, M. R., Williams, P. I., Bower, K., Kondo, Y., Schneider, J., Drewnick, F., Borrmann, S., Weimer, S., Demerjian, K., Salcedo, D., Cottrell, L., Griffin, R., Takami, A., Miyoshi, T., Hatakeyama, S., Shimono, A., Sun, J. Y., Zhang, Y. M., Dzepina, K., Kimmel, J. R., Sueper, D., Jayne, J. T., Herndon, S. C., Trimborn, A. M., Williams, L. R., Wood, E. C., Middlebrook, A. M., Kolb, C. E., Baltensperger, U., and Worsnop, D. R. (2009). Evolution of Organic Aerosols in the Atmosphere. *Science*, 326(5959), 1525–1529. <https://doi.org/10.1126/science.1180353>.
- Jokinen, T., Berndt, T., Makkonen, R., Kerminen, V.-M., Junninen, H., Paasonen, P., Stratmann, F., Herrmann, H., Guenther, A. B., Worsnop, D. R., Kulmala, M., Ehn, M., & Sipilä, M. (2015). Production of extremely low volatile organic compounds from biogenic emissions: Measured yields and atmospheric implications. *Proceedings of the National Academy of Sciences*, 112(23), 7123–7128. <https://doi.org/10.1073/pnas.1423977112>.
- Jokinen, T., Sipilä, M., Junninen, H., Ehn, M., Lönn, G., Hakala, J., Petäjä, T., Mauldin, R. L., Kulmala, M., & Worsnop, D. R. (2012). Atmospheric sulphuric acid and neutral cluster measurements using CI-APi-TOF. *Atmospheric Chemistry and Physics*, 12(9), 4117–4125. <https://doi.org/10.5194/acp-12-4117-2012>.
- Jokinen, T., Sipilä, M., Richters, S., Kerminen, V.-M., Paasonen, P., Stratmann, F., Worsnop, D., Kulmala, M., Ehn, M., Herrmann, H., & Berndt, T. (2014). Rapid Autoxidation Forms Highly Oxidized RO₂ Radicals in the Atmosphere. *Angewandte Chemie International Edition*, 53(52), 14596–14600. <https://doi.org/10.1002/anie.201408566>.
- Krechmer, J., Lopez-Hilfiker, F., Koss, A., Hutterli, M., Stoermer, C., Deming, B., Kimmel, J., Warneke, C., Holzinger, R., Jayne, J., Worsnop, D., Fuhrer, K., Gonin, M., and de Gouw, J. (2018), Evaluation of a New Reagent-Ion Source and Focusing Ion-Molecule Reactor for

- Use in Proton-Transfer-Reaction Mass Spectrometry, *Analytical chemistry*, 90(20), 12011–12018, doi:10.1021/acs.analchem.8b02641.
- Kroll, J. H., & Seinfeld, J. H. (2008). Chemistry of secondary organic aerosol: Formation and evolution of low-volatility organics in the atmosphere. *Atmospheric Environment*, 42(16), 3593–3624. <https://doi.org/10.1016/j.atmosenv.2008.01.003>.
- Kurtén, T., Tiusanen, K., Roldin, P., Rissanen, M., Luy, J.-N., Boy, M., Ehn, M., & Donahue, N. (2016). α -Pinene Autoxidation Products May Not Have Extremely Low Saturation Vapor Pressures Despite High O:C Ratios. *The Journal of Physical Chemistry A*, 120(16), 2569–2582. <https://doi.org/10.1021/acs.jpca.6b02196>.
- Lee, B. H., Lopez-Hilfiker, F. D., Mohr, C., Kurtén, T., Worsnop, D. R., & Thornton, J. A. (2014). An Iodide-Adduct High-Resolution Time-of-Flight Chemical-Ionization Mass Spectrometer: Application to Atmospheric Inorganic and Organic Compounds. *Environmental Science & Technology*, 48(11), 6309–6317. <https://doi.org/10.1021/es500362a>.
- Lopez-Hilfiker, F. D., Iyer, S., Mohr, C., Lee, B. H., Ambro, E. L., Kurtén, T., & Thornton, J. A. (2016). Constraining the sensitivity of iodide adduct chemical ionization mass spectrometry to multifunctional organic molecules using the collision limit and thermodynamic stability of iodide ion adducts. *Atmospheric Measurement Techniques*, 9(4), 1505–1512. <https://doi.org/10.5194/amt-9-1505-2016>.
- Makarov, A., and Denisov, E. (2009), Dynamics of ions of intact proteins in the Orbitrap mass analyzer, *Journal of the American Society for Mass Spectrometry*, 20(8), 1486-1495, doi:10.1016/j.jasms.2009.03.024.
- Meija, J., & Caruso, J. A. (2004). Deconvolution of isobaric interferences in mass spectra. *Journal of the American Society for Mass Spectrometry*, 15(5), 654–658. <https://doi.org/10.1016/j.jasms.2003.12.016>.
- Messina, P., Lathière, J., Sindelarova, K., Vuichard, N., Granier, C., Ghattas, J., Cozic, A., & Hauglustaine, D. A. (2016). Global biogenic volatile organic compound emissions in the ORCHIDEE and MEGAN models and sensitivity to key parameters. *Atmospheric Chemistry and Physics*, 16(22), 14169–14202. <https://doi.org/10.5194/acp-16-14169-2016>.
- Michalski, A., Damoc, E., Hauschild, J.-P., Lange, O., Wieghaus, A., Makarov, A., Nagaraj, N., Cox, J., Mann, M., & Horning, S. (2011). Mass Spectrometry-based Proteomics Using Q Exactive, a High-performance Benchtop Quadrupole Orbitrap Mass Spectrometer. *Molecular & Cellular Proteomics*, 10(9), M111.011015. <https://doi.org/10.1074/mcp.M111.011015>.
- Perry, R. H., Cooks, R. G., & Noll, R. J. (2008). Orbitrap mass spectrometry: Instrumentation, ion motion and applications. *Mass Spectrometry Reviews*, 27(6), 661–699. <https://doi.org/10.1002/mas.20186>.
- Riva, M., Rantala, P., Krechmer, J. E., Peräkylä, O., Zhang, Y., Heikkinen, L., Garmash, O., Yan, C., Kulmala, M., Worsnop, D., & Ehn, M. (2019). Evaluating the performance of five different chemical ionization techniques for detecting gaseous oxygenated organic species. *Atmospheric Measurement Techniques*, 12(4), 2403-2421. doi: 10.5194/amt-12-2403-2019.
- Riva, M., Ehn, M., Li, D., Tomaz, S., Bourgoin, F., Perrier, S., and George, C. (2019), CI-Orbitrap: An Analytical Instrument To Study Atmospheric Reactive Organic Species, *Analytical chemistry*, 91(15), 9419-9423, doi:10.1021/acs.analchem.9b02093.

- Rosenfeld, D., Lohmann, U., Raga, G. B., O'Dowd, C. D., Kulmala, M., Fuzzi, S., Reissell, A., & Andreae, M. O. (2008). Flood or Drought: How Do Aerosols Affect Precipitation? *Science*, 321(5894), 1309–1313. <https://doi.org/10.1126/science.1160606>.
- Stark, H., Yatavelli, R. L. N., Thompson, S. L., Kimmel, J. R., Cubison, M. J., Chhabra, P. S., Canagaratna, M. R., Jayne, J. T., Worsnop, D. R., & Jimenez, J. L. (2015). Methods to extract molecular and bulk chemical information from series of complex mass spectra with limited mass resolution. *International Journal of Mass Spectrometry*, 389, 26–38. <https://doi.org/10.1016/j.ijms.2015.08.011>.
- Tröstl, J., Chuang, W. K., Gordon, H., Heinritzi, M., Yan, C., Molteni, U., Ahlm, L., Frege, C., Bianchi, F., Wagner, R., Simon, M., Lehtipalo, K., Williamson, C., Craven, J. S., Duplissy, J., Adamov, A., Almeida, J., Bernhammer, A.-K., Breitenlechner, M., Brilke, S., Dias, A., Ehrhart, S., Flagan, R. C., Franchin, A., Fuchs, C., Guida, R., Gysel, M., Hansel, A., Hoyle, C. R., Jokinen, T., Junninen, H., Kangasluoma, J., Keskinen, H., Kim, J., Krapf, M., Kurten, A., Laaksonen, A., Lawler, M., Leiminger, M., Mathot, S., Mohler, O., Nieminen, T., Onnela, A., Petaja, T., Piel, F. M., Miettinen, P., Rissanen, M. P., Rondo, L., Sarnela, N., Schobesberger, S., Sengupta, K., Sipila, M., Smith, J. N., Steiner, G., Tome, A., Virtanen, A., Wagner, A. C., Weingartner, E., Wimmer, D., Winkler, P. M., Ye, P., Carslaw, K. S., Curtius, J., Dommen, J., Kirkby, J., Kulmala, M., Riipinen, I., Worsnop, D. R., Donahue, N. M., and Baltensperger, U. (2016). The role of low-volatility organic compounds in initial particle growth in the atmosphere. *Nature*, 533(7604), 527–531. <https://doi.org/10.1038/nature18271>.
- Ziemann, P. J., and Atkinson, R. (2012). Kinetics, products, and mechanisms of secondary organic aerosol formation, *Chemical Society reviews*, 41(19), 6582-6605, doi:10.1039/c2cs35122f.
- Zuth, C., Vogel, A. L., Ockenfeld, S., Huesmann, R., & Hoffmann, T. (2018). Ultrahigh-Resolution Mass Spectrometry in Real Time: Atmospheric Pressure Chemical Ionization Orbitrap Mass Spectrometry of Atmospheric Organic Aerosol. *Analytical Chemistry*, 90(15), 8816–8823. <https://doi.org/10.1021/acs.analchem.8b00671>.

Chapter IV: Ammonium CI-Orbitrap: a
tool for characterizing the reactivity of
oxygenated organic molecules

Chapter IV: Ammonium CI-Orbitrap: a tool for characterizing the reactivity of oxygenated organic molecules

Dandan Li¹, Dongyu Wang², Lucia Caudillo³, Wiebke Scholz⁴, Mingyi Wang^{5,6}, Guillaume Marie³, Sophie Tomaz¹, Pekka Rantala⁷, Mihnea Surdu², CLOUD COLLABORATION, Sébastien Perrier¹, Jasper Kirkby^{3,8}, Neil M. Donahue⁵, Christian George¹, Imad El-Haddad², Matthieu Riva¹

1 Univ Lyon, Université Claude Bernard Lyon 1, CNRS, IRCELYON, 69626, Villeurbanne, France

6 Institute for Atmospheric and Earth System Research/Physics, Faculty of Science, University of Helsinki, 00014, Helsinki, Finland

2 Laboratory of Atmospheric Chemistry, Paul Scherrer Institute, 5232, Villigen, Switzerland

3 Institute for Atmospheric and Environmental Sciences, Goethe University Frankfurt, 60438, Frankfurt am Main, Germany

4 Institute for Ion Physics and Applied Physics, University of Innsbruck, 6020, Innsbruck, Austria

5 Center for Atmospheric Particle Studies, Carnegie Mellon University, Pittsburgh, PA, 15213, USA

6 now at Division of Chemistry and Chemical Engineering, California Institute of Technology, Pasadena, CA 91125, USA

6 Department of Atmospheric Sciences, University of Washington, Seattle, WA 98195, USA

7 Institute for Atmospheric and Earth System Research/Physics, Faculty of Science, University of Helsinki, 00014, Helsinki, Finland

Manuscript in preparation

IV.1. Introduction

Aerosols are known to affect the climate by either directly scattering or absorbing solar radiation, or acting as seeds for cloud formation (Fan et al., 2016; Haywood and Boucher, 2000). A major fraction of submicron aerosol mass particles consists of organic aerosols, with secondary organic aerosol (SOA) being the largest source (Jimenez et al., 2009; Hallquist et al., 2009). Oxygenated organic molecules (OOMs) generated from the oxidation of volatile organic compounds (VOCs) contribute to the formation and growth of SOA (Ehn et al., 2014; Mellouki et al., 2015). OOMs can be generated by autoxidation of peroxy radical (RO_2) (Bianchi et al., 2019), where RO_2 undergoes an intramolecular H atom shift, followed by O_2 addition forming a new and more oxidized RO_2 (Crounse et al., 2013; Rissanen et al., 2014; Bianchi et al., 2019). These propagation steps are repeated until termination by either bimolecular or unimolecular reactions, yielding closed-shell molecules (Bianchi et al., 2019). Among the OOMs, the highly oxygenated organic molecules (HOMs), typically containing multifunctional groups and exhibiting (extremely) low saturation vapor pressure, can nucleate with inorganic species, e.g., sulfuric acid (Ehn et al., 2014; Kirkby et al., 2016; Bianchi et al., 2016) leading to the formation of new particles. Less oxygenated molecules (i.e., containing 2 to 5 oxygen atoms) play a vital role in the growth of newly formed atmospheric particles, by either condensation or through multiphase chemistry (Bianchi et al., 2019; Ehn et al., 2014; Hallquist et al., 2009). Therefore, the identification and quantification of the wide diversity of OOMs are essential to understand the formation and growth of SOA (Kirkby et al., 2016; Bianchi et al., 2016; Trostl et al., 2016; Jokinen et al., 2015; Glasius and Goldstein, 2016).

Mass spectrometry (MS) is a widely used analytical technique in atmospheric chemistry (Wang et al., 2017; Wang et al., 2020; Breitenlechner et al., 2017; Bianchi et al., 2019) and has made remarkable achievements in detecting, characterizing, and quantifying OOMs (Ehn et al., 2010; Riva et al., 2019a; Breitenlechner et al., 2017). Moreover, the application of chemical ionization (CI) enables the detection of a wide variety of organic and inorganic analytes (Bianchi et al., 2019; Ehn et al., 2014; Jokinen et al., 2012; Lee et al., 2014). Different MS and ionization chemistries exhibit disparate selectivity and sensitivity to OOMs (Bianchi et al., 2019; Riva et al., 2020b; Riva et al., 2019b; Berndt et al., 2018b; Berndt et al., 2018a). For example, negative ion-based chemistry, including nitrate (NO_3^-), can optimally detect HOMs. However using such ion

based chemistry, only a small subset of the OOMs can be measured (Lee et al., 2014; Berndt et al., 2015; Berndt et al., 2018b; Riva et al., 2019b). Positive ion-based chemistries have also been developed and present good responses to HOMs as well as the less oxidized products, providing the possibility of achieving carbon-closure (Praplan et al., 2015; Berndt et al., 2018a; Berndt et al., 2018b; Hansel et al., 2018; Riva et al., 2020b; Riva et al., 2019b). However, these methods are mainly based on proton transfer, which often results in the fragmentations of the analytes (Yuan et al., 2017; Breitenlechner et al., 2017; Li et al., 2020). Time-of-flight (TOF) mass spectrometers using ammonium (NH_4^+) or amines as reagent ions can detect a wide variety of OOMs but suffer from a lack of mass resolving power, making the peak identification challenging especially for complex systems, i.e., atmospheric conditions (Berndt et al., 2018b; Berndt et al., 2018a; Riva et al., 2019b). Finally, the recently developed ultrahigh-resolution Orbitrap mass spectrometer using propylamine achieved unambiguous identification of overlapping peaks and accurate quantification of OOMs. However this analytical technique was used in very diluted environments to ensure a linear response of the OOMs and for a very simplified atmospheric system (Riva et al., 2020b; Riva et al., 2019b).

Here we explored the capability of NH_4^+ ion-based CI-Orbitrap mass spectrometer (Q-Exactive Orbitrap, Thermo Scientific) for detecting OOMs generated from α -pinene ozonolysis in the Cosmic Leaving OUTdoors Droplets (CLOUD) chamber at European Organization for Nuclear Research (CERN) under various environmental conditions. The performances of the CI-(NH_4^+)-Orbitrap were compared to the state-of-the-art online mass spectrometers including a nitrate CI atmospheric pressure interface long time of flight mass spectrometer (CI-(NO_3^-)-APi-LTOF; Tofwerk AG), a proton transfer reaction time of flight mass spectrometer (PTR3-TOF; Ionicon Analytik GmbH), and an iodide CI time of flight mass spectrometer equipped with a Filter Inlet for Gases and AEROSols (I^- -FIGAERO-CIMS, Tofwerk AG).

IV.2. Experimental approach and product analysis

IV.2.1. CLOUD chamber experiments

All experiments were conducted in the CLOUD chamber, a 26 m³ stainless steel vessel at CERN. This chamber enables to achieve an extremely standards of cleanliness and is described in detail in

Kirkby et al. (Kirkby et al., 2011; Kirkby et al., 2016). The evaporation of cryogenic liquid nitrogen (N_2) and liquid oxygen (O_2) was blended at a ratio of 79:21 to produce pure synthetic air, which flushed the chamber constantly. Variable amounts of trace gases, including O_3 , VOCs, NO_x , SO_2 , and CO were accurately injected into the system and monitored. 250 optical fiber-optic systems installed on top of the chamber were utilized to initiate photolytic reactions, including Hg-Xe UV lamps, and UV excimer laser. The CLOUD chamber was cleaned by irrigating the walls with ultra-pure water, then heated to 373 K, and flushed with humidified pure air and high ozone, declining the contaminant levels such as VOCs to sub pptv level. During the cleaning process, particles were wiped out using a high-voltage electric field.

The results presented here are from the CLOUD14 campaign performed in autumn 2019. During the CLOUD14 campaign, the total flow was kept at 250 standard litre per minute (slpm) providing an average residence time of 105 minutes. α -Pinene was introduced to the chamber by passing a small flow of dry air over a temperature-controlled evaporator containing the liquid compound. Ozone was generated by flowing a small fraction of the air through a quartz tube surrounded by UVC lights (i.e., wavelength < 240 nm). Experiments were performed at 223 and 323 ± 0.1 K. The RH in the chamber was controlled by flowing a portion of the air through a Nafion® humidifier using ultrapure water (18 MΩ cm, Millipore Corporation). The chamber was used in continuous-flow mode. The contents of the chamber were ceaselessly detected and analyzed by a wide range of external instruments connected to the sampling probes ~1 m protruding into the chamber.

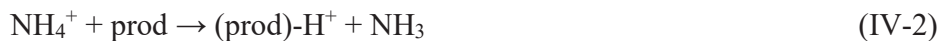
IV.2.2. Product analysis by CI-(NH_4^+)-Orbitrap

The chemical composition of closed-shell molecules was retrieved in real time by means of CI-Orbitrap sampling from the CLOUD chamber through a sampling inlet (750 mm long 10 mm inner diameter Teflon flexible tube) at a flow rate of 10 slpm. The CI inlet mounted on the Orbitrap was a home-built version with minor modifications regarding the commercial inlet, (more details (Riva et al., 2019a)). The ion-molecule reaction (IMR) proceeded at atmospheric pressure with a residence time of 200-300 ms. The same operating parameters used in our previous studies (RF level 60, automatic gain control 1×10^6 charges, maximum injection time 1000 ms, multi RF ratio 1.2, mass resolution 140 000 at m/z 200), were used, thereby minimizing the declustering

processes and maximizing the linearity range (Riva et al., 2019a; Riva et al., 2020a; Cai et al., 2022).

The high resolution Orbitrap mass spectra data were analyzed using a newly-developed software “Orbitool” with a graphical user interface (GUI) (<https://orbitrap.catalyse.cnrs.fr>), more details in ref (Cai et al., 2021). Orbitool enables data averaging, noise determination and reduction, single peak fitting, mass calibration, assignment of molecular formulas and export of time series. Signals were averaged over 5 min before determining the noise and performing mass calibration.

NH_4^+ has already been utilized in proton-transfer reaction mass spectrometry (PTR-MS) (Lindinger et al., 1998) and to the novel PTR3-TOF (Berndt et al., 2018b; Hansel et al., 2018). This ion based chemistry was used for the detection of oxygenated volatile organic compounds (OVOC) and was conducted in the similar operation as in our initial study (Riva et al., 2019a). NH_3 was added into the ion source taking 2 sccm from the head space of a 1% liquid ammonia water mixture (Ammonium hydroxide solution 25% NH_3 basis, ACS reagent, Sigma-Aldrich). The product molecules (prod) were softly charged by binding to ammonium ions, forming (prod)- NH_4^+ adduct ions or protonated products (prod)- H^+ , following equations (1) and (2).



No signals of the reagent ion can be recorded due to the cut-off of the Orbitrap ($m/z \geq 50$). As a result, the absence of the reagent ions made it difficult to normalize the raw abundance and then to quantify the products. However, 62 amines including $\text{C}_4\text{H}_{12}\text{N}^+$, $\text{C}_6\text{H}_{14}\text{N}^+$ were observed with NH_4^+ as the reagent ion, which were formally derivatives of ammonia. Among them, 13 amines were observed in high abundance and remained constant throughout the measurement period (Figure IV-1). As a result, they were used to normalize the signal intensity of the analytes to account for any potential variation within the ionization process (Riva et al., 2019b).

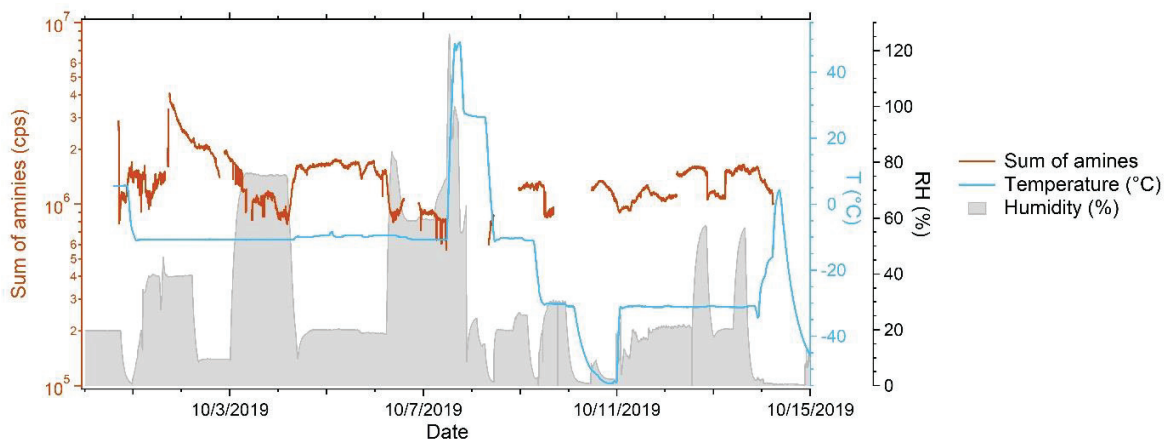


Figure IV-1: Time evolution of sum of the 13 amines used to normalize signal intensity. Temperature and humidity are also reported throughout the different experiments when the NH₄⁺-Orbitrap was used.

The concentrations of certain groups of compounds, including monomeric species such as C₁₀H₁₄O_x and C₁₀H₁₆O_x, were estimated based on correlation analysis between NH₄⁺-Orbitrap and NO₃⁻-LTOF/PTR3-TOF, providing semi quantification using equation (3). Correlation analysis was performed on the time series of co-detected compounds by NH₄⁺-Orbitrap and NO₃⁻-LTOF/PTR3-TOF, having the same elemental composition. Compounds with a Pearson correlation coefficient (R^2) > 0.9 were selected and the slope of the linear regression fit was used to estimate the concentration of the compounds measured by NH₄⁺-Orbitrap; according to the following equation:

$$[prod]_{Orbi_LTOF/PTR3} = c_{Orbi_LTOF/PTR3} \times \frac{[(prod)-NH_4^+] + [(prod)-H^+]}{\sum [Amine]} \quad (IV-3)$$

where c is the calibration factor, obtained from the correlation analysis. Finally a temperature dependent sampling-line loss correction factor was applied to retrieve the concentration of the compounds, following the method described by Simon et al. (Simon et al., 2020).

IV.2.3 Product analysis by CI-(NO₃⁻)-APi-LTOF

Detection of RO₂ radicals and closed shell products was also performed by the CI-(NO₃⁻)-LTOF which has been described elsewhere (Jokinen et al., 2012; Kurten et al., 2014). Therefore, only relevant details to this study are provided. NO₃⁻-LTOF offered a mass resolving power up of 12

000 and OOMs (mass 300-650 Da) were detected as clusters ions with the $(\text{HNO}_3)_n(\text{NO}_3^-)$ anions, with $n = 0-2$. The primary ions were produced by a corona discharge needle exposure to a sheath gas enriched by HNO_3 . Laminar flow diffusional loss was assumed in the 30 cm sampling line. A core-sampling technique was applied to prevent losses in the sampling inlet (Knopf et al., 2015). 5.13 slpm were sampled from the center of a core flow inlet (total flow (30 lspm)). This setup reduced the sampling loss rate of HOMs to less than 30% (Simon et al., 2020). The data were processed using Tofware (Version 3.2, Aerodyne Inc., USA) and MATLAB R2019b (MathWorks, Inc., USA). In addition, background signals, mass-dependent transmission efficiency (Heinritzi et al., 2016), and sampling losses (Simon et al., 2020) were determined and the different corrections applied. The NO_3^- -LTOF was directly calibrated using sulfuric acid (Kurten et al., 2012). A calibration factor C was determined to be $\sim 4.13 \times 10^{10}$ molecules cm^{-3} during the CLOUD 14 campaign (Caudillo et al., 2021).

IV.2.4 Product analysis by PTR3-TOF

The PTR3-TOF ionized organic compounds by proton transfer. H_3O^+ ions were produced by a corona discharge using humidified nitrogen (Breitenlechner et al., 2017). In order to reduce sample losses, a 2 slpm was drawn from a 10 slpm laminar flow through a critical orifice into the tripole where the ion-molecule reactions took place. The pressure in this region was maintained at ~ 80 mbar. The distribution of primary ions and sample molecules can be adjusted by a tunable radio frequency signal applied to the tripole rods. The greater pressure in the tripole and longer reaction time result in a 500-fold increased the sensitivity of the PTR3-TOF compared to conventional PTR instruments.

During the CLOUD 14 experiments, the collision energy was controlled between 62-72 Td. These settings helped reducing the humidity dependence for detection of organic compounds. The PTR3-TOF was calibrated using a gas standard mixture containing 1 ppm of 3-hexanone, heptanone and α -pinene in nitrogen. The concentration of oxygenated products was estimated using the sensitivity of 3-hexanone as lower-limit values due to possible fragmentation. The product ions were detected with a TOF mass spectrometer (Tofwerk AG, Switzerland). All data were analyzed with TOF-Tracer software running on Julia 0.6 (<https://github.com/lukasfischer83/TOF-Tracer>). In this study, data were further corrected for the

duty cycle transmission of TOF and temperature dependent sampling line losses (Stolzenburg et al., 2018).

IV.2.5 Product analysis by I⁻-FIGAERO-CIMS

The I⁻-FIGAERO-CIMS is capable of characterizing both the gas and particle phases (Lopez-Hilfiker et al., 2014). In gas phase mode, trace gases are directly sampled into a 100-mbar turbulent ion-molecule reactor. Simultaneously particles are collected onto a polytetrafluoroethylene (PTFE) filter via a separate dedicated sampling port. In the particle phase mode, the filter is automatically moved into a pure N₂ gas stream flowing into the ion-molecule reactor. N₂ is progressively heated to evaporate the aerosol particles via temperature-programmed thermal desorption. Both modes are fully automated and programmable for continuous online sampling. Analytes are then chemically ionized and extracted into a TOF mass analyzer (Wang et al., 2020). In this study, gas phase data are used for the side-by-side comparison.

Iodide ions (I⁻) are used as the reagent ions and formed by passing a 1.0 slpm flow of ultrahigh purity N₂ over a diffusion tube filled with methyl iodide (CH₃I), and then through an ²¹⁰Po radioactive source. In the sampling mode, the reagent ion flow is mixed with a sample flow in the IMR at ~150 mbar. A coaxial core sampling is used to minimize the vapor wall loss in the sampling line. The total flow is kept at 18.0 slpm and the core flow at 4.5 slpm; the CIMS samples at the center of the core flow with a flow rate of 1.6 slpm. The gas-phase background signal is determined by routinely introducing zero air directly into the inlet to displace the gaseous sample. Data were analyzed using Tofware (version 2.5.11_FIGAERO) giving 10 s average mass spectra. The ion signal was normalized by the sum of reagent ion signal (i.e., m/z 127: I⁻ and m/z 145: H₂OI⁻).

IV.2.6 Volatility of OOMs

It is challenging to directly measure the vapor pressure of individual OOMs due to the difficulty to synthesize oxidation products having various functional groups. To overcome experimental challenges, model calculations have been developed to estimate the vapor pressure, using for example structure-based estimations and formula-based estimations (Isaacman-Vanwertz and Aumont, 2021). Volatility basis set (VBS), a categorization framework based on quantifiable organic property-volatility, has been established and is frequently used to characterize oxidation

chemistry (Donahue et al., 2011; Li et al., 2016). The VBS parameterization is useful for classifying the wide range of OVOCs into multiple volatility groups. Hence OOMs were classified into various volatility classes including extremely low volatility organic compounds (ELVOC) and low volatility organic compounds (LVOC) based on their effective saturation concentration, C^* , in the unit of $\mu\text{g m}^{-3}$ (Bianchi et al., 2019). In this study the VBS parameterization optimized by Li et al was applied (Li et al., 2016; Isaacman-Vanwertz and Aumont, 2021).

$$\log_{10}C^*(298K) = (n_C^0 - n_C)b_C - n_O b_O - 2 \frac{n_C n_O}{(n_C + n_O)} b_{CO} - n_N b_N - n_S b_S \quad (4)$$

where n_C , n_O , n_N , and n_S were the number of carbon, oxygen, nitrogen, and sulfur atoms of the specific molecule, separately; n_C^0 was the reference carbon number; b_C , b_O , b_N , and b_S were the contribution of each atom to $\log_{10}C^*$, separately; b_{CO} was the carbon-oxygen nonideality (Donahue et al., 2011). Values of b coefficient can be found in Li et al.(Li et al., 2016). The formula used to estimate the vapor pressure is amended to convert all NO_3 groups into OH groups to reduce the bias from the compounds containing nitrates (Daumit et al., 2013; Isaacman-Vanwertz and Aumont, 2021).

Due to the different temperatures in the CLOUD14 experiments, $C^*(298K)$ was adjusted to the measured experimental temperature in equations (5) and (6):

$$\log_{10}C^*(T) = \log_{10}C^*(298K) + \frac{\Delta H_{vap}}{R \ln(10)} \times \left(\frac{1}{298} - \frac{1}{T}\right) \quad (5)$$

$$\Delta H_{vap}(\text{kJ mol}^{-1}) = -11 \cdot \log_{10}C^*(298K) + 129 \quad (6)$$

where T was the temperature in kelvin; $C^*(298K)$ was the saturation mass concentration at 298 K; ΔH_{vap} is the evaporation enthalpy and R is the gas constant ($8.3134 \text{ J K}^{-1} \text{ mol}^{-1}$). The potential presence of isomers may result in uncertainty in this method since the only input is molecular formula.

In this study, all oxidation products were grouped into six volatility regimes; ultralow-volatility (ULVOCs), $C^* < 10^{-8.5} \mu\text{g m}^{-3}$, extremely low volatility (ELVOCs), $10^{-8.5} < C^* < 10^{-4.5} \mu\text{g m}^{-3}$, low-volatility (LVOCs), $10^{-4.5} < C^* < 10^{-0.5} \mu\text{g m}^{-3}$, semi-volatile (SVOCs), $10^{-0.5} < C^* < 10^{2.5} \mu\text{g m}^{-3}$, intermediate-volatility organic compounds (IVOC), $10^{2.5} < C^* < 10^{6.5} \mu\text{g m}^{-3}$, and VOC, $10^{6.5} < C^* \mu\text{g m}^{-3}$ based on VBS.

IV.3. Results and discussion

IV.3.1 Characterization of NH₄⁺-Orbitrap

Firstly, we explored the ability of the higher mass resolving power of the Orbitrap for separating overlapping peaks compared to other TOF mass analyzers (Riva et al., 2019a; Riva et al., 2020b). The overlapping peaks affected the identification and quantification of the less intense peaks more than the most intense peaks. Therefore, the relative intensities of neighboring peaks should also be considered when estimating their ease of separation.

The mass resolving power is defined as

$$\text{Mass Resolving Power} = m / \Delta m \quad (7)$$

where m is the mass-to-charge ratio of the analyte ion, and Δm is the full width at half maximum (FWHM). Higher mass resolving power allowed unambiguous peak assignment. For a pair of overlapping peaks of equal intensity, the distance between their respective peak center, referred to hereafter simply as peak distance, dm , needed to be greater than 0.8 of the FWHM of the overlapping peaks, such that they could be reasonably deconvolved without any a priori knowledge, as shown in Fig. IV-2.

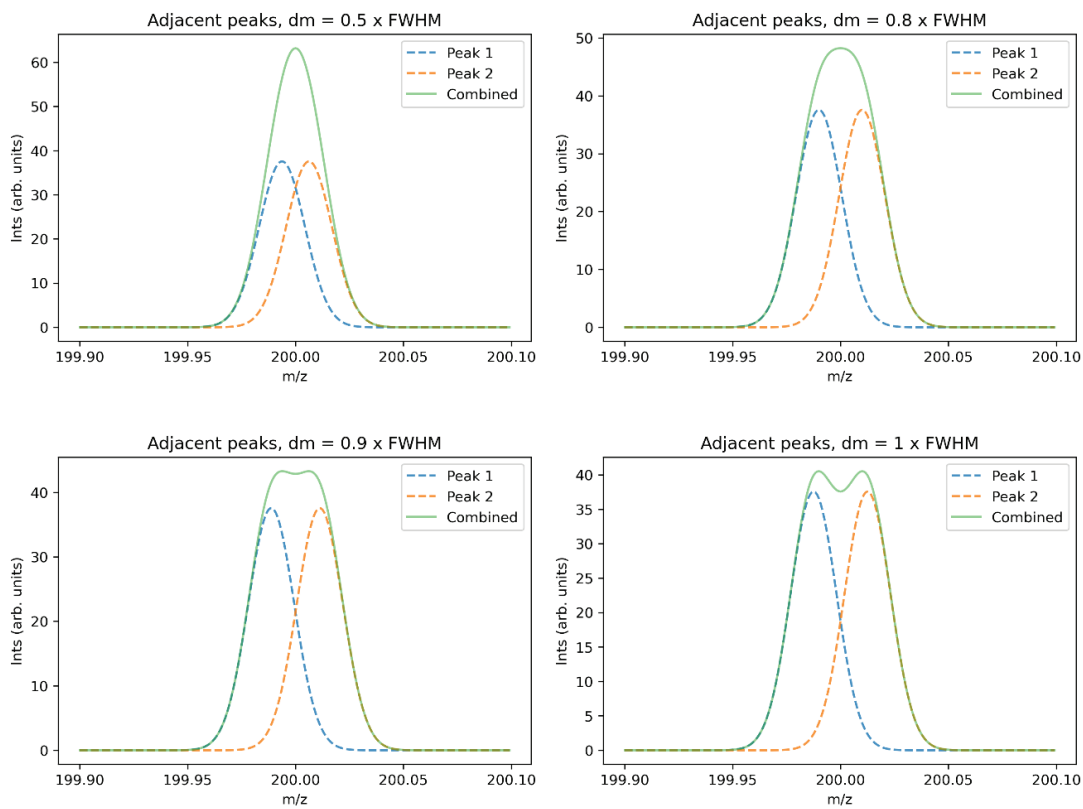


Figure IV-2: Simulated TOF spectra of overlapping peaks of equal intensity near m/z 200 assuming a mass resolving power of 8,000, somewhere between that of a Tofwerk HTOF (“high-resolution time-of-flight”) and LTOF (“long high-resolution time-of-flight) mass spectrometers. Noise wasn’t added to the data.

Depending on their experiences, individual may be able to visually identify the presence of overlapping peaks at lower or higher dm values. We arbitrarily defined the minimum dm (normalized to that of FWHM, or Δm) as the value at which the observed spectrum (“Combined” trace in Fig. IV-2 and IV-3) had a local minimum between the centers of the overlapping peaks (i.e., there is a virtual “dip” in the observed ion peak). The minimum dm value increased with the intensity ratio of overlapping peaks, ranging roughly from 0.85 (for equally intense peaks) to 1.43 (for peaks differing one order-of-magnitude in their respective intensities), as shown in Fig. IV-3. In practice, noise and the presence of additional neighboring peaks would further complicate peak deconvolution, offset somewhat by the level of experiences. For simplicity, we used a normalized dm of 1 (i.e., $dm = \Delta m$) as a threshold for unambiguous deconvolution of neighboring peaks.

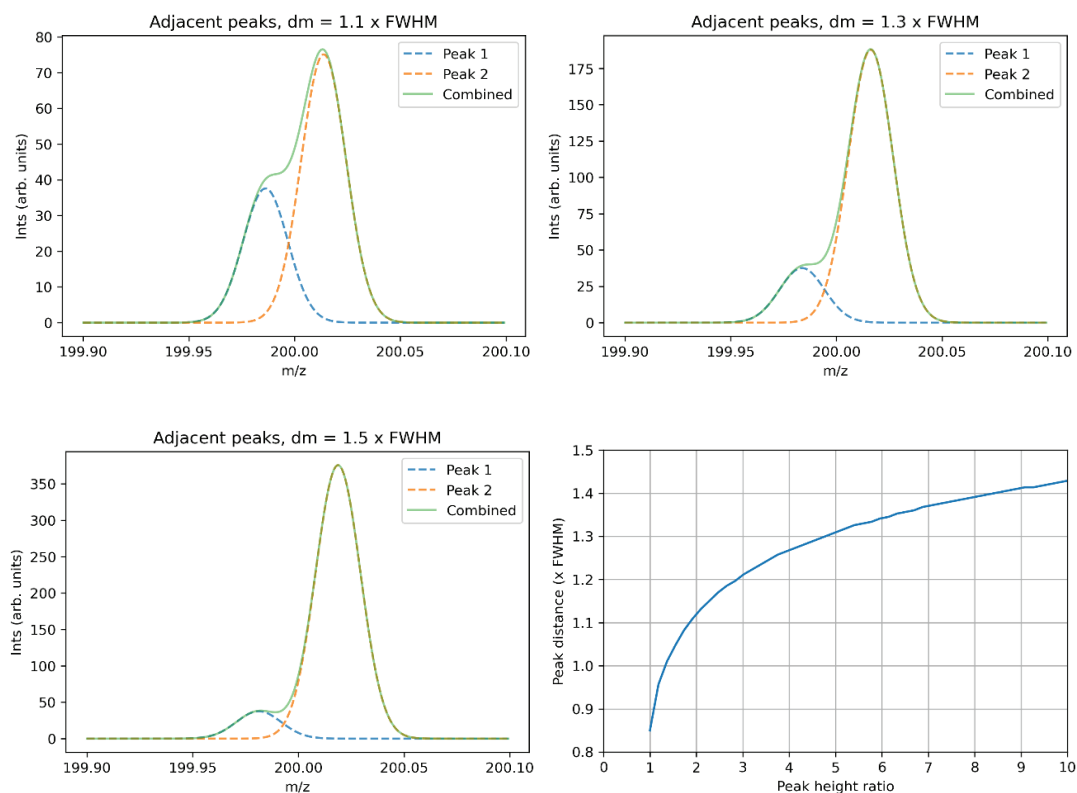


Figure IV-3: Simulated TOF spectra of overlapping peaks of equal intensity near m/z 200 assuming a mass resolving power of 8,000, somewhere between that of a Tofwerk HTOF (“high-resolution time-of-flight”) and LTOF (“long high-resolution time-of-flight) mass spectrometers. The overlapping area represents a greater proportion of the peak area of the less intense peak. Noise wasn’t added to the data.

Figure IV-4 shows the histogram of the distances between neighboring peaks normalized against the FWHM for the Orbitrap mass analyzer and a TOF analyzer having a mass resolving power of 10 000. In each histogram, one count indicates that an ion had at least one neighboring ion with a relative intensity of 20%, 50% or 100% (with higher relative intensity being more selective). Neighboring ions separated by distances exceeding 2 times the FWHM are considered well-separated. For ions with multiple neighboring ions within the $2 \times$ FWHM separation distance window, the distance to the first neighboring that satisfies the aforementioned relative intensity threshold is reported. Overall, NH_4^+ -Orbitrap can separate most of the observed ions (> 99%),

while the CI-(NH₄⁺)-TOF, depending on the relative intensity threshold set, can separate only 32% to 46% of all the ions by at least 1 FWHM.

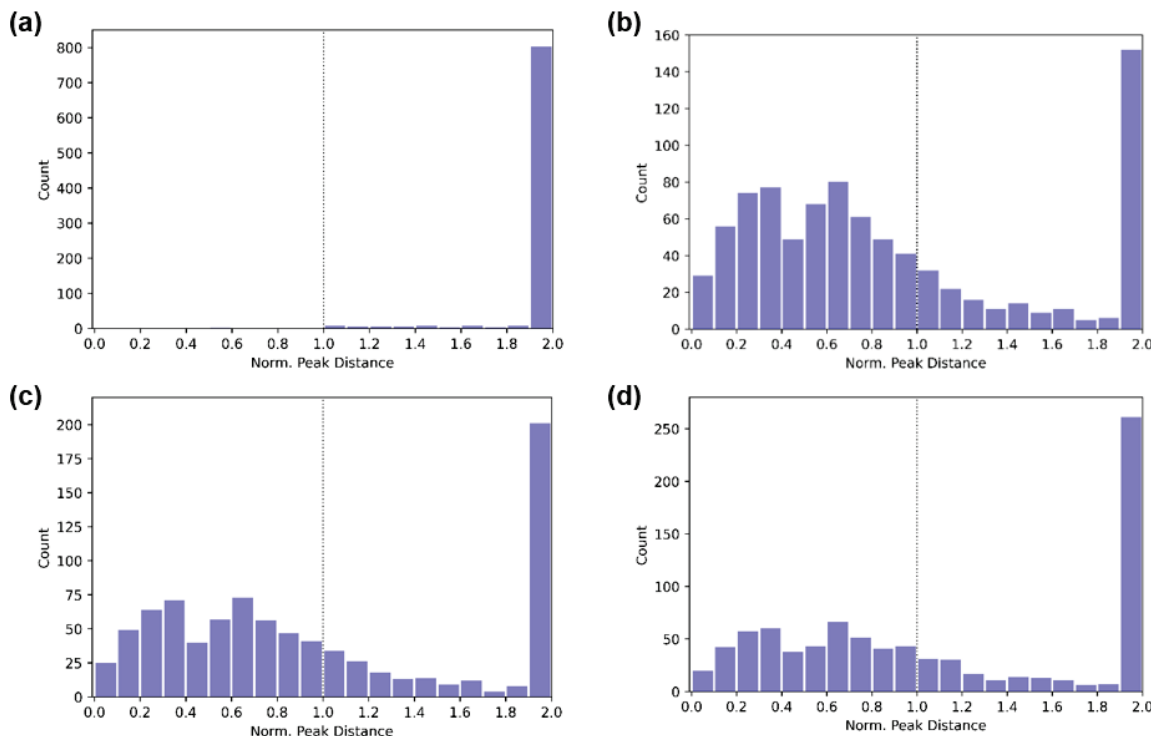


Figure IV-4: Distance of neighboring peaks normalized to the FWHM, which is a function of the mass resolving power of the mass analyzer and the nominal mass of the ion. For each ion, the distance to the closest neighbor with a relative peak intensity that exceeds 20%, 50%, or 100% is recorded. The average mass spectra observed during Run 2213 by the NH₄⁺-Orbitrap is used to generate the analysis. (a) Orbitrap mass analyzer (mass resolution \sim 140 000) >99% of ions are separated by at least 1 FWHM from their neighbors with a relative intensity threshold being set at 20%. (b) TOF mass analyzer (mass resolution \sim 10,000) >46% of ions are separated by at least 1 FWHM from their neighbors with a relative intensity threshold being set at 100%. (c) TOF mass analyzer >39% of ions are separated by at least 1 FWHM from their neighbors with a relative intensity threshold is set at 50%. (d) TOF mass analyzer >32% of ions are separated by at least 1 FWHM from their neighbors with a relative intensity threshold is set at 20%.

Orbitrap has been reported to have a non-linear response to compounds present at extremely low concentrations, which is neither instrumental nor reagent ion dependent as shown in our

previous results (Riva et al., 2020a; Cai et al., 2022). A similar evaluation was performed for the NH₄⁺-Orbitrap by comparing the measured vs the theoretical isotopic intensities. As shown in Fig. IV-5, the NH₄⁺-Orbitrap provides a linear response for ion intensity greater than $\sim 1 \times 10^4$ cps, which corresponds the limit of quantification (LoQ, corresponding to lowest normalized signal observed within the linear range) of the Orbitrap $\sim 1 \times 10^6$ molecules cm⁻³ estimated using the calibration factor derived from NO₃⁻-LTOF (see section 2.2), which is consistent with previous study (Riva et al., 2020a).

IV.3.2 Characterization of OVOC by four instruments

Illustrated in Fig. IV-5 are Kendrick mass defect plots of OOMs measured by CI-(NH₄⁺)-Orbitrap, CI-(NO₃⁻)-LTOF, PTR3-TOF, and I⁻-FIGAERO-CIMS, identifying species of 460, 189, 90, and 23, respectively. The NH₄⁺-Orbitrap detected the widest range of products, including HOMs and the less oxidized species (i.e., O < 6). Out of the 460 compounds, 11% were amine contaminations. The number of O atoms in OOMs varied from 1 to 11 in monomers (C₂-C₁₀) and from 2 to 16 for dimeric products (C₁₄-C₂₀), with an average elemental oxygen-to-carbon ratio (O:C) of 0.4 ± 0.2. As expected, the NO₃⁻-LTOF exhibited a very good sensitivity towards HOMs, with the highest O:C of 0.7 ± 0.4. The PTR3-TOF mainly detected compounds below m/Q 300 Th with an average O:C of 0.4 ± 0.3. However, it is important to point out that the PTR3-TOF was optimized to achieve sensitive measurements of ammonia and amines, impacting its capability to detect OOMs. Gas-phase concentrations of OOMs were too low to be efficiently detected in real-time via the gas-phase sampling port of the I⁻-FIGAERO-CIMS. As a result, fewer monomers of C₈₋₁₀ and dimers of C₁₉₋₂₀ were observed using the I⁻-FIGAERO-CIMS, with an average O:C of 0.5 ± 0.2.

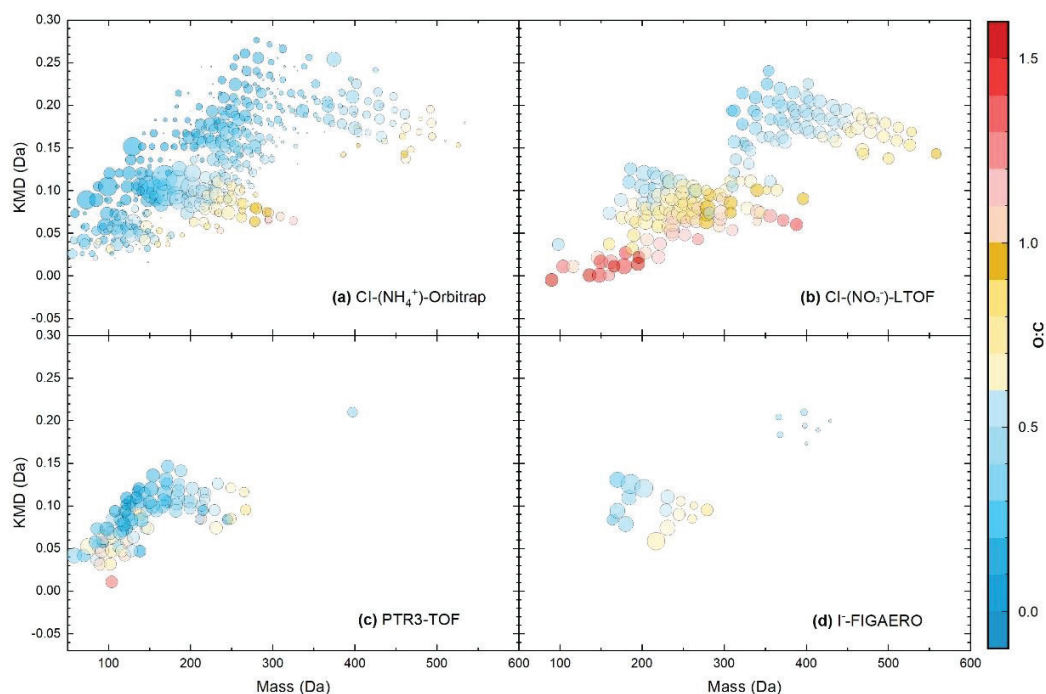


Figure IV-5: Mass defect plots for organic compounds measured by (a) CI- (NH_4^+) -Orbitrap, (b) CI- (NO_3^-) -LTOF, (c) PTR3-TOF and (d) I $^-$ -FIGAERO. The x-axis represents the mass-to-charge ratio of the neutral analyte and the y-axis represents the corresponding mass defect, which is the difference between their exact mass and nominal mass.(Schobesberger et al., 2013) Markers were all sized by the logarithm of their corresponding signals and colored by the O:C value. Run 2213: α -pinene oxidation products at -10 °C and 20% RH. α -pinene was ~0.41 ppbv and O₃ ~110 ppbv, NO₂ ~1.75 ppbv, NO ~0.12 ppbv and CO ~1000 ppbv.

IV.3.3 Instrumental comparisons: correlations

Due to the selectivity and the sensitivity of the analytical methods, not all ions were observed by each mass spectrometer, and thus only a fraction (~22%) of the identified species can be compared. To identify how NH₄⁺-Orbitrap performed compare to the other mass spectrometers, a correlation including all co-detected ions was realized. Table IV-1 summarizes the experimental conditions the runs used for performing this analysis. The data set covers a wide variety of conditions, such as the different concentration of α -pinene, NO_x, SO₂, and CO, as well as RH. The good correlations imply that both instruments were likely measuring the same compounds. A Pearson correlation coefficient R^2 was calculated, using the time evolution of OOMs, having the same elemental

composition measured by the different mass spectrometers. Figure IV-6 displays the correlation coefficient of detected compounds, with marker size scaled by R^2 . NH_4^+ -Orbitrap showed an excellent correlation ($R^2 > 0.80$) for ~30% of the compounds co-detected with the NO_3^- -LTOF. In addition, it showed high correlations with PTR3-TOF including 89 species having a correlation R^2 greater than 0.50. I⁻-FIGAERO-CIMS showed correlations $R^2 > 0.90$ for certain families of compounds, like $\text{C}_{10}\text{H}_{15}\text{O}_{5-7}\text{N}$ and $\text{C}_{20}\text{H}_{31}\text{O}_{7,9}\text{N}$. By comparing the coverage regions of the instruments across multiple experimental conditions, the NH_4^+ -Orbitrap was capable of covering the widest range of compounds and showed an overall good agreement with other mass spectrometers.

Table IV-1: Main experimental conditions of selected runs analyzed by NH_4^+ -Orbitrap.

Run	α -pinene (ppbv)	O_3 (ppbv)	NO_x (ppbv)	CO (ppbv)	SO_2 (ppbv)	RH (%)	T (°C)
2211	2	110	0	130	0	10→80	-10
2213	0.41	110	1.75	1000	0	20	-10

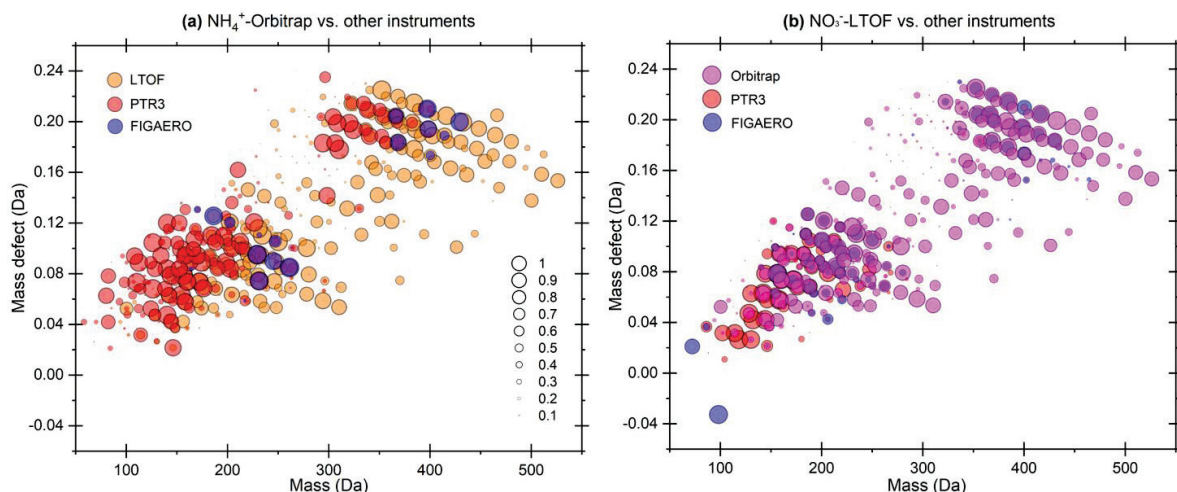


Figure IV-6: Mass defect plots depicting the compounds of which time series correlation was observed by (a) CI-(NH_4^+)-Orbitrap and (b) CI-(NO_3^-)-LTOF with other MS instruments. Each circle represents a molecule and marker size represents the correlation R^2 of time series of the molecule between two different MS instruments. Run 2211 and 2213 were used.

Figure IV-7 summarizes the performance of each mass spectrometer in detecting monomeric compounds, such as $C_{10}H_{16}O_n$. The y-axis is arbitrary and represents a qualitative characterization of the oxygen content when compounds were detected by different CI schemes. Similar to previous results, the I^- -FIGAERO-CIMS detected OOMs with several oxygens starting from 3, but were not optimal for the detection of monomers with O numbers greater than 7 (Riva et al., 2019b). The NO_3^- -LTOF was mainly selective towards HOMs with O number greater than 6 (Riva et al., 2019b). The PTR3-TOF had limited capabilities in detecting OOMs with more than 5 O atoms due to the optimization of the instrument to obtain a very sensitive measurement of ammonia. The amine reagent ions have proven promising abilities for detecting OOMs, but was limited to being used in comparable clean systems due to the considerable depletion of the reagent ion and the presence of overlapping peaks (Berndt et al., 2017; Berndt et al., 2018b; Riva et al., 2019b). While showing a similar OOMs detection range to amines, NH_4^+ provides a linear response to higher loading. As shown in Fig. IV-8, background peaks were not impacted by atmospheric relevant additions of O_3 and α -pinene.

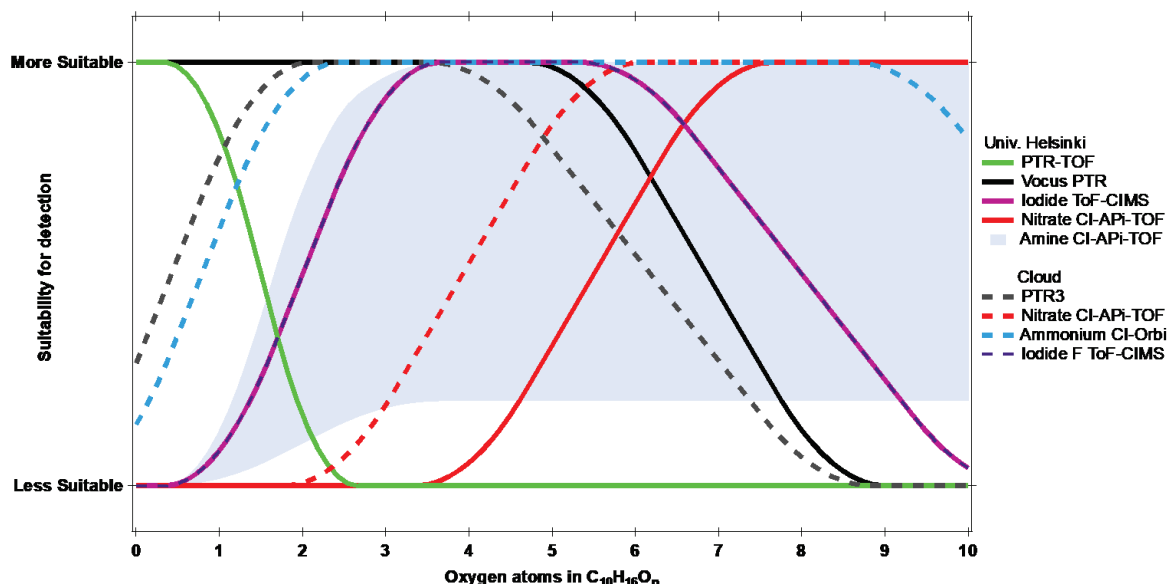


Figure IV-7: Estimated detection suitability of the different CIMS techniques for monomers from α -pinene ozonolysis, plotted as a function of the number of oxygen atoms. Image modified from Riva et al.(Riva et al., 2019b)

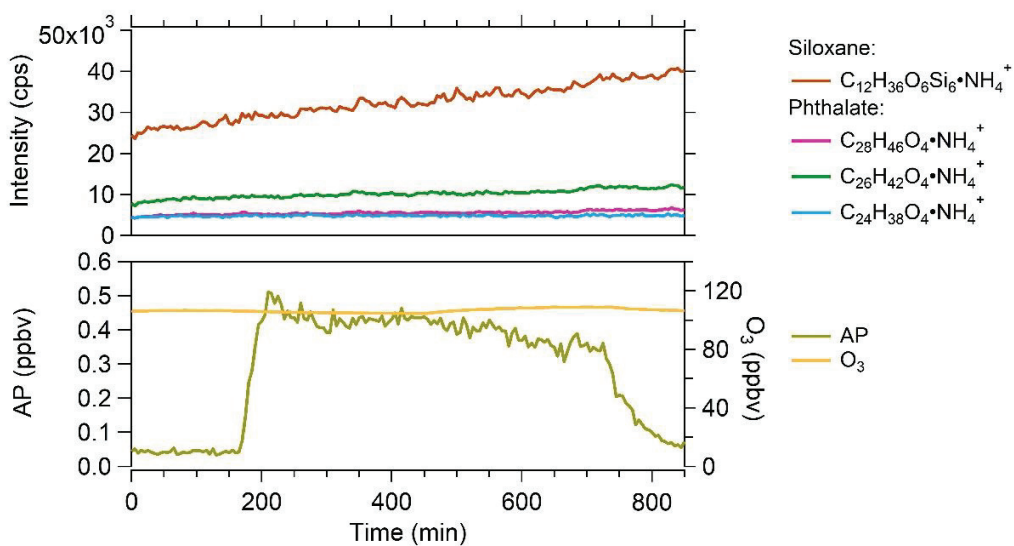


Figure IV-8: Constant time evolution of background ions showing the linearity of reagent ion NH_4^+ . Siloxanes and phthalates clustered with NH_4^+ were not impacted by the addition of α -pinene, which means that the ionization technique remains linear under atmospheric relevant conditions. Run 2213: α -pinene oxidation products at -10 °C and 20% RH. α -pinene was ~0.41 ppbv and O_3 ~110 ppbv, NO_2 ~1.75 ppbv, NO ~0.12 ppbv and CO ~1000 ppbv.

IV.3.4 Instrumental comparisons: concentration estimates

Concentrations of the identified compounds were estimated for NH_4^+ -Orbitrap, as described in section IV.2.2. The sensitivity of NH_4^+ -Orbitrap using other instruments was determined to provide semi-quantitative information. For instance, concentrations of the most abundant C_{10} -monomers (i.e., $C_{10}H_{14/16}O_n$) were estimated using different calibration factors (Fig. IV-9), which were measured during a steady-state conditions (i.e., Run 2211 with $[O_3] = 100$ ppbv and $[\alpha$ -pinene] = 2 ppbv, RH = 10%). Using calibration factors obtained from two independent correlation analysis (i.e., using the PTR3-TOF and the NO_3^- -LTOF), concentration of C_{10} -monomers measured by NH_4^+ -Orbitrap are within a factor of 2, showing a fairly good agreement between the different instruments and underlining the robustness of the methodology.

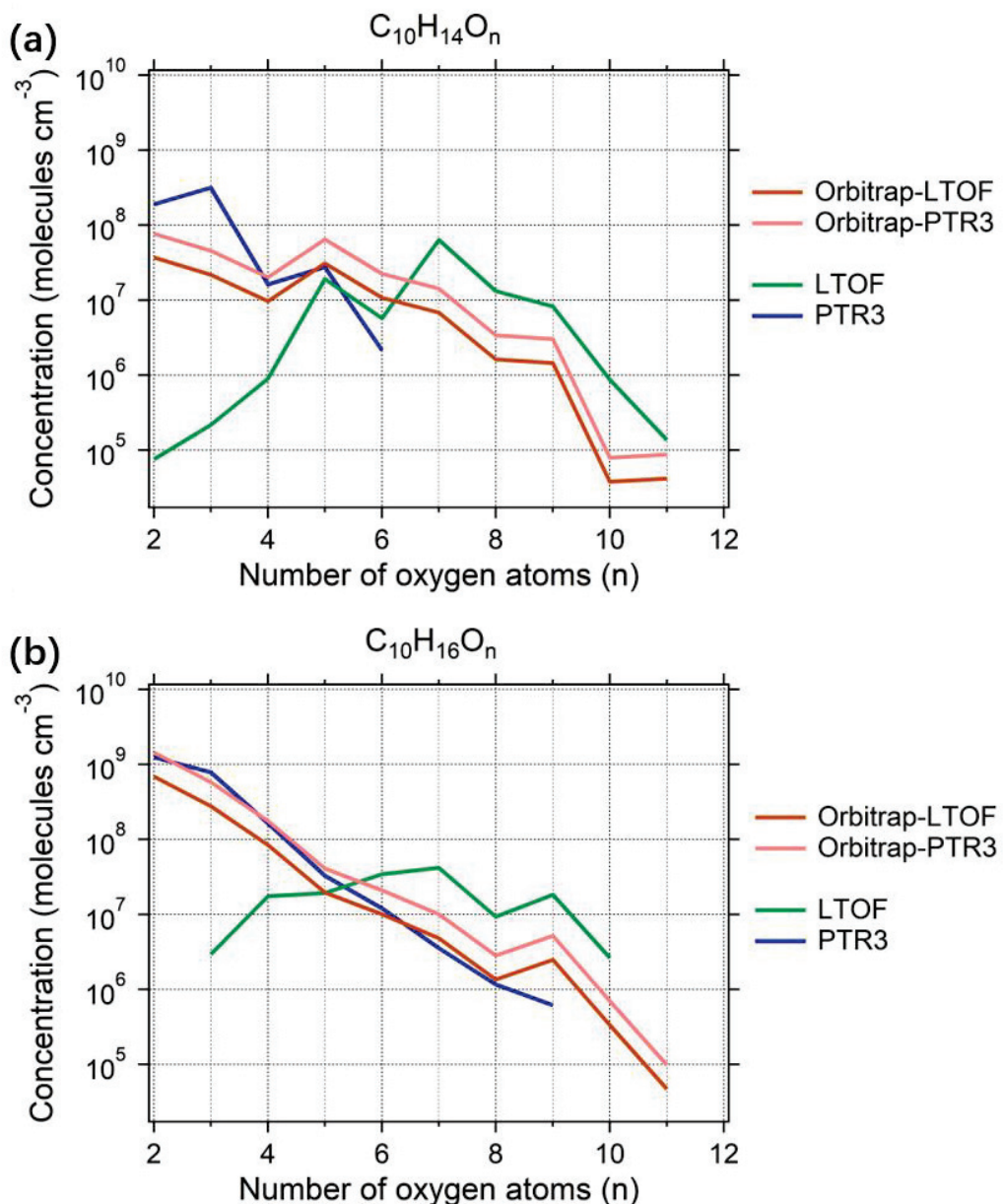


Figure IV-9: Estimated concentrations of the main C_{10} -monomer oxidation products. Run 2211 was used.

As previously reported, Orbitrap provided a non-linear response to compounds present at extremely low concentrations, which is neither instrumental nor reagent ion dependent as shown in our previous results (Riva et al., 2020a; Cai et al., 2022). A similar evaluation was performed for the NH_4^+ -Orbitrap by comparing the measured vs. the theoretical isotopic intensities. As shown

in Fig. IV-10, the NH_4^+ -Orbitrap provided a linear response for ion intensity greater than $\sim 5 \times 10^3$ cps, which corresponded to the limit of quantification (LoQ, corresponding to lowest normalized signal observed within the linear range) of the Orbitrap $\sim 5 \times 10^5$ molecules cm^{-3} estimated using the calibration factor derived from NO_3^- -LTOF, which is consistent with previous study (Riva et al., 2020a).

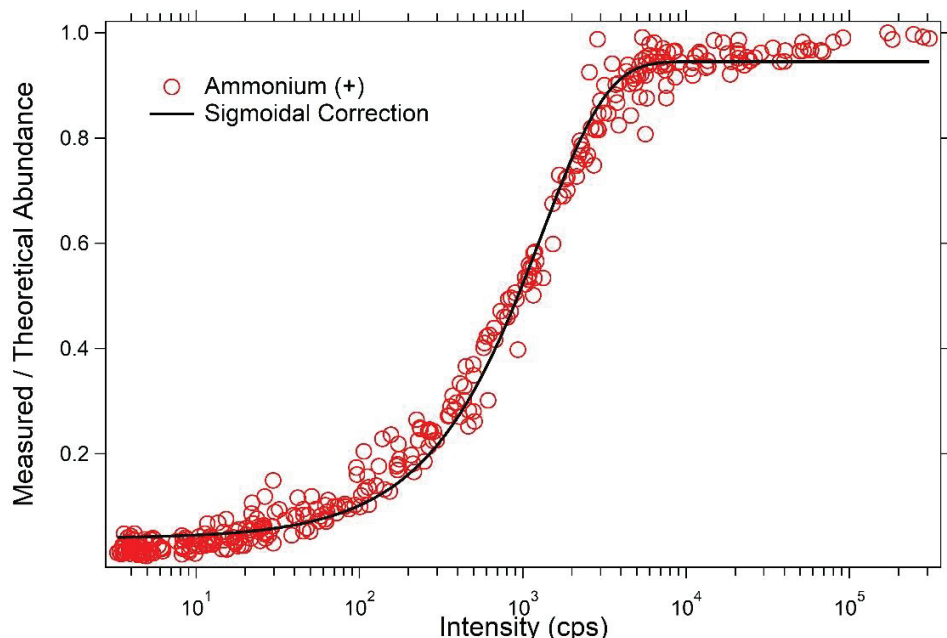


Figure 10: Linearity of the Orbitrap as a function of signal intensity measured with ammonium (NH_4^+) reagent ions. The black fit is the “sigmoidal correction function” based on a sigmoidal fitting algorithm.

Applying the calibration factors to all measured OVOCs (Fig. IV-11), concentrations measured by the NH_4^+ -Orbitrap determined by two different calibration factors. Comparing to other mass spectrometers, the NH_4^+ -Orbitrap seemed to capture the largest fraction of the reacted carbon. Out of the largest contributors to the reacted carbon, pinonaldehyde (i.e., $\text{C}_{10}\text{H}_{16}\text{O}_2$) was not efficiently detected by NO_3^- -LTOF, which is consistent with the higher selectivity of the reagent ions. While PTR3-TOF mainly detected C_{8-10} monomers. Overall, NH_4^+ -Orbitrap brings potential for a better quantification of the large variety of OOMs produced from the VOC oxidation.

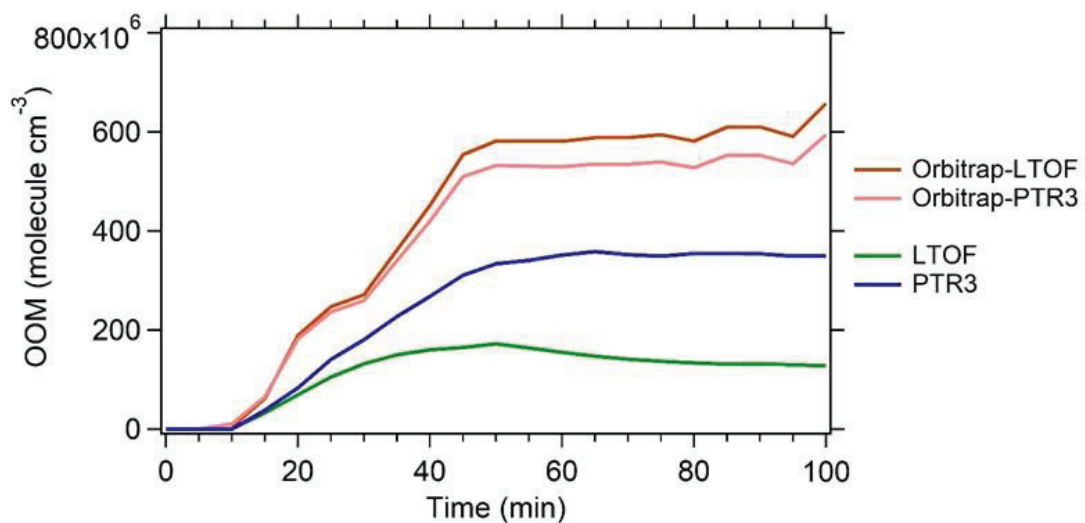


Figure IV-11: Estimated concentrations of all measured OOMs in the photooxidation of α -pinene. All monomers C₈₋₁₀ and dimers C₁₈₋₂₀ measured by CI-(NH₄⁺)-Orbitrap, CI-(NO₃⁻)-LTOF, and PTR3-TOF were summed up. The concentrations of OOM measured by NH₄⁺-Orbitrap were quantified by the calibration factors derived from correlation analysis between NH₄⁺-Orbitrap and NO₃⁻-LTOF (Orbitrap-LTOF, light green) or PTR3-TOF (Orbitrap-PTR3, light blue), respectively. Run 2213 was used.

IV.3.5 RH dependance of NH₄⁺-Orbitrap

The sensitivity of the reagent-adduct ionization has been reported to be affected by the presence of water vapor for a wide variety of reagent ions (Lee et al., 2014; Breitenlechner et al., 2017). The impact of RH on the detection of OOMs by the NH₄⁺-Orbitrap was also studied. While the concentrations of gas phase precursor and oxidant remained constant the RH was raised from 10% to 80%, resulting in a constant production rate (Surdu et al., 2023) and an increase in the condensation sink (Fig. IV-12), the signal of organic vapor behaved inconsistently during the RH ramp. As shown in Fig. IV-13, the NH₄⁺-Orbitrap showed an important RH dependence. For instance, the less (i.e., O < 5) oxygenated molecules increased with increasing RH, especially compounds with carbon numbers C₈; the signal of highly (i.e., O > 10) oxygenated molecules decreased as a function of RH. The evolution of the signal intensity of the ions measured by the

NH_4^+ -Orbitrap might be explained by multiple reasons, such as water affecting the ionization efficiency or altering the physicochemical processes.

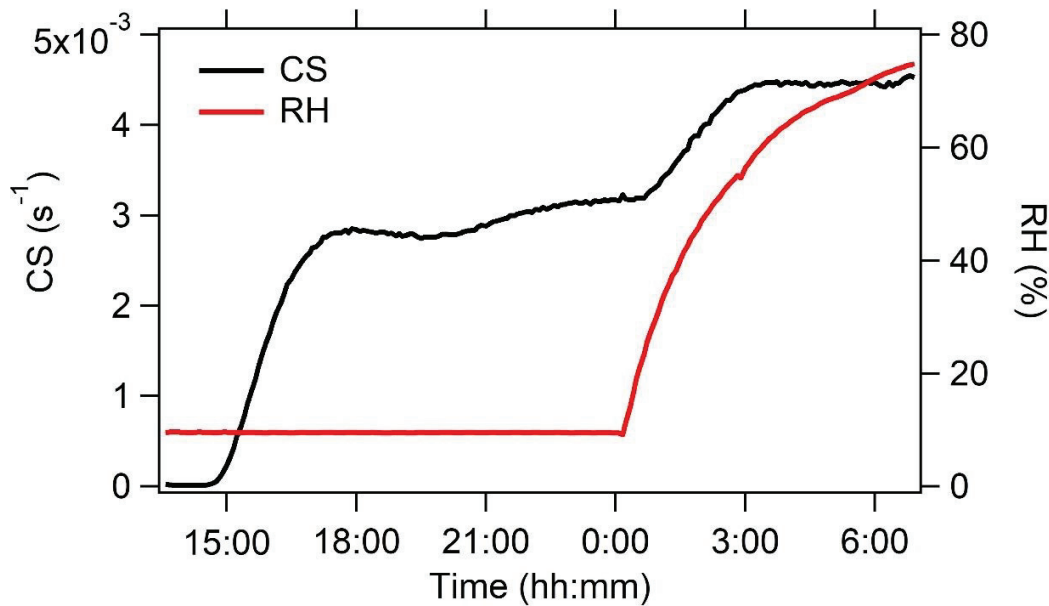


Figure IV-12: Time series of condensation sink (CS) where the RH is ramped up. Run 2211 were used.

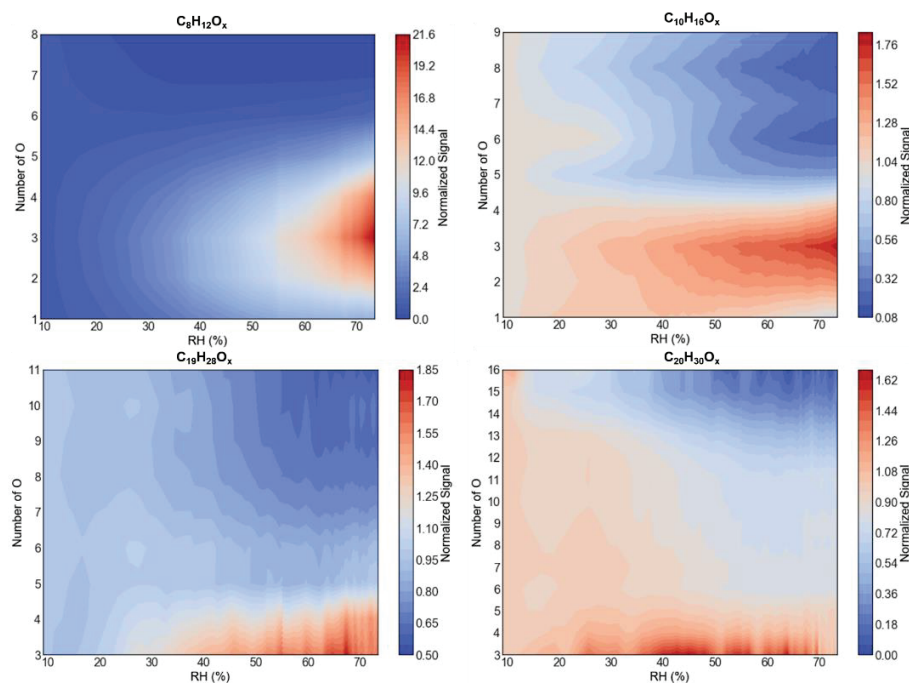


Figure IV-13: The effect of relative humidity on the distribution of the most abundant monomers and dimers measured by NH_4^+ -Orbitrap. The RH ramped from $\sim 10\%$ to $\sim 80\%$. The normalized signal represents the signal variation ratio at certain RH compared to that at RH = 10%, normalized signal = $\frac{\text{signal}_{RH}}{\text{signal}_{10\%}}$. Run 2211 were used.

Firstly, the efficiency to a particular compound partly relied on whether water vapor competes with the ammonium ion, lowering the sensitivity, or whether it acted as a third body to stabilize the ammonium-organic analyte cluster by removing extra energy from the collision, raising the sensitivity (Lee et al., 2014). NH_4^+ primary ions can cluster with water molecules when humidity increased, thereby reducing the clustering of the NH_4^+ with organic analytes (Breitenlechner et al., 2017). However, the formed $\text{NH}_4^+X_n$ (X being NH_3 or H_2O ; $n = 1,2$) clusters might also act as reagent ions and ionized OOMs through ligand switching reactions, which are expected to be fast and thus improve the charging efficiency (Hansel et al., 2018). Compared to previous NH_4^+ -CIMS, the $\text{NH}_4^+X_n$ reagent ions are expected to be larger due to the absence of the field in the ion-molecular-reaction zone in Orbitrap, resulting in greater ligand exchanging and increasing the sensitivity for the less oxygenated species (Canaval et al., 2019). For RH-independent compounds, this may be due to the existence of very stable complex with NH_4^+ reagent ion, or sufficient internal

vibrational modes to disperse extra energy from the collision (Lee et al., 2014). The highly oxygenated dimers in the category of ULVOCs and ELVOCs which largely partition to the particle phase regardless of the presence of water, might be possible that water may also affect the physicochemical processes (i.e., multiphase chemistry, partitioning,...), in this case possibly causing the decomposition of highly oxygenated molecules in the particle phase to create the less and moderately oxygenated products, e.g., C₈H₁₂O₁₋₅ (up to a 30-fold increase in the gas phase) (Pospisilova et al., 2020), and/or leading to an increase in the driving force of gas-particle partitioning of highly oxygenated species (Surdu et al., 2023).

IV.3.6 Volatility distribution by four instruments

Figure IV-14 shows the distribution oxidation products measured by four MS instruments according to their saturation vapor concentrations ($\log_{10}C_{\text{sat}}$) estimated using the modified Li et al. approach (Li et al., 2016; Isaacman-Vanwertz and Aumont, 2021). OOMs were grouped into six volatility regimes; ultralow-volatility (ULVOCs), extremely low volatility (ELVOCs), low-volatility (LVOCs), semi-volatile (SVOCs), intermediate-volatility organic compounds (IVOC) and VOC based on volatility basis sets (VBS), where ULVOCs and ELVOCs initiate cluster growth and form new particles. Each volatility bin summed up the signal intensity of OOMs within the volatility range. The mean contributions of these compound groups are shown in the VBS pie charts. The ULVOC, ELVOC, and LVOC classes were well captured by NH₄⁺-Orbitrap and NO₃⁻-LTOF. While PTR3-TOF were only able to characterize the SVOC and IVOC classes. IVOC and VOC groups in PTR3-TOF and NH₄⁺-Orbitrap were generally less oxygenated VOCs (i.e., O < 5). IVOC made up the biggest mass contributions for NH₄⁺-Orbitrap, and LVOC dominated in NO₃⁻-LTOF. Hence, the detection of NH₄⁺-Orbitrap covered the widest range of volatilities, clearly highlighting the benefit of using this technique for the formation and fate of OOMs. In the past, reagent switching was not practical, and users would run two mass spectrometer systems in parallel or use a Multi-scheme chemical IONization inlet (MION) with only one mass spectrometer to obtain the fullest possible mass spectrum (Rissanen et al., 2019; Huang et al., 2021). With NH₄⁺-Orbitrap it is now possible to cover the entire range of compounds which was not the case with most CI techniques.

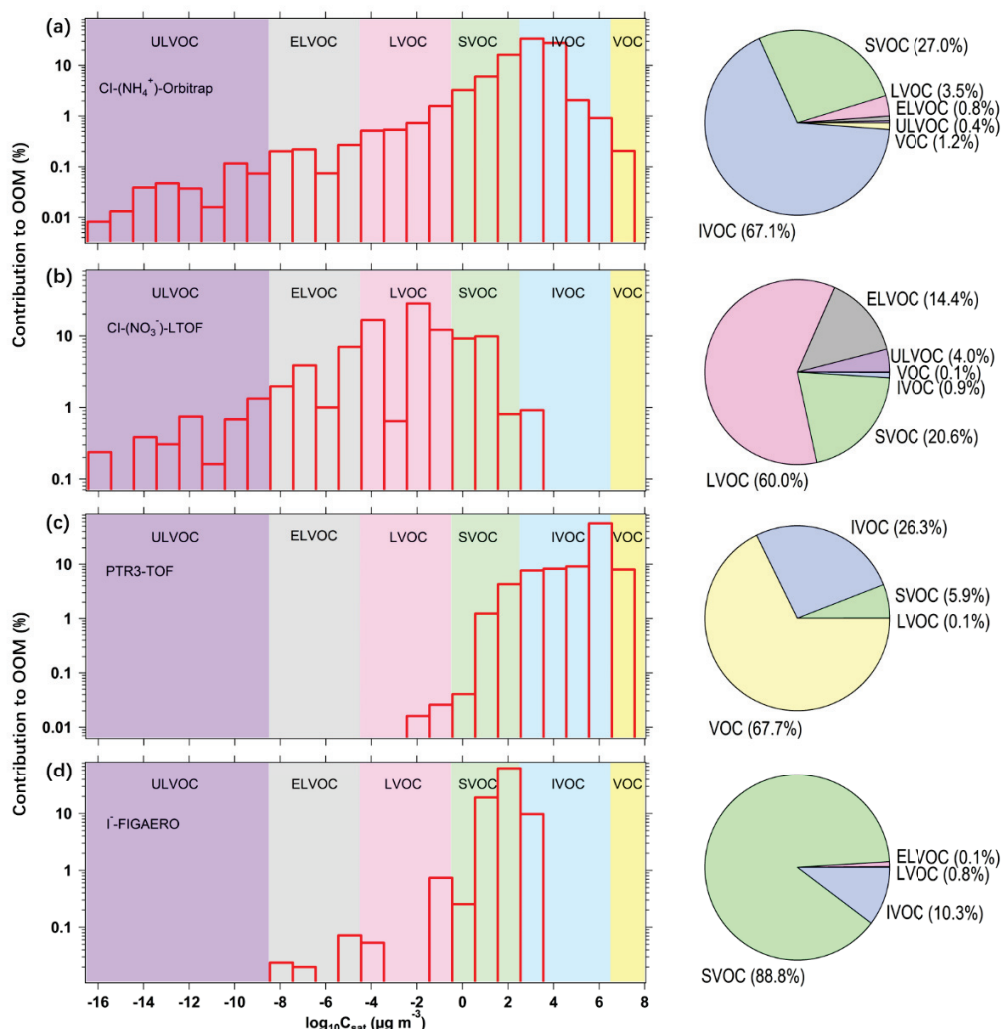


Figure IV-14: Volatility distribution comparison for organic compounds detected by (a) CI-(NH₄⁺)-Orbitrap, (b) CI-(NO₃⁻)-LTOF, (c) PTR3-TOF and (d) I⁻-FIGAERO. The background colors represent the saturation concentration (C_{sat}) in the range of ultra-low volatility (ULVOCs, purple), extremely low volatility (ELVOCs, gray), low volatility (LVOCs, pink), semi-volatile (SVOCs, green), intermediate volatility (IVOCs, blue) and volatile organic compounds (VOCs). The right pie charts are the corresponding contributions of VOC, IVOC, SVOC, LVOC, ELVOC, and ULVOC classes. Run 2213 was used.

IV.4. Conclusion

In conclusion, this study presents an intercomparison between CI-(NH₄⁺)-Orbitrap, CI-(NO₃⁻)-LTOF, PTR3-TOF, and I⁻-FIGAERO-CIMS based on the identification and quantification of OOMs formed from the ozonolysis of α-pinene under various environmental conditions. We used for the first time, NH₄⁺ adduct ions with the Orbitrap mass spectrometer to measure the oxygenated species. NH₄⁺-Orbitrap is a promising CIMS technique for a comprehensive measurement of the whole product distribution and provides a more complete understanding of the molecular composition and volatility of OOMs. In addition, NH₄⁺-Orbitrap measurements can be used as input to test or interpret environmental measurements to better predict the evolution of organic compounds using transport and climate models. However, it remains challenging to obtain an accurate quantification of the trace gaseous substances. It is worth expecting that NH₄⁺-Orbitrap can be not only useful for laboratory-based studies, but also to field observations, to provide a deeper understanding of atmospheric oxidation processes.

IV.5. References

- Berndt, T., Herrmann, H., and Kurten, T.: Direct Probing of Criegee Intermediates from Gas-Phase Ozonolysis Using Chemical Ionization Mass Spectrometry, *Journal of the American Chemical Society*, 139, 13387-13392, 10.1021/jacs.7b05849, 2017.
- Berndt, T., Mentler, B., Scholz, W., Fischer, L., Herrmann, H., Kulmala, M., and Hansel, A.: Accretion Product Formation from Ozonolysis and OH Radical Reaction of alpha-Pinene: Mechanistic Insight and the Influence of Isoprene and Ethylene, *Environmental science & technology*, 52, 11069-11077, 10.1021/acs.est.8b02210, 2018a.
- Berndt, T., Scholz, W., Mentler, B., Fischer, L., Herrmann, H., Kulmala, M., and Hansel, A.: Accretion Product Formation from Self- and Cross-Reactions of RO₂ Radicals in the Atmosphere, *Angewandte Chemie*, 57, 3820-3824, 10.1002/anie.201710989, 2018b.
- Berndt, T., Richters, S., Kaethner, R., Voigtlander, J., Stratmann, F., Sipila, M., Kulmala, M., and Herrmann, H.: Gas-Phase Ozonolysis of Cycloalkenes: Formation of Highly Oxidized RO₂ Radicals and Their Reactions with NO, NO₂, SO₂, and Other RO₂ Radicals, *The journal of physical chemistry. A*, 119, 10336-10348, 10.1021/acs.jpca.5b07295, 2015.
- Bianchi, F., Kurten, T., Riva, M., Mohr, C., Rissanen, M. P., Roldin, P., Berndt, T., Crounse, J. D., Wennberg, P. O., Mentel, T. F., Wildt, J., Junninen, H., Jokinen, T., Kulmala, M., Worsnop, D. R., Thornton, J. A., Donahue, N., Kjaergaard, H. G., and Ehn, M.: Highly Oxygenated Organic Molecules (HOM) from Gas-Phase Autoxidation Involving Peroxy Radicals: A Key Contributor to Atmospheric Aerosol, *Chemical reviews*, 119, 3472-3509, 10.1021/acs.chemrev.8b00395, 2019.
- Bianchi, F., Tröstl, J., Junninen, H., Frege, C., Henne, S., Hoyle, C. R., Molteni, U., Herrmann, E., Adamov, A., Bukowiecki, N., Chen, X., Duplissy, J., Gysel, M., Hutterli, M., Kangasluoma,

- J., Kontkanen, J., Kürten, A., Manninen, H. E., Münch, S., Peräkylä, O., Petäjä, T., Rondo, L., Williamson, C., Weingartner, E., Curtius, J., Worsnop, D. R., Kulmala, M., Dommen, J., and Baltensperger, U.: New particle formation in the free troposphere: A question of chemistry and timing, *Science*, 352, 1109-1112, 10.1126/science.aad5456, 2016.
- Breitenlechner, M., Fischer, L., Hainer, M., Heinritzi, M., Curtius, J., and Hansel, A.: PTR3: An Instrument for Studying the Lifecycle of Reactive Organic Carbon in the Atmosphere, *Analytical chemistry*, 89, 5824-5831, 10.1021/acs.analchem.6b05110, 2017.
- Cai, R., Huang, W., Meder, M., Bourgain, F., Aizikov, K., Riva, M., Bianchi, F., and Ehn, M.: Improving the Sensitivity of Fourier Transform Mass Spectrometer (Orbitrap) for Online Measurements of Atmospheric Vapors, *Analytical chemistry*, 94, 15746-15753, 10.1021/acs.analchem.2c03403, 2022.
- Cai, R., Li, Y., Clément, Y., Li, D., Dubois, C., Fabre, M., Besson, L., Perrier, S., George, C., Ehn, M., Huang, C., Yi, P., Ma, Y., and Riva, M.: Orbitool: a software tool for analyzing online Orbitrap mass spectrometry data, *Atmos. Meas. Tech.*, 14, 2377-2387, 10.5194/amt-14-2377-2021, 2021.
- Canaval, E., Hyttinen, N., Schmidbauer, B., Fischer, L., and Hansel, A.: NH₄⁺ Association and Proton Transfer Reactions With a Series of Organic Molecules, *Frontiers in Chemistry*, 7, 10.3389/fchem.2019.00191, 2019.
- Caudillo, L., Rörup, B., Heinritzi, M., Marie, G., Simon, M., Wagner, A. C., Müller, T., Granzin, M., Amorim, A., Ataei, F., Baalbaki, R., Bertozzi, B., Brasseur, Z., Chiu, R., Chu, B., Dada, L., Duplissy, J., Finkenzeller, H., Gonzalez Carracedo, L., He, X. C., Hofbauer, V., Kong, W., Lamkaddam, H., Lee, C. P., Lopez, B., Mahfouz, N. G. A., Makhmutov, V., Manninen, H. E., Marten, R., Massabò, D., Mauldin, R. L., Mentler, B., Molteni, U., Onnela, A., Pfeifer, J., Philippov, M., Piedehierro, A. A., Schervish, M., Scholz, W., Schulze, B., Shen, J., Stolzenburg, D., Stozhkov, Y., Surdu, M., Tauber, C., Tham, Y. J., Tian, P., Tomé, A., Vogt, S., Wang, M., Wang, D. S., Weber, S. K., Welti, A., Yonghong, W., Yusheng, W., Zauner-Wieczorek, M., Baltensperger, U., El Haddad, I., Flagan, R. C., Hansel, A., Höhler, K., Kirkby, J., Kulmala, M., Lehtipalo, K., Möhler, O., Saathoff, H., Volkamer, R., Winkler, P. M., Donahue, N. M., Kürten, A., and Curtius, J.: Chemical composition of nanoparticles from α -pinene nucleation and the influence of isoprene and relative humidity at low temperature, *Atmos. Chem. Phys.*, 21, 17099-17114, 10.5194/acp-21-17099-2021, 2021.
- Crounse, J. D., Nielsen, L. B., Jørgensen, S., Kjaergaard, H. G., and Wennberg, P. O.: Autoxidation of Organic Compounds in the Atmosphere, *The Journal of Physical Chemistry Letters*, 4, 3513-3520, 10.1021/jz4019207, 2013.
- Daumit, K. E., Kessler, S. H., and Kroll, J. H.: Average chemical properties and potential formation pathways of highly oxidized organic aerosol, *Faraday discussions*, 165, 181-202, 10.1039/c3fd00045a, 2013.
- Donahue, N. M., Epstein, S. A., Pandis, S. N., and Robinson, A. L.: A two-dimensional volatility basis set: 1. organic-aerosol mixing thermodynamics, *Atmospheric Chemistry and Physics*, 11, 3303-3318, 10.5194/acp-11-3303-2011, 2011.
- Ehn, M., Junninen, H., Petäjä, T., Kurtén, T., Kerminen, V. M., Schobesberger, S., Manninen, H. E., Ortega, I. K., Vehkämäki, H., Kulmala, M., and Worsnop, D. R.: Composition and temporal behavior of ambient ions in the boreal forest, *Atmospheric Chemistry and Physics*, 10, 8513-8530, 10.5194/acp-10-8513-2010, 2010.

- Ehn, M., Thornton, J. A., Kleist, E., Sipila, M., Junninen, H., Pullinen, I., Springer, M., Rubach, F., Tillmann, R., Lee, B., Lopez-Hilfiker, F., Andres, S., Acir, I. H., Rissanen, M., Jokinen, T., Schobesberger, S., Kangasluoma, J., Kontkanen, J., Nieminen, T., Kurten, T., Nielsen, L. B., Jorgensen, S., Kjaergaard, H. G., Canagaratna, M., Maso, M. D., Berndt, T., Petaja, T., Wahner, A., Kerminen, V. M., Kulmala, M., Worsnop, D. R., Wildt, J., and Mentel, T. F.: A large source of low-volatility secondary organic aerosol, *Nature*, 506, 476-479, 10.1038/nature13032, 2014.
- Fan, J., Wang, Y., Rosenfeld, D., and Liu, X.: Review of Aerosol–Cloud Interactions: Mechanisms, Significance, and Challenges, *Journal of the Atmospheric Sciences*, 73, 4221-4252, 10.1175/jas-d-16-0037.1, 2016.
- Glasius, M. and Goldstein, A. H.: Recent Discoveries and Future Challenges in Atmospheric Organic Chemistry, *Environmental science & technology*, 50, 2754-2764, 10.1021/acs.est.5b05105, 2016.
- Hallquist, M., Wenger, J. C., Baltensperger, U., Rudich, Y., Simpson, D., Claeys, M., Dommen, J., Donahue, N. M., George, C., Goldstein, A. H., Hamilton, J. F., Herrmann, H., Hoffmann, T., Iinuma, Y., Jang, M., Jenkin, M. E., Jimenez, J. L., Kiendler-Scharr, A., Maenhaut, W., McFiggans, G., Mentel, T. F., Monod, A., Prévôt, A. S. H., Seinfeld, J. H., Surratt, J. D., Szmigielski, R., and Wildt, J.: The formation, properties and impact of secondary organic aerosol: current and emerging issues, *Atmos. Chem. Phys.*, 9, 5155-5236, 10.5194/acp-9-5155-2009, 2009.
- Hansel, A., Scholz, W., Mentler, B., Fischer, L., and Berndt, T.: Detection of RO₂ radicals and other products from cyclohexene ozonolysis with NH₄⁺ and acetate chemical ionization mass spectrometry, *Atmospheric Environment*, 186, 248-255, 10.1016/j.atmosenv.2018.04.023, 2018.
- Haywood, J. and Boucher, O.: Estimates of the direct and indirect radiative forcing due to tropospheric aerosols: A review, *Reviews of geophysics*, 38, 513-543, 2000.
- Heinritzi, M., Simon, M., Steiner, G., Wagner, A. C., Kürten, A., Hansel, A., and Curtius, J.: Characterization of the mass-dependent transmission efficiency of a CIMS, *Atmospheric Measurement Techniques*, 9, 1449-1460, 10.5194/amt-9-1449-2016, 2016.
- Huang, W., Li, H., Sarnela, N., Heikkilä, L., Tham, Y. J., Mikkilä, J., Thomas, S. J., Donahue, N. M., Kulmala, M., and Bianchi, F.: Measurement report: Molecular composition and volatility of gaseous organic compounds in a boreal forest – from volatile organic compounds to highly oxygenated organic molecules, *Atmospheric Chemistry and Physics*, 21, 8961-8977, 10.5194/acp-21-8961-2021, 2021.
- Isaacman-VanWertz, G. and Aumont, B.: Impact of organic molecular structure on the estimation of atmospherically relevant physicochemical parameters, *Atmospheric Chemistry and Physics*, 21, 6541-6563, 10.5194/acp-21-6541-2021, 2021.
- Jimenez, J. L., Canagaratna, M. R., Donahue, N. M., Prevot, A. S. H., Zhang, Q., Kroll, J. H., DeCarlo, P. F., Allan, J. D., Coe, H., Ng, N. L., Aiken, A. C., Docherty, K. S., Ulbrich, I. M., Grieshop, A. P., Robinson, A. L., Duplissy, J., Smith, J. D., Wilson, K. R., Lanz, V. A., Hueglin, C., Sun, Y. L., Tian, J., Laaksonen, A., Raatikainen, T., Rautiainen, J., Vaattovaara, P., Ehn, M., Kulmala, M., Tomlinson, J. M., Collins, D. R., Cubison, M. J., Dunlea, J., Huffman, J. A., Onasch, T. B., Alfarra, M. R., Williams, P. I., Bower, K., Kondo, Y., Schneider, J., Drewnick, F., Borrmann, S., Weimer, S., Demerjian, K., Salcedo, D., Cottrell, L., Griffin, R., Takami, A., Miyoshi, T., Hatakeyama, S., Shimono, A., Sun, J. Y., Zhang,

- Y. M., Dzepina, K., Kimmel, J. R., Sueper, D., Jayne, J. T., Herndon, S. C., Trimborn, A. M., Williams, L. R., Wood, E. C., Middlebrook, A. M., Kolb, C. E., Baltensperger, U., and Worsnop, D. R.: Evolution of Organic Aerosols in the Atmosphere, *Science*, 326, 1525-1529, doi:10.1126/science.1180353, 2009.
- Jokinen, T., Sipilä, M., Junninen, H., Ehn, M., Lönn, G., Hakala, J., Petäjä, T., Mauldin, R. L., Kulmala, M., and Worsnop, D. R.: Atmospheric sulphuric acid and neutral cluster measurements using CI-APi-TOF, *Atmospheric Chemistry and Physics*, 12, 4117-4125, 10.5194/acp-12-4117-2012, 2012.
- Jokinen, T., Berndt, T., Makkonen, R., Kerminen, V. M., Junninen, H., Paasonen, P., Stratmann, F., Herrmann, H., Guenther, A. B., Worsnop, D. R., Kulmala, M., Ehn, M., and Sipila, M.: Production of extremely low volatile organic compounds from biogenic emissions: Measured yields and atmospheric implications, *Proceedings of the National Academy of Sciences of the United States of America*, 112, 7123-7128, 10.1073/pnas.1423977112, 2015.
- Kirkby, J., Curtius, J., Almeida, J., Dunne, E., Duplissy, J., Ehrhart, S., Franchin, A., Gagne, S., Ickes, L., Kurten, A., Kupc, A., Metzger, A., Riccobono, F., Rondo, L., Schobesberger, S., Tsagkogeorgas, G., Wimmer, D., Amorim, A., Bianchi, F., Breitenlechner, M., David, A., Dommen, J., Downard, A., Ehn, M., Flagan, R. C., Haider, S., Hansel, A., Hauser, D., Jud, W., Junninen, H., Kreissl, F., Kvashin, A., Laaksonen, A., Lehtipalo, K., Lima, J., Lovejoy, E. R., Makhmutov, V., Mathot, S., Mikkila, J., Minginette, P., Mogo, S., Nieminen, T., Onnela, A., Pereira, P., Petaja, T., Schnitzhofer, R., Seinfeld, J. H., Sipila, M., Stozhkov, Y., Stratmann, F., Tome, A., Vanhanen, J., Viisanen, Y., Vrtala, A., Wagner, P. E., Walther, H., Weingartner, E., Wex, H., Winkler, P. M., Carslaw, K. S., Worsnop, D. R., Baltensperger, U., and Kulmala, M.: Role of sulphuric acid, ammonia and galactic cosmic rays in atmospheric aerosol nucleation, *Nature*, 476, 429-433, 10.1038/nature10343, 2011.
- Kirkby, J., Duplissy, J., Sengupta, K., Frege, C., Gordon, H., Williamson, C., Heinritzi, M., Simon, M., Yan, C., Almeida, J., Tröstl, J., Nieminen, T., Ortega, I. K., Wagner, R., Adamov, A., Amorim, A., Bernhammer, A.-K., Bianchi, F., Breitenlechner, M., Brilke, S., Chen, X., Craven, J., Dias, A., Ehrhart, S., Flagan, R. C., Franchin, A., Fuchs, C., Guida, R., Hakala, J., Hoyle, C. R., Jokinen, T., Junninen, H., Kangasluoma, J., Kim, J., Krapf, M., Kürten, A., Laaksonen, A., Lehtipalo, K., Makhmutov, V., Mathot, S., Molteni, U., Onnela, A., Peräkylä, O., Piel, F., Petäjä, T., Praplan, A. P., Pringle, K., Rap, A., Richards, N. A. D., Riipinen, I., Rissanen, M. P., Rondo, L., Sarnela, N., Schobesberger, S., Scott, C. E., Seinfeld, J. H., Sipilä, M., Steiner, G., Stozhkov, Y., Stratmann, F., Tomé, A., Virtanen, A., Vogel, A. L., Wagner, A. C., Wagner, P. E., Weingartner, E., Wimmer, D., Winkler, P. M., Ye, P., Zhang, X., Hansel, A., Dommen, J., Donahue, N. M., Worsnop, D. R., Baltensperger, U., Kulmala, M., Carslaw, K. S., and Curtius, J.: Ion-induced nucleation of pure biogenic particles, *Nature*, 533, 521, 10.1038/nature17953, 2016.
- Knopf, D. A., Poschl, U., and Shiraiwa, M.: Radial diffusion and penetration of gas molecules and aerosol particles through laminar flow reactors, denuders, and sampling tubes, *Analytical chemistry*, 87, 3746-3754, 10.1021/ac5042395, 2015.
- Kurten, A., Rondo, L., Ehrhart, S., and Curtius, J.: Calibration of a chemical ionization mass spectrometer for the measurement of gaseous sulfuric acid, *The journal of physical chemistry. A*, 116, 6375-6386, 10.1021/jp212123n, 2012.

- Kurten, A., Jokinen, T., Simon, M., Sipila, M., Sarnela, N., Junninen, H., Adamov, A., Almeida, J., Amorim, A., Bianchi, F., Breitenlechner, M., Dommen, J., Donahue, N. M., Duplissy, J., Ehrhart, S., Flagan, R. C., Franchin, A., Hakala, J., Hansel, A., Heinritzi, M., Hutterli, M., Kangasluoma, J., Kirkby, J., Laaksonen, A., Lehtipalo, K., Leiminger, M., Makhmutov, V., Mathot, S., Onnela, A., Petaja, T., Praplan, A. P., Riccobono, F., Rissanen, M. P., Rondo, L., Schobesberger, S., Seinfeld, J. H., Steiner, G., Tome, A., Trostl, J., Winkler, P. M., Williamson, C., Wimmer, D., Ye, P., Baltensperger, U., Carslaw, K. S., Kulmala, M., Worsnop, D. R., and Curtius, J.: Neutral molecular cluster formation of sulfuric acid-dimethylamine observed in real time under atmospheric conditions, *Proceedings of the National Academy of Sciences of the United States of America*, 111, 15019-15024, 10.1073/pnas.1404853111, 2014.
- Lee, B. H., Lopez-Hilfiker, F. D., Mohr, C., Kurten, T., Worsnop, D. R., and Thornton, J. A.: An iodide-adduct high-resolution time-of-flight chemical-ionization mass spectrometer: application to atmospheric inorganic and organic compounds, *Environmental science & technology*, 48, 6309-6317, 10.1021/es500362a, 2014.
- Li, H., Riva, M., Rantala, P., Heikkinen, L., Daellenbach, K., Krechmer, J. E., Flaud, P.-M., Worsnop, D., Kulmala, M., Villenave, E., Perraudeau, E., Ehn, M., and Bianchi, F.: Terpenes and their oxidation products in the French Landes forest: insights from Vocus PTR-TOF measurements, *Atmospheric Chemistry and Physics*, 20, 1941-1959, 10.5194/acp-20-1941-2020, 2020.
- Li, Y., Pöschl, U., and Shiraiwa, M.: Molecular corridors and parameterizations of volatility in the chemical evolution of organic aerosols, *Atmospheric Chemistry and Physics*, 16, 3327-3344, 10.5194/acp-16-3327-2016, 2016.
- Lindner, W., Hansel, A., and Jordan, A.: On-line monitoring of volatile organic compounds at pptv levels by means of proton-transfer-reaction mass spectrometry (PTR-MS) medical applications, food control and environmental research, *International Journal of Mass Spectrometry and Ion Processes*, 173, 191-241, [https://doi.org/10.1016/S0168-1176\(97\)00281-4](https://doi.org/10.1016/S0168-1176(97)00281-4), 1998.
- Lopez-Hilfiker, F. D., Mohr, C., Ehn, M., Rubach, F., Kleist, E., Wildt, J., Mentel, T. F., Lutz, A., Hallquist, M., Worsnop, D., and Thornton, J. A.: A novel method for online analysis of gas and particle composition: description and evaluation of a Filter Inlet for Gases and AEROSols (FIGAERO), *Atmospheric Measurement Techniques*, 7, 983-1001, 10.5194/amt-7-983-2014, 2014.
- Mellouki, A., Wallington, T. J., and Chen, J.: Atmospheric chemistry of oxygenated volatile organic compounds: impacts on air quality and climate, *Chemical reviews*, 115, 3984-4014, 10.1021/cr500549n, 2015.
- Pospisilova, V., Lopez-Hilfiker, F. D., Bell, D. M., El Haddad, I., Mohr, C., Huang, W., Heikkinen, L., Xiao, M., Dommen, J., Prevot, A. S. H., Baltensperger, U., and Slowik, J. G.: On the fate of oxygenated organic molecules in atmospheric aerosol particles, *Science Advances*, 6, eaax8922, doi:10.1126/sciadv.aax8922, 2020.
- Praplan, A. P., Schobesberger, S., Bianchi, F., Rissanen, M. P., Ehn, M., Jokinen, T., Junninen, H., Adamov, A., Amorim, A., Dommen, J., Duplissy, J., Hakala, J., Hansel, A., Heinritzi, M., Kangasluoma, J., Kirkby, J., Krapf, M., Kürten, A., Lehtipalo, K., Riccobono, F., Rondo, L., Sarnela, N., Simon, M., Tomé, A., Tröstl, J., Winkler, P. M., Williamson, C., Ye, P., Curtius, J., Baltensperger, U., Donahue, N. M., Kulmala, M., and Worsnop, D. R.:

- Elemental composition and clustering behaviour of α -pinene oxidation products for different oxidation conditions, *Atmospheric Chemistry and Physics*, 15, 4145-4159, 10.5194/acp-15-4145-2015, 2015.
- Rissanen, M. P., Mikkilä, J., Iyer, S., and Hakala, J.: Multi-scheme chemical ionization inlet (MION) for fast switching of reagent ion chemistry in atmospheric pressure chemical ionization mass spectrometry (CIMS) applications, *Atmospheric Measurement Techniques*, 12, 6635-6646, 10.5194/amt-12-6635-2019, 2019.
- Rissanen, M. P., Kurten, T., Sipila, M., Thornton, J. A., Kangasluoma, J., Sarnela, N., Junninen, H., Jorgensen, S., Schallhart, S., Kajos, M. K., Taipale, R., Springer, M., Mentel, T. F., Ruuskanen, T., Petaja, T., Worsnop, D. R., Kjaergaard, H. G., and Ehn, M.: The formation of highly oxidized multifunctional products in the ozonolysis of cyclohexene, *Journal of the American Chemical Society*, 136, 15596-15606, 10.1021/ja507146s, 2014.
- Riva, M., Brüggemann, M., Li, D., Perrier, S., George, C., Herrmann, H., and Berndt, T.: Capability of CI-Orbitrap for Gas-Phase Analysis in Atmospheric Chemistry: A Comparison with the CI-APi-TOF Technique, *Analytical chemistry*, 92, 8142-8150, 10.1021/acs.analchem.0c00111, 2020a.
- Riva, M., Brüggemann, M., Li, D., Perrier, S., George, C., Herrmann, H., and Berndt, T.: Capability of CI-Orbitrap for Gas-Phase Analysis in Atmospheric Chemistry: A Comparison with the CI-APi-TOF Technique, *Analytical chemistry*, 10.1021/acs.analchem.0c00111, 2020b.
- Riva, M., Ehn, M., Li, D., Tomaz, S., Bourgoin, F., Perrier, S., and George, C.: CI-Orbitrap: An Analytical Instrument To Study Atmospheric Reactive Organic Species, *Analytical chemistry*, 91, 9419-9423, 10.1021/acs.analchem.9b02093, 2019a.
- Riva, M., Rantala, P., Krechmer, J. E., Peräkylä, O., Zhang, Y., Heikkinen, L., Garmash, O., Yan, C., Kulmala, M., Worsnop, D., and Ehn, M.: Evaluating the performance of five different chemical ionization techniques for detecting gaseous oxygenated organic species, *Atmos. Meas. Tech.*, 12, 2403-2421, 10.5194/amt-12-2403-2019, 2019b.
- Schobesberger, S., Junninen, H., Bianchi, F., Lonn, G., Ehn, M., Lehtipalo, K., Dommen, J., Ehrhart, S., Ortega, I. K., Franchin, A., Nieminen, T., Riccobono, F., Hutterli, M., Duplissy, J., Almeida, J., Amorim, A., Breitenlechner, M., Downard, A. J., Dunne, E. M., Flagan, R. C., Kajos, M., Keskinen, H., Kirkby, J., Kupc, A., Kurten, A., Kurten, T., Laaksonen, A., Mathot, S., Onnela, A., Praplan, A. P., Rondo, L., Santos, F. D., Schallhart, S., Schnitzhofer, R., Sipila, M., Tome, A., Tsagkogeorgas, G., Vehkamaki, H., Wimmer, D., Baltensperger, U., Carslaw, K. S., Curtius, J., Hansel, A., Petaja, T., Kulmala, M., Donahue, N. M., and Worsnop, D. R.: Molecular understanding of atmospheric particle formation from sulfuric acid and large oxidized organic molecules, *Proceedings of the National Academy of Sciences of the United States of America*, 110, 17223-17228, 10.1073/pnas.1306973110, 2013.
- Simon, M., Dada, L., Heinritzi, M., Scholz, W., Stolzenburg, D., Fischer, L., Wagner, A. C., Kürten, A., Rörup, B., He, X.-C., Almeida, J., Baalbaki, R., Baccarini, A., Bauer, P. S., Beck, L., Bergen, A., Bianchi, F., Bräkling, S., Brilke, S., Caudillo, L., Chen, D., Chu, B., Dias, A., Draper, D. C., Duplissy, J., El-Haddad, I., Finkenzeller, H., Frege, C., Gonzalez-Carracedo, L., Gordon, H., Granzin, M., Hakala, J., Hofbauer, V., Hoyle, C. R., Kim, C., Kong, W., Lamkaddam, H., Lee, C. P., Lehtipalo, K., Leiminger, M., Mai, H., Manninen, H. E., Marie, G., Marten, R., Mentler, B., Molteni, U., Nichman, L., Nie, W., Ojdanic, A., Onnela, A., Partoll, E., Petäjä, T., Pfeifer, J., Philippov, M., Quéléver, L. L. J., Ranjithkumar, A.,

- Rissanen, M. P., Schallhart, S., Schobesberger, S., Schuchmann, S., Shen, J., Sipilä, M., Steiner, G., Stozhkov, Y., Tauber, C., Tham, Y. J., Tomé, A. R., Vazquez-Pufleau, M., Vogel, A. L., Wagner, R., Wang, M., Wang, D. S., Wang, Y., Weber, S. K., Wu, Y., Xiao, M., Yan, C., Ye, P., Ye, Q., Zauner-Wieczorek, M., Zhou, X., Baltensperger, U., Dommen, J., Flagan, R. C., Hansel, A., Kulmala, M., Volkamer, R., Winkler, P. M., Worsnop, D. R., Donahue, N. M., Kirkby, J., and Curtius, J.: Molecular understanding of new-particle formation from α -pinene between -50 and $+25$ °C, *Atmospheric Chemistry and Physics*, 20, 9183-9207, 10.5194/acp-20-9183-2020, 2020.
- Stolzenburg, D., Fischer, L., Vogel, A. L., Heinritzi, M., Schervish, M., Simon, M., Wagner, A. C., Dada, L., Ahonen, L. R., Amorim, A., Baccarini, A., Bauer, P. S., Baumgartner, B., Bergen, A., Bianchi, F., Breitenlechner, M., Brilke, S., Mazon, S. B., Chen, D., Dias, A., Draper, D. C., Duplissy, J., Haddad, I. E., Finkenzeller, H., Frege, C., Fuchs, C., Garmash, O., Gordon, H., He, X., Helm, J., Hofbauer, V., Hoyle, C. R., Kim, C., Kirkby, J., Kontkanen, J., Kürten, A., Lampilahti, J., Lawler, M., Lehtipalo, K., Leiminger, M., Mai, H., Mathot, S., Mentler, B., Molteni, U., Nie, W., Nieminen, T., Nowak, J. B., Ojdanic, A., Onnela, A., Passananti, M., Petäjä, T., Quéléver, L. L. J., Rissanen, M. P., Sarnela, N., Schallhart, S., Tauber, C., Tomé, A., Wagner, R., Wang, M., Weitz, L., Wimmer, D., Xiao, M., Yan, C., Ye, P., Zha, Q., Baltensperger, U., Curtius, J., Dommen, J., Flagan, R. C., Kulmala, M., Smith, J. N., Worsnop, D. R., Hansel, A., Donahue, N. M., and Winkler, P. M.: Rapid growth of organic aerosol nanoparticles over a wide tropospheric temperature range, *Proceedings of the National Academy of Sciences*, 115, 9122-9127, doi:10.1073/pnas.1807604115, 2018.
- Surdu, M., Lamkaddam, H., Wang, D. S., Bell, D. M., Xiao, M., Lee, C. P., Li, D., Caudillo, L., Marie, G., Scholz, W., Wang, M., Lopez, B., Piedehierro, A. A., Ataei, F., Baalbaki, R., Bertozzi, B., Bogert, P., Brasseur, Z., Dada, L., Duplissy, J., Finkenzeller, H., He, X.-C., Höhler, K., Korhonen, K., Krechmer, J. E., Lehtipalo, K., Mahfouz, N. G. A., Manninen, H. E., Marten, R., Massabò, D., Mauldin, R., Petäjä, T., Pfeifer, J., Philippov, M., Rörup, B., Simon, M., Shen, J., Umo, N. S., Vogel, F., Weber, S. K., Zauner-Wieczorek, M., Volkamer, R., Saathoff, H., Möhler, O., Kirkby, J., Worsnop, D. R., Kulmala, M., Stratmann, F., Hansel, A., Curtius, J., Welti, A., Riva, M., Donahue, N. M., Baltensperger, U., and El Haddad, I.: Molecular Understanding of the Enhancement in Organic Aerosol Mass at High Relative Humidity, *Environmental science & technology*, 57, 2297-2309, 10.1021/acs.est.2c04587, 2023.
- Trostl, J., Chuang, W. K., Gordon, H., Heinritzi, M., Yan, C., Molteni, U., Ahlm, L., Frege, C., Bianchi, F., Wagner, R., Simon, M., Lehtipalo, K., Williamson, C., Craven, J. S., Duplissy, J., Adamov, A., Almeida, J., Bernhammer, A. K., Breitenlechner, M., Brilke, S., Dias, A., Ehrhart, S., Flagan, R. C., Franchin, A., Fuchs, C., Guida, R., Gysel, M., Hansel, A., Hoyle, C. R., Jokinen, T., Junninen, H., Kangasluoma, J., Keskinen, H., Kim, J., Krapf, M., Kurten, A., Laaksonen, A., Lawler, M., Leiminger, M., Mathot, S., Mohler, O., Nieminen, T., Onnela, A., Petaja, T., Piel, F. M., Miettinen, P., Rissanen, M. P., Rondo, L., Sarnela, N., Schobesberger, S., Sengupta, K., Sipila, M., Smith, J. N., Steiner, G., Tome, A., Virtanen, A., Wagner, A. C., Weingartner, E., Wimmer, D., Winkler, P. M., Ye, P., Carslaw, K. S., Curtius, J., Dommen, J., Kirkby, J., Kulmala, M., Riipinen, I., Worsnop, D. R., Donahue, N. M., and Baltensperger, U.: The role of low-volatility organic compounds in initial particle growth in the atmosphere, *Nature*, 533, 527-531, 10.1038/nature18271, 2016.

- Wang, M., Kong, W., Marten, R., He, X.-C., Chen, D., Pfeifer, J., Heitto, A., Kontkanen, J., Dada, L., Kürten, A., Yli-Juuti, T., Manninen, H. E., Amanatidis, S., Amorim, A., Baalbaki, R., Baccarini, A., Bell, D. M., Bertozzi, B., Bräkling, S., Brilke, S., Murillo, L. C., Chiu, R., Chu, B., De Menezes, L.-P., Duplissy, J., Finkenzeller, H., Carracedo, L. G., Granzin, M., Guida, R., Hansel, A., Hofbauer, V., Krechmer, J., Lehtipalo, K., Lamkaddam, H., Lampimäki, M., Lee, C. P., Makhmutov, V., Marie, G., Mathot, S., Mauldin, R. L., Mentler, B., Müller, T., Onnela, A., Partoll, E., Petäjä, T., Philippov, M., Pospisilova, V., Ranjithkumar, A., Rissanen, M., Rörup, B., Scholz, W., Shen, J., Simon, M., Sipilä, M., Steiner, G., Stolzenburg, D., Tham, Y. J., Tomé, A., Wagner, A. C., Wang, D. S., Wang, Y., Weber, S. K., Winkler, P. M., Wlasits, P. J., Wu, Y., Xiao, M., Ye, Q., Zauner-Wieczorek, M., Zhou, X., Volkamer, R., Riipinen, I., Dommen, J., Curtius, J., Baltensperger, U., Kulmala, M., Worsnop, D. R., Kirkby, J., Seinfeld, J. H., El-Haddad, I., Flagan, R. C., and Donahue, N. M.: Rapid growth of new atmospheric particles by nitric acid and ammonia condensation, *Nature*, 581, 184-189, 10.1038/s41586-020-2270-4, 2020.
- Wang, X., Hayeck, N., Brüggemann, M., Yao, L., Chen, H., Zhang, C., Emmelin, C., Chen, J., George, C., and Wang, L.: Chemical Characteristics of Organic Aerosols in Shanghai: A Study by Ultrahigh-Performance Liquid Chromatography Coupled With Orbitrap Mass Spectrometry, *Journal of Geophysical Research: Atmospheres*, 122, 11,703-711,722, 10.1002/2017jd026930, 2017.
- Yuan, B., Koss, A. R., Warneke, C., Coggon, M., Sekimoto, K., and de Gouw, J. A.: Proton-Transfer-Reaction Mass Spectrometry: Applications in Atmospheric Sciences, *Chemical reviews*, 117, 13187-13229, 10.1021/acs.chemrev.7b00325, 2017.

Chapter V: Nitrate radicals suppress
biogenic new particle formation from
monoterpene oxidation

Chapter V: Nitrate radicals suppress biogenic new particle formation from monoterpene oxidation

Dandan Li^{1,†}, Wei Huang^{2,†}, Dongyu Wang³, Mingyi Wang^{4,5}, Joel A. Thornton⁶, Lucía Caudillo⁷, Birte Rörup², Ruby Marten³, Wiebke Scholz⁸, Henning Finkenzeller⁹, Guillaume Marie⁷, Urs Baltensperger³, David M. Bell³, Zoé Brasseur², Joachim Curtius⁷, Lubna Dada³, Jonathan Duplissy^{2,10}, Xianda Gong¹¹, Armin Hansel⁸, Xu-Cheng He², Victoria Hofbauer⁴, Heikki Junninen^{2,12}, Jordan E. Krechmer¹³, Andreas Kürten⁷, Houssni Lamkaddam³, Katrianne Lehtipalo^{2,14}, Brandon Lopez⁴, Yingge Ma¹⁵, Naser G. A. Mahfouz^{4,16}, Hanna E. Manninen¹⁷, Bernhard Mentler⁸, Sébastien Perrier¹, Tuukka Petäjä², Joschka Pfeifer¹⁷, Maxim Philippov¹⁸, Meredith Schervish⁴, Siegfried Schobesberger¹⁹, Jiali Shen², Mihnea Surdu³, Sophie Tomaz¹, Rainer Volkamer⁹, Xinkai Wang¹, Stefan K. Weber^{7,17}, André Welti¹⁴, Douglas R. Worsnop^{2,13}, Yusheng Wu², Chao Yan², Marcel Zauner-Wieczorek⁷, Markku Kulmala², Jasper Kirkby^{7,17}, Neil M. Donahue⁴, Christian George¹, Imad El-Haddad^{3,*}, Federico Bianchi^{2,*}, Matthieu Riva^{1,*}

¹ Univ Lyon, Université Claude Bernard Lyon 1, CNRS, IRCELYON, 69626, Villeurbanne, France

² Institute for Atmospheric and Earth System Research/Physics, Faculty of Science, University of Helsinki, 00014, Helsinki, Finland

³ Laboratory of Atmospheric Chemistry, Paul Scherrer Institute, 5232, Villigen, Switzerland

⁴ Center for Atmospheric Particle Studies, Carnegie Mellon University, Pittsburgh, PA, 15213, USA

⁵ now at Division of Chemistry and Chemical Engineering, California Institute of Technology, Pasadena, CA 91125, USA

⁶ Department of Atmospheric Sciences, University of Washington, Seattle, WA 98195, USA

⁷ Institute for Atmospheric and Environmental Sciences, Goethe University Frankfurt, 60438, Frankfurt am Main, Germany

⁸ Institute for Ion Physics and Applied Physics, University of Innsbruck, 6020, Innsbruck, Austria

⁹ Department of Chemistry & CIRES, University of Colorado Boulder, Boulder, CO 80309, USA

¹⁰ Helsinki Institute of Physics (HIP)/Physics, Faculty of Science, University of Helsinki, 00014, Helsinki, Finland

¹¹ Leibniz Institute for Tropospheric Research, 04318, Leipzig, Germany

¹² now at Institute of Physics, University of Tartu, 50090, Tartu, Estonia

¹³ Aerodyne Research Inc., Billerica, Massachusetts 01821, USA

¹⁴ Finnish Meteorological Institute, 00560, Helsinki, Finland

¹⁵ State Environmental Protection Key Laboratory of Formation and Prevention of Urban Air Pollution Complex, Shanghai Academy of Environment Sciences, 200233, Shanghai, P. R. China

¹⁶ now at Atmospheric and Oceanic Sciences, Princeton University, Princeton, NJ 08540, USA

¹⁷ CERN, the European Organization for Nuclear Research, CH-1211 Geneve 23, Switzerland

¹⁸ P.N. Lebedev Physical Institute of the Russian Academy of Sciences, 119991, Moscow, Russia

¹⁹ Department of Applied Physics, University of Eastern Finland, 70211, Kuopio, Finland

† These authors contributed equally to this work

Article soon to be submitted

V.1. Introduction

More than half of cloud condensation nuclei (CCN) are formed through gas-to-particle conversion of oxidation products, a process called new particle formation (NPF)^{6,9}. Gaseous species responsible for atmospheric NPF include sulfuric acid, nitric acid, iodine oxoacids, and highly oxygenated organic molecules (HOMs)^{5,10-13}. HOMs are formed from the gas-phase oxidation of biogenic and anthropogenic volatile organic compounds (VOCs) through multiple autoxidation reactions of peroxy radicals (RO_2)^{1,3,14}. It is well established that HOMs play an important role both in nucleation itself and in particle growth, either alone or by stabilizing sulfuric acid clusters^{4,15,16}.

Pure organic nucleation appears to be driven by highly functionalized accretion products, which are of ultralow- or extremely low volatility and are thought to be peroxides (ROOR) formed via rapid RO_2 self/cross-reactions^{4,17-20}. Daytime VOC oxidation is usually initiated by reactions with hydroxyl radicals (OH) and ozone (O_3)^{21,22}, whereas nocturnal VOC oxidation is often initiated by nitrate radicals (NO_3) in addition to O_3 ²³⁻²⁵. Although dimers are mainly formed during nighttime, notably from ozone chemistry, NPF involving organic species at night is rarely reported^{5,26,27}. The mechanism suppressing biogenic NPF at night remains uncertain, although it is suspected that NO_3 chemistry may play a role^{28,29}. For example, it has been suggested that NO_3 oxidation of α -pinene, the most abundant monoterpene globally, is a less efficient source of SOA than oxidation by either OH or O_3 ^{30,31}. However, a recent study has shown a higher SOA yield from the α -pinene + NO_3 system depending on different RO_2 fates³². It is important to note that involvement in nucleation and growth is a subset of SOA formation, and therefore it stands to

reason that NO_3 oxidation might also be an inefficient source of particles. As a result, the exact role of NO_3 radicals on the formation and growth of particles remains highly uncertain.

V.2. Materials and methods

V.2.1. Kinetic and product characterization in the oxidation flow reactor

The oxidation of α -pinene initiated by ozone and nitrate radical (NO_3) was conducted in an 18-liter Pyrex glass oxidation flow reactor (OFR, 12 cm i.d. \times 158 cm length) under dry conditions, at room temperature of 296 ± 1 K and atmospheric pressure (Aregahegn et al., 2013). The total flow rate was kept at 16 standard litres per minute (slpm) using synthetic air (N_2/O_2 80:20) and the residence time was 67.5 s. The volatile organic compound (VOC) precursors, (+)- α -pinene (Sigma-Aldrich, $\geq 99\%$), ozone, and NO_2 were injected continuously using mass flow controllers (MFC, Bronkhorst). Input VOC concentration was fixed at approximately 8 ± 1 ppbv and retrieved using a quadrupole mass spectrometer (IONICON, PTR-QMS 300). NO_3 radicals were generated from the oxidation of NO_2 with O_3 in an external 1-liter pre-reactor at atmospheric pressure and room temperature. The pre-reactor was dimmed to prevent the photolysis of NO_3 by room lights. 500 standard $\text{cm}^3 \text{min}^{-1}$ (scm) of O_2 was passed through a stable ozone generator (Fisher Scientific, SOG-1) to generate ~ 900 ppbv of O_3 within the pre-reactor (corresponding to $\sim 50 \pm 5$ ppbv after dilution in the flow tube). O_3 is mixed with a variable NO_2 flow in the pre-reactor to produce different NO_3 radical concentrations. The total flow in pre-reactor was fixed at 1 slpm, giving a reaction time of 60 s. Then the mixture of NO_3 , O_3 , and excess NO_2 enters OFR and reacts with α -pinene. The concentrations of O_3 and NO_2 in OFR outflow (ranging from 1.9 to 75 ± 2 ppbv in the flow tube) were retrieved using a Thermo 49C, and a Ecophysics CLD 88p equipped with a photolytic converter PLC 860, respectively. The particle formation was measured by a condensation particle counter (TSI CPC 3772) and remained negligible ($< 100 \text{ cm}^{-3}$) during all flow tube experiments. A chemical ionization coupled to a Q-Exactive Orbitrap mass spectrometer (CI-Orbitrap, Thermo Scientific) monitored the oxidation products.

V.2.2. Particle formation in CLOUD chamber

New particle formation experiments were performed at CERN in the CLOUD (Cosmics Leaving OUtdoor Droplets) chamber, a 3-m-diameter electropolished stainless steel vessel of 26.1 m^3 . This

chamber enables to achieve a high standard of cleanliness and discussed in detail by Kirkby et al. (2016). The evaporation of cryogenic liquid nitrogen (N_2) and liquid oxygen (O_2) was blended at a ratio of 79:21 to produce pure synthetic air, which flushed the chamber constantly. Variable amounts of trace gases, for example, O_3 , VOCs, NOx, SO_2 , and CO were precisely injected into the system as needed and monitored. 250 optical fiber-optic systems installed on top of the chamber are utilized to initiate photolytic reactions, including Hg-Xe UV lamps, and UV excimer laser. The CLOUD chamber is cleaned by irrigating the walls with ultra-pure water, heating to 373 K, and flushing with humidified pure air and the high ozone concentration, declining the contaminant levels such as VOCs to less 1 ppbv. The particles were wiped out under a high voltage electric field. During the CLOUD 14 campaign, the total flow was kept at 250 slpm with an average residence time of 105 mins. With mounting in a thermal housing, the CLOUD chamber temperature was maintained at 264 ± 0.1 K and relative humidity at 20% for the NO_3 run. The contents of the chamber were ceaselessly detected and analyzed by a wide range of external instruments connected to the sampling probes ~ 1 m protruding into the chamber. The chamber instrumentation for the results reported here comprised an atmospheric pressure chemical ionization inlet coupled to an ultrahigh-resolution Orbitrap mass spectrometer (CI-Orbitrap) for retrieving the chemical composition of gaseous (highly) oxygenated volatile organic compounds (OVOC) (Riva et al., 2019), a nitrate chemical ionization atmospheric pressure interface long time of flight mass spectrometer (CI-(NO_3^-)-APi-LTOF, Aerodyne Research Inc. and Tofwerk AG) from the University of Frankfurt (Kurten et al., 2014) for providing the reference of highly oxygenated molecules (HOMs) concentration, an iodide-adduct chemical ionization time of flight mass spectrometer equipped with a Filter Inlet for Gases and AEROsols (FIGAERO-CIMS) for the composition of particle phase, a proton transfer reaction time-of-flight (PTR-TOF) mass spectrometer for organic precursors concentrations (Breitenlechner et al., 2017), a CPC battery at 2.5-12 nm thresholds (mobility diameters), a di-ethylene glycol CPC (DEG-CPC) at 2.0 nm threshold (Dada et al., 2020), a nano-scanning electrical mobility spectrometer (nSEMS) for 1.5-25 nm particle size (Mai and Flagan, 2018), trace gas analyzers to measure ozone (O_3 , Thermo Fisher Scientific Inc. 42i-TLE), nitric oxide (NO, ECO Physics, CLD 780TR) and nitrogen dioxide monitor (CAPS NO_2 , Aerodyne Research Inc.) and dew point mirrors (EdgeTech) for RH of the chamber.

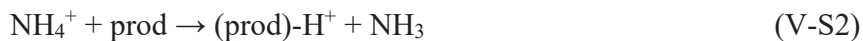
V.2.3. Field campaign in Siikaneva, Finland

The ambient observation was conducted between March 10 and June 15, 2016 in a wetland, Siikaneva, southern Finland ($61^{\circ} 49' 59.4''\text{N}$, $24^{\circ} 92' 11' 32.4''\text{E}$). It is located ~ 5 km west of the Station for Measuring Ecosystem – Atmosphere Relations (SMEAR) II station, which is located in a boreal forest at Hyytiälä. Air temperature was measured with Rotronic HC2 sensor (Rotronic 88 AG, Switzerland). Global radiation was measured by a Kipp & Zonen CNR4 radiometer (OTT HydroMet B.V., The Netherlands). A proton transfer reaction time-of-flight mass spectrometer (PTR-TOF, Ionicon Analytik GmbH) using H_3O^+ as the ion source was used to measure VOC concentrations. A chemical ionization atmospheric pressure interface time-of-flight mass spectrometers (CI-APi-TOF, Aerodyne Research Inc.) using NO_3^- as the reagent ion was deployed to measure the molecular composition of ambient neutral clusters. Number concentrations of particles with a mobility diameter larger than 2.5 nm were recorded with a condensation particle counter (CPC3776, TSI Inc). Number concentration and size distribution of atmospheric ions and neutral particles with a mobility diameter of 0.8–42 nm were measured with a neutral cluster and air ion spectrometer (NAIS, Airel Ltd.).

V.2.4. Orbitrap technology

CI-Orbitrap technology has been described elsewhere and prior studies have reported its capabilities to study atmospheric reactive organic species successfully (Riva et al., 2020; Riva et al., 2019). For this study, ammonium and nitrate ions ($\text{NH}_4^+ / \text{NO}_3^-$) were used as reagent ion of CI-Orbitrap for the detection of an extensive range of OVOCs. NO_3^- ionization has been described elsewhere (Riva et al., 2019), and NH_4^+ adduct ion chemistry has already been utilized with PTR-MS as discussed by Lindinger et al. (1998) and with the novel PTR3-TOF by Hansel et al. (2018) or Berndt et al. (2018) and shown excellent sensitivity to detect OVOCs. Therefore, for this study, OVOCs refer to oxidized organic compounds that can be detected, including HOMs ($\text{O} > 6$) and the lower oxidized molecules ($\text{O} = 2–5$) in positive mode.

NH_3 was added to the ion source taking 5 sccm from the headspace of a 1% of liquid ammonium hydroxide solution (25% NH_3 basis, ACS reagent, Sigma-Aldrich). The product molecules (prod) were softly charged by binding to ammonium ions, forming (prod)- NH_4^+ adduct ions or protonated products (prod)- H^+ , following equations V-S1 and V-S2.



The Orbitrap was externally mass-calibrated using a 2 mM sodium acetate solution (Aldrich, >99% purity) in an electrospray ionization source. The drift in mass accuracy remained within 2 ppm throughout the experiments. The formula assignment of measured ions was constrained by known oxidation chemistry and elemental composition, i.e., ions are assumed to contain only carbon, hydrogen, oxygen, and nitrogen atoms (up to three N atoms to account for adduction of NH_4^+).

V.2.5. Volatility of HOMs.

Since HOM are difficult to synthesis and their vapor pressures are too low for the methods currently used to detect volatility, direct measurements of the volatilities of individual HOM are very challenging. Numerous model calculations, such as so-called group contribution approaches⁶³ or parameterizations based on the oxidation state^{64,65}. We use a volatility parameterization to calculate effective saturation mass concentration (C_{sat}) of individual organic compounds according to their structure-based estimations and formula-based estimations using the modified Li et al. approach^{48,65} as in equation (3):

$$\log_{10} C_{\text{sat}}(298K) = (n_C^0 - n_C)b_C - n_O b_O - 2 \frac{n_{CNO}}{(n_C + n_O)} b_{CO} - n_N b_N - n_S b_S \quad (3)$$

where n_C , n_O , n_N , and n_S are the number of carbon, oxygen, nitrogen, and sulfur atoms of the specific molecule, separately; n_C^0 is the reference carbon number; b_C , b_O , b_N , and b_S are the contribution of each atom to $\log_{10} C_{\text{sat}}$, separately; b_{CO} is the carbon-oxygen nonideality⁶⁴. Values of b coefficient can be found in Li et al.⁶⁵. The formula used to estimate the vapor pressure is amended to convert all NO_3 groups into OH groups to reduce the bias from the compounds containing nitrates^{48,66}.

Due to the different temperatures in the CLOUD 14 experiments, we adjusted the $C_{\text{sat}}(298K)$ to the measured experimental temperature in equations (4) and (5):

$$\log_{10} C_{\text{sat}}(T) = \log_{10} C_{\text{sat}}(298K) + \frac{\Delta H_{\text{vap}}}{R \ln(10)} \times \left(\frac{1}{298} - \frac{1}{T} \right) \quad (4)$$

$$\Delta H_{\text{vap}}(\text{kJ mol}^{-1}) = -11 \cdot \log_{10} C_{\text{sat}}(298K) + 129 \quad (5)$$

where T is the temperature in kelvin; $C_{sat}(298K)$ is the saturation mass concentration at 298 K; ΔH_{vap} is the evaporation enthalpy and R is the gas constant ($8.3134 \text{ J K}^{-1} \text{ mol}^{-1}$). The potential presence of isomers may result in uncertainty in this method since the only input is molecular formula.

In this study, all oxidation products were grouped into six volatility regimes; ultralow-volatility (ULVOCs), $C_{sat} < 10^{-8.5} \mu\text{g m}^{-3}$, extremely low volatility (ELVOCs), $10^{-8.5} < C_{sat} < 10^{-4.5} \mu\text{g m}^{-3}$, low-volatility (LVOCs), $10^{-4.5} < C_{sat} < 10^{-0.5} \mu\text{g m}^{-3}$, semi-volatile (SVOCs), $10^{-0.5} < C_{sat} < 10^{2.5} \mu\text{g m}^{-3}$, intermediate-volatility organic compounds (IVOC), $10^{2.5} < C_{sat} < 10^{6.5} \mu\text{g m}^{-3}$, and VOC, $10^{6.5} < C_{sat} \mu\text{g m}^{-3}$ based on VBS.

V.2.6. Kinetic model simulations.

The behaviors of NO_3 , N_2O_5 , RO_2 ($\text{C}_{10}\text{H}_{15}\text{O}_4$, $\text{C}_{10}\text{H}_{17}\text{O}_3$ and $\text{C}_{10}\text{H}_{16}\text{NO}_5$), the corresponding less oxidized monomers formed from the oxidation reaction of α -pinene by O_3/OH and NO_3 radicals under typical experimental conditions were simulated simply using the F0AM v3.1 (Wolfe et al., 2016) box model employing MCM v3.3.1 (Jenkin et al., 1997). The RO_2 autoxidation reactions and NO_3 chemistry-related packages were not considered in the model.

V.3. Results

Here we examine the reactivity of α -pinene with varying levels of NO_3 radicals and the influence of different HOM composition on NPF. We draw on three datasets: experiments conducted in the CLOUD chamber (Cosmics Leaving OUtdoor Droplets) at CERN (European Organization for Nuclear Research); laboratory oxidation flow reactor (OFR) experiments; and field measurements in a wetland surrounded by boreal forests (Siikaneva, Finland) (see Methods for experimental details). Controlled laboratory experiments were performed using α -pinene, as it is one of the most abundant biogenic VOCs in the atmosphere (Kanakidou et al., 2005) and one of the key precursors for the production of HOMs (Kirkby et al., 2016). We oxidized α -pinene in the presence of O_3 and NO_3 radicals produced from the reaction of NO_2 with O_3 . Various mass spectrometers equipped with chemical ionization inlets using different reagent ions (i.e., NH_4^+ , NO_3^-) were deployed to determine the chemical composition of neutral gas-phase oxygenated VOCs (OVOCs), including HOMs.

V.3.1. NPF with different oxidants

Figure V-1 shows the evolution of reactant and reaction product concentrations together with the resulting particle formation rates measured in the CLOUD chamber. We broke the experiment into three stages to examine different radical chemistry under otherwise identical conditions, including approximately 1000 parts per billion (ppbv) of carbon monoxide to scavenge the OH radicals formed from the ozonolysis of α -pinene and homogeneous illumination from four Hg-Xe arc lamps (UVH, Figure V-S1). We first examined the reaction of α -pinene with O₃. At $t = 0$ min, nitrogen dioxide (NO₂) was continuously injected to form NO₃. The production rate of NO₃ was 0.3 ppbv h⁻¹, similar to that observed in the atmosphere (Liebmann et al., 2018), and the NO₃ concentration was estimated using a 0-D box model (F0AM) (Wolfe et al., 2016). Finally, at $t = 80$ min, LEDs at 385 nm (LS3) were switched on to form nitrogen monoxide (NO) via NO₂ photolysis and convert NO₃ into NO₂. The three conditions were thus: pure ozonolysis; ozonolysis perturbed by NO₃; and ozonolysis perturbed by NO_x.

Non-nitrogen containing OVOCs (CHO) formed through the ozonolysis of α -pinene comprise monomers C_{9,10}H_{12,14,16,18}O_{≥2} (CHO monomers) and dimers C_{19,20}H_{28,30,32}O_{≥4} (CHO dimers), which predominated during its ozonolysis. NO₂ injection and NO₃ formation resulted in a sharp decrease in the concentrations of CHO dimers (Figure V-1B). Ultimately, CHO dimers were completely suppressed as NO₃ radicals rose toward a concentration of only 0.6 pptv, even though measured O₃ and α -pinene concentrations remained constant (Figure V-1A). Meanwhile, we observed a large formation of nitrogen-containing species (CHON), including monomers C_{9,10}H_{13,15,17}O_{≥4}N (CHON monomers) and two classes of dimers (CHON dimers): C_{19,20}H_{29,31,33}O_{≥5}N (CHON₁ dimers) and C₂₀H₃₂O_{≥8}N₂ (CHON₂ dimers), with the concentrations of CHON dimers being higher those of CHO dimers during pure ozonolysis (~1.4-fold) (Figure V-1B). Good agreement between NH₄⁺-Orbitrap and NO₃⁻-LTOF (a nitrate CI atmospheric pressure interface long time of flight mass spectrometer) (Kurten et al., 2014) for the detection of CHO and CHON species indicates similar sensitivity for the different mass spectrometers (Figure V-S2).

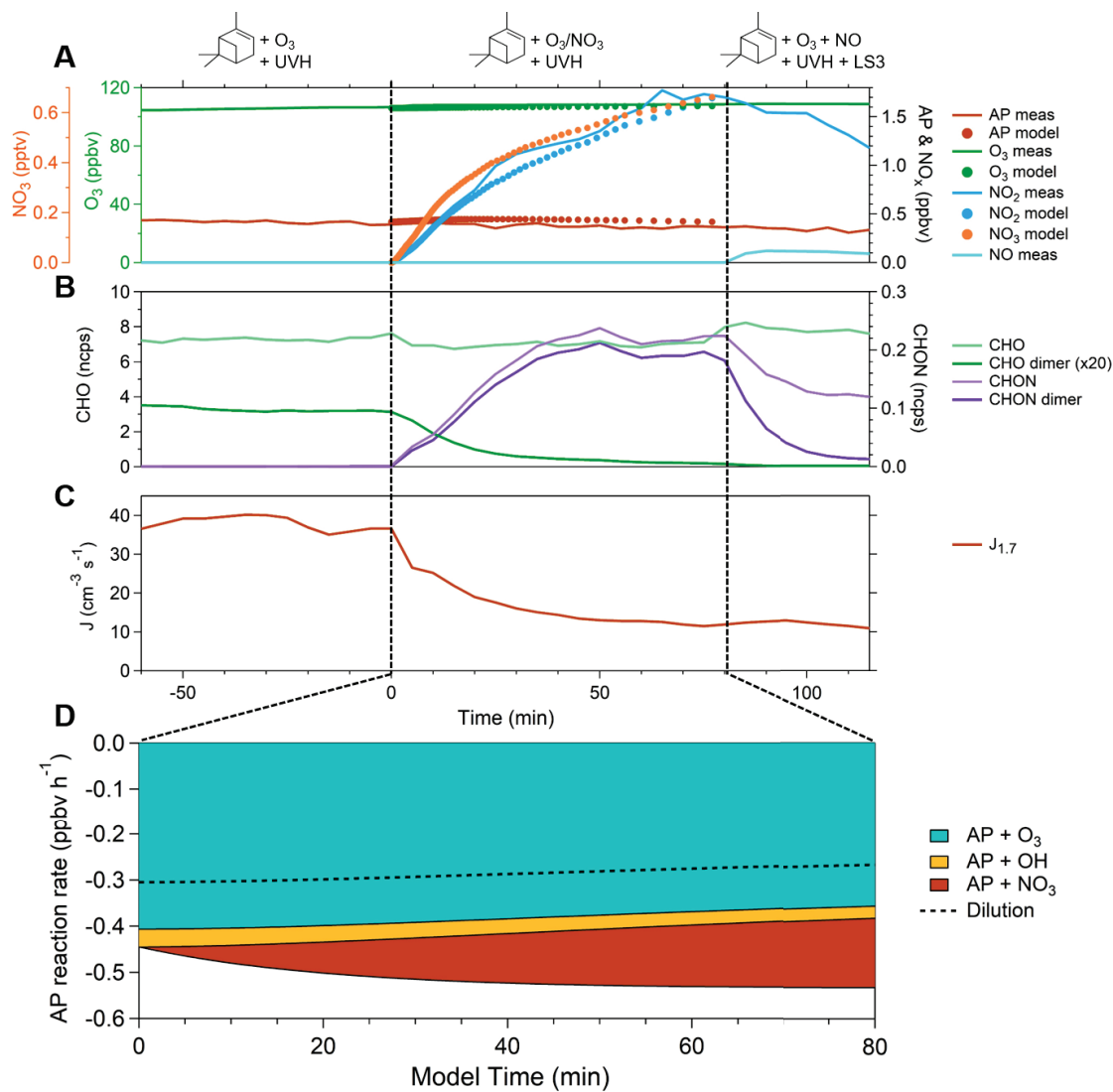


Figure V-1: Effect of NO₃ radicals and NO on OVOC and particle formation in CLOUD. (A) Evolution of measured (solid line) and simulated (markers) α -pinene, O₃, NO_x, and the simulated NO₃ radical concentrations in the CLOUD chamber. Constant α -pinene (~1.3 ppb) and O₃ (~108 ppb) were injected continuously into the chamber. The experiment was conducted at 20% RH and 263 K. UVH: Hg-Xe UV lamps; LS3: LEDs at 385 nm. When constant NO₂ (~2.5 ppb) was injected into the chamber at $t = 0$ min, NO₃ was generated from the reaction of NO₂ with O₃. When LS3 were turned on at $t = 80$ min, NO₂ was photolyzed to NO. (B) Evolution of non-nitrogen containing total OVOCs (CHO), dimers (CHO dimer $\times 20$), and nitrogen-containing total OVOCs (CHON) and dimers (CHON dimer) measured by CI-(NH₄⁺)-Orbitrap. The signal of

CHO dimers was multiplied by a factor of 20 for better visualization. (C) Evolution of the particle formation rates (J) at 1.7 nm. (D) Evolution of the α -pinene reaction rate during the NO_3 perturbed ozonolysis stage.

Added NO_3 increased the overall concentration of dimers due to the greater formation of CHON dimers. During this stark change in dimer composition, the net formation rate of particles at 1.7 nm ($J_{1.7}$) decreased by a factor of 4, implying that NO_3 chemistry strongly suppresses α -pinene NPF. After switching on the lights at $t = 80$ min, the NO_3 radicals were scavenged mainly by reaction with NO as well as by photolysis; subsequently, oxidation proceeded via ozonolysis under high NO_x conditions. The presence of NO_x terminated the bimolecular reactions of CHO RO_2 generated from the $\text{O}_3/\text{OH} + \alpha$ -pinene and formed CHON monomers (Figure V-1B and V-S3), whereas the formation pathway of CHON dimers was cut off due to the absence of nitrooxy peroxy radicals, which are generated from the NO_3 radical addition to α -pinene (CHON RO_2). As Figure V-1C shows, the particle formation rates did not change even at higher CHO concentrations when the lights were turned on, which is consistent with previously observed lower J values at higher NO_x (Yan et al., 2020). This indicates that NO_3 chemistry suppresses particle formation to a similar extent as NO does (Yan et al., 2020), even though NO_3 initiated oxidation of α -pinene yields a large concentration of dimeric compounds, unlike NO.

The evolution of the α -pinene reacted in the NO_3 chemistry stage is shown in Figure V-1D. The same amount of α -pinene reacted with O_3 in the presence of NO_3 radicals, while the total reacted α -pinene increased by 10%. NO_3 chemistry suppression of NPF occurred even though most of the α -pinene oxidation was still driven by O_3 (Figure V-1D and V-S4), and even though the overall concentration of dimers produced with NO_3 present was substantially higher than that during the pure ozonolysis (Lehtipalo et al., 2018). Our F0AM simulations show that, almost all CHO RO_2 radicals predominantly undergo self-/cross-reactions and also reactions with HO_2 pathway, indicating the presence of NO_3 and NO_x did not fundamentally modify the dimer branching ratios of RO_2 radicals (Figure V-S5). The results suggest that CHON RO_2 produced from NO_3 oxidation are highly reactive and dimers formed through NO_3 chemistry must be significantly more volatile than dimers formed from O_3 chemistry. This is similar to isoprene suppression of biogenic NPF where the resulting oxidation products (i.e., $\text{C}_{14}\text{-C}_{15}$ dimers) are more volatile than those from monoterpenes alone (Heinritzi et al., 2020; McFiggans et al., 2019).

Importantly, the sharp decrease in particle formation rates occurred at very low NO_3 concentrations relative to O_3 , even though the reaction with O_3 remained the dominant α -pinene oxidation process (Figure V-1D and V-S4). Thus, NO_3 chemistry fundamentally alters the product distributions and volatility, even when it represents only a small fraction of the total α -pinene reactivity, i.e., less than 30% (Figure V-S4).

V.3.2. HOM distribution at different NO_3 levels

To further investigate the influence of different steady-state concentrations of NO_3 radicals on α -pinene oxidation, we performed extensive OFR experiments in the presence of O_3 , OH, and NO_3 radicals. In addition to an experiment without any NO_2 addition, we also investigated eight NO_2 to O_3 ratios between 0.03:1 (close to the ratio of 0.023:1 for the CLOUD experiments) and 1.5:1 (Figure V-S6). Over this range, no NPF occurred due to the short residence time inside OFR, and the simulation shows that the rate of the α -pinene reaction with O_3 remained constant, but the total α -pinene reactivity increased by a factor of 3 relative to O_3/OH chemistry (Figure V-S7a). Ultimately up to ~80% of the α -pinene loss was from NO_3 oxidation at the highest $\text{NO}_2:\text{O}_3$ (Figure V-S7b). Meanwhile, fraction of α -pinene oxidized by OH radicals decreased from 44% to 6% because NO_2 scavenged the OH. Similarly, other than reaction with NO_2 (resulting in approximately 50 to 2000 pptv of N_2O_5 in the OFR), NO_3 radicals were almost completely consumed by α -pinene, and the reactions of $\text{CHO RO}_2 + \text{NO}_3$ and $\text{CHO RO}_2 + \text{NO}_2$ did not play a significant role in modifying the product distribution (Figure V-S8).

Like the CLOUD observations, the presence of NO_3 radicals fundamentally alters the product distribution (Figure V-9). All CHON dimers identified in the CLOUD chamber were found in OFR, but more CHON monomers and OH-initiated species were observed in OFR due to its short residence time and the absence of OH scavenger (Figure V-10). Figure V-2 shows the sensitivity of oxidation products generated from α -pinene and the fraction reacting with NO_3 vs. O_3/OH . Specifically, at maximal NO_3 concentrations, CHO dimers intensity is ~10 times lower compared to experiments performed without NO_3 (Figure V-2A). CHO monomers are much less sensitive to the increasing level of NO_3 radicals in α -pinene oxidation, with only a 2.3-fold decrease, which is probably due to the cross reactions of CHO RO_2 and CHON RO_2 . This is consistent with our F0AM simulation, which shows a 1.4-fold decrease for the less oxidized CHO monomers (i.e., O_{2-5})

concentrations (Figure V-S11). However, the sharper reduction of the most oxidized CHO (i.e., O_{>6}) as the NO₃ contribution increases (up to 10-fold decrease) indicates that the suppression of ozonolysis products by NO₃ is most important for the most highly oxygenated monomer and dimer products (Figure V-2A and V-2B, and V-S12).

In contrast to CHO dimers (10-folds decrease), the concentrations of products identified as CHO RO₂ (with an odd number of H atoms, including C₁₀H₁₅O₄₋₁₀ and C₁₀H₁₇O₃₋₇) do not differ much in the presence of NO₃ versus O₃/OH chemistry, with slight fluctuations across all different NO₃ reactivities (Figure V-2B). In contrast to a 20% reduction in simulated C₁₀H₁₅O_x radicals, the measured C₁₀H₁₅O_x rose with NO₃ radicals, likely due to the additional CHO RO₂ produced by the H-abstraction pathway from the reaction of NO₃ radicals with α -pinene which was not included in the model (Figure V-S11, V-S12e, and V-S13). Concentrations of C₁₀H₁₇O_{5,7} radicals from OH chemistry decreased by a factor of 9 due to the lowered reactivity of α -pinene with OH and more loss via bimolecular reactions (Figure V-S7, and V-S12f). CHON RO₂ (including C₁₀H₁₆O_{5,6,7,9}N) started to play an important or even dominant role as soon as NO₃ radicals were produced (Figure V-S13, and V-S14e).

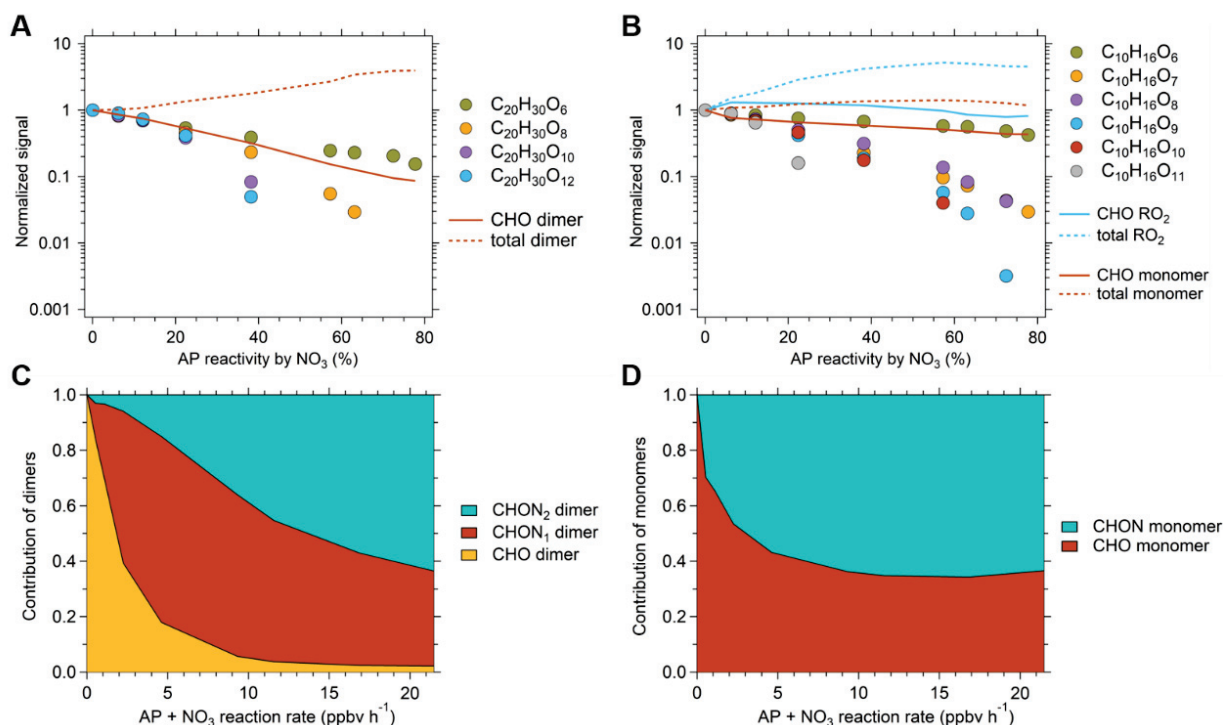


Figure V-2: Sensitivity of NO₃ radicals to the formation of OVOCs in an oxidation flow reactor. (A and B) Normalized signals of non-N containing dimers (CHO dimers) and total dimers (total dimers) (A), and non-N containing monomers (CHO monomers), total monomers (total monomers), non-N containing RO₂ radicals (CHO RO₂), and total RO₂ radicals (total RO₂) (B) as a function of α -pinene reactivity by NO₃ radicals measured by CI-(NH₄⁺)-Orbitrap in oxidation flow reactor (OFR) experiments. Ion signals are normalized to the signal in pure O₃ chemistry for comparison. A missing data point indicates that the signal intensity is below the detection limit of the instrument (10^5 molecule cm⁻³). Experiments were conducted at ~8 ppbv α -pinene, ~50 ppbv O₃, 296 K and RH < 1%. Nine different NO₂ concentrations were injected varying from 0 to 75 ppbv in flow tube. Every point represents the steady state concentrations of products. (C and D) Contribution of non-N containing dimers (CHO dimers), 1 N-containing dimers (CHON₁ dimers), and 2 N-containing dimers (CHON₂ dimers) to total dimers (C), and non-N containing monomers (CHO monomers) and N-containing monomers (CHON monomers) to total monomers (D) plotted against α -pinene oxidation rate by NO₃ radicals.

Unlike O₃/OH chemistry, NO₃ chemistry yields a solitary RO₂ species (i.e., C₁₀H₁₆NO₅), the autoxidation of which is very limited. This is shown by comparing the signal of a “parent” RO₂ to its more oxygenated autoxidation products (Figure V-S13). Although uncertainties remained in the quantification of RO₂ radical concentrations, chemical ionizations were reported to exhibit the same sensitivity for the O₃-derived RO₂ radicals (Berndt et al., 2016), and NH₄⁺-Orbitrap did not show any distinct sensitivity to CHON species compared to CHO species (Figure V-S2). The average ratio of C₁₀H₁₅O₄ to (C₁₀H₁₅O₆ + C₁₀H₁₅O₈), which are ozonolysis products, was 4.0 ± 0.3 . In contrast, the ratio of C₁₀H₁₆NO₅ to (C₁₀H₁₆NO₇ + C₁₀H₁₆NO₉), from NO₃ oxidation, was 72 ± 14 (Figure V-S13). Such a large difference is likely caused by the ring-retaining structure of C₁₀H₁₆NO₅ preventing the H-shift isomerization involved in the autoxidation of peroxy radicals (Berndt et al., 2016; Kurten et al., 2017). The concentrations of CHON RO₂, CHON₁ dimers, and CHON monomers seemed to be constant when the α -pinene reactivity by NO₃ reached ~40%, indicating that newly formed CHON RO₂ proceed immediately via a propagation cycle to form RO radicals or via an accretion reaction to form CHON₂ dimers at higher NO₃ levels (Figure V-S14).

The contribution to total dimers of CHON₁ dimers generated from the cross reaction between CHON RO₂ and CHO RO₂ increased with an increasing contribution of NO₃ to α -pinene reactivity

and peaked (67%) when the α -pinene reaction rate with NO_3 radicals was greater than 5 ppbv h^{-1} , corresponding to $\sim 40\%$ of total α -pinene reactivity, after which its dominance was gradually replaced by CHON_2 dimers produced from CHON RO_2 self/cross-reactions (Figure V-2C, and V-S7). The proportion of CHON monomers to total monomers also reached its highest value (60%) at this α -pinene reaction rate (i.e., 5 ppbv h^{-1}), and then remained constant (Figure V-2D). Results obtained with the CI-Orbitrap operated in negative mode (NO_3^-) further support the role of CHON RO_2 in the distribution of OVOCs (Figure V-S15). However, it should be mentioned that the nitrate reagent ion is selective towards HOMs, i.e., $n_0 > 6$ for CHO monomers and $n_0 > 8$ for CHON monomers, which explains the general decreasing trend of OVOCs (i.e., monomers and dimers) measured by the CI-(NO_3^-)-Orbitrap. Overall, the OFR results indicate that the presence of CHON RO_2 competes against autoxidation and CHO dimers formation, two mechanisms responsible for monoterpene NPF, resulting in a net reduction of CHO species formed from O_3/OH oxidation.

V.3.3. Change of HOM volatility distribution by NO_3

Higher volatilities of CHON dimers than CHO dimers in the particle phase are confirmed by thermal desorption measurements performed by a FIGAERO-CIMS (Filter Inlet for Gases and AEROSols coupled to a chemical ionization time of flight mass spectrometer) (Lopez-Hilfiker et al., 2014) (Figure V-3A). It is worth mentioning that unlike monomers, thermal fragmentation contributions are negligible for larger compounds like dimers during particle desorption with the FIGAERO (Huang et al., 2018; Wang and Ruiz, 2018). The maximum desorption temperatures (T_{\max}) of particulate CHON dimers were much lower (40–85 °C) than T_{\max} of particulate CHO dimers (~ 110 °C), corresponding to saturation vapor concentrations (C_{sat}) of 10^{-3} to $10^1 \mu\text{g m}^{-3}$ for CHON dimers and 10^{-5} to $10^{-7} \mu\text{g m}^{-3}$ for CHO dimers (Wang et al., 2020a). The saturation vapor concentrations of particulate OVOCs in the CLOUD chamber experiments are predicted using the volatility basis set (VBS) parameterizations (Isaacman-VanWertz and Aumont, 2021; Stolzenburg et al., 2018). Parameterized $\log_{10}C_{\text{sat}}$ agree well with the measured $\log_{10}C_{\text{sat}}$ for particulate CHO species (Figure V-S16a). In addition, measured $\log_{10}C_{\text{sat}}$ of particulate dimers show a good correlation ($R^2 = 0.85$) with their estimated $\log_{10}C_{\text{sat}}$ using the modified Li et al. approach (Isaacman-VanWertz and Aumont, 2021) accounting for nitrate functionalities (Figure V-S16b).

Therefore, we estimated the volatility distribution of the full-range OVOCs measured by CI-(NH₄⁺)-Orbitrap in the CLOUD chamber (Figure V-3B, and V-S17) using the modified Li et al. approach (Isaacman-VanWertz and Aumont, 2021). As shown in Figure V-3B, we grouped monomers C₉₋₁₀ and dimers C₁₈₋₂₀ measured in the CLOUD chamber into five volatility regimes based on their log₁₀C_{sat} values (Donahue et al., 2012; Schervish and Donahue, 2020); ultra-low volatility (ULVOCs), extremely low-volatility (ELVOCs), low-volatility (LVOCs), semi-volatile (SVOCs), and intermediate-volatility organic compounds (IVOCs). Only the ULVOCs and some ELVOCs initiate cluster growth and form new particles (Schervish and Donahue, 2020; Simon et al., 2020). In each volatility bin, we show the signal of the sum of OVOCs that fall in this volatility range. Due to the negligible CHON RO₂ autoxidation, the volatility distribution of OVOCs shifts towards relatively higher volatility in the presence of NO₃ radicals compared to the distribution from pure O₃ chemistry (Figure V-3B). The resulting average signal-weighted C_{sat} value is 2 times higher in the presence of NO₃ radicals. However, the effect is most dramatic in the tail, for compounds directly involved in NPF. The contribution of ELVOCs drops by a factor of 2 (i.e., from 1.7% to 0.8%), and the ULVOCs, which contribute most efficiently to pure biogenic nucleation (Schervish and Donahue, 2020; Simon et al., 2020), comprise 0.6% of the total measured OVOCs in the pure O₃ system but decrease to 0.1% in the presence of NO₃ radicals (Figure V-3C). The lowest volatility bins of the ULVOC range (log₁₀C_{sat}<-13 µg m⁻³) vanish entirely. A 5-fold reduction of the ULVOC yield was also quantified using the NO₃⁻-LTOF.

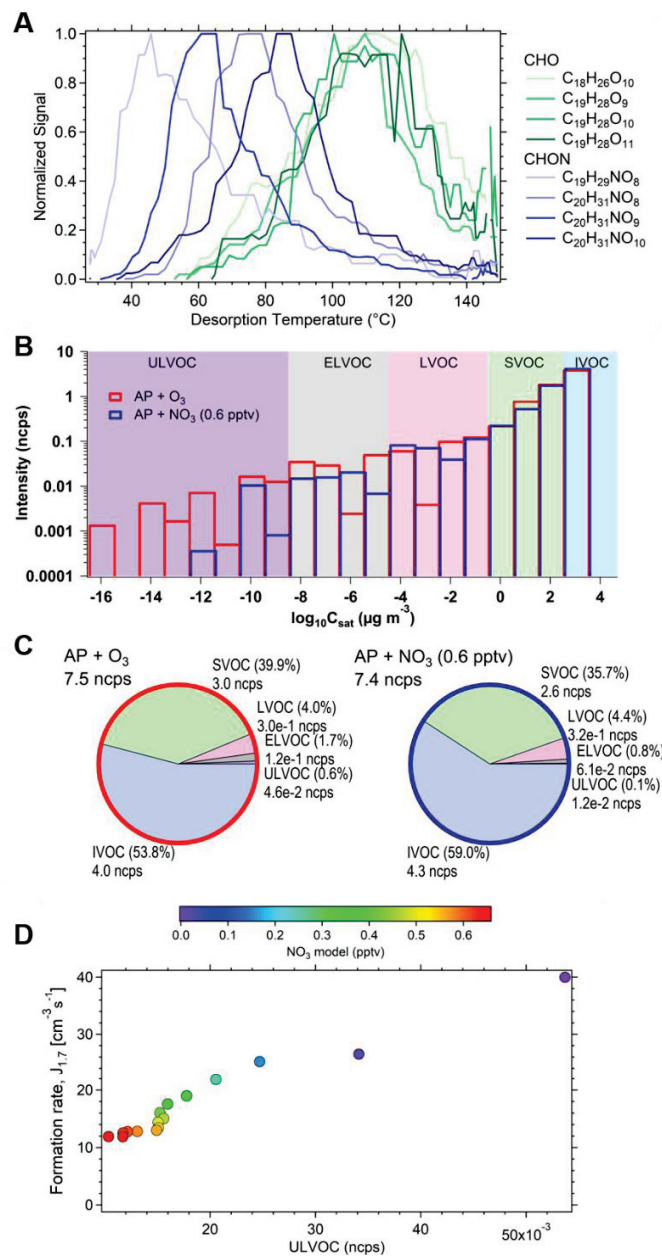


Figure V-3: Higher volatilities of OVOCs in the presence of NO_3 radicals illustrating the suppression of NPF in CLOUD. (A) Desorption signals of selected CHO dimers and CHON dimers in the particle phase measured by FIGAERO-CIMS. Ion signals are normalized to the maximum signal on a linear scale for clarity. (B) Monomers C_{9-10} and dimers C_{18-20} measured by CI-(NH_4^+)-Orbitrap binned to a volatility distribution showing their relative abundance in pure O_3 and NO_3 chemistry, respectively; simulated NO_3 concentration was ~0.6 pptv. The background

colors represent the saturation concentration (C_{sat}) in the range of ultra-low volatility (ULVOCs, purple), extremely low volatility (ELVOCs, gray), low volatility (LVOCs, pink), semi-volatile (SVOCs, green), and intermediate volatility (IVOCs, blue) organic compounds. (C)

Corresponding contributions of IVOCs, SVOCs, LVOCs, ELVOCs, and ULVOCs classes in pure O₃ and NO₃ chemistry. These percentages do not relate to the yields but to the measured intensities. (D) Formation rate of particles plotted as a function of ULVOC concentration, colored by the concentrations of simulated NO₃ radicals.

As the OVOC composition changed during the experiment, the decrease of the measured particle formation rates at 1.7 nm by a factor of 4 (see also Figure V-1C) is likely driven by the decreasing concentration of ULVOCs caused by an increase in the NO₃ radical concentration (Figure V-1D and V-3D). Overall, the results demonstrate that NO₃ radicals inhibit the production of the least volatile compounds and ultimately impede the formation of new particles.

V.3.4. Nocturnal NPF in a wetland

We further investigated the role of NO₃ radicals in suppressing NPF from the ozonolysis of monoterpenes by conducting nighttime observations in a wetland surrounded by boreal forests in Siikaneva, Finland. At this location, we did observe rare nocturnal NPF events (Figure V-S18), which were accompanied by a decoupled layer formation capturing the emissions from the wetland inside this stable boundary layer and nearly no mixing with the rest of the atmosphere (Junninen et al., 2022). Similar OVOC species as in the CLOUD chamber were detected in this ambient environment (Figure V-S19). Monoterpenes were found to be dominating VOCs at this site (Figure V-S20), and the most abundant monoterpene species there were found to be α -pinene and Δ^3 -carene (Vettikkat et al., 2023). These species were thus used to calculate the reactivity of different monoterpene isomers in wetland, in order to represent the reactivity range in Siikaneva by assuming the total monoterpene concentration is that of one monoterpene. The resulting reactivity of ozonolysis with these two monoterpenes and the generated concentrations of CHO dimers were on average 3 times and 2 times higher during the nighttime NPF event compared to nonevent night, respectively, with the dominating monoterpene ozonolysis reactivity in Siikaneva from α -pinene (Figure V-4, V-S21a). Further, concentrations of CHO monomers and CHO dimers were 4 and 10 times higher than those of CHON monomers and CHON dimers during the NPF event, respectively,

with total CHO species representing 80% of total OVOCs. In contrast, sharp increases of CHON monomers and CHON dimers were observed only during the nonevent when no decoupling process occurred but in well-mixed conditions with the rest of the atmosphere (Junninen et al., 2022). The presence of CHON dimers, which are markers for NO_3 chemistry, indicates the presence of NO_3 during the nonevent night (Junninen et al., 2022; Yan et al., 2016), which was estimated at nearly 1 ppqv, resulting in a reactivity of monoterpene 0.2 pptv h^{-1} during the nonevent night ($\text{NO}_2:\text{O}_3 \approx 0.007:1$) with the reactivity of monoterpene by NO_3 radicals in Siikaneva mainly coming from α -pinene (Figure V-S21b). These were associated with a corresponding drop in ULVOC and ELVOC concentration both by a factor of 6 (Figure V-4G). Consistent with the CLOUD experiments, the particle number concentration was up to one order of magnitude (3-fold in median) lower during the nonevent nights compared to event nights (Figure V-4A).

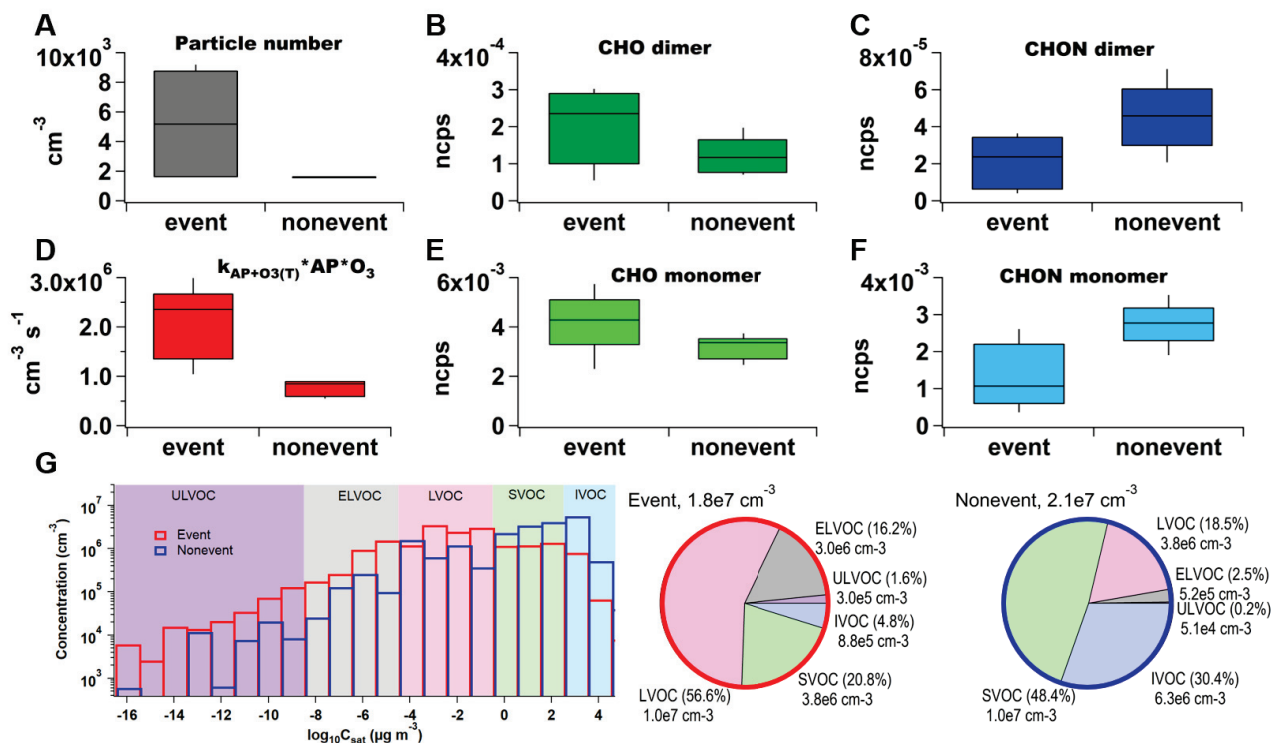


Figure V-4: Nocturnal NPF event and nonevent recorded at Siikaneva, Finland. (A, B, C, D, E and F) Box plots of number concentrations of particles greater than 2.5 nm (A), CHO dimers (B), CHON dimers (C), α -pinene ozonolysis rate (D), CHO monomers (E), and CHON monomers (F) in one NPF event and one nonevent. (G) Binned volatility distribution of monomers C₉₋₁₀ and dimers C₁₉₋₂₀ measured by CI-(NO₃⁻)-APi-TOF showing their concentration for a NPF event and

a nonevent. The pie charts on the right represent the corresponding contributions of IVOCs, SVOCs, LVOCs, ELVOCs, and ULVOCs classes.

V.4. Discussion

Taken together, these results form the basis of a molecular understanding of why biogenic NPF is not commonly observed at night, especially in monoterpene-dominated environments. The NO_3^- -derived RO_2 radicals not only yield higher volatility dimers but also completely alter the fate of RO_2 radicals from other oxidants and thus the capacity to form new particles. The nitrogen-containing organic vapors formed from NO_3^- chemistry are not of sufficiently low volatility to initiate the formation and growth of particles. When only 20-30% of the α -pinene reactivity is driven by NO_3^- , ULVOC yields are reduced by a factor of 5 and particle formation rates by a factor of 4. In the ambient atmosphere, particle number is cut by up to an order of magnitude in boreal environments when NO_3^- chemistry is involved.

In general, the quantity and volatility distribution of HOMs, HOM- RO_2 , and RO_2 produced from concurrent complex chemical reactions can substantially alter the formation of new particles in the atmosphere. This is especially important for organic NPF governed by covalently bound dimers, where cross-reactions between different RO_2 control the ULVOC tail of the volatility distribution, and exact NPF rates depend even on the volatility distribution within that tail. In some cases, such as for isoprene suppression of monoterpene nucleation, it is the mixture of organic precursors that influences the outcome (Heinritzi et al., 2020; McFiggans et al., 2019). In others, such as for NO_x suppression, it is inhibition of dimer formation that affects the outcome (Yan et al., 2020). Here, for NO_3^- suppression, it is the oxidant that influences the outcome. Our results highlight a need for more realistic consideration of NPF processes in the atmosphere, especially when multiple oxidants/processes are involved. In addition, the influence of NO_3^- derived from NO_x represents an anthropogenic perturbation on a biogenic system, which have broader implications for the understanding of aerosol sources and CCN in the modern atmosphere.

V.5. References

Almeida, J., Schobesberger, S., Kurten, A., Ortega, I. K., Kupiainen-Maatta, O., Praplan, A. P., Adamov, A., Amorim, A., Bianchi, F., Breitenlechner, M., David, A., Dommen, J., Donahue, N. M., Downard, A., Dunne, E., Duplissy, J., Ehrhart, S., Flagan, R. C., Franchin,

- A., Guida, R., Hakala, J., Hansel, A., Heinritzi, M., Henschel, H., Jokinen, T., Junninen, H., Kajos, M., Kangasluoma, J., Keskinen, H., Kupc, A., Kurten, T., Kvashin, A. N., Laaksonen, A., Lehtipalo, K., Leiminger, M., Leppa, J., Loukonen, V., Makhmutov, V., Mathot, S., McGrath, M. J., Nieminen, T., Olenius, T., Onnela, A., Petaja, T., Riccobono, F., Riipinen, I., Rissanen, M., Rondo, L., Ruuskanen, T., Santos, F. D., Sarnela, N., Schallhart, S., Schnitzhofer, R., Seinfeld, J. H., Simon, M., Sipila, M., Stozhkov, Y., Stratmann, F., Tome, A., Trostl, J., Tsagkogeorgas, G., Vaattovaara, P., Viisanen, Y., Virtanen, A., Vrtala, A., Wagner, P. E., Weingartner, E., Wex, H., Williamson, C., Wimmer, D., Ye, P., Yli-Juuti, T., Carslaw, K. S., Kulmala, M., Curtius, J., Baltensperger, U., Worsnop, D. R., Vehkamaki, H., and Kirkby, J. (2013), Molecular understanding of sulphuric acid-amine particle nucleation in the atmosphere, *Nature*, 502(7471), 359-363, doi:10.1038/nature12663.
- Aregahegn, K. Z., Nozière, B., and George, C. (2013), Organic aerosol formation photo-enhanced by the formation of secondary photosensitizers in aerosols, *Faraday discussions*, 165, 123, doi:10.1039/c3fd00044c.
- Asaf, D., Pedersen, D., Matveev, V., Peleg, M., Kern, C., Zingler, J., Platt, U., and Luria, M. (2009), Long-Term Measurements of NO₃ Radical at a Semiarid Urban Site: 1. Extreme Concentration Events and Their Oxidation Capacity, *Environmental science & technology*, 43(24), 9117-9123, doi:10.1021/es900798b.
- Bates, K. H., Burke, G. J. P., Cope, J. D., and Nguyen, T. B. (2022), Secondary organic aerosol and organic nitrogen yields from the nitrate radical (NO₃) oxidation of alpha-pinene from various RO₂ fates. *Atmospheric Chemistry Physics*, 22(2), 1467-1482, doi:10.5194/acp-22-1467-2022.
- Berndt, T., Richters, S., Jokinen, T., Hyttinen, N., Kurten, T., Otkjaer, R. V., Kjaergaard, H. G., Stratmann, F., Herrmann, H., Sipila, M., Kulmala, M., and Ehn, M. (2016), Hydroxyl radical-induced formation of highly oxidized organic compounds, *Nature communications*, 7, 13677, doi:10.1038/ncomms13677.
- Berndt, T., Scholz, W., Mentler, B., Fischer, L., Herrmann, H., Kulmala, M., and Hansel, A. (2018), Accretion Product Formation from Self- and Cross-Reactions of RO₂ Radicals in the Atmosphere, *Angewandte Chemie*, 57(14), 3820-3824, doi:10.1002/anie.201710989.
- Bianchi, F., Kurten, T., Riva, M., Mohr, C., Rissanen, M. P., Roldin, P., Berndt, T., Crounse, J. D., Wennberg, P. O., Mentel, T. F., Wildt, J., Junninen, H., Jokinen, T., Kulmala, M., Worsnop, D. R., Thornton, J. A., Donahue, N., Kjaergaard, H. G., and Ehn, M. (2019), Highly Oxygenated Organic Molecules (HOM) from Gas-Phase Autoxidation Involving Peroxy Radicals: A Key Contributor to Atmospheric Aerosol, *Chemical reviews*, 119(6), 3472-3509, doi:10.1021/acs.chemrev.8b00395.
- Bianchi, F., Tröstl, J., Junninen, H., Frege, C., Henne, S., Hoyle, C. R., Molteni, U., Herrmann, E., Adamov, A., Bukowiecki, N., Chen, X., Duplissy, J., Gysel, M., Hutterli, M., Kangasluoma, J., Kontkanen, J., Kürten, A., Manninen, H. E., Münch, S., Peräkylä, O., Petäjä, T., Rondo, L., Williamson, C., Weingartner, E., Curtius, J., Worsnop, D. R., Kulmala, M., Dommen, J., and Baltensperger, U. (2016), New particle formation in the free troposphere: A question of chemistry and timing, *Science*, 352(6289), 1109-1112, doi:10.1126/science.aad5456.
- Bonn, B., and Moortgat, G. K. (2002), New particle formation during α- and β-pinene oxidation by O₃, OH and NO₃, and the influence of water vapour: particle size distribution studies, *Atmospheric Chemistry Physics*, 2(3), 183-196, doi:10.5194/acp-2-183-2002.

- Breitenlechner, M., Fischer, L., Hainer, M., Heinritzi, M., Curtius, J., and Hansel, A. (2017), PTR3: An Instrument for Studying the Lifecycle of Reactive Organic Carbon in the Atmosphere, *Analytical chemistry*, 89(11), 5824-5831, doi:10.1021/acs.analchem.6b05110.
- Dada, L., Lehtipalo, K., Kontkanen, J., Nieminen, T., Baalbaki, R., Ahonen, L., Duplissy, J., Yan, C., Chu, B., Petaja, T., Lehtinen, K., Kerminen, V. M., Kulmala, M., and Kangasluoma, J. (2020), Formation and growth of sub-3-nm aerosol particles in experimental chambers, *Nature protocols*, 15(3), 1013-1040, doi:10.1038/s41596-019-0274-z.
- Donahue, N. M., Kroll, J. H., Pandis, S. N., and Robinson, A. L. (2012), A two-dimensional volatility basis set – Part 2: Diagnostics of organic-aerosol evolution, *Atmospheric Chemistry and Physics*, 12(2), 615-634, doi:10.5194/acp-12-615-2012.
- Ehn, M., Thornton, J. A., Kleist, E., Sipila, M., Junninen, H., Pullinen, I., Springer, M., Rubach, F., Tillmann, R., Lee, B., Lopez-Hilfiker, F., Andres, S., Acir, I. H., Rissanen, M., Jokinen, T., Schobesberger, S., Kangasluoma, J., Kontkanen, J., Nieminen, T., Kurten, T., Nielsen, L. B., Jorgensen, S., Kjaergaard, H. G., Canagaratna, M., Maso, M. D., Berndt, T., Petaja, T., Wahner, A., Kerminen, V. M., Kulmala, M., Worsnop, D. R., Wildt, J., and Mentel, T. F. (2014), A large source of low-volatility secondary organic aerosol, *Nature*, 506(7489), 476-479, doi:10.1038/nature13032.
- Fry, J. L., Draper, D. C., Barsanti, K. C., Smith, J. N., Ortega, J., Winkler, P. M., Lawler, M. J., Brown, S. S., Edwards, P. M., Cohen, R. C., and Lee, L. (2014), Secondary organic aerosol formation and organic nitrate yield from NO_3 oxidation of biogenic hydrocarbons, *Environmental science & technology*, 48(20), 11944-11953, doi:10.1021/es502204x.
- Geyer, A., Aliche, B., Konrad, S., Schmitz, T., Stutz, J., and Platt, U. (2001), Chemistry and oxidation capacity of the nitrate radical in the continental boundary layer near Berlin, *Journal of Geophysical Research: Atmospheres*, 106(D8), 8013-8025, doi:10.1029/2000jd900681.
- Gordon, H., Kirkby, J., Baltensperger, U., Bianchi, F., Breitenlechner, M., Curtius, J., Dias, A., Dommen, J., Donahue, N. M., Dunne, E. M., Duplissy, J., Ehrhart, S., Flagan, R. C., Frege, C., Fuchs, C., Hansel, A., Hoyle, C. R., Kulmala, M., Kürten, A., Lehtipalo, K., Makhmutov, V., Molteni, U., Rissanen, M. P., Stozkhov, Y., Tröstl, J., Tsagkogeorgas, G., Wagner, R., Williamson, C., Wimmer, D., Winkler, P. M., Yan, C., and Carslaw, K. S. (2017), Causes and importance of new particle formation in the present-day and preindustrial atmospheres, *Journal of Geophysical Research: Atmospheres*, 122(16), 8739-8760, doi:10.1002/2017jd026844.
- Gordon, H., Sengupta, K., Rap, A., Duplissy, J., Frege, C., Williamson, C., Heinritzi, M., Simon, M., Yan, C., Almeida, J., Trostl, J., Nieminen, T., Ortega, I. K., Wagner, R., Dunne, E. M., Adamov, A., Amorim, A., Bernhammer, A. K., Bianchi, F., Breitenlechner, M., Brilke, S., Chen, X., Craven, J. S., Dias, A., Ehrhart, S., Fischer, L., Flagan, R. C., Franchin, A., Fuchs, C., Guida, R., Hakala, J., Hoyle, C. R., Jokinen, T., Junninen, H., Kangasluoma, J., Kim, J., Kirkby, J., Krapf, M., Kurten, A., Laaksonen, A., Lehtipalo, K., Makhmutov, V., Mathot, S., Molteni, U., Monks, S. A., Onnela, A., Perakyla, O., Piel, F., Petaja, T., Praplan, A. P., Pringle, K. J., Richards, N. A., Rissanen, M. P., Rondo, L., Sarnela, N., Schobesberger, S., Scott, C. E., Seinfeld, J. H., Sharma, S., Sipila, M., Steiner, G., Stozkhov, Y., Stratmann, F., Tome, A., Virtanen, A., Vogel, A. L., Wagner, A. C., Wagner, P. E., Weingartner, E., Wimmer, D., Winkler, P. M., Ye, P., Zhang, X., Hansel, A., Dommen, J., Donahue, N. M., Worsnop, D. R., Baltensperger, U., Kulmala, M., Curtius, J., and Carslaw, K. S. (2016),

- Reduced anthropogenic aerosol radiative forcing caused by biogenic new particle formation, *Proceedings of the National Academy of Sciences of the United States of America*, 113(43), 12053-12058, doi:10.1073/pnas.1602360113.
- Hakola, H., Hellén, H., Hemmilä, M., Rinne, J., and Kulmala, M. (2012), In situ measurements of volatile organic compounds in a boreal forest, *Atmospheric Chemistry and Physics*, 12(23), 11665-11678, doi:10.5194/acp-12-11665-2012.
- He, X. C., Tham, Y. J., Dada, L., Wang, M., Finkenzeller, H., Stolzenburg, D., Iyer, S., Simon, M., Kurten, A., Shen, J., Rorup, B., Rissanen, M., Schobesberger, S., Baalbaki, R., Wang, D. S., Koenig, T. K., Jokinen, T., Sarnela, N., Beck, L. J., Almeida, J., Amanatidis, S., Amorim, A., Ataei, F., Baccarini, A., Bertozi, B., Bianchi, F., Brilke, S., Caudillo, L., Chen, D., Chiu, R., Chu, B., Dias, A., Ding, A., Dommen, J., Duplissy, J., El Haddad, I., Gonzalez Carracedo, L., Granzin, M., Hansel, A., Heinritzi, M., Hofbauer, V., Junninen, H., Kangasluoma, J., Kemppainen, D., Kim, C., Kong, W., Krechmer, J. E., Kvashin, A., Laitinen, T., Lamkaddam, H., Lee, C. P., Lehtipalo, K., Leiminger, M., Li, Z., Makhmutov, V., Manninen, H. E., Marie, G., Marten, R., Mathot, S., Mauldin, R. L., Mentler, B., Mohler, O., Muller, T., Nie, W., Onnela, A., Petaja, T., Pfeifer, J., Philippov, M., Ranjithkumar, A., Saiz-Lopez, A., Salma, I., Scholz, W., Schuchmann, S., Schulze, B., Steiner, G., Stozhkov, Y., Tauber, C., Tome, A., Thakur, R. C., Vaisanen, O., Vazquez-Pufleau, M., Wagner, A. C., Wang, Y., Weber, S. K., Winkler, P. M., Wu, Y., Xiao, M., Yan, C., Ye, Q., Ylisirnio, A., Zauner-Wieczorek, M., Zha, Q., Zhou, P., Flagan, R. C., Curtius, J., Baltensperger, U., Kulmala, M., Kerminen, V. M., Kurten, T., Donahue, N. M., Volkamer, R., Kirkby, J., Worsnop, D. R., and Sipila, M. (2021), Role of iodine oxoacids in atmospheric aerosol nucleation, *Science*, 371(6529), 589-595, doi:10.1126/science.abe0298.
- Heinritzi, M., Dada, L., Simon, M., Stolzenburg, D., Wagner, A. C., Fischer, L., Ahonen, L. R., Amanatidis, S., Baalbaki, R., Baccarini, A., Bauer, P. S., Baumgartner, B., Bianchi, F., Brilke, S., Chen, D., Chiu, R., Dias, A., Dommen, J., Duplissy, J., Finkenzeller, H., Frege, C., Fuchs, C., Garmash, O., Gordon, H., Granzin, M., El Haddad, I., He, X., Helm, J., Hofbauer, V., Hoyle, C. R., Kangasluoma, J., Keber, T., Kim, C., Kürten, A., Lamkaddam, H., Laurila, T. M., Lampilahti, J., Lee, C. P., Lehtipalo, K., Leiminger, M., Mai, H., Makhmutov, V., Manninen, H. E., Marten, R., Mathot, S., Mauldin, R. L., Mentler, B., Molteni, U., Müller, T., Nie, W., Nieminen, T., Onnela, A., Partoll, E., Passananti, M., Petäjä, T., Pfeifer, J., Pospisilova, V., Quéléver, L. L. J., Rissanen, M. P., Rose, C., Schobesberger, S., Scholz, W., Scholze, K., Sipilä, M., Steiner, G., Stozhkov, Y., Tauber, C., Tham, Y. J., Vazquez-Pufleau, M., Virtanen, A., Vogel, A. L., Volkamer, R., Wagner, R., Wang, M., Weitz, L., Wimmer, D., Xiao, M., Yan, C., Ye, P., Zha, Q., Zhou, X., Amorim, A., Baltensperger, U., Hansel, A., Kulmala, M., Tomé, A., Winkler, P. M., Worsnop, D. R., Donahue, N. M., Kirkby, J., and Curtius, J. (2020), Molecular understanding of the suppression of new-particle formation by isoprene, *Atmospheric Chemistry and Physics*, 20(20), 11809-11821, doi:10.5194/acp-20-11809-2020.
- Huang, W., Saathoff, H., Pajunoja, A., Shen, X., Naumann, K. H., Wagner, R., Virtanen, A., Leisner, T., and Mohr, C. (2018), α -Pinene secondary organic aerosol at low temperature: chemical composition and implications for particle viscosity, *Atmospheric Chemistry Physics*, 18(4), 2883-2898, doi:10.5194/acp-18-2883-2018.

- Isaacman-VanWertz, G., and Aumont, B. (2021), Impact of organic molecular structure on the estimation of atmospherically relevant physicochemical parameters, *Atmospheric Chemistry and Physics*, 21(8), 6541-6563, doi:10.5194/acp-21-6541-2021.
- Jimenez, J. L., Canagaratna, M. R., Donahue, N. M., Prevot, A. S. H., Zhang, Q., Kroll, J. H., DeCarlo, P. F., Allan, J. D., Coe, H., Ng, N. L., Aiken, A. C., Docherty, K. S., Ulbrich, I. M., Grieshop, A. P., Robinson, A. L., Duplissy, J., Smith, J. D., Wilson, K. R., Lanz, V. A., Hueglin, C., Sun, Y. L., Tian, J., Laaksonen, A., Raatikainen, T., Rautiainen, J., Vaattovaara, P., Ehn, M., Kulmala, M., Tomlinson, J. M., Collins, D. R., Cubison, M. J., Dunlea, J., Huffman, J. A., Onasch, T. B., Alfarra, M. R., Williams, P. I., Bower, K., Kondo, Y., Schneider, J., Drewnick, F., Borrmann, S., Weimer, S., Demerjian, K., Salcedo, D., Cottrell, L., Griffin, R., Takami, A., Miyoshi, T., Hatakeyama, S., Shimono, A., Sun, J. Y., Zhang, Y. M., Dzepina, K., Kimmel, J. R., Sueper, D., Jayne, J. T., Herndon, S. C., Trimborn, A. M., Williams, L. R., Wood, E. C., Middlebrook, A. M., Kolb, C. E., Baltensperger, U., and Worsnop, D. R. (2009), Evolution of Organic Aerosols in the Atmosphere, *Science*, 326(5959), 1525-1529, doi:doi:10.1126/science.1180353.
- Jokinen, T., Berndt, T., Makkonen, R., Kerminen, V. M., Junninen, H., Paasonen, P., Stratmann, F., Herrmann, H., Guenther, A. B., Worsnop, D. R., Kulmala, M., Ehn, M., and Sipila, M. (2015), Production of extremely low volatile organic compounds from biogenic emissions: Measured yields and atmospheric implications, *Proceedings of the National Academy of Sciences of the United States of America*, 112(23), 7123-7128, doi:10.1073/pnas.1423977112.
- Junninen, H., Ahonen, L., Bianchi, F., Quéléver, L., Schallhart, S., Dada, L., Manninen, H. E., Leino, K., Lampilahti, J., Buenrostro Mazon, S., Rantala, P., Räty, M., Kontkanen, J., Negri, S., Aliaga, D., Garmash, O., Alekseychik, P., Lipp, H., Tamme, K., Levula, J., Sipilä, M., Ehn, M., Worsnop, D., Zilitinkevich, S., Mammarella, I., Rinne, J., Vesala, T., Petäjä, T., Kerminen, V.-M., and Kulmala, M. (2022), Terpene emissions from boreal wetlands can initiate stronger atmospheric new particle formation than boreal forests, *Communications Earth & Environment*, 3(1), 93, doi:10.1038/s43247-022-00406-9.
- Junninen, H., Hulkko, M., Riipinen, I., Nieminen, T., Hirsikko, A., Suni, T., Boy, M., Lee, S.-H., Vana, M., Tammet, H., Kerminen, V.-M., and Kulmala, M. (2017), Observations on nocturnal growth of atmospheric clusters, *Tellus B: Chemical and Physical Meteorology*, 60(3), 365-371, doi:10.1111/j.1600-0889.2008.00356.x.
- Kürten, A., Bergen, A., Heinritzi, M., Leiminger, M., Lorenz, V., Piel, F., Simon, M., Sitals, R., Wagner, A. C., and Curtius, J. (2016), Observation of new particle formation and measurement of sulfuric acid, ammonia, amines and highly oxidized organic molecules at a rural site in central Germany, *Atmospheric Chemistry and Physics*, 16(19), 12793-12813, doi:10.5194/acp-16-12793-2016.
- Kanakidou, M., Seinfeld, J. H., Pandis, S. N., Barnes, I., Dentener, F. J., Facchini, M. C., Van Dingenen, R., Ervens, B., Nenes, A., Nielsen, C. J., Swietlicki, E., Putaud, J. P., Balkanski, Y., Fuzzi, S., Horth, J., Moortgat, G. K., Winterhalter, R., Myhre, C. E. L., Tsigaridis, K., Vignati, E., Stephanou, E. G., and Wilson, J. (2005), Organic aerosol and global climate modelling: a review, *Atmospheric Chemistry Physics*, 5(4), 1053-1123, doi:10.5194/acp-5-1053-2005.
- Kerminen, V. M., Petäjä, T., Manninen, H. E., Paasonen, P., Nieminen, T., Sipilä, M., Junninen, H., Ehn, M., Gagné, S., Laakso, L., Riipinen, I., Vehkamäki, H., Kurten, T., Ortega, I. K.,

- Dal Maso, M., Brus, D., Hyvärinen, A., Lihavainen, H., Leppä, J., Lehtinen, K. E. J., Mirme, A., Mirme, S., Hörrak, U., Berndt, T., Stratmann, F., Birmili, W., Wiedensohler, A., Metzger, A., Dommen, J., Baltensperger, U., Kiendler-Scharr, A., Mentel, T. F., Wildt, J., Winkler, P. M., Wagner, P. E., Petzold, A., Minikin, A., Plass-Dülmer, C., Pöschl, U., Laaksonen, A., and Kulmala, M. (2010), Atmospheric nucleation: highlights of the EUCAARI project and future directions, *Atmospheric Chemistry Physics*, 10(22), 10829-10848, doi:10.5194/acp-10-10829-2010.
- Kirkby, J., Duplissy, J., Sengupta, K., Frege, C., Gordon, H., Williamson, C., Heinritzi, M., Simon, M., Yan, C., Almeida, J., Tröstl, J., Nieminen, T., Ortega, I. K., Wagner, R., Adamov, A., Amorim, A., Bernhammer, A.-K., Bianchi, F., Breitenlechner, M., Brilke, S., Chen, X., Craven, J., Dias, A., Ehrhart, S., Flagan, R. C., Franchin, A., Fuchs, C., Guida, R., Hakala, J., Hoyle, C. R., Jokinen, T., Junninen, H., Kangasluoma, J., Kim, J., Krapf, M., Kürten, A., Laaksonen, A., Lehtipalo, K., Makhmutov, V., Mathot, S., Molteni, U., Onnela, A., Peräkylä, O., Piel, F., Petäjä, T., Praplan, A. P., Pringle, K., Rap, A., Richards, N. A. D., Riipinen, I., Rissanen, M. P., Rondo, L., Sarnela, N., Schobesberger, S., Scott, C. E., Seinfeld, J. H., Sipilä, M., Steiner, G., Stozhkov, Y., Stratmann, F., Tomé, A., Virtanen, A., Vogel, A. L., Wagner, A. C., Wagner, P. E., Weingartner, E., Wimmer, D., Winkler, P. M., Ye, P., Zhang, X., Hansel, A., Dommen, J., Donahue, N. M., Worsnop, D. R., Baltensperger, U., Kulmala, M., Carslaw, K. S., and Curtius, J. (2016), Ion-induced nucleation of pure biogenic particles, *Nature*, 533, 521, doi:10.1038/nature17953.
- Kulmala, M., Hämeri, K., Aalto, P. P., Mäkelä, J. M., Pirjola, L., Nilsson, E. D., Buzorius, G., Rannik, Ü., Dal Maso, M., Seidl, W., Hoffman, T., Janson, R., Hansson, H. C., Viisanen, Y., Laaksonen, A., and O'dowd, C. D. (2001), Overview of the international project on biogenic aerosol formation in the boreal forest (BIOFOR), *Tellus B: Chemical and Physical Meteorology*, 53(4), 324-343, doi:10.3402/tellusb.v53i4.16601.
- Kulmala, M., Vehkamäki, H., Petäjä, T., Dal Maso, M., Lauri, A., Kerminen, V.-M., Birmili, W., and McMurry, P. (2004), Formation and growth rates of ultrafine atmospheric particles: a review of observations, *Journal of Aerosol Science*, 35(2), 143-176.
- Kurten, A., Jokinen, T., Simon, M., Sipila, M., Sarnela, N., Junninen, H., Adamov, A., Almeida, J., Amorim, A., Bianchi, F., Breitenlechner, M., Dommen, J., Donahue, N. M., Duplissy, J., Ehrhart, S., Flagan, R. C., Franchin, A., Hakala, J., Hansel, A., Heinritzi, M., Hutterli, M., Kangasluoma, J., Kirkby, J., Laaksonen, A., Lehtipalo, K., Leiminger, M., Makhmutov, V., Mathot, S., Onnela, A., Petaja, T., Praplan, A. P., Riccobono, F., Rissanen, M. P., Rondo, L., Schobesberger, S., Seinfeld, J. H., Steiner, G., Tome, A., Trostl, J., Winkler, P. M., Williamson, C., Wimmer, D., Ye, P., Baltensperger, U., Carslaw, K. S., Kulmala, M., Worsnop, D. R., and Curtius, J. (2014), Neutral molecular cluster formation of sulfuric acid-dimethylamine observed in real time under atmospheric conditions, *Proceedings of the National Academy of Sciences of the United States of America*, 111(42), 15019-15024, doi:10.1073/pnas.1404853111.
- Kurten, T., Moller, K. H., Nguyen, T. B., Schwantes, R. H., Misztal, P. K., Su, L., Wennberg, P. O., Fry, J. L., and Kjaergaard, H. G. (2017), Alkoxy Radical Bond Scissions Explain the Anomalously Low Secondary Organic Aerosol and Organonitrate Yields From alpha-Pinene + NO₃, *Journal of Physical Chemistry Letters*, 8(13), 2826-2834, doi:10.1021/acs.jpcllett.7b01038.

- Kurtenbach, R., Ackermann, R., Becker, K. H., Geyer, A., Gomes, J. A. G., Lörzer, J. C., Platt, U., and Wiesen, P. (2002), Verification of the Contribution of Vehicular Traffic to the Total NMVOC Emissions in Germany and the Importance of the NO₃ Chemistry in the City Air, *Journal of Atmospheric Chemistry*, 42(1), 395-411, doi:10.1023/A:1015778616796.
- Lehtipalo, K., Yan, C., Dada, L., Bianchi, F., Xiao, M., Wagner, R., Stolzenburg, D., Ahonen, L. R., Amorim, A., Baccarini, A., Bauer, P. S., Baumgartner, B., Bergen, A., Bernhammer, A. K., Breitenlechner, M., Brilke, S., Buchholz, A., Mazon, S. B., Chen, D., Chen, X., Dias, A., Dommen, J., Draper, D. C., Duplissy, J., Ehn, M., Finkenzeller, H., Fischer, L., Frege, C., Fuchs, C., Garmash, O., Gordon, H., Hakala, J., He, X., Heikkinen, L., Heinritzi, M., Helm, J. C., Hofbauer, V., Hoyle, C. R., Jokinen, T., Kangasluoma, J., Kerminen, V. M., Kim, C., Kirkby, J., Kontkanen, J., Kurten, A., Lawler, M. J., Mai, H., Mathot, S., Mauldin, R. L., 3rd, Molteni, U., Nichman, L., Nie, W., Nieminen, T., Ojdanic, A., Onnela, A., Passananti, M., Petaja, T., Piel, F., Pospisilova, V., Quelever, L. L. J., Rissanen, M. P., Rose, C., Sarnela, N., Schallhart, S., Schuchmann, S., Sengupta, K., Simon, M., Sipila, M., Tauber, C., Tome, A., Trostl, J., Vaisanen, O., Vogel, A. L., Volkamer, R., Wagner, A. C., Wang, M., Weitz, L., Wimmer, D., Ye, P., Ylisirnio, A., Zha, Q., Carslaw, K. S., Curtius, J., Donahue, N. M., Flagan, R. C., Hansel, A., Riipinen, I., Virtanen, A., Winkler, P. M., Baltensperger, U., Kulmala, M., and Worsnop, D. R. (2018), Multicomponent new particle formation from sulfuric acid, ammonia, and biogenic vapors, *Science Advances*, 4(12), eaau5363, doi:10.1126/sciadv.aau5363.
- Liebmann, J., Karu, E., Sobanski, N., Schuladen, J., Ehn, M., Schallhart, S., Quéléver, L., Hellen, H., Hakola, H., Hoffmann, T., Williams, J., Fischer, H., Lelieveld, J., and Crowley, J. N. (2018), Direct measurement of NO₃ radical reactivity in a boreal forest, *Atmospheric Chemistry and Physics*, 18(5), 3799-3815, doi:10.5194/acp-18-3799-2018.
- Lim, Y. B., and Ziemann, P. J. (2005), Products and Mechanism of Secondary Organic Aerosol Formation from Reactions of n-Alkanes with OH Radicals in the Presence of NO_x, *Environmental science & technology*, 39(23), 9229-9236, doi:10.1021/es051447g.
- Lopez-Hilfiker, F. D., Mohr, C., Ehn, M., Rubach, F., Kleist, E., Wildt, J., Mentel, T. F., Lutz, A., Hallquist, M., Worsnop, D., and Thornton, J. A. (2014), A novel method for online analysis of gas and particle composition: description and evaluation of a Filter Inlet for Gases and AEROSols (FIGAERO), *Atmospheric Measurement Techniques*, 7(4), 983-1001, doi:10.5194/amt-7-983-2014.
- Mai, H., and Flagan, R. C. (2018), Scanning DMA Data Analysis I. Classification Transfer Function, *Aerosol Science and Technology*, 52(12), 1382-1399, doi:10.1080/02786826.2018.1528005.
- McFiggans, G., Mentel, T. F., Wildt, J., Pullinen, I., Kang, S., Kleist, E., Schmitt, S., Springer, M., Tillmann, R., Wu, C., Zhao, D., Hallquist, M., Faxon, C., Le Breton, M., Hallquist, A. M., Simpson, D., Bergstrom, R., Jenkin, M. E., Ehn, M., Thornton, J. A., Alfarra, M. R., Bannan, T. J., Percival, C. J., Priestley, M., Topping, D., and Kiendler-Scharr, A. (2019), Secondary organic aerosol reduced by mixture of atmospheric vapours, *Nature*, 565(7741), 587-593, doi:10.1038/s41586-018-0871-y.
- Molteni, U., Bianchi, F., Klein, F., El Haddad, I., Frege, C., Rossi, M. J., Dommen, J., and Baltensperger, U. (2018), Formation of highly oxygenated organic molecules from aromatic compounds, *Atmospheric Chemistry and Physics*, 18(3), 1909-1921, doi:10.5194/acp-18-1909-2018.

- Ng, N. L., Brown, S. S., Archibald, A. T., Atlas, E., Cohen, R. C., Crowley, J. N., Day, D. A., Donahue, N. M., Fry, J. L., Fuchs, H., Griffin, R. J., Guzman, M. I., Herrmann, H., Hodzic, A., Iinuma, Y., Jimenez, J. L., Kiendler-Scharr, A., Lee, B. H., Luecken, D. J., Mao, J., McLaren, R., Mutzel, A., Osthoff, H. D., Ouyang, B., Picquet-Varrault, B., Platt, U., Pye, H. O. T., Rudich, Y., Schwantes, R. H., Shiraiwa, M., Stutz, J., Thornton, J. A., Tilgner, A., Williams, B. J., and Zaveri, R. A. (2017), Nitrate radicals and biogenic volatile organic compounds: oxidation, mechanisms, and organic aerosol, *Atmospheric Chemistry and Physics*, 17(3), 2103-2162, doi:10.5194/acp-17-2103-2017.
- Riva, M., Ehn, M., Li, D., Tomaz, S., Bourgain, F., Perrier, S., and George, C. (2019), CI-Orbitrap: An Analytical Instrument To Study Atmospheric Reactive Organic Species, *Analytical chemistry*, 91(15), 9419-9423, doi:10.1021/acs.analchem.9b02093.
- Rose, C., Zha, Q., Dada, L., Yan, C., Lehtipalo, K., Junninen, H., Mazon, S. B., Jokinen, T., Sarnela, N., Sipilä, M., Petäjä, T., Kerminen, V.-M., Bianchi, F., and Kulmala, M. (2018), Observations of biogenic ion-induced cluster formation in the atmosphere, *Science Advances*, 4(4), eaar5218, doi:doi:10.1126/sciadv.aar5218.
- Schervish, M., and Donahue, N. M. (2020), Peroxy Radical Chemistry and the Volatility Basis Set, *Atmospheric Chemistry and Physics*, 20(2), 1183-1199, doi:10.5194/acp-20-1183-2020.
- Simon, M., Dada, L., Heinritzi, M., Scholz, W., Stolzenburg, D., Fischer, L., Wagner, A. C., Kürten, A., Rörup, B., He, X.-C., Almeida, J., Baalbaki, R., Baccarini, A., Bauer, P. S., Beck, L., Bergen, A., Bianchi, F., Bräkling, S., Brilke, S., Caudillo, L., Chen, D., Chu, B., Dias, A., Draper, D. C., Duplissy, J., El-Haddad, I., Finkenzeller, H., Frege, C., Gonzalez-Carracedo, L., Gordon, H., Granzin, M., Hakala, J., Hofbauer, V., Hoyle, C. R., Kim, C., Kong, W., Lamkaddam, H., Lee, C. P., Lehtipalo, K., Leiminger, M., Mai, H., Manninen, H. E., Marie, G., Marten, R., Mentler, B., Molteni, U., Nichman, L., Nie, W., Ojdanic, A., Onnela, A., Partoll, E., Petäjä, T., Pfeifer, J., Philippov, M., Quéléver, L. L. J., Ranjithkumar, A., Rissanen, M. P., Schallhart, S., Schobesberger, S., Schuchmann, S., Shen, J., Sipilä, M., Steiner, G., Stozhkov, Y., Tauber, C., Tham, Y. J., Tomé, A. R., Vazquez-Pufleau, M., Vogel, A. L., Wagner, R., Wang, M., Wang, D. S., Wang, Y., Weber, S. K., Wu, Y., Xiao, M., Yan, C., Ye, P., Ye, Q., Zauner-Wieczorek, M., Zhou, X., Baltensperger, U., Dommen, J., Flagan, R. C., Hansel, A., Kulmala, M., Volkamer, R., Winkler, P. M., Worsnop, D. R., Donahue, N. M., Kirkby, J., and Curtius, J. (2020), Molecular understanding of new-particle formation from α -pinene between -50 and $+25$ °C, *Atmospheric Chemistry and Physics*, 20(15), 9183-9207, doi:10.5194/acp-20-9183-2020.
- Stolzenburg, D., Fischer, L., Vogel, A. L., Heinritzi, M., Schervish, M., Simon, M., Wagner, A. C., Dada, L., Ahonen, L. R., Amorim, A., Baccarini, A., Bauer, P. S., Baumgartner, B., Bergen, A., Bianchi, F., Breitenlechner, M., Brilke, S., Mazon, S. B., Chen, D., Dias, A., Draper, D. C., Duplissy, J., Haddad, I. E., Finkenzeller, H., Frege, C., Fuchs, C., Garmash, O., Gordon, H., He, X., Helm, J., Hofbauer, V., Hoyle, C. R., Kim, C., Kirkby, J., Kontkanen, J., Kürten, A., Lampilahti, J., Lawler, M., Lehtipalo, K., Leiminger, M., Mai, H., Mathot, S., Mentler, B., Molteni, U., Nie, W., Nieminen, T., Nowak, J. B., Ojdanic, A., Onnela, A., Passananti, M., Petäjä, T., Quéléver, L. L. J., Rissanen, M. P., Sarnela, N., Schallhart, S., Tauber, C., Tomé, A., Wagner, R., Wang, M., Weitz, L., Wimmer, D., Xiao, M., Yan, C., Ye, P., Zha, Q., Baltensperger, U., Curtius, J., Dommen, J., Flagan, R. C., Kulmala, M., Smith, J. N., Worsnop, D. R., Hansel, A., Donahue, N. M., and Winkler, P. M. (2018), Rapid growth of

- organic aerosol nanoparticles over a wide tropospheric temperature range, *Proceedings of the National Academy of Sciences*, 115(37), 9122-9127, doi:doi:10.1073/pnas.1807604115.
- Tomaz, S., Wang, D., Zabalegui, N., Li, D., Lamkaddam, H., Bachmeier, F., Vogel, A., Monge, M. E., Perrier, S., Baltensperger, U., George, C., Rissanen, M., Ehn, M., El Haddad, I., and Riva, M. (2021), Structures and reactivity of peroxy radicals and dimeric products revealed by online tandem mass spectrometry, *Nature communications*, 12(1), 300, doi:10.1038/s41467-020-20532-2.
- Trostl, J., Chuang, W. K., Gordon, H., Heinritzi, M., Yan, C., Molteni, U., Ahlm, L., Frege, C., Bianchi, F., Wagner, R., Simon, M., Lehtipalo, K., Williamson, C., Craven, J. S., Duplissy, J., Adamov, A., Almeida, J., Bernhammer, A. K., Breitenlechner, M., Brilke, S., Dias, A., Ehrhart, S., Flagan, R. C., Franchin, A., Fuchs, C., Guida, R., Gysel, M., Hansel, A., Hoyle, C. R., Jokinen, T., Junninen, H., Kangasluoma, J., Keskinen, H., Kim, J., Krapf, M., Kurten, A., Laaksonen, A., Lawler, M., Leiminger, M., Mathot, S., Mohler, O., Nieminen, T., Onnela, A., Petaja, T., Piel, F. M., Miettinen, P., Rissanen, M. P., Rondo, L., Sarnela, N., Schobesberger, S., Sengupta, K., Sipila, M., Smith, J. N., Steiner, G., Tome, A., Virtanen, A., Wagner, A. C., Weingartner, E., Wimmer, D., Winkler, P. M., Ye, P., Carslaw, K. S., Curtius, J., Dommen, J., Kirkby, J., Kulmala, M., Riipinen, I., Worsnop, D. R., Donahue, N. M., and Baltensperger, U. (2016), The role of low-volatility organic compounds in initial particle growth in the atmosphere, *Nature*, 533(7604), 527-531, doi:10.1038/nature18271.
- Vettikkat, L., Miettinen, P., Buchholz, A., Rantala, P., Yu, H., Schallhart, S., Petäjä, T., Seco, R., Männistö, E., Kulmala, M., Tuittila, E. S., Guenther, A. B., and Schobesberger, S.: High emission rates and strong temperature response make boreal wetlands a large source of isoprene and terpenes, *Atmos. Chem. Phys.*, 23, 2683-2698, 10.5194/acp-23-2683-2023, 2023.
- Wang, D. S., and Hildebrandt Ruiz, L. (2018), Chlorine-initiated oxidation of n-alkanes under high-NO_x conditions: insights into secondary organic aerosol composition and volatility using a FIGAERO-CIMS, *Atmospheric Chemistry and Physics*, 18(21), 15535-15553, doi:10.5194/acp-18-15535-2018.
- Wang, M., Chen, D., Xiao, M., Ye, Q., Stolzenburg, D., Hofbauer, V., Ye, P., Vogel, A. L., Mauldin, R. L., 3rd, Amorim, A., Baccarini, A., Baumgartner, B., Brilke, S., Dada, L., Dias, A., Duplissy, J., Finkenzeller, H., Garmash, O., He, X. C., Hoyle, C. R., Kim, C., Kvashnin, A., Lehtipalo, K., Fischer, L., Molteni, U., Petaja, T., Pospisilova, V., Quelever, L. L. J., Rissanen, M., Simon, M., Tauber, C., Tome, A., Wagner, A. C., Weitz, L., Volkamer, R., Winkler, P. M., Kirkby, J., Worsnop, D. R., Kulmala, M., Baltensperger, U., Dommen, J., El-Haddad, I., and Donahue, N. M. (2020a), Photo-oxidation of Aromatic Hydrocarbons Produces Low-Volatility Organic Compounds, *Environmental science & technology*, 54(13), 7911-7921, doi:10.1021/acs.est.0c02100.
- Wang, M., Kong, W., Marten, R., He, X.-C., Chen, D., Pfeifer, J., Heitto, A., Kontkanen, J., Dada, L., Kürten, A., Yli-Juuti, T., Manninen, H. E., Amanatidis, S., Amorim, A., Baalbaki, R., Baccarini, A., Bell, D. M., Bertozzi, B., Bräkling, S., Brilke, S., Murillo, L. C., Chiu, R., Chu, B., De Menezes, L.-P., Duplissy, J., Finkenzeller, H., Carracedo, L. G., Granzin, M., Guida, R., Hansel, A., Hofbauer, V., Krechmer, J., Lehtipalo, K., Lamkaddam, H., Lampimäki, M., Lee, C. P., Makhmutov, V., Marie, G., Mathot, S., Mauldin, R. L., Mentler, B., Müller, T., Onnela, A., Partoll, E., Petäjä, T., Philippov, M., Pospisilova, V., Ranjithkumar, A., Rissanen, M., Rörup, B., Scholz, W., Shen, J., Simon, M., Sipilä, M.,

- Steiner, G., Stolzenburg, D., Tham, Y. J., Tomé, A., Wagner, A. C., Wang, D. S., Wang, Y., Weber, S. K., Winkler, P. M., Wlasits, P. J., Wu, Y., Xiao, M., Ye, Q., Zauner-Wieczorek, M., Zhou, X., Volkamer, R., Riipinen, I., Dommen, J., Curtius, J., Baltensperger, U., Kulmala, M., Worsnop, D. R., Kirkby, J., Seinfeld, J. H., El-Haddad, I., Flagan, R. C., and Donahue, N. M. (2020b), Rapid growth of new atmospheric particles by nitric acid and ammonia condensation, *Nature*, 581(7807), 184-189, doi:10.1038/s41586-020-2270-4.
- Wang, M., Xiao, M., Bertozzi, B., Marie, G., Rorup, B., Schulze, B., Bardakov, R., He, X. C., Shen, J., Scholz, W., Marten, R., Dada, L., Baalbaki, R., Lopez, B., Lamkaddam, H., Manninen, H. E., Amorim, A., Ataei, F., Bogert, P., Brasseur, Z., Caudillo, L., De Menezes, L. P., Duplissy, J., Ekman, A. M. L., Finkenzeller, H., Carracedo, L. G., Granzin, M., Guida, R., Heinritzi, M., Hofbauer, V., Hohler, K., Korhonen, K., Krechmer, J. E., Kurten, A., Lehtipalo, K., Mahfouz, N. G. A., Makhmutov, V., Massabo, D., Mathot, S., Mauldin, R. L., Mentler, B., Muller, T., Onnela, A., Petaja, T., Philippov, M., Piedehierro, A. A., Pozzer, A., Ranjithkumar, A., Schervish, M., Schobesberger, S., Simon, M., Stozhkov, Y., Tome, A., Umo, N. S., Vogel, F., Wagner, R., Wang, D. S., Weber, S. K., Welti, A., Wu, Y., Zauner-Wieczorek, M., Sipila, M., Winkler, P. M., Hansel, A., Baltensperger, U., Kulmala, M., Flagan, R. C., Curtius, J., Riipinen, I., Gordon, H., Lelieveld, J., El-Haddad, I., Volkamer, R., Worsnop, D. R., Christoudias, T., Kirkby, J., Mohler, O., and Donahue, N. M. (2022), Synergistic $\text{HNO}_3\text{-H}_2\text{SO}_4\text{-NH}_3$ upper tropospheric particle formation, *Nature*, 605(7910), 483-489, doi:10.1038/s41586-022-04605-4.
- Wolfe, G. M., Marvin, M. R., Roberts, S. J., Travis, K. R., and Liao, J. (2016), The Framework for 0-D Atmospheric Modeling (F0AM) v3.1, *Geosci. Model Dev.*, 9(9), 3309-3319, doi:10.5194/gmd-9-3309-2016.
- Yan, C., Nie, W., Äijälä, M., Rissanen, M. P., Canagaratna, M. R., Massoli, P., Junninen, H., Jokinen, T., Sarnela, N., Häme, S. A. K., Schobesberger, S., Canonaco, F., Yao, L., Prévôt, A. S. H., Petäjä, T., Kulmala, M., Sipilä, M., Worsnop, D. R., and Ehn, M. (2016), Source characterization of highly oxidized multifunctional compounds in a boreal forest environment using positive matrix factorization, *Atmospheric Chemistry and Physics*, 16(19), 12715-12731, doi:10.5194/acp-16-12715-2016.
- Yan, C., Nie, W., Vogel, A. L., Dada, L., Lehtipalo, K., Stolzenburg, D., Wagner, R., Rissanen, M. P., Xiao, M., Ahonen, L., Fischer, L., Rose, C., Bianchi, F., Gordon, H., Simon, M., Heinritzi, M., Garmash, O., Roldin, P., Dias, A., Ye, P., Hofbauer, V., Amorim, A., Bauer, P. S., Bergen, A., Bernhammer, A.-K., Breitenlechner, M., Brilke, S., Buchholz, A., Mazon, S. B., Canagaratna, M. R., Chen, X., Ding, A., Dommen, J., Draper, D. C., Duplissy, J., Frege, C., Heyn, C., Guida, R., Hakala, J., Heikkinen, L., Hoyle, C. R., Jokinen, T., Kangasluoma, J., Kirkby, J., Kontkanen, J., Kürten, A., Lawler, M. J., Mai, H., Mathot, S., Mauldin, R. L., Molteni, U., Nichman, L., Nieminen, T., Nowak, J., Ojdanic, A., Onnela, A., Pajunoja, A., Petäjä, T., Piel, F., Quéléver, L. L. J., Sarnela, N., Schallhart, S., Sengupta, K., Sipilä, M., Tomé, A., Tröstl, J., Väisänen, O., Wagner, A. C., Ylisirniö, A., Zha, Q., Baltensperger, U., Carslaw, K. S., Curtius, J., Flagan, R. C., Hansel, A., Riipinen, I., Smith, J. N., Virtanen, A., Winkler, P. M., Donahue, N. M., Kerminen, V.-M., Kulmala, M., Ehn, M., and Worsnop, D. R. (2020), Size-dependent influence of NO_x on the growth rates of organic aerosol particles, *Science Advances*, 6(22), eaay4945, doi:doi:10.1126/sciadv.aay4945.

Zhao, Y., Thornton, J. A., and Pye, H. O. T. (2018), Quantitative constraints on autoxidation and dimer formation from direct probing of monoterpene-derived peroxy radical chemistry, *Proceedings of the National Academy of Sciences of the United States of America*, 115(48), 12142-12147, doi:10.1073/pnas.1812147115.

V.6. Supplementary information

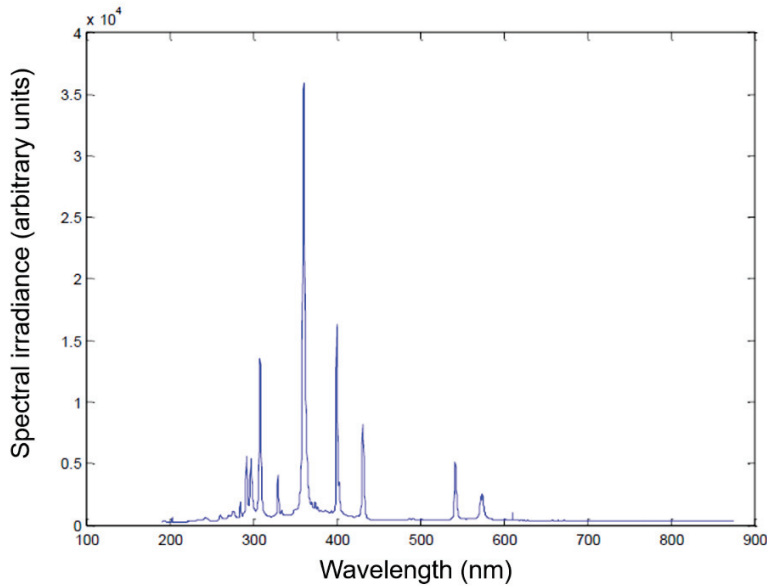


Figure V-S1: Spectrum of mercury-doped xenon arc lamps (UVH) in the CLOUD chamber. Four 200 W Hamamatsu Hg-Xe lamps (UVH) provide light across the entire UV-Vis spectral range and illuminate the chamber homogeneously.

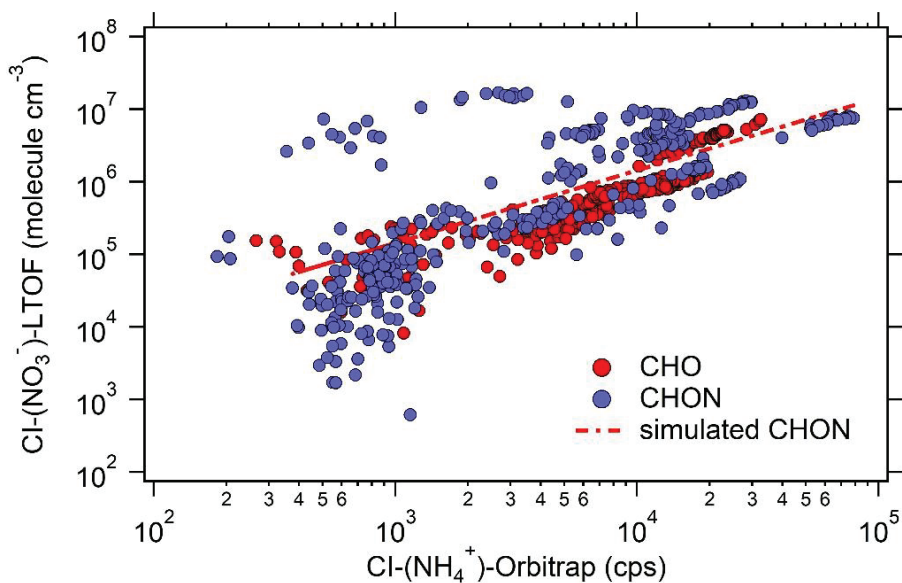


Figure V-S2: Sensitivity of CI- (NH_4^+) -Orbitrap for the detection of CHO and CHON in the CLOUD chamber. Time evolution intercomparison of CHO (red marker) and CHON (blue marker) measured by CI- (NH_4^+) -Orbitrap and CI- (NO_3^-) -LTOF. Time evolution of CHO species with correlation coefficients $R^2 > 0.9$ between NH_4^+ -Orbitrap (cps in unit) and NO_3^- -LTOF (molecule cm^{-3} in unit) are used to obtain the calibration factor applied to estimate the concentration of CHON measured by NH_4^+ -Orbitrap (red dashed line). The outliers for CHON measured by CI- (NO_3^-) -LTOF is the time evolution of one compound ($\text{C}_{10}\text{H}_{15}\text{NO}_{10}$).

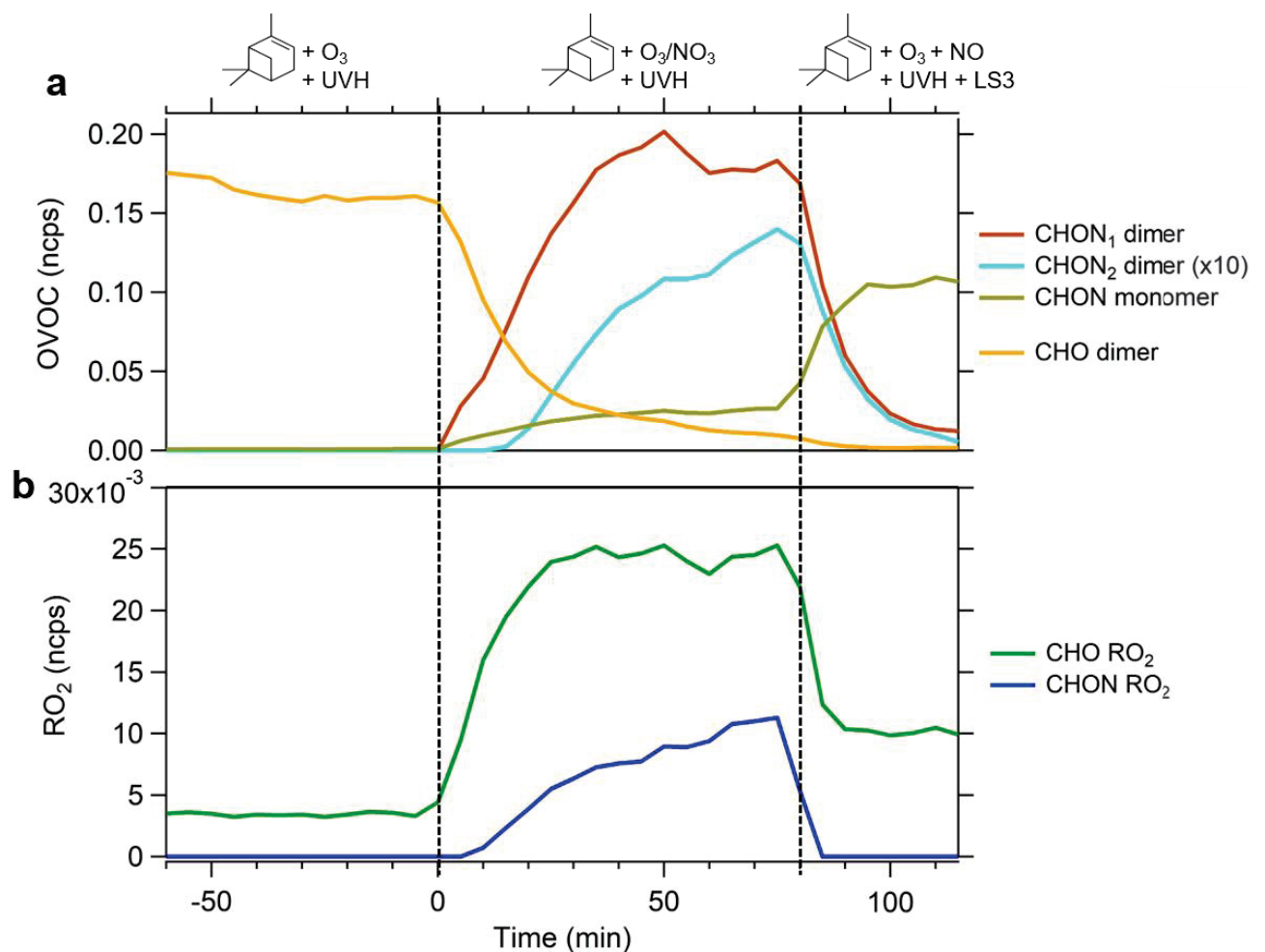


Figure V-S3. Effect of NO_3 radicals and NO on OVOC in CLOUD. Evolution of 1 N-containing dimers (CHON₁ dimer), 2 N-containing dimers (CHON₂ dimer), N-containing monomers (CHON monomer) and non-N containing dimer (CHO dimer) (**a**) and N-containing RO₂ radicals (CHON RO₂) and non-N containing RO₂ radicals (CHO RO₂) (**b**).

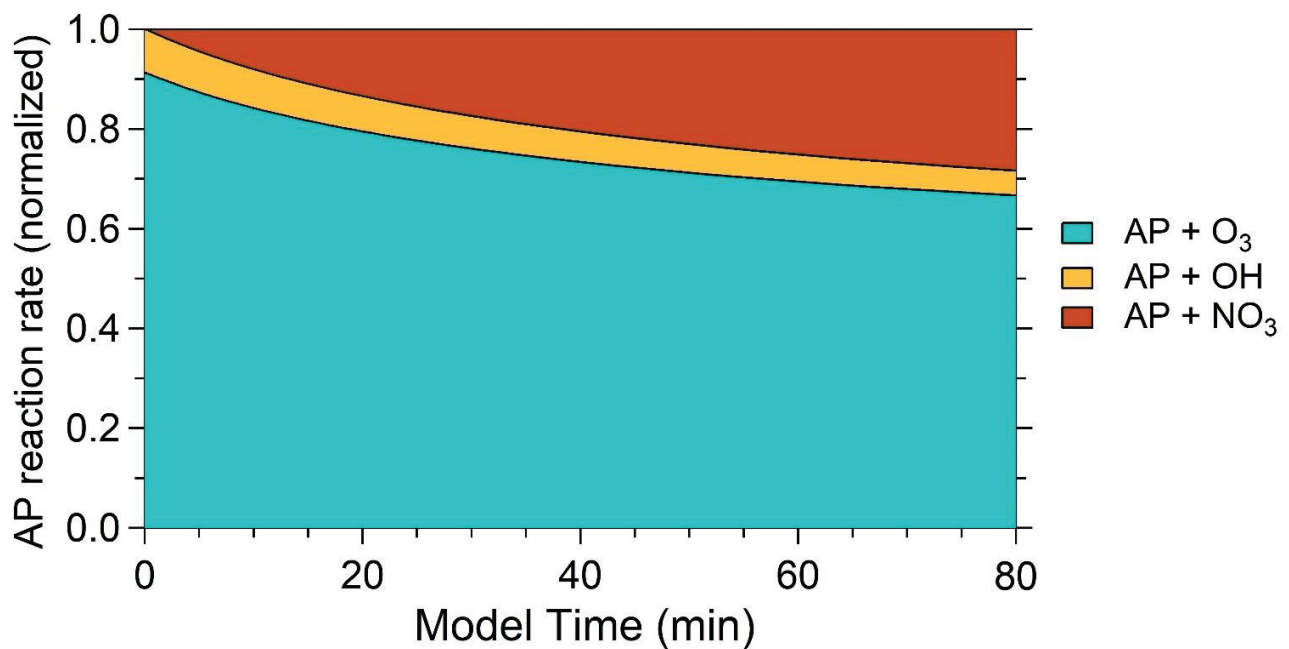


Figure V-S4: Evolution of normalized α -pinene reaction rate during the NO_3 perturbed ozonolysis stage in the CLOUD chamber. The contributions of different oxidants to the reacted α -pinene were simulated using F0AM model when NO_3 was present in the chamber during 0-80 mins.

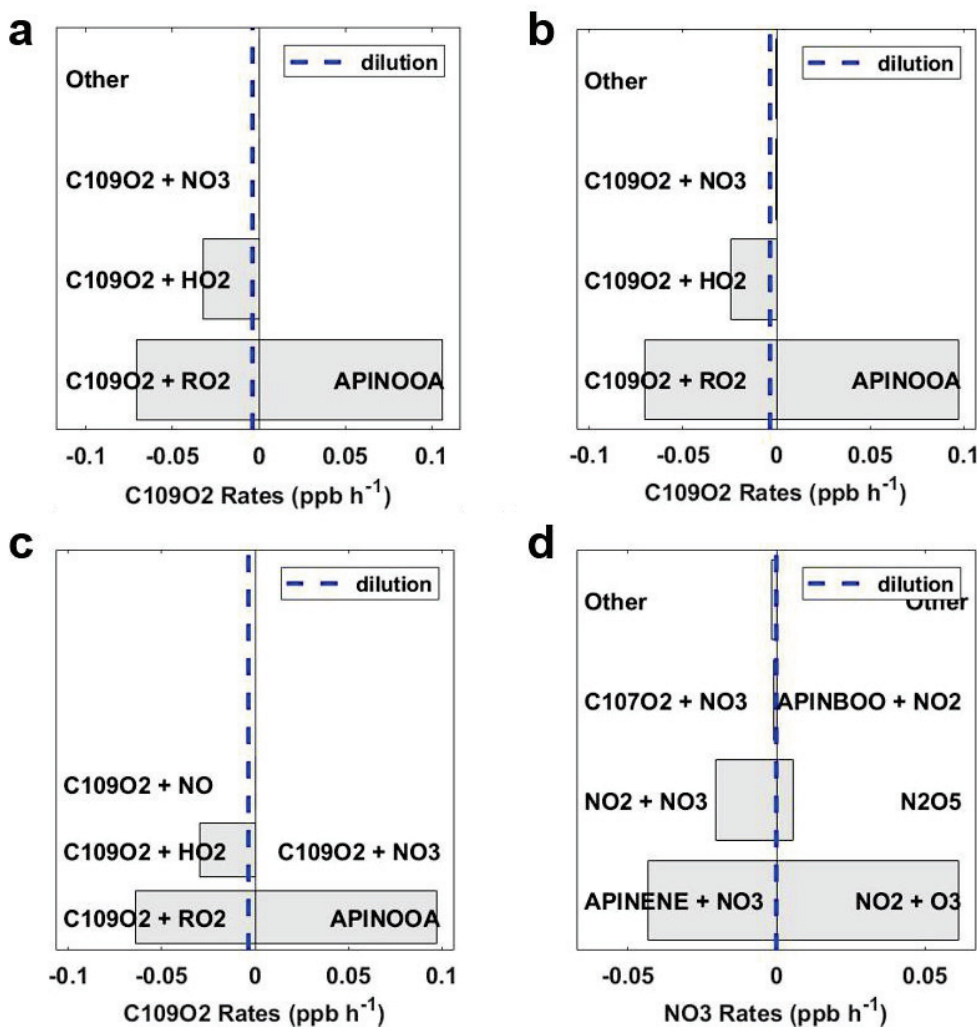


Figure V-S5. Fate of $\text{C}_{10}\text{H}_{15}\text{O}_4$ and NO_3 radicals simulated in CLOUD chamber. Production and loss rates of $\text{C}_{10}\text{H}_{15}\text{O}_4$ ($\text{C}109\text{O}_2$) radical during pure ozonolysis (a), during ozonolysis perturbed by NO_3 (b), and during ozonolysis perturbed by NO_x (c). Production and loss rates of formed NO_3 radical during NO_2 injected into the chamber at $t = 0\text{--}80$ min (d). APINOOA, $\text{C}107\text{O}_2$ and APINBOO in the figure refer to Criegee Intermediate, $\text{C}_{10}\text{H}_{15}\text{O}_4$ and $\text{C}_{10}\text{H}_{17}\text{O}_3$, respectively.

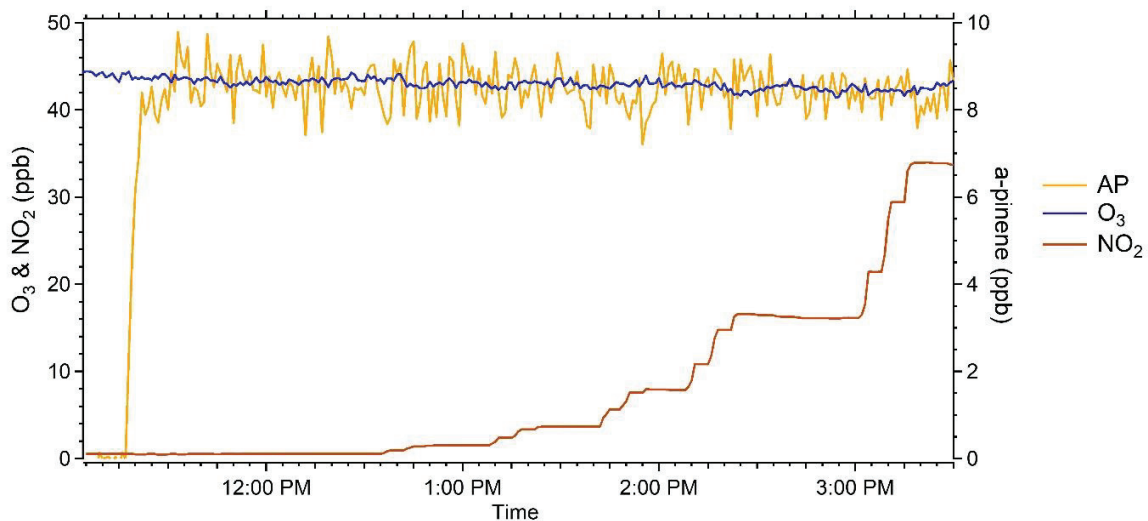


Figure V-S6: Precursors for oxidation flow reactor (OFR) experiments. A run of the evolution of trace gas α -pinene, O_3 , and NO_2 in the OFR outflow. Constant α -pinene and O_3 were injected to the OFR. The concentration of NO_2 in the OFR varied from 0–75 ppbv. Experiments were conducted at 296 K and RH < 1%.

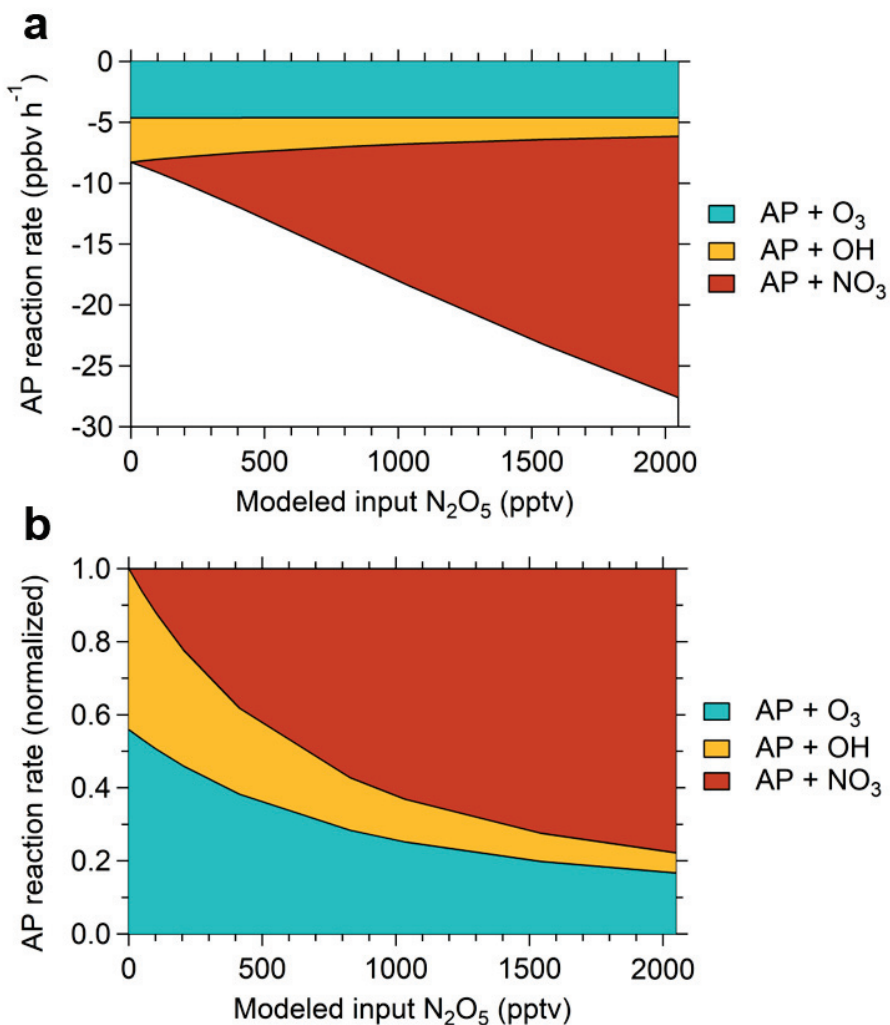


Figure V-S7: Simulated reactivity of α -pinene at different NO_3 levels in OFR experiments. Absolute reaction rate of α -pinene (a) and normalized reaction rate of α -pinene (b) as a function of modeled input N_2O_5 concentration. The contributions of different oxidants to the reacted α -pinene at nine NO_3 concentrations were simulated using F0AM model.

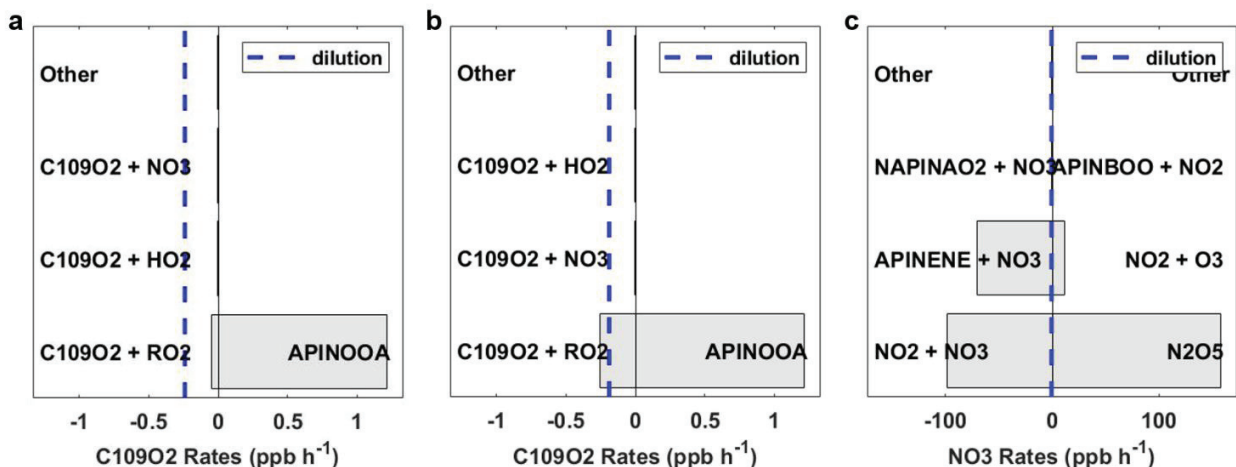


Figure V-S8. Fate of NO_3 and $\text{C}_{10}\text{H}_{15}\text{O}_4$ radicals simulated in OFR experiments. Production and loss rates of $\text{C}_{10}\text{H}_{15}\text{O}_4$ (C_{109}O_2) radicals in O_3/OH chemistry (a), and at highest $\text{NO}_2:\text{O}_3$ (b). Production and loss rates of NO_3 at highest $\text{NO}_2:\text{O}_3$ (c). The concentration of α -pinene + O_3 were used as input in (a), α -pinene + O_3 + NO_2 in (b) and O_3 + NO_2 in (c). The input concentration of α -pinene, O_3 , and NO_2 were 10 ppbv, 50 ppbv, and 75 ppbv, respectively. APINOOA, NAPINAO₂ and APINBOO in the figure refer to Criegee Intermediate, $\text{C}_{10}\text{H}_{16}\text{NO}_5$ and $\text{C}_{10}\text{H}_{17}\text{O}_3$, respectively.

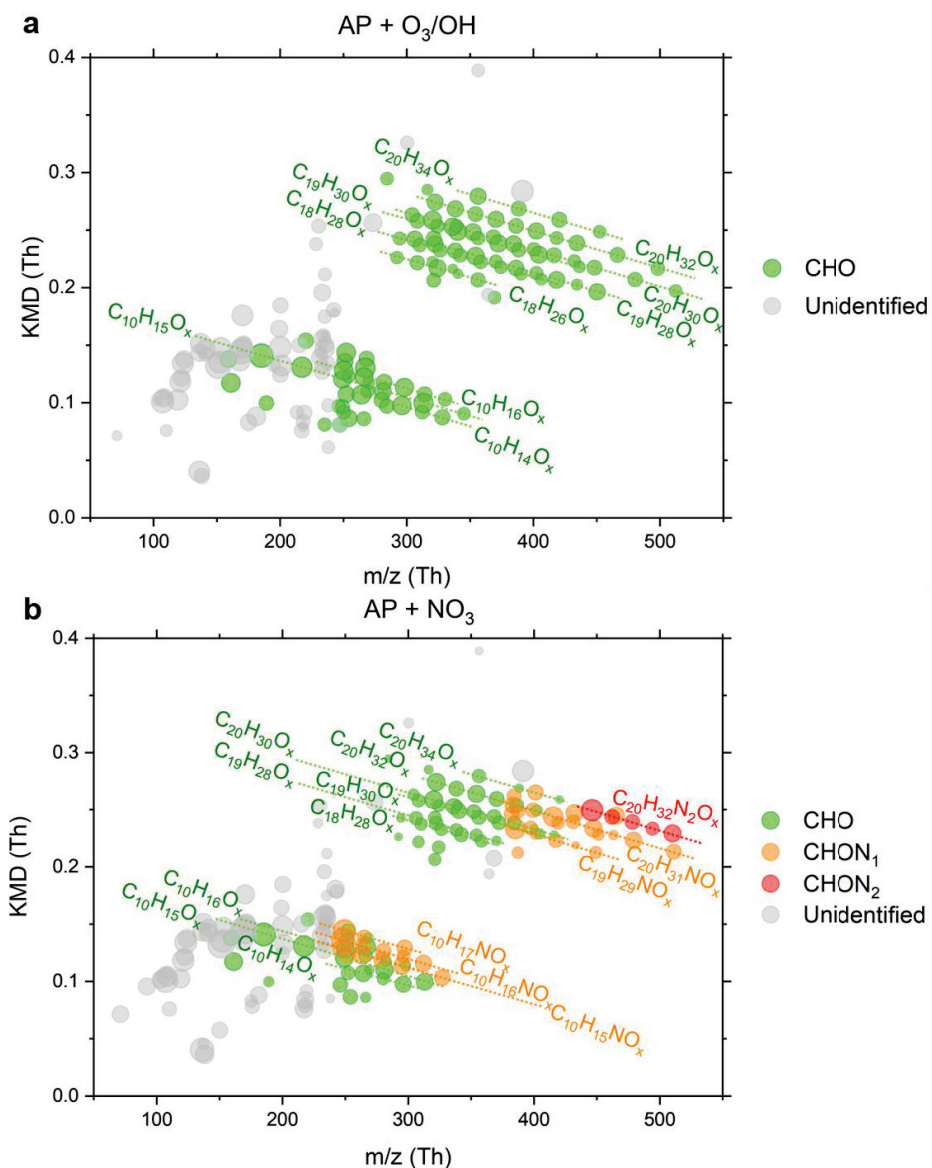


Figure V-S9: Kendrick mass defect plots of gaseous compounds observed in the reactions of α -pinene with O₃/OH (**a**) and NO₃ radical at highest NO₂:O₃ (**b**). The circles are the measured ions colored by groups: CHO, CHON₁, CHON₂, and unidentified compounds, the sizes of which correspond to their logarithmic intensities. The unidentified compounds represent products with apparent evolution but unassigned molecular formulae.

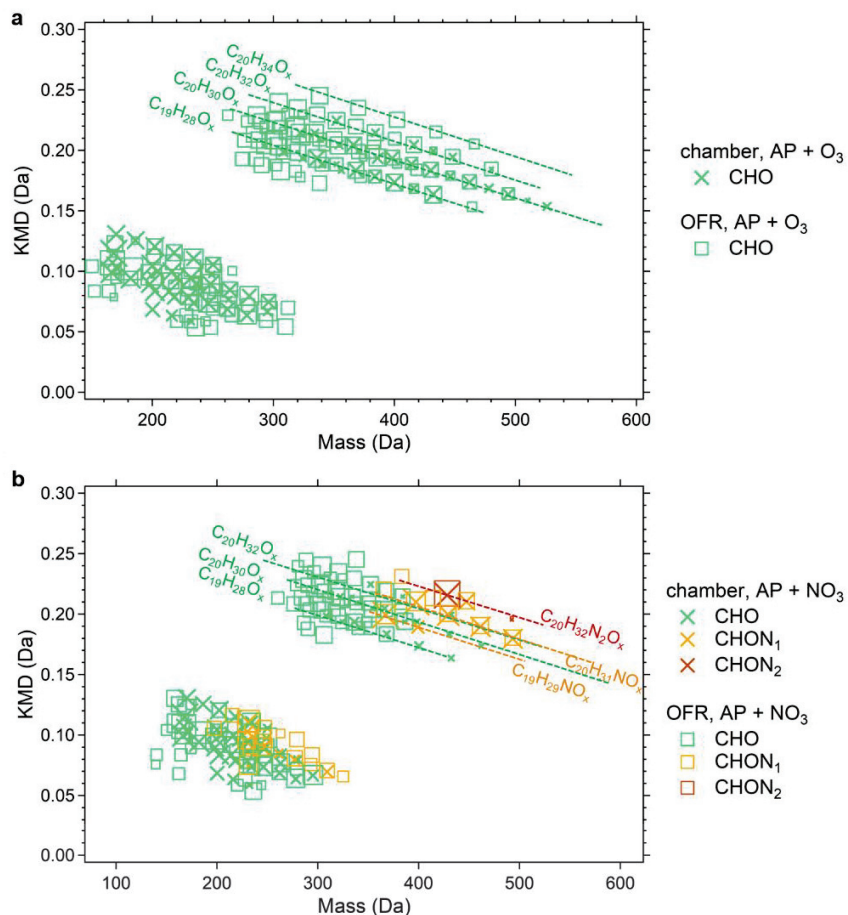


Figure V-S10. Kendrick mass defect plots of OVOCs observed in the CLOUD chamber and OFR experiments. Mass defect plots for C₉₋₁₀ monomers and C₁₉₋₂₀ dimers from pure ozonolysis in the chamber versus from O₃/OH chemistry in OFR experiments (**a**). Mass defect plots for C₉₋₁₀ monomers and C₁₉₋₂₀ dimers from ozonolysis perturbed by NO₃ in the chamber versus from OFR at lowest NO₂:O₃ (**b**). Data at which about 30% of α -pinene was oxidized by NO₃ radicals were used for comparison between CLOUD and OFR experiments. The circles are the measured molecules colored by groups: CHO, CHON₁, and CHON₂, the sizes of which correspond to their logarithmic intensities. Cross and square markers correspond to chamber and OFR data measured by CI-(NH₄⁺)-Orbitrap, respectively. The abscissa represents the measured mass of the compounds which has subtracted the reagent ions.

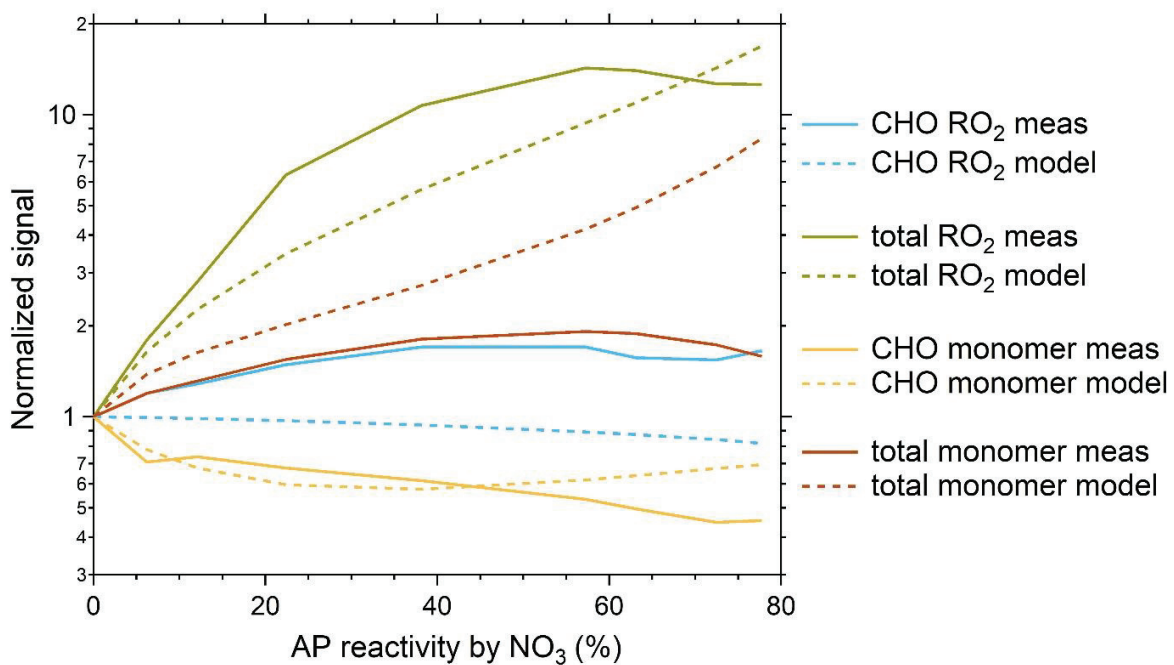


Figure V-S11: Low oxygenated OVOCs measured by CI-(NH₄⁺)-Orbitrap and simulated in OFR experiments. Normalized signals of low oxygenated CHO RO₂ (i.e., C₁₀H₁₅O₄ from O₃), total RO₂ (CHO RO₂ and C₁₀H₁₆NO₅ from NO₃), CHO monomers (C₁₀H₁₄O₃, C₁₀H₁₆O₂₋₄, and C₁₀H₁₈O₃), and total monomer (CHO monomers, C₁₀H₁₅NO₄, and C₁₀H₁₇NO_{4,5}) as a function of α-pinene reactivity by NO₃ radicals. Results measured by CI-(NH₄⁺)-Orbitrap are given in solid lines and those simulated by F0AM in dashed lines.

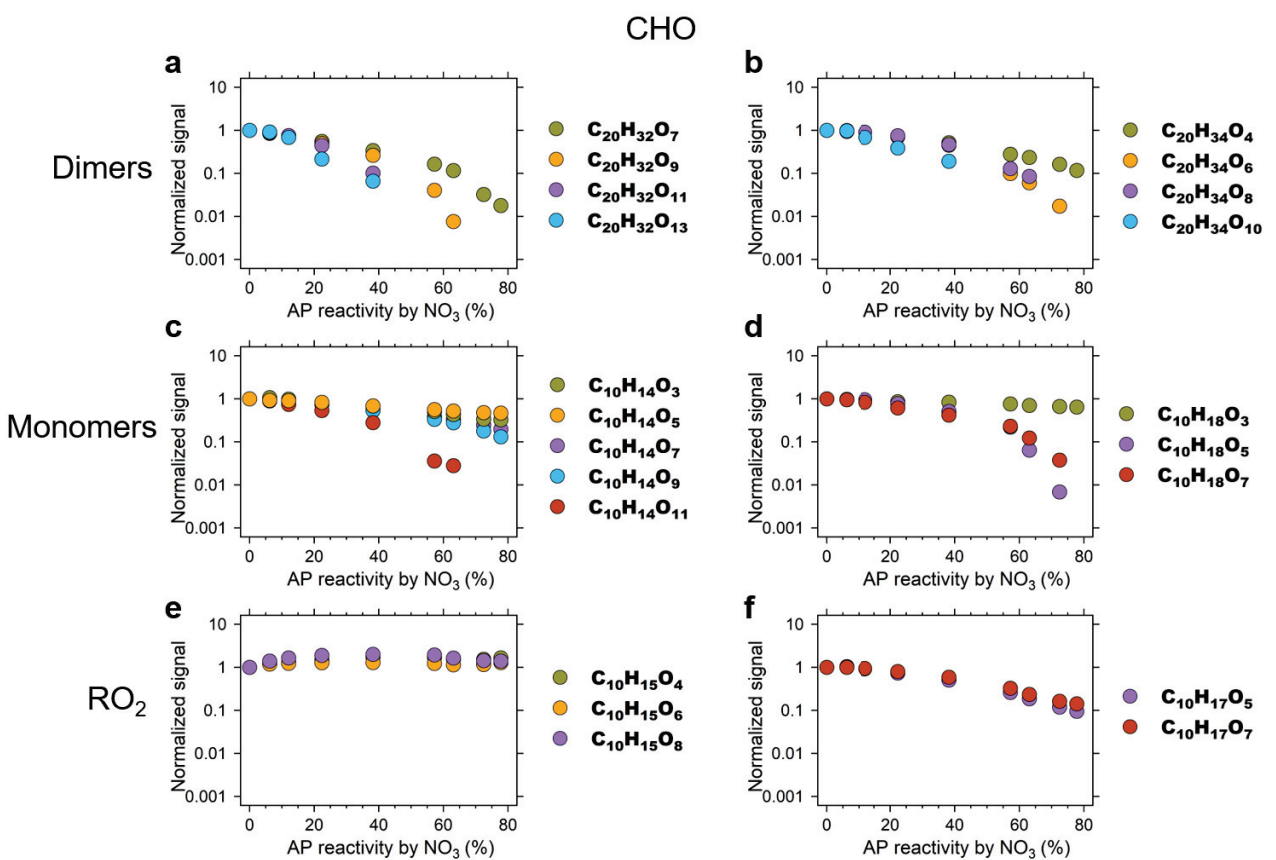


Figure V-S12: CHO in OFR experiments measured by CI- (NH_4^+) -Orbitrap. Normalized signals of dimers $\text{C}_{20}\text{H}_{32}\text{O}_x$ (a) and $\text{C}_{20}\text{H}_{34}\text{O}_x$ (b), monomers $\text{C}_{10}\text{H}_{14}\text{O}_x$ (c) and $\text{C}_{10}\text{H}_{18}\text{O}_x$ (d), peroxy radicals $\text{C}_{10}\text{H}_{15}\text{O}_x$ (e) and $\text{C}_{10}\text{H}_{17}\text{O}_x$ (f) derived from O_3/OH chemistry as a function of α -pinene reactivity by NO_3 radicals.

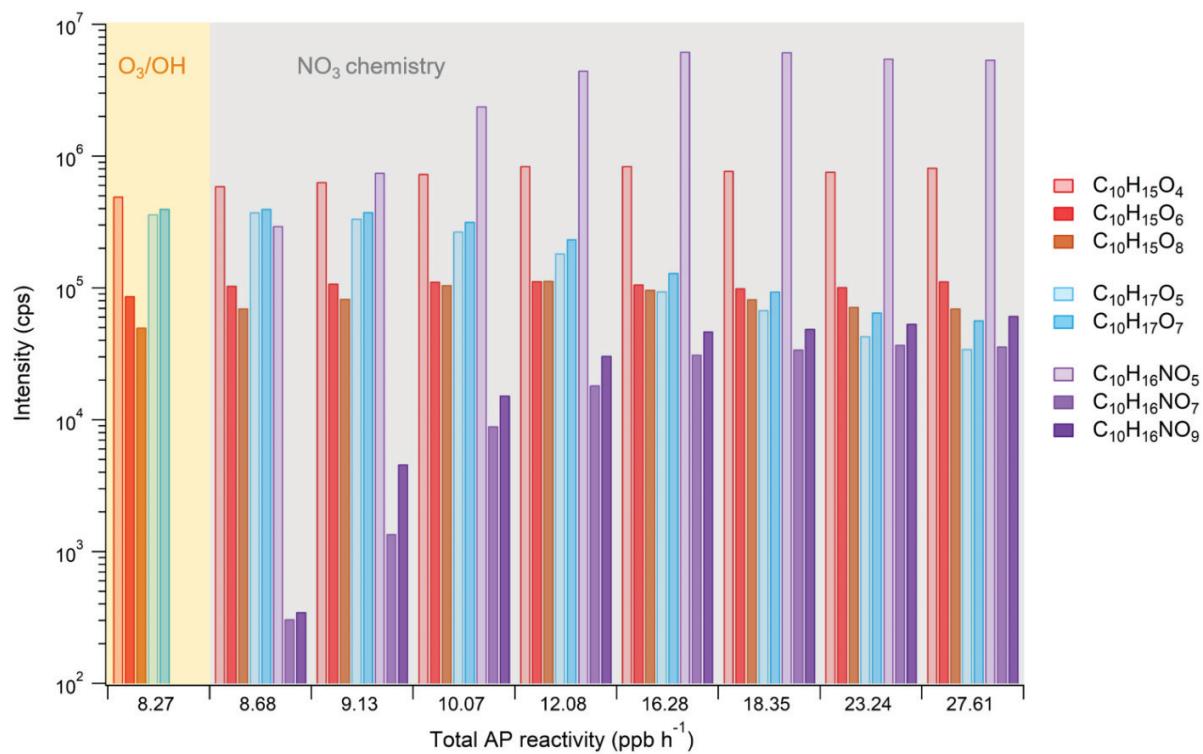


Figure V-S13: Distribution of peroxy radicals measured by CI-(NH₄⁺)-Orbitrap in OFR experiments. Intensity of peroxy radicals C₁₀H₁₅O_x from O₃, C₁₀H₁₇O_x from OH and C₁₀H₁₆NO_x from NO₃ reaction distributed by total α -pinene reactivity. Results from O₃/OH chemistry are shaded in yellow and those from NO₃ chemistry in gray.

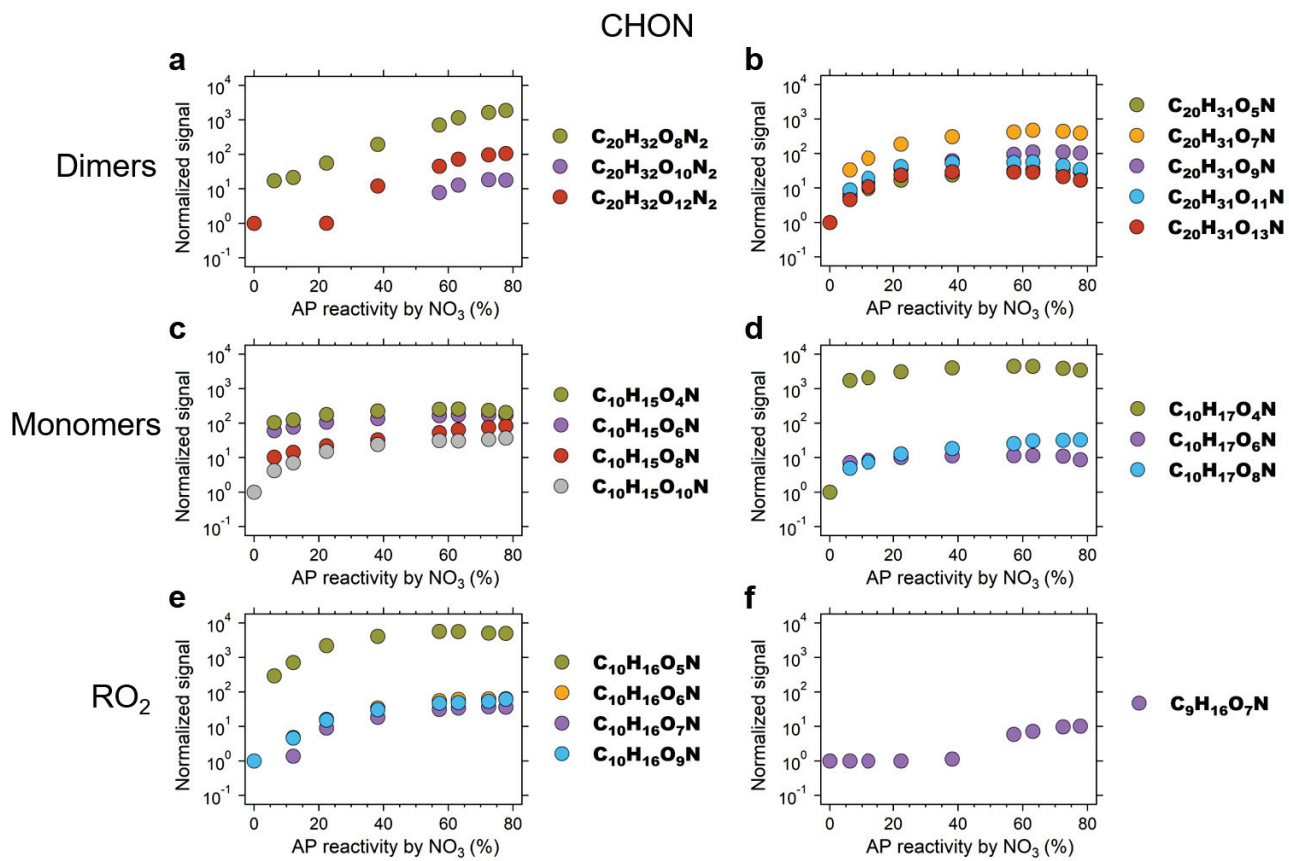


Figure V-S14: CHON in OFR experiments measured by CI- (NH_4^+) -Orbitrap. Normalized signals of dinitroxy dimers $\text{C}_{20}\text{H}_{32}\text{O}_x\text{N}_2$ (a) and nitroxy dimers $\text{C}_{20}\text{H}_{31}\text{O}_x\text{N}$ (b), organic nitrates $\text{C}_{10}\text{H}_{15}\text{O}_x\text{N}$ (c) and $\text{C}_{10}\text{H}_{17}\text{O}_x\text{N}$ (d), peroxy radicals $\text{C}_{10}\text{H}_{16}\text{O}_x\text{N}$ (e) and $\text{C}_9\text{H}_{16}\text{O}_x\text{N}$ (f) derived from NO_3 chemistry as a function of α -pinene reactivity by NO_3 radicals.

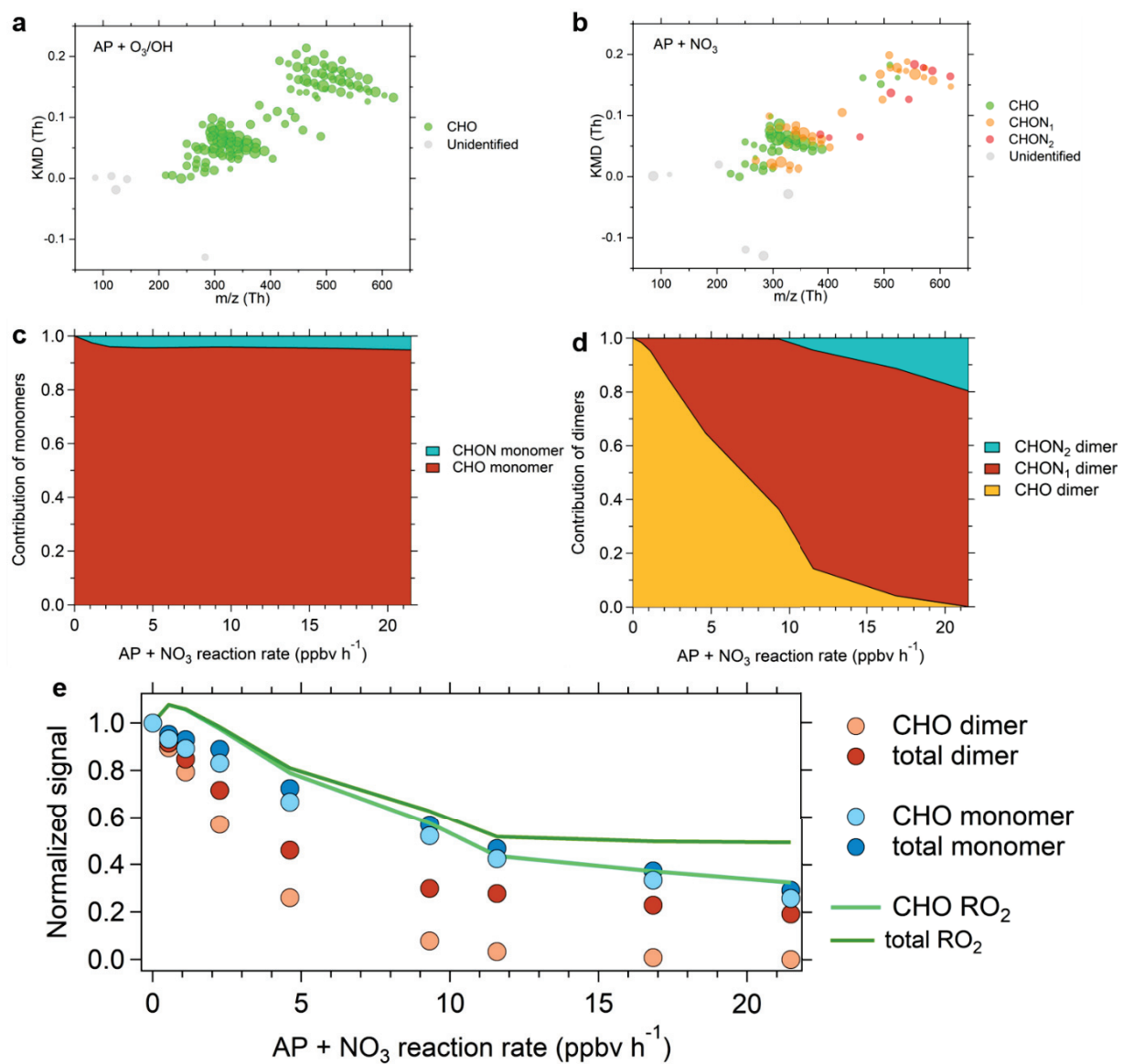


Figure V-S15: Sensitivity of NO₃ radicals to the formation of OVOCs in OFR experiments measured by CI-(NO₃⁻)-Orbitrap. (a and b) Kendrick mass defect plots of gaseous compounds observed in the reaction of α -pinene with O₃/OH (a) and NO₃ radical (b). The circles are the measured ions colored by groups: CHO, CHON₁, CHON₂, and unidentified compounds, the sizes of which correspond to their logarithmic intensities. The unidentified compounds represent products with apparent evolution but unassigned molecular formulae. (c and d) Contribution of CHO monomers and CHON monomers to total monomers (c), CHO dimers, CHON₁ dimers, and CHON₂ dimers to total dimers (d) plotted against α -pinene oxidation rate by NO₃ radicals. (e)

Normalized signals of CHO monomers, CHO dimers, and CHO RO₂ as a function of α -pinene oxidation rate by NO₃ radicals. Ion signals are normalized to the signal in pure O₃ chemistry for comparison.

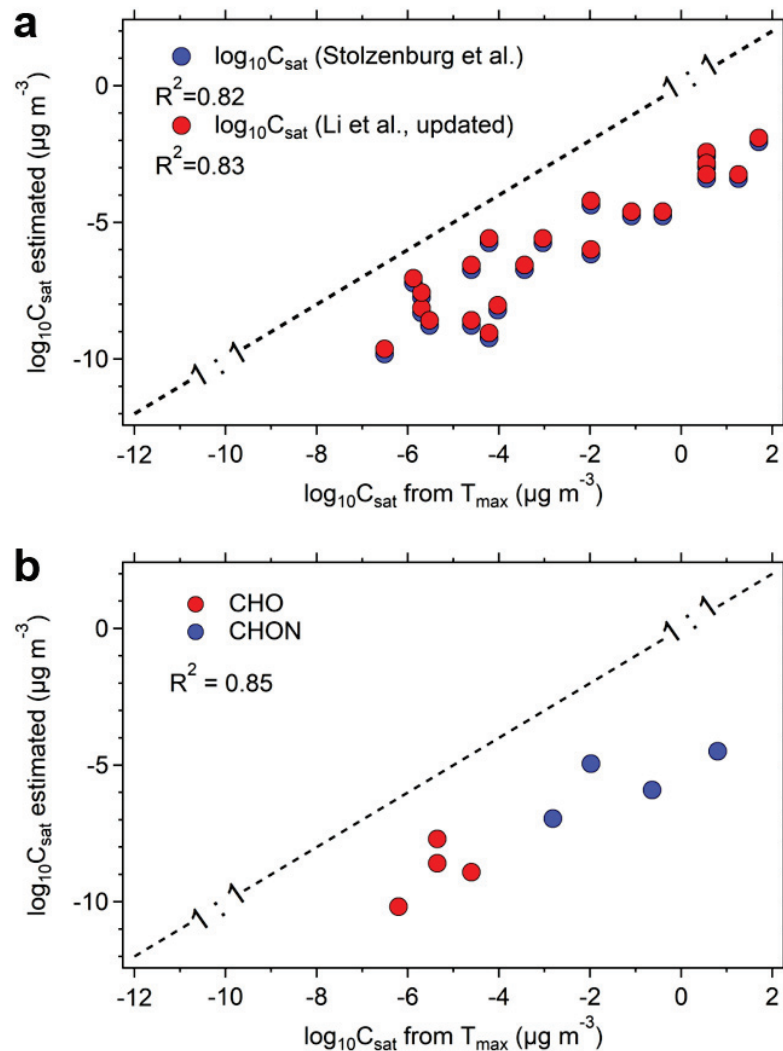


Figure V-S16: Volatility of CHO in the particle phase measured by FIGAERO-CIMS vs. estimated by the VBS parameterizations in the CLOUD chamber. (a) Saturation vapor concentrations ($\log_{10}C_{\text{sat}}$) of CHO species formed from α -pinene ozonolysis in the particle phase are predicted by two parameterizations of Stolzenburg et al. (2018) (colored in blue) and Li et al. (updated by Isaacman-VanWertz and Aumont, 2021) (colored in red). The measured $\log_{10}C_{\text{sat}}$ are calculated using the thermal-desorption volatility calibration curve obtained by calibrants

correlating their $\log_{10}C_{\text{sat}}$ with $1/T_{\text{max}}$ using FIGAERO-CIMS (Wang et al., 2020). The gas phase parameterizations are applied assuming compounds with same molecular formulae to have the same structure as in the particle phase. (b) Saturation vapor concentrations of selected CHO dimers and CHON dimers in the particle phase measured versus predicted by modified Li et al. approach. A good correlation R^2 of 0.85 validates the consistency between direct FIGAERO volatility measurements and VBS parameterizations.

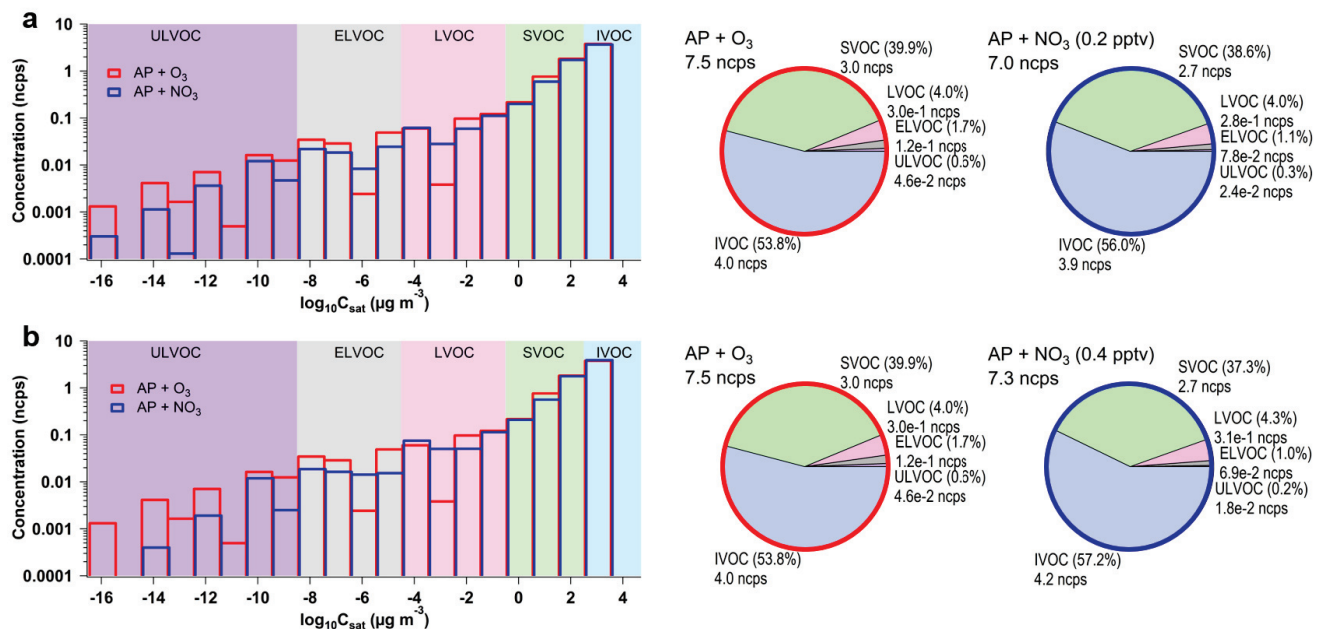


Figure V-S17: Volatility distribution of OVOCs measured by CI-(NH₄⁺)-Orbitrap in the CLOUD chamber. Monomers C₉₋₁₀ and dimers C₁₈₋₂₀ binned to a volatility distribution showing the measured relative abundance in pure O₃ and NO₃ chemistry, respectively; simulated NO₃ concentration was ~0.2 pptv (a) and ~0.4 pptv (b). The background colors represent the saturation concentration (C_{sat}) in the range of ultra-low volatility (ULVOCs, purple), extremely low volatility (ELVOCs, gray), low volatility (LVOCs, pink), semi-volatile (SVOCs, green) and intermediate volatility (IVOCs, blue) organic compounds.

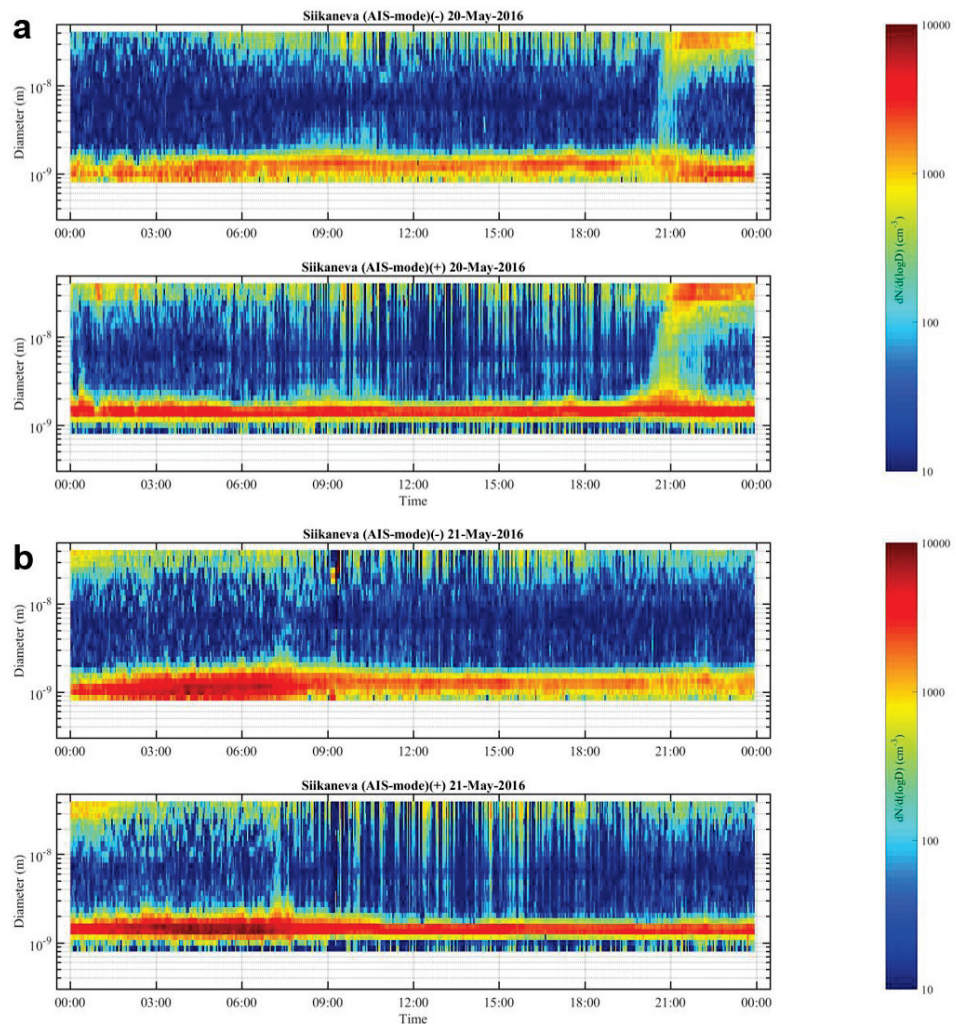


Figure V-S18: Nocturnal NPF event and nonevent measured by AIS during Siikaneva campaign.

Example of a nucleation event (a) and non-nucleation event (b) at night showing the size evolution of positive and negative ions. The color scale shows the number concentration of ions.

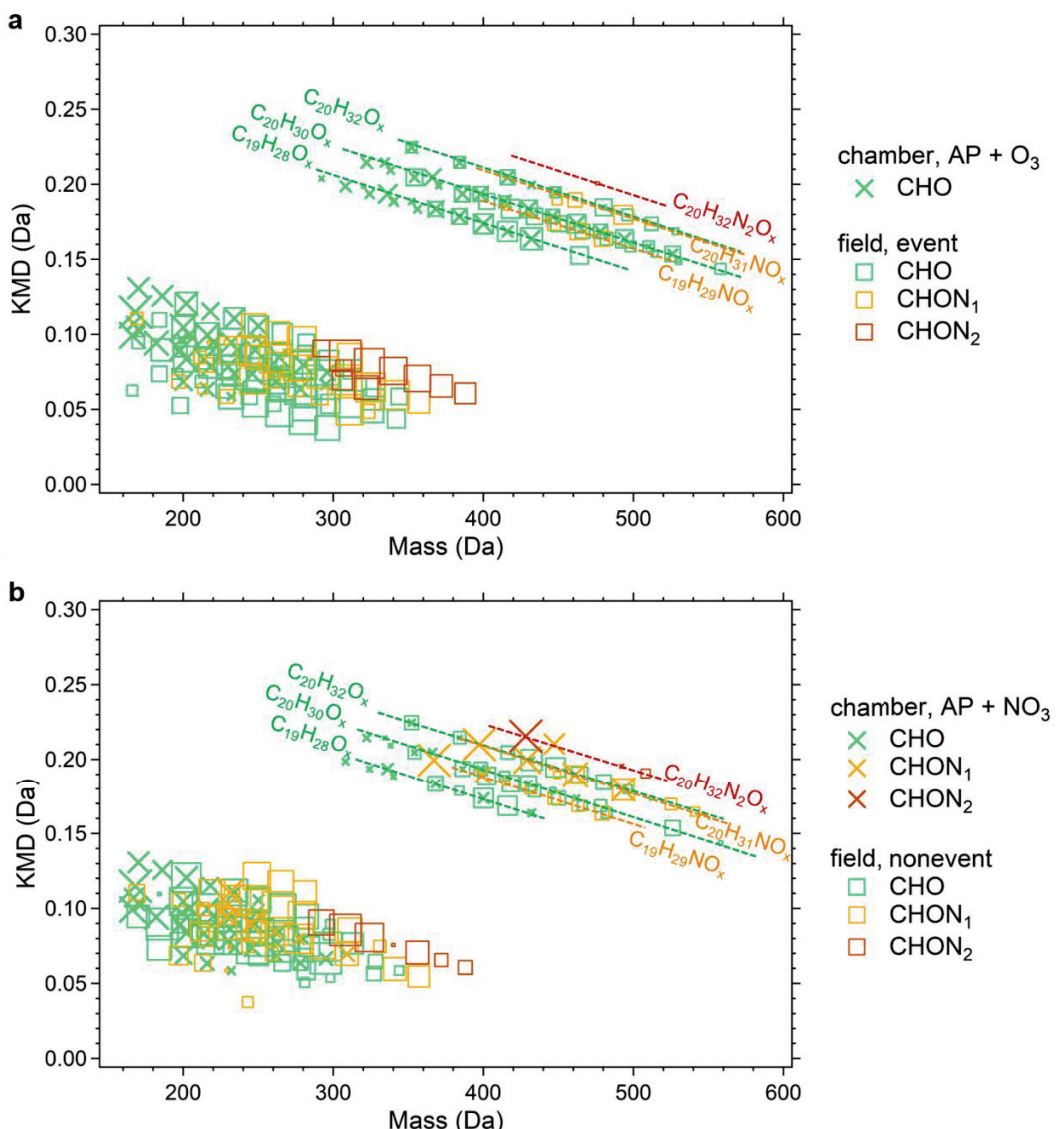


Figure V-S19: Kendrick mass defect plots of oxygenated compounds observed in the CLOUD chamber and wetland. Mass defect plots for C₉₋₁₀ monomers and C₁₉₋₂₀ dimers in O₃ stage of chamber versus a nocturnal NPF event (a) and in NO₃ stage of chamber versus a nonevent (b). The circles are the measured molecules colored by groups: CHO, CHON₁, and CHON₂, the sizes of which correspond to their logarithmic intensities. Cross and square markers correspond to chamber and campaign data measured by CI-(NH₄⁺)-Orbitrap and CI-(NO₃⁻)-APi-TOF, respectively. The abscissa represents the measured mass of the compounds which has subtracted the reagent ions.

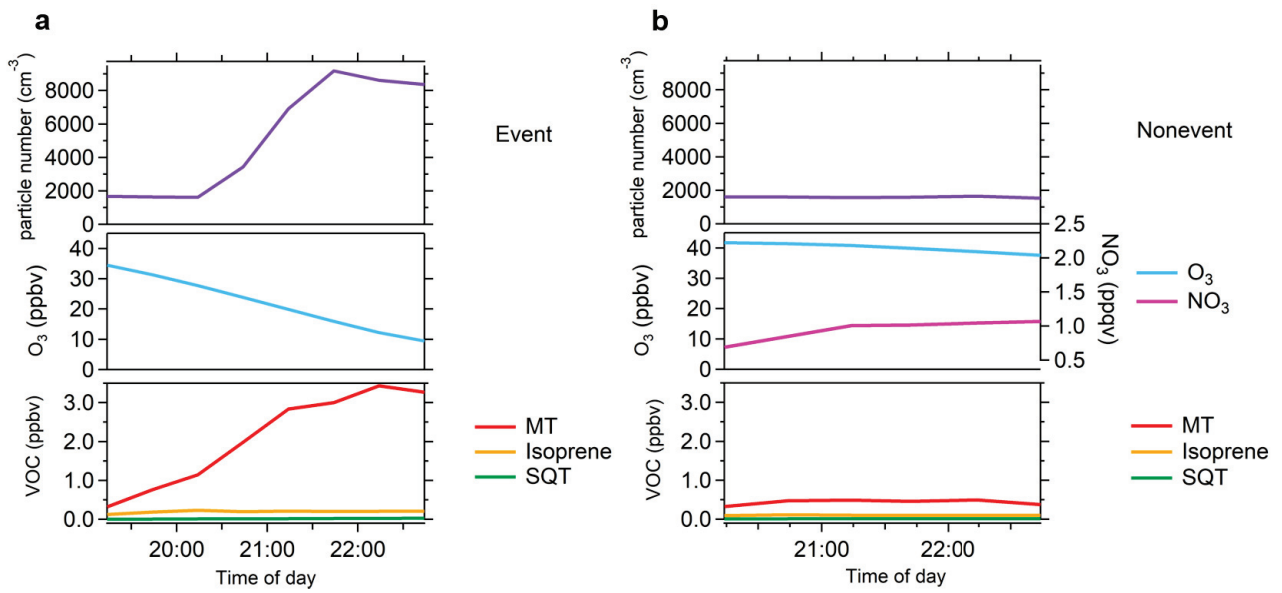
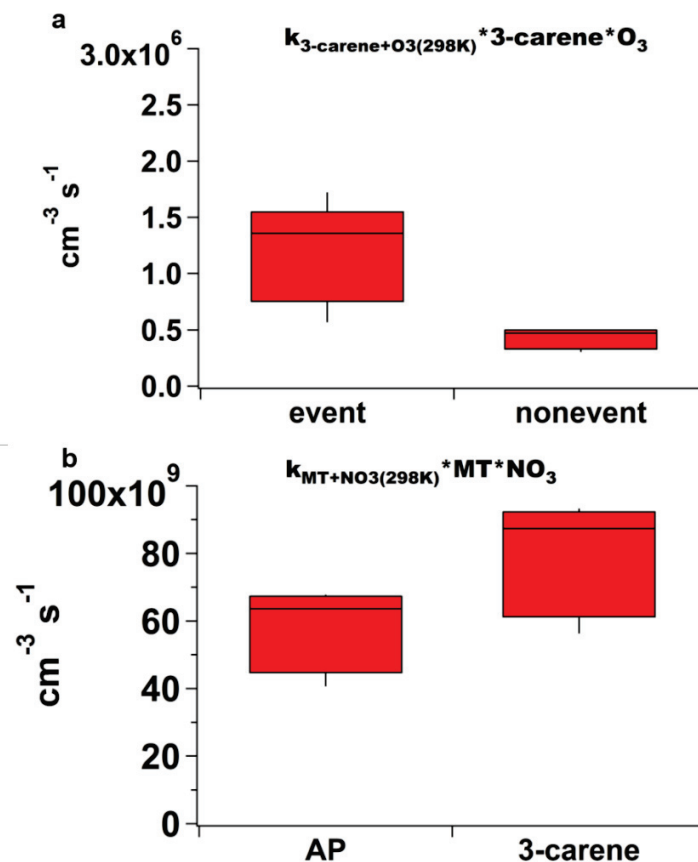


Figure V-S20: Time evolution of particle number, VOC, O_3 and estimated NO_3 in a nocturnal NPF event and nonevent during Siikaneva campaign. (a) Concentration evolution of particle number, monoterpene (MT), isoprene, sesquiterpenes (SQT), and O_3 in the NPF event. (b) Concentration evolution of particle number, monoterpene (MT), isoprene, sesquiterpenes (SQT), O_3 and estimated NO_3 in the non-nucleation event. Unfortunately, NO_x measurement was not available in Siikaneva, in particular for event night with decoupling process. Concentration of NO_3 in nonevent (no decoupling process occurred) was estimated from the NO_x concentration measured at Hyytiälä in a boreal forest, ~5 km east of Siikaneva.



Supplementary Figure 21. Monoterpene reaction rate in a nocturnal NPF event and nonevent during Siikaneva campaign. **(a)** Ozonolysis rate of $\Delta^3\text{-carene}$ in the NPF event and nonevent. **(b)** Reactivity of $\alpha\text{-pinene}$ and $\Delta^3\text{-carene}$ by NO_3 radical in the nonevent. Concentration of monoterpenes were measured, but the composition could not be classified due to the instrumental limitation during the campaign. $\alpha\text{-Pinene}$ is the most abundant monoterpene in May at Hyytiälä, followed by $\Delta^3\text{-carene}$ ⁴. Hence, reactivities of $\alpha\text{-pinene}$ and $\Delta^3\text{-carene}$ are calculated and represent the reactivity range by assuming the total monoterpene concentration is that of one monoterpene. The reaction rate of these monoterpenes with estimated NO_3 radical in the nonevent are also assessed at 298 K, given that the most reaction rate constants are only available at room temperature from International Union of Pure and Applied Chemistry (IUPAC, <https://iupac.aeris-data.fr/en/home/>). Considering the $\Delta^3\text{-carene}$ concentration being a factor of ~2 lower than that of $\alpha\text{-pinene}$ ⁴, the dominating monoterpene reactivity by O_3 and by NO_3 radical in Siikaneva are both from $\alpha\text{-pinene}$.

Supplemental references:

- Stolzenburg, D., Fischer, L., Vogel, A. L., Heinritzi, M., Schervish, M., Simon, M., Wagner, A. C., Dada, L., Ahonen, L. R., Amorim, A., Baccarini, A., Bauer, P. S., Baumgartner, B., Bergen, A., Bianchi, F., Breitenlechner, M., Brilke, S., Mazon, S. B., Chen, D., Dias, A., Draper, D. C., Duplissy, J., Haddad, I. E., Finkenzeller, H., Frege, C., Fuchs, C., Garmash, O., Gordon, H., He, X., Helm, J., Hofbauer, V., Hoyle, C. R., Kim, C., Kirkby, J., Kontkanen, J., Kürten, A., Lampilahti, J., Lawler, M., Lehtipalo, K., Leiminger, M., Mai, H., Mathot, S., Mentler, B., Molteni, U., Nie, W., Nieminen, T., Nowak, J. B., Ojdanic, A., Onnela, A., Passananti, M., Petäjä, T., Quéléver, L. L. J., Rissanen, M. P., Sarnela, N., Schallhart, S., Tauber, C., Tomé, A., Wagner, R., Wang, M., Weitz, L., Wimmer, D., Xiao, M., Yan, C., Ye, P., Zha, Q., Baltensperger, U., Curtius, J., Dommen, J., Flagan, R. C., Kulmala, M., Smith, J. N., Worsnop, D. R., Hansel, A., Donahue, N. M., and Winkler, P. M. (2018), Rapid growth of organic aerosol nanoparticles over a wide tropospheric temperature range, *Proceedings of the National Academy of Sciences*, 115(37), 9122-9127, doi:doi:10.1073/pnas.1807604115.
- Vettikat, L., Miettinen, P., Buchholz, A., Rantala, P., Yu, H., Schallhart, S., Petäjä, T., Seco, R., Männistö, E., Kulmala, M., Tuittila, E. S., Guenther, A. B., and Schobesberger, S.: High emission rates and strong temperature response make boreal wetlands a large source of isoprene and terpenes, *Atmos. Chem. Phys.*, 23, 2683-2698, 10.5194/acp-23-2683-2023, 2023.
- Wang, M., Chen, D., Xiao, M., Ye, Q., Stolzenburg, D., Hofbauer, V., Ye, P., Vogel, A. L., Mauldin, R. L., 3rd, Amorim, A., Baccarini, A., Baumgartner, B., Brilke, S., Dada, L., Dias, A., Duplissy, J., Finkenzeller, H., Garmash, O., He, X. C., Hoyle, C. R., Kim, C., Kvashnin, A., Lehtipalo, K., Fischer, L., Molteni, U., Petaja, T., Pospisilova, V., Quelever, L. L. J., Rissanen, M., Simon, M., Tauber, C., Tome, A., Wagner, A. C., Weitz, L., Volkamer, R., Winkler, P. M., Kirkby, J., Worsnop, D. R., Kulmala, M., Baltensperger, U., Dommen, J., El-Haddad, I., and Donahue, N. M. (2020), Photo-oxidation of Aromatic Hydrocarbons Produces Low-Volatility Organic Compounds, *Environmental science & technology*, 54(13), 7911-7921, doi:10.1021/acs.est.0c02100.
- Vettikat, L., Miettinen, P., Buchholz, A., Rantala, P., Yu, H., Schallhart, S., Petäjä, T., Seco, R., Männistö, E., Kulmala, M., Tuittila, E. S., Guenther, A. B., and Schobesberger, S.: High emission rates and strong temperature response make boreal wetlands a large source of isoprene and terpenes, *Atmos. Chem. Phys.*, 23, 2683-2698, 10.5194/acp-23-2683-2023, 2023.

Chapter VI: Conclusions and perspectives

Chapter VI: Conclusions and perspectives

In this work, we firstly investigated the possibility of coupling a chemical ionization (CI) inlet to an ultrahigh-resolution mass spectrometer. The new developed CI-Orbitrap presents a higher mass resolving power (i.e., $R = 140\ 000$ at $m/z\ 200$) compared to state-of-the-art online mass spectrometers. Hence, uncertainties in identifying and quantifying overlapping peaks are substantially reduced by using CI-Orbitrap. We demonstrated its capacity to accurately separate ions detected using nitrate ion (NO_3^-)-based chemistry from a complex gas phase mixture produced from the oxidation of monoterpenes. The capability of the CI-Orbitrap in measuring RO_2 radicals as well as OVOCs at atmospherically relevant concentrations was also compared to simultaneous CI-APi-TOF measurements. By carefully choosing a sigmoidal correction function, we were able to show that the current restrictions of this novel analytical method can be largely overcome. Additionally, the analysis using the CI-Orbitrap can precisely quantify organic species at concentrations as low as 1×10^5 molecules cm^{-3} , allowing for the unmistakable identification of OVOCs generated in the gas phase. Therefore, the chemistry and the physicochemical properties of complex gaseous molecules can be better understood to a certain degree. Overall, the development of this new analytical tool may mark a crucial advancement in our ability to understand the formation and fate of atmospheric reactive organic species.

Given the success of using nitrate ion-based chemistry with the CI-Orbitrap, ammonium (NH_4^+) ion-based scheme was explored to characterize the widest range of oxidation products and radical species formed from the oxidation of VOCs. The intercomparison of the performance of various mass spectrometers, including CI-($\text{NH}_4^+/\text{NO}_3^-$)-Orbitrap, CI-(NO_3^-)-LTOF, PTR3-TOF, and CI-(I^-)-FIGAERO at identifying and quantifying OVOCs formed from α -pinene ozonolysis, revealed that the CI-(NH_4^+)-Orbitrap is a very promising analytical system to obtain a detailed assessment of the entire OVOC distribution. NH_4^+ ion-based scheme displays a constant trend despite subsequent loading, suggesting a linear response of ionization under atmospherically relevant conditions. Of these four mass spectrometers, CI-(NH_4^+)-Orbitrap identified the largest range of products, including highly oxygenated organic molecules (HOMs) and the least oxidized species. Hence, measurements by CI-(NH_4^+)-Orbitrap may be used as an input to evaluate or

Chapter VI: Conclusions and perspectives

interpret environmental observations to enhance the accuracy of models. Quantification of the product signals remains challenging for all mass spectrometers as there is no absolute and robust calibration method. Hence, more studies are needed to obtain an accurate quantification of the signals recorded by CI mass spectrometry techniques, and more specifically for the CI-(NH₄⁺)-Orbitrap for future applications in atmospheric measurements.

Oxygenated organic molecules (OOMs), which are produced from the oxidation of VOCs, contribute to the formation and growth of organic aerosol. When it comes to daytime VOC oxidation is mainly driven by hydroxyl radicals and ozone (O₃). At night, besides O₃, nitrate radicals (NO₃) are involved in the degradation of VOCs and the formation of a wide variety of OVOCs, including HOMs. Interestingly, nighttime new particle formation (NPF) is less frequently documented than daytime NPF, even though subsequent concentrations of dimeric species are also reported at night, particularly from O₃ chemistry. Here, we show that NO₃ chemistry inhibits NPF during the oxidation of monoterpenes, and likely explain the lack of NPF event at night in environment dominated by monoterpene emissions. We combined NPF experiments performed at the CLOUD facility, radical experiments using an oxidation flow reactor, as well as field observations in a wetland that do show intermittent nocturnal NPF. The NO₃-derived RO₂ radicals not only produce greater volatility dimers, but entirely modify the fate of other RO₂ radicals, produced from O₃/OH chemistry, ultimately impacting their ability to form particles. The organic vapors containing nitrogen produced by NO₃ chemistry do not have a low enough volatility to initiate the nucleation and growth particles. Hence, the yields of ultra-low volatility volatile organic compounds (ULVOC) decreased by a factor of 5 and particle formation rates dropped by a factor of 4 when only 20–30% of the monoterpene reactivity is driven by NO₃ radicals. Laboratory experiments are supported by ambient observations showing that particle number was reduced by up to an order of magnitude when NO₃ chemistry is present. Our findings explain why NPF does not happen all the time and everywhere to some extent. Further research is needed on the reactivity of NO₃-derived RO₂ radicals compared to O₃/OH derived RO₂ radicals. The NO₃ oxidation for other precursors, i.e., isoprene and aromatics, also needs to be examined for which precursors NO₃ chemistry is important. In other words, following studies should be conducted to identify if the process revealed here is only important for monoterpenes or more general of various VOCs. To better constrained NPF, especially in monoterpene-dominated environments, modeling needs to

Chapter VI: Conclusions and perspectives

consider the impact of NO_3 chemistry. Indeed, it would be important to better extrapolate how $\text{NO}_3\text{-RO}_2$ can inhibit NPF and quantify how widespread the NO_3 chemistry suppress NPF, thereby providing wider implications of anthropogenic perturbation on a biogenic system.

Résumé

Ce travail de thèse s'est attaché à développer une nouvelle interface d'ionisation chimique (CI) afin de la coupler à un spectromètre de masse à ultra haute résolution (Orbitrap). Ainsi le CI-Orbitrap présente un pouvoir de résolution en masse plus élevé (un facteur 10), réduisant considérablement les incertitudes dans l'identification et la quantification des espèces chimiques. Par ailleurs, l'Orbitrap permet de réaliser des expériences de spectrométrie de masse en tandem (MS^2) permettant ainsi de déterminer les énergies de liaison entre les ions réactifs et les analytes ainsi que d'élaborer les structures de molécules hautement oxygénées. Cette technologie permet ainsi d'améliorer considérablement la compréhension des processus d'oxydation des composés organiques volatils (COV). Fort de ces développements, un nouvel agent ionisant a été testé afin d'évaluer sa capacité à mesurer la plus grande gamme de COV et de COV oxygénés. Ainsi l'ammonium (NH_4^+) a été utilisé comme agent ionisant, notamment lors de campagne de mesures effectuées au CERN. Une intercomparaison, avec une large variété de spectromètre de masse, a ainsi pu être réalisée et démontre que le CI- (NH_4^+) -Orbitrap permet d'identifier et de quantifier la plus grande gamme de COV oxygénés formés lors de l'oxydation en phase gazeuse de COV. Cette technique analytique apparaît donc très prometteuse pour obtenir une analyse approfondie de la formation et l'évolution des COV oxygénés dans l'atmosphère. Forst du CI- (NH_4^+) -Orbitrap, les processus d'oxydation de l'alpha-pinène (monoterpène le plus présent dans l'atmosphère) ont pu être étudiés dans des mélanges complexes. Plus spécifiquement les processus de chimie nocturne, impliquant l'ozone et le radical nitrate (NO_3) ont été étudiés. Les différents résultats issus d'expériences en laboratoire et provenant de campagne de mesure dans la forêt boréale démontrent que les radicaux NO_3 impactent fortement la formation de nouvelles particules dans l'atmosphère. En effet, les produits formés, contenant notamment des atomes d'azote, ne disposent pas d'une volatilité suffisamment faible pour initier les processus de nucléation et la croissance des particules. Les rendements de COV à ultra-faible volatilité (ULVOC) ont diminué d'un facteur 5 et les taux de formation de particules ont chuté d'un facteur 4 lorsque seulement 20 à 30 % de la réactivité du monoterpène est due aux radicaux NO_3 . Les observations ambiantes ont également démontré que le nombre de particules était fortement réduit lorsque la chimie du NO_3 est présente. Ces résultats participent à expliquer le très faible nombre d'observations de formation de nouvelles particules pendant la nuit dans l'atmosphère.

Abstract

This work firstly investigated the possibility of coupling a chemical ionization inlet to an ultrahigh-resolution mass spectrometer. The new developed CI-APi-Orbitrap presents a higher mass resolving power, substantially reducing the uncertainties in identifying and quantifying overlapping peaks. It separated ions detected using nitrate ions base chemistry from a complex gas phase mixture produced from the oxidation of monoterpenes accurately. The binding energies between the reagent ions and product molecules were directly explored and the structures of highly oxygenated molecules were acquired using the MS^2 feature of CI- (NO_3^-) -Orbitrap, greatly increasing the understanding of the oxidation and fate of VOC oxidation. In addition, we find that ammonium (NH_4^+) ion-based scheme characterizes the widest range of oxidation products and radical species formed from VOCs oxidation, compared to CI- (NO_3^-) -LTOF, PTR3-TOF, and CI- (I^-) -FIGAERO. Despite high loading, the NH_4^+ ion-based scheme exhibits a constant trend, indicating a linear response to ionization at atmospherically relevant conditions. The CI- (NH_4^+) -Orbitrap is a highly promising analytical system to obtain a thorough analysis of the entire OVOC distribution. With CI- (NH_4^+) -Orbitrap, we detected nitrooxy peroxy radicals formed from NO_3 chemistry, and nitrogen-containing accretion products formed from the reaction of different peroxy radicals. The ring-retaining structure of nitrooxy peroxy radicals prevents the H-shift isomerization involved in the autoxidation of peroxy radicals, limiting the autoxidation to form higher oxygenated molecules. As a result, the organic vapors containing nitrogen produced by NO_3 chemistry do not have a low enough volatility to start the nucleation and growth particles. And the NO_3 -derived RO_2 radicals entirely modify the fate of RO_2 radicals from other oxidants, which in turn affects their ability to form particles. In other words, nitrooxy peroxy radicals suppress the production of ultra-low volatility organic compounds responsible for NPF. The yields of ultra-low volatility volatile organic compounds (ULVOC) decreased by a factor of 5 and particle formation rates dropped by a factor of 4 when only 20–30% of the monoterpene reactivity is driven by NO_3 radicals. NPF experiments at the CLOUD facility, radical experiments using an oxidation flow reactor, as well as field observations in a wetland that do show intermittent nocturnal NPF, were combined to show that NO_3 chemistry inhibits NPF during the oxidation of monoterpenes, and thus at night. Ambient observations showed that particle number was reduced by up to an order of magnitude when NO_3 chemistry is present.